MULTI-SCALE CONTROLS ON SPATIAL PATTERNS OF SOIL WATER STORAGE IN THE HUMMOCKY REGIONS OF NORTH AMERICA

A Thesis

Submitted to the College of

Graduate Studies and Research

in Partial Fulfillment of the Requirements

for the Degree of Doctor of Philosophy

in the Department of Soil Science

University of Saskatchewan

Saskatoon

By

Asim Biswas

PERMISSION TO USE

In presenting this thesis in partial fulfillment of the requirements for Postgraduate degree from the University of Saskatchewan, I agree that the Libraries of this University may make it freely available for inspection. I further agree that permission for copying of this thesis in any manner, in whole or in part, for scholarly purposes may be granted by the professor or professors who supervised my thesis work or, in their absence, by the head of the department or the Dean of the College within which my thesis work was done. It is understood that any copying or publication or use of this thesis or parts thereof for financial gain shall not be allowed without my written permission. It is also understood that due recognition shall be given to me and to the University of Saskatchewan in any scholarly use that may be made of any material in my thesis.

DISCLAIMER

Reference in this thesis to any specific commercial products, process, or service by trade name, trademark, manufacturer, or otherwise, does not constitute or imply its endorsement, recommendation, or favoring by the University of Saskatchewan. The views and opinions of the author expressed herein do not state or reflect those of the University of Saskatchewan, and shall not be used for advertising or product endorsement purposes.

Requests for permission to copy or to make other use of material in this thesis in whole or part should be addressed to:

Head of the Department of Soil Science
University of Saskatchewan
51 Campus Drive
Saskatoon, Saskatchewan, S7N 5A8

ABSTRACT

The intensification of land-water management due to agriculture, forestry, and urbanization is a global phenomenon increasing the pressure on world's water resources and threatening water security in North America. The Prairie Pothole Region of North America covers approximately 775,000 km^2 and contains millions of wetlands that serve important hydrological and ecological functions. The unique hummocky topography and the variable effect of different processes contribute to high spatio-temporal variability in soil water, posing major challenges in hydrological studies. The objectives of this study were to a) examine the spatial pattern of soil water storage and its scale and location characteristics; and b) to identify its controls at multiple scales. Soil water content at 20 cm intervals down to 140 cm was measured along a transect extending over several knoll–depression cycles in a hummocky landscape. High water storage in depressions and low water storage on the knolls created a spatial pattern that was inversely related to elevation. Spatial patterns were strongly similar within any given season (intra-season rank correlation coefficient as high as 0.99), moreso than between the same season over different years (inter-annual rank correlation coefficient as high as 0.97). Less similar spatial patterns were observed between different seasons (inter-season rank correlation coefficients as high as 0.90). While the intra-season and inter-annual spatial patterns were similar at scales >18 m, the inter-season spatial patterns were similar at much large scales (>72 m). This may be due to the variations in landform elements and micro-topography. The similarity at scales >72 m were present at any time and depth. However, small- and medium-scale spatial patterns changed with depth and with season due to a change in the hydrological processes. The relative dominance of a given set of processes operating both within a season and for the same season over different years yielded strong intra-season and inter-annual similarity at scales >18 m. Moreover, similarity was stronger with increasing depth, and was thought to be due to the dampening effect of overlying soil layers that are more dynamic. Similarity of spatial patterns over time helps to identify the location that best represents the field averaged soil water and improves sampling efficiency. Change in the similarity of scales of spatial pattern helps identify the change in sampling domain as controlled by hydrological processes. The scale information can be used to improve prediction for use in environmental management and modeling of

different surface and subsurface hydrological processes. The similarity of spatial pattern between the surface and subsurface layers help make inferences on deep layer hydrological processes as well as groundwater dynamics from surface water measurements.

ACKNOWLEDGEMENTS

I owe the largest debt of gratitude to my parents and brothers. The inspiration and support from them was always unconditional and unqualified. I cannot say enough thanks to my family.

It would not have been possible to undertake and complete the research required to write these manuscripts and the dissertation without the support of my supervisor, Dr. Bing Si. As a good friend and mentor, he made my Ph.D. experience most enjoyable yet challenging. Deepest gratitude to my research advisory committee members, Drs. Richard Farrell, Steven Siciliano, Xulin Guo, and Angela Bedard-Haughn for their guidance along the way up today.

I owe many thanks to Dr. Tom Yates, who first started the work in the same study site and developed the transect. Thanks are owed to other professors and scientists in and outside of the university. Drs. Daniel Pennock, Darwin Anderson, Amin Elshorbagy, Garth van der Kamp, Junwei Huang are too few to mention.

I owe a special thanks to my friend, brother, and colleague Henry, who was always there with me for anything at any time. Thanks to all my friends and their family at inside and outside of university life who made me feel home away from my home and my days going. Among them, I have to mention the name of Gourango, Priyanka, Siraj, and Tuli at the top. I would like to thank the members of Soil Physics team, who helped me at field data collection and laboratory work and made my office days enjoyable.

The financial support from the Natural Science and Engineering Research Council of Canada, International Polar Year Project, Dean's scholarship at the University of Saskatchewan are highly acknowledged. I also acknowledge the financial support from the Department of Soil Science, the College of Agriculture and Bioresources and the College of Graduate Studies and Research at the University of Saskatchewan. I thank to Debbie and Dean from the Workplace Safety and Environment Protection for helping me with the field equipment. Thanks to the Canadian Wildlife Service for providing the permission to use St. Denis study site.

Thanks to all who were there for me at different times and their names are not mentioned here. Lastly, I am grateful that God has placed me here and cared for me.

DEDICATION

I dedicate this Dissertation to my loving Parents and Brothers

TABLE OF CONTENTS

LIST OF TABLES

LIST OF FIGURES

LIST OF ABBREVIATIONS

ABE	absolute biased error
AR1	univariate lag-1 auto regressive
BD	bulk density
BM	benchmark
$CaCO_3$	calcium carbonate
CASMM	catchment average soil moisture monitoring site
CoV	coefficient of variation
CP	capacitance probe
CV	concave
CW	cultivated wetland
CWT	continuous wavelet transform
CX	convex
DEM	digital elevation map
DWT	discrete wavelet transform
EMD	empirical mode decomposition
FFT	fast Fourier transform
GIS	geographical information system
H[ ]	Hilbert transform
HAS	Hilbert spectral analysis
HHT	Hilbert-Huang transform
IFFT	inverse fast Fourier transform
IMF	intrinsic mode function
IP	impedance probe
k_a	dielectric constant
LAI	leaf area index
LE	lower envelope
LiDAR	light detection and ranging
m	number of measurement time
MABE	mean absolute biased error
MODWT	maximal overlap discrete wavelet transform
MRD	mean relative difference
N	number of sample points
NMM	neutron moisture meter
OC	organic carbon
p	significance level

PC	principle component
PCA	principle component analysis
PPR	prairie pothole region
PVC	polyvinyl chloride
r	correlation coefficient
r^2	coefficient of determination
RE	relative elevation
RMSE	root mean squared error
r_s	rank correlation coefficient
S	smoothing function
s	scale
SAGA	system for automated geoscientific analyses
SD	standard deviation
SDNWA	St. Denis national wildlife area
SDRD	standard deviation of mean relative difference
SWS	soil water storage
TDR	time domain reflectometry
UE	upper envelope
UW	uncultivated wetland
VHP	Vitel hydra probe
VIF	variance inflation factor
W	wavelet coefficients
x	location
δ	relative difference in soil water content
η	dimensional space
θ	soil water content
μ	population mean
Π	rectangle function
σ	standard deviation
Σ	summation function
σ^2	variance
τ	location
$\psi[\ ]$	mother wavelet function
ω	dimensionless frequency

1.0 INTRODUCTION

Life depends on water. In turn, quality of life is tied to healthy and sustainable water supplies that balance the environment, economic well-being, and human health. Across the world, there are increasing concerns about the long-term quality and accessibility of water for public consumption and proper functioning of ecosystems. Adding to the pressure on increasingly scarce water resources are population growth, economic development, climate change, land use changes, and environmental pollution. Canada is by no means exempt from these pressures. Water contributes $23 billion annually to Canada's economy, yet the country's water resources face unprecedented challenges (Environment Canada, 2004). Agriculture, forestry and industry all compete with an increasing urban population for what is essentially a finite resource of high quality water. During the last century, changes in land use and climate have generated significant concerns about the environmental sustainability of Canada's major river systems. Heavy demands on the South Saskatchewan River system for irrigation in Alberta, human consumption in Saskatchewan and power generation in Manitoba are threatening the water resources in the Canadian prairies.

A majority of the Canadian Prairie landscape is comprised of hummocky terrain that contains a very complex sequence of slopes extending from different sized rounded depressions to irregular complex knolls and knobs (Pennock, 2005). The hummocky terrain was formed by the last deglaciation, which shaped the topography of the landscape. Once the glacier retreated, there were millions of large ice chunks left buried in soil, which created small depressions upon melting. These depressions are known as potholes and the area in which they are prevalent is known as Prairie Pothole Region (PPR) of North America (Figure 1.1). The PPR covers a vast area (~775,000 km^2) that contains between 5 to 60 potholes per km^2 (National Wetlands Working Group, 1997). The potholes serve important hydrological and ecological functions. For example, a pothole can act as a sink for agriculturally derived nutrients (van der Valk, 1989; Whigham and Jordon, 2003) that creates the risk of eutrophication (Environment Canada, 2001). Potholes can also store surface water that will attenuate flood flows (Hubbard and Linder, 1986; Gleason and Tangen, 2008). The PPR is known as the 'duck factory' of North America, providing 10% of waterfowl nesting habitat and producing 50 to 80 % of the North American

waterfowl population (Smith et al., 1964; Ogaard et al., 1981; LaBaugh et al., 1998; Johnson et al., 2005). In addition, potholes are important in filtering water, buffering the impacts of upland land uses, removing and storing greenhouse gases from the atmosphere and reducing soil erosion (Ducks Unlimited Canada, 2006). Therefore, the distribution of water in this landscape determines the ground water dynamics, chances of runoff generation or changes in stream flow volume.

Figure 1.1. Prairie Pothole Region (PPR) of North America (Minke, 2009)

The distribution of soil water in the landscape is controlled by several factors and processes including soil properties, topography, vegetation, climatic processes, ground water, and water routing processes (Western and Blöschl, 1999; Gómez-Plaza et al., 2001; Tallon and Si, 2004). Both the individual and combined effects of these factors make soil water highly variable over space and in time (Bell et al., 1980; Munoz-Pardo et al., 1990; Gómez-Plaza et al., 2000; Hupet and Vanclooster, 2005; Brocca et al., 2009, 2010). Fortunately, these factors are not completely random; rather they exhibit certain spatial patterns in field. The spatial pattern of the controlling factors is reflected in the spatial pattern of soil water content (Kachanoski and de

Jong, 1988; Grayson and Western, 1998). Moreover, the spatial pattern of various controlling factors and processes are scale dependent (Webster, 1977; Trangmar et al., 1985; Goovaerts, 1998) and the scaling heterogeneity of the factors make the spatial pattern of soil water highly scale dependent (Entin et al., 2000; Choi et al., 2007). Therefore, the spatial series of soil water storage can be characterized as a combination of different frequency components, which are representative of different scale processes. For example, some processes vary frequently in space and are represented by high frequency components (small-scale processes), while others vary slowly and are represented by low frequency components (large-scale processes) (Si, 2003). Understanding the scales of the spatial pattern of soil water improves the prediction of hydrologic and general circulation models, weather prediction, and the understanding of different processes including evapotranspiration and runoff (Famiglietti and Wood, 1994), precipitation (Koster et al., 2000) and atmospheric variability (Delworth and Manabe, 1993). It also helps in simulation of land surface processes (Giorgi and Avissar, 1997) and characterization of biogeochemical cycling as well as that of water and energy.

Spatial patterns of controlling factors can have an increasing or decreasing trend. For example, the gradual change in topography, lithology, parent material, climate or vegetation can also impose a trend in the spatial pattern of soil water (Van Wambeke and Dulal, 1978). The trend results in non-uniform spatial mean(s) and variance(s) and makes the spatial series nonstationary (Kachanoski and de Jong, 1988). Moreover, the effect from different scale processes as represented by different frequency components can be localized in space making it difficult to identify the dominant scale of variation (Kachanoski and de Jong, 1988; Gómez-Plaza et al., 2000; Kim and Barros, 2002). In addition, sometimes the effect from different factors are non-additive and do not follow the principle of superposition (Yan and Gao, 2007) leading to a system that is nonlinear. In a nonlinear system, the response in soil water storage cannot be obtained by simply observing the response to one factor at a time and subsequently adding the individual observational results together (Pai and Palazotto, 2008). Therefore, in understanding the spatial distribution of soil water in the landscape, it is necessary to address both the nonstationarity and nonlinearity that is associated with the spatial series of soil water.

The main objective of this research was to examine the spatial pattern of soil water storage in the hummocky landscape of the Prairie Pothole Region of North America. To meet the

main objective, the first sub-objective was to develop new methodologies in dealing with various issues associated with the spatial distribution of soil water storage. The second sub-objective was to examine the scale and landscape characteristics of the spatial distribution of soil water storage. The third sub-objective was to identify the dominant factors controlling soil water storage at multiple scales.

In doing so, new methodologies were developed and applied to the soil water data collected from St. Denis National Wildlife Area, central Saskatchewan, Canada. New methodologies were compared with well-established methodologies in literature. The overall results were sub-divided into 7 sections, each of them was written as a standalone research paper, which are either published, accepted for publication or have been submitted for publication in peer reviewed international journals. Each paper starts with a preface and contains the appropriate literature review required to set the context for the work and discuss the results within the paper. Each paper also contains a complete materials and methods section with the necessary theoretical basis for the analysis techniques. Thus, there will be a degree of redundancy of information, which is unavoidable when using this format. The advantage of having peer-reviewed work in the thesis outweighs any disadvantages this format may present to the reader. Steps have been taken to reduce redundancy, such as combining the abbreviations and references from the individual manuscripts into one complete bibliography (Chapter 11). The coherency through the thesis is provided by a general literature review in Chapter 2 and a synthesis of results and implications for future research is given in Chapter 10.

The results section starts with a manuscript (Chapter 3), which examined the similarity of the spatial pattern of soil water storage at different seasons and depths and identified a location with field-averaged soil water over time, known as a benchmark location. The benchmark location has the potential to reduce the number of samples necessary to characterize field soil water in the landscape. The similarity of the scales of the spatial pattern of nonstationary soil water and the characteristic landscape elements associated with the similarity or dissimilarity at dominant scales were identified in Chapter 4 using wavelet coherency analysis. The similarity of the spatial pattern of soil water storage at the surface to the subsurface layers (Chapter 5) was also examined at different seasons using wavelet coherency analysis.

While Chapters 3 to 5 discuss spatial patterns and their different scale and landscape characteristics, Chapters 6 to 9 discuss the controls of soil water storage in the landscape. Chapter 6 presents the correlation between soil water storage and its various controlling factors at the measurement scale using Pearson correlation coefficients, while Chapter 7 presents the correlation at multiple scales using wavelet coherency analysis. Chapter 8 identifies the effect of local and nonlocal controls of soil water storage. Finally, Chapter 9 separates the variations in soil water storage at multiple scales and provides the scale-specific predictive relationship using Hilbert-Huang transform.

Hilbert-Huang transform is a new spatial analysis method in soil science and is compared with well-established wavelet transform to examine the scales and location of variability in Appendix A and Appendix B. The permission to publish and republish the sections and chapters of this dissertation is given to different journals and the names are listed in Appendix D. Publications related to the Ph.D. work is listed in Appendix E.

2.0 REVIEW OF LITERATURE

2.1 Soil Water

The amount of water stored in soil constitutes < 0.001 percent of the global total water storage and < 0.05 percent of the global fresh water storage (Shiklomanov, 1993). However, it is the principal limiting factor in semi-arid agricultural production and a key element in environmental health. Soil water determines the rate of evapotranspiration by controlling water availability to plants (Gómez-Plaza et al., 2000; Mohanty et al., 2000; Porporato et al., 2004). It also determines environmental health by affecting the migration of sediment, toxins and chemicals to environmentally sensitive areas such as surface water bodies and ground water. Soil water has also been recognized as a key parameter of various environmental processes by hydrologists, meteorologists, and climate scientists. It controls the interaction between the land surface and atmosphere as the changes in the soil water affect both energy and water cycles. Soil water plays an important role in determining the amount of runoff that occurs after rainfall or snowmelt (Bronstert and Bárdossy, 1999; Raats, 2001; Wilson et al., 2004; Vereecken et al., 2007) and thus the likelihood of drought and flood that may affect an area. It provides a link between surface energy and water balances (Famiglietti and Wood, 1994; Crow and Wood, 2002; Albertson and Montaldo, 2003; Pan et al., 2003; Rodríguez-Iturbe and Porporato, 2004) and thereby determines the hydrological response of an area (Wilson et al., 2004). Soil water content is also a key input in validating several hydrologic and climatic models (Rodríguez-Iturbe et al., 1999). It also determines the emission of different gases including greenhouse gases, thus soil water is taking part in the study of climate change (Renault and Stengel, 1994; Lark et al., 2004; Yates et al., 2007).

2.2 Spatial Variability of Soil Water

Understanding these environmental processes as controlled by soil water is a major challenge in hydrology (Quinn, 2004) because the distribution of soil water is controlled by several factors and processes including soil properties, topography, vegetation, climatic processes, ground water, and water routing processes (Western and Blöschl, 1999; Gómez-Plaza et al., 2001; Tallon and Si, 2004). The individual or combined effects of these factors and

processes yield large spatio-temporal heterogeneity in soil water distribution within a field (Bell et al., 1980; Francis et al., 1986; Munoz-Pardo et al., 1990; Fitzjohn et al., 1998; Seyfried, 1998; Gómez-Plaza et al., 2000; Schume et al., 2003; Hupet and Vanclooster, 2002, 2005; Lin et al., 2006; Brocca et al., 2008, 2009, 2010). Therefore, a large number of samples are required to characterize the soil water content in a field.

Spatial variability in soil water can be characterized through the coefficient of variation and from the probability density function of sampled soil water using statistical analysis. The relationship between the variance or the coefficients of variations of soil water content and its mean value allows us to: a) optimize the number of sampling points to represent the field averaged soil water with a fair accuracy (Hills and Reynolds, 1969; Reynolds, 1974; Bell et al., 1980; Owe et al., 1982); b) estimate the error associated with measurements; c) assess the variability of soil water within a known area; and d) define the wetness condition for which remote sensing monitoring is most accurate (Charpentier and Groffman, 1992; Brocca et al., 2007). Mostly there is a decreasing trend in soil water variability with the decrease in mean soil water. However, contradictory conclusions have often been reported on whether the soil water variability is positively (Famiglietti et al., 1998; Martínez-Fernández and Ceballos, 2003) or negatively (Famiglietti et al., 1999; Hupet and Vanclooster, 2002) correlated to average soil water content. Recently Choi et al. (2007) reported a negative exponential relationship between the coefficient of variation and the average soil water content. The relative variability in average soil water content decreases as the sampling extent increases, and thus the relationship follows power law decay function (Rodríquez-Iturbe et al., 1995; Choi et al., 2007).

Another important issue in the statistical analysis concerns the statistical distribution of soil water content. Knowledge about the statistical distribution of soil water is important because several hydrological, ecological, and atmospheric processes are related to soil water. Several authors have indicated a normal distribution of soil water content from spot measurements over grids or transect (Hills and Reynolds, 1969; Bell et al., 1980; Hawley et al., 1983; Vachaud et al., 1985; Francis et al., 1986; Munoz-Pardo et al., 1990; Nyberg, 1996; Anctil et al., 2002; Buttafuoco et al., 2005). However, Loague (1992) reported the normal distribution of soil water content measured only along the transect and not over a grid or points. The distribution of soil water can be negatively skewed/non-normal under very wet conditions, to positively

skewed/non-normal under dry conditions with normal in the mid-range of mean soil water content (Famiglietti et al., 1999).

The spatial variability of soil water is the reflection of the spatial variability of hydrological processes, which is controlled by various factors such as climate, soil texture, vegetation and topography in any natural catchment or agricultural land (Mohanty and Skaggs, 2001; Choi et al., 2007). The spatial variability in factors yields the variability in the spatial distribution of soil water. However, it is fortunate that the factors or processes controlling soil water distribution are not completely random in field; rather they follow a spatial pattern. For example, any factors measured at places in close proximity are more likely to be similar than those measured further apart (Gajem et al., 1981; Viera et al., 1982; Oliver, 1987). This means that the factors are auto-correlated and the autocorrelation varies with space yielding a pattern. Therefore, the spatial patterns in the controlling factors or processes can be defined as a perceptual structure, placement or arrangement of the factors or processes on earth, which includes the space between the objects. The regularity or the systematic variation is also termed the 'organization' (Western et al., 1999) and the spatial organization implies variation characterized by consistent spatial patterns (Blöschl, 1999). With the increasing regularity or the systematic variability, the soil water distribution may even exhibit spatial continuity (Western et al., 1999) that means the soil water pattern may be continuous in space.

Geostatistical analysis can describe the variance between point values sampled in a spatial field as a function of their distance. Various authors have used geostatistical analysis to characterize the spatial pattern in soil water (Warrick et al., 1990; Nyberg, 1996; Bárdossy and Lehmann, 1998; Western et al., 1998; Entin et al., 2000; Wang et al., 2001; Anctil et al., 2002; Meyles et al., 2003; Petrone et al., 2004; Western et al., 2004; Brocca et al., 2007; Lakhankar et al., 2010). The main feature of this analysis is the range, which is defined as the distance at which the variogram (plot of semivariance as a function of lag distance or separation between measurements) levels off (the sill) and beyond which the observation appear independent (Figure 2.1). The correlation length is the measure of the spatial continuity in soil water and is directly related to the range (Figure 2.1; Western et al., 1998, 2004). Western and Blöschl (1999) observed the range between 0.7 m to 650 m; however, the range is dependent on the scale of the study and the density of the measurement. Spatial continuity or the organized spatial pattern of

factors controls the hydrologic processes and thus determines the spatial pattern in soil water content (Kachanoski and de Jong, 1988; Grayson and Western, 1998; Blöschl, 1999; Western et al., 1999).

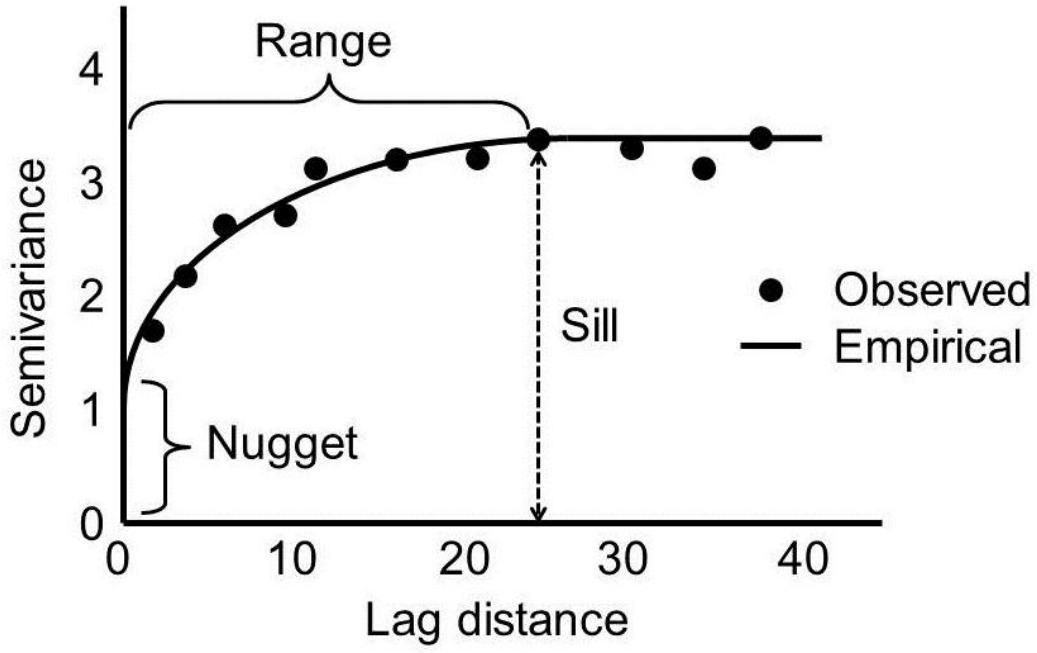

Figure 2.1. A typical example of semivariogram showing different components.

2.3 Similarity of Soil Water Spatial Patterns Over Time

In spite of high spatio-temporal variability, if a field is repeatedly surveyed for soil water, some points would always be wetter and some points would be drier than the field average. Therefore, if we rank the soil water content within a field, the points would maintain their rank at different measurement times. Hence, the spatial pattern of soil water content measured at one time will be similar to the spatial pattern of soil water content measured at another time. The similarity of the spatial pattern of soil water content at different times was examined by Vachaud et al. (1985). In doing so, authors assigned a statistical value to each location. For example, they ranked the observation from the smallest to the largest values and identified the cumulative probability distribution as normal. They identified a location with probability of 50%, which characterized the average soil water for the entire field. The other locations with one standard deviation or two-standard deviation were the characteristics of extreme values. This time

invariant association between the spatial locations and the classical statistical parameters (mostly the mean and standard deviation) of soil water was defined as the 'time stability' of the rank of individual observations in the probability distribution function (Vachaud et al., 1985). Therefore, the time stability of soil water spatial pattern is the reflection of the similarity of spatial pattern over time (Kachanoski and de Jong, 1988). Hence, the stability is in the order or rank of the soil water at different spatial points that does not change at some probability. The similarity in the order or rank of the individual points is also termed as the 'order stability' or 'rank stability' (Tallon and Si, 2004; Chen, 2006).

Vachaud et al. (1985) used two different techniques to evaluate the time stability of soil water spatial pattern. The first one concerns the difference $\Delta_{i,t}$ between individual measurements of soil water content $\theta_{i,t}$ at location *i* and time *t* and the mean water content $\overline{\theta_t}$ at the same time;

$$\Delta_{i,t} = \theta_{i,t} - \overline{\theta_t} \qquad [2.1]$$

where $\overline{\theta_t} = \left(1/n\right)\sum_{i-1}^{n} \theta_{i,t}$ and *n* is the number of measurement locations. The relative difference was calculated as

$$\delta_{i,t} = \frac{\Delta_{i,t}}{\overline{\theta_t}} \qquad [2.2]$$

For any location *i*, the mean relative difference (MRD) can be calculated as

$$\overline{\delta_i} = \frac{1}{m}\sum_{t=1}^{m} \delta_{i,t}\ , \qquad [2.3]$$

and the standard deviation of mean relative difference (SDRD) can be calculated for the whole occasions of soil water measurements as

$$\sigma\left(\delta_i\right) = \sqrt{\frac{\sum\left(\delta_{i,t} - \overline{\delta_i}\right)^2}{m-1}} \qquad [2.4]$$

where *m* is the number of sampling occasions. The MRD can be ranked to identify the points that overestimate ($\overline{\delta_i} > 0$) or underestimate ($\overline{\delta_i} < 0$) the field averaged water storage regardless of observation time.

The second technique used was the nonparametric Spearman's test. If $R_{i,t}$ is the rank of soil water $\theta_{i,t}$ at i^{th} location and t^{th} time and $R_{i,t'}$ is the rank of soil water at the same location but at different time t', the Spearman's rank correlation coefficients can be calculated as

$$r_s = 1 - \frac{6 \cdot \sum_{i=1}^{n} (R_{i,t} - R_{i,t'})^2}{n(n^2 - 1)}, \qquad [2.5]$$

where n is the number of observations. A value of r_s =1 corresponded to identity of rank for any location or perfect time stability between time t and t'. The closer r_s to 1, the more stable the process at that specific location (Vachaud et al., 1985).

Vachaud et al. (1985) first developed and tested this method at three sites in France, Spain, and Tunisia with differing climate, land cover, and varying sample sizes. Later, various authors have picked up this concept and applied it in their soil water variability studies over a range of study areas, sampling schemes, investigation depths, study periods, land uses, landscapes, and measuring techniques (Table 2.1). The time stability concept has been used in examining the similarity of the spatial pattern of various other soil properties (Goovaerts and Chiang, 1993), infiltration and its application to irrigation (Jaynes and Hunsaker, 1989), soil matric potential (Van Pelt and Wierenga, 2001), EC (Farahani and Buchleiter, 2004), Na-content and Na absorption ratio (Castrignanó et al., 1994; Douaik et al., 2006, 2007), and throughfall (Keim et al., 2005).

Table 2.1. Main characteristics of soil water time stability analysis reported in the literature.

Authors	Year	Study area	Land use	Soil type	Slope (%)	Area/length	Sampling Instr.†	Sampled depth (cm)	NSP‡	NS§	Argt¶	SP (m)#	Dominant control!!
Vachaud et al.	1985	Grenoble, France	Grass	Silty clay sand	0	2E+03 m^2	NMM	100	17	24	G	10	Texture
		Sevilla, Spain	Agric	/	/	/	NMM	100	9	8	I	/	
		Mornag, Tunisia	/	Silt clay sand	0	100 m	Grav	100	19	2	T	5	
						1E+04 m^2	NMM	100	25	3	G	20	
Kachanoski and de Jong	1988	Saskatchewan, Canada	/	/	8	720 m	NMM-Grav	10-170	72	3	T	10	Topo.
Munoz-Pardo et al.	1990	Medjaz el bab, Tunisia	Agric	Sandy loam	0	1.2E04 m^2	Grav	100	3	81	G	12.5	Texture
Comegna and Basile	1994	Naples, Italy	Agric	Sandy	0	0.3 ha	NMM	150	75	6	T+G	12	Soil properties
Famiglietti et al.	1998	Rattlesnake hill, USA	Grass	Gravely clay, clay	5.3	200 m2	Grav	5	21	88	T	10	Wet- soil properties Dry- topo.
Grayson and Western	1998	Tarrawarra,	Grass	Silt loam	8	1.1E+05 m^2	TDR	30	500	13	G	15	Soil depth,
		Australia	Grass	Silt loam	8	1.1E+05 m^2	NMM	60	20	84	G	70	Topo.
		Tarrawarra,	Grass	Silt loam	8	1.0E+05 m^2	NMM	120	34	85	I	35	
		Australia	/	/	/	1E+09 m	NMM	50	41	14	T	7E+7	
		R-5 Chickasha											
		Lockyersleigh											
Western et al.	1999	Tarrawarra, Australia	Grass	Silt-loam	8	10.5E04	TDR	30	13	500	G	15	Topo.
Gómez-Plaza et al.	2000	Murcia, Spain	Grass-burnt	Loam	29	300 m	TDR	15	16	14	T	20	Topo., vegetation
			Grass-burnt		30	300 m			16				
			Grass		31	200 m			11				
Mohanty and Skaggs	2001	SGP97 LW03	Pasture	Sandy loam	Rolling	6.4E+05 m^2	Grav-IP	6	49	23	G	100	Combined soil, topo., vegetation
		SGP97 LW13	Pasture	Silty loam	Rolling					25			
		SGP97 LW21	Wheat/grass	Silty loam	0					17			
Van Pelt and Wierenga	2001	Leyendecker, NM	Wheat/cotton	Silty clay loam	0	1E+04 m^2	NMM	15-50	60	14	G	6-22	Texture
Hupet and Vanclooster	2002	Louvin, Belgium	Agric.	Organic soil	0	6300 m^2	TDR-NMM	0-125	60	28	G	15	Vegetation
Grant et al.	2004	Boise, Idaho	Sagebrush	Fine loam – clay	~40	3.6E+05 m^2	NMM	75	12	16	I	175	Texture
									19	12		135	
Martínez-Fernández and Ceballos	2003	Duero basin, Spain	Agric.	Sandy-loam	8	1.3E+09 m^2	TDR	5, 25, 50, 100	23	74	I	5E+07	Soil water condition

† sampling instrument (NMM, neutron moisture meter; IP, impedance probe; Grav, gravimetric method; TDR, time domain reflectometry; CP, capacitance probe; VHP, Vitel Hydra probe); ‡ number of sample points; § sample numbers; ¶ sampling arrangement (G, grid; T, transect; I, irregular); # sampling spacing; /, information not available; !! dominant control (topo., topography; Ppt., precipitation)

Table 2.1: Main characteristics of soil water time stability analysis reported in the literature (contd.).

Authors	Year	Study area	Land use	Soil type	Slope (%)	Area/length	Sampling Instr.†	Sampled depth (cm)	NSP‡	NS§	Argt¶	SP (m)#	Dominant control!!
Tallon and Si	2004	Saskatchewan, Canada	Agric.	Silty clay loam	Rolling	612 m	CP	30, 60, 90 120, 160	95	~12	T	6	Soil properties, topo.
Cosh et al.	2004	Walnut Creek, Iowa	Corn	Silt loam	/	1E+11 m^2	TDR	5	12	43	I	/	Soil properties
Jacobs et al.	2004	SMEX02 WC11 SMEX02 WC12 SMEX02 WC13 SMEX02 WC14	Corn Corn Soybean Soybean	Silty loam	Rolling 0 Rolling Rolling	4E+09 m	IP	6	91 132 140 94	13	T	12.5-25	Soil properties, topo.
Petrone et al.	2004	Quebec, Canada	Agric.	Peat	0 0 0	1.2E+03 m^2 9E+04 m^2 254 m	TDR	15	336 57 508	3 3 2	G G T	2 30 0.5	Vegetation, soil water condition
Western et al.	2004	Tarrawarra 1, Austr. Tarrawarra 1, 2, Aust. Point Nepeau, Austr. Carran's, NZ Satellite station, NZ Clayden's, NZ	Grass	Silt-loam Silt-loam Sand Silt-loam+clay Clay-loam Clay	8 8 8 14 16 14	10E04 m^2 45E04 m^2 13E04 m^2 5E04 m^2 60E04 m^2 13E04 m^2	TDR	30	8 8 6 6 6 6	145 470 589 485 368 273	G	30 40 15 10 40 20	Topo. Soil properties
Martínez-Fernández and Ceballos	2005	Duero basin, Spain	Agric. Forest	Sandy loam Silty loam	Rolling Rolling	1.3E+09 m^2 6.2E+08 m^2	TDR	5-100	23 18	40 m 52 m	I	5E+7 6000	Texture, vegetation
Pachepsky et al.	2005	Bekkevoort, Belgium	Grass removed	Sandy loam	Gently sloping	8 m	TDR	15, 35, 55, 75, 95	12	384 days	T	0.5	Soil properties
Starr	2005	Houlton, Maine	Cropland	Gravelly sandy loam, Gravelly loam, shaly silt loam, silt loam	Rolling	/	TDR	30	155	5-9	T	30	Topo.
Cosh et al.	2006	Little Washita Oklahoma	Rangeland cropland	Sand and silts - clay	0	6.1E+08 m^2	VHP	5	13+1	21 m	I	/	Land cover type

† sampling instrument (NMM, neutron moisture meter; IP, impedance probe; Grav, gravimetric method; TDR, time domain reflectometry; CP, capacitance probe; VHP, Vitel Hydra probe); ‡ number of sample points; § sample numbers; ¶ sampling arrangement (G, grid; T, transect; I, irregular); # sampling spacing; /, information not available; !! dominant control (topo., topography; Ppt., precipitation)

Table 2.1: Main characteristics of soil water time stability analysis reported in the literature (contd.).

Authors	Year	Study area	Land use	Soil type	Slope (%)	Area/length	Sampling Instr.†	Sampled depth (cm)	NSP‡	NS§	Argt¶	SP (m)#	Dominant control!!
Bosch et al.	2006	Georgia (SMEX03)	Forest cropland Pasture	Loamy sand	0-5	3.8E+09 m^2	CP	6	19	10	I	/	Combined from texture, topo., land management
Lin	2006	Pennsylvania, USA	Forest	Silt loam	25-48	7.9 ha	Theta probe	6	77	~ 1 yr	T	/	Combined topo. and soil properties
Starks et al.	2006	Little Washita Oklahoma (SGP97-SMEX03)	Rangeland cropland	Sandy loam / silt Loam / loamy sand	0	6.1E+08 m^2	VHP	0-15, 15-30, 30-45, 45-60, 0-60	8	40	I	/	Soil properties
Teuling et al.	2006	Belgium Tarrawarra, Australia Chickasha, Oklahoma	Agric. Pasture Grass	Silt-loam Silt-loam, clay /	0 Undulating 3	0.65 ha 10.5 ha 10 ha	TDR, NMM NMM NMM	50 150 60	28 20 34	45 days I 59 days 84 days	G I I	/ / /	Soil water condition
Zhou et al.	2007	Pennsylvania, USA	Forest	Silt-loam	25-40	7.9 ha	TDR	100	77	~ 1 yr	I	/	Soil water condition, water table
Cosh et al.	2008	Walnut Gulch, AZ	Shrub and grass			150 km^2	VHP	5	21	41 m	I	/	Soil properties
Guber et al.	2008	Beltsville, Maryland	Corn	Coarse-loamy	1-4	25 ha	CP	180	24	610 days	I	/	Soil properties
Williams et al.	2008	Dry Creek, Idaho	Grass and shrub	Coarse-loamy	30	0.02 km^2	TDR	5, 15, 45, 75, 105	57	38	G	20	Slope, soil texture, soil depth
Brocca et al.	2007, ‘09	Tiber valley, Italy	Grass	Silty-clay Silt-clay-loam Sandy-loam	0 7 12	405 m^2 5000 m^2 8800 m^2	TDR	15	45 50 108	14 14 7	G	3 14 7	Topo.

† sampling instrument (NMM, neutron moisture meter; IP, impedance probe; Grav, gravimetric method; TDR, time domain reflectometry; CP, capacitance probe; VHP, Vitel Hydra probe); ‡ number of sample points; § sample numbers; ¶ sampling arrangement (G, grid; T, transect; I, irregular); # sampling spacing; /, information not available; !! dominant control (topo., topography; Ppt., precipitation)

Table 2.1: Main characteristics of soil water time stability analysis reported in the literature (contd.).

Authors	Year	Study area	Land use	Soil type	Slope (%)	Area/length	Sampling Instr.†	Sampled depth (cm)	NSP‡	NS§	Argt¶	SP (m)#	Dominant control!!
Hu et al.	2008, '09, '10a	Shaanxi Province, China	Grass and shrub	Sandy-loam	Undulating	20 ha	NMM	100	12	20	I	/	Soil properties, bulk density, organic carbon
Zhao et al.	2010	China	Perennial grass	Sandy-loam	Rolling	24 ha	Theta probe	6	100	36 m	G	15	Vegetation, land management

† sampling instrument (NMM, neutron moisture meter; IP, impedance probe; Grav, gravimetric method; TDR, time domain reflectometry; CP, capacitance probe; VHP, Vitel Hydra probe); ‡ number of sample points; § sample numbers; ¶ sampling arrangement (G, grid; T, transect; I, irregular); # sampling spacing; /, information not available; !! dominant control (topo., topography; Ppt., precipitation)

One of the important applications of the time stability concept has been the identification of time stable locations, which can considerably reduce the number of sampling locations in obtaining the mean soil water content for an area of interest (Vachaud et al., 1985) and holds considerable promise for minimizing costs. Repeated survey of soil water in a field showed that some locations in the field are consistently wetter or drier than the field averaged soil water. Therefore, the sample locations maintain their rank irrespective of dry or wet conditions and the location that closely represents the field averaged soil water will continue to do so over the period of measurement (Vachaud et al., 1985). Hence, the relative difference between the average soil water of that location and the whole field will be close to zero and thus the soil water measurement of that location can be used to represent the field averaged soil water at any time. The location is described as the catchment average soil moisture monitoring (CASMM) site (Grayson and Western, 1998) or benchmark location (Tallon and Si, 2004). Vachaud et al. (1985) mentioned that the identification of time stable location (benchmark location) is realistic because the factors controlling the spatial pattern of soil water content are stable with time. Monitoring soil water at benchmark locations is useful in deciding various agronomic management practices such as irrigation scheduling, fertility monitoring and fertilizer recommendation, modeling soil water balance in a field, and understanding hydrological processes. Information on time stable spatial patterns has actively been used in remote sensing of soil water in upscaling the water content from several or even single point measurement to the average soil water content across a footprint area (Mohanty and Skaggs, 2001; Cosh et al., 2004; Jacobs et al., 2004). It has also been used in establishing field or catchment-wide antecedent soil water condition for runoff simulations (Western et al., 2003), relating spatio-temporal variation in soil water to the onset of subsurface flow as measured with a network of peizometers (Penna et al., 2006) and upscaling of soil moisture information in irrigated and dry-land crops (Rolston et al., 1991; Rocha et al., 2005). Use of temporally stable patterns to downscale remotely sensed data of soil water has also been suggested (Narayan and Lakshmi, 2005). Pachepsky et al. (2005), Fernández-Gálvez et al. (2006) and Guber et al. (2008) used time stability of the spatial pattern to estimate the soil water contents at rarely sampled locations or at missing points.

2.4 Methods for Identifying Time Stable Locations

According to the definition of time stability, the time stable location is the location that has MRD close to zero with least SDRD (Vachaud et al., 1985). These are the most widely used indices in identifying the time stable sampling locations (Grayson and Western, 1998; Gómez-Plaza et al., 2000; Cosh et al., 2006, 2008; Brocca et al., 2009). In addition to this, various other indices that identify the time stable location can also be found in the literature. Jacobs et al. (2004) introduced root mean squared error (RMSE) of the relative difference, which is computed from the mean relative difference and associated variance and was expressed as

$$RMSE_i = \sqrt{\left(\bar{\delta}_i^2 + \sigma^2\left(\delta_i\right)\right)}. \quad [2.6]$$

Using the rank ordered $RMSE_i$, the location with lowest RMSE was identified as the most time stable location. The RMSE can be used to evaluate the time stable site for an entire range of soil water measurements within a field as calculated or comparison among the fields as

$$RMSE_{i,j} = \sqrt{\left(\bar{\delta}_{i,j}^2 + \sigma^2\left(\delta_{i,j}\right)\right)}, \quad [2.7]$$

where $\bar{\delta}_{i,j}$ is the MRD and $\sigma\left(\delta_{i,j}\right)$ is the SDRD for i^{th} location and j^{th} field. Therefore, Jacobs et al. (2004) compared the time stability within a field as well as among different fields. Similarly, Guber et al. (2008) extended the time stability analysis and included the depth in the calculation. They employed a new time stability index T_{ik}, which was computed as the width of the 90% tolerance interval of empirical probability distribution functions of relative soil water content, i.e., $\delta_{i,k,t}\left(P=0.95\right)-\delta_{i,k,t}\left(p=0.05\right)$, where $\delta_{i,k,t}$ is the MRD at i^{th} location and k^{th} depth and t^{th} time. Smaller the value of T_{ik}, stronger the time stability. Furthermore, Guber et al. (2008) used the root mean squared difference,

$$D_{i,k} = \sqrt{\frac{\sum_t^{N_{i,k}} \left(\bar{\theta}_{t,k} - \theta_{i,t,k} / \bar{\delta}_{i,k}\right)}{N_{i,k} - 1}}, \quad [2.8]$$

where $N_{i,k}$ is the total number of observation and $\bar{\delta}_{i,k}$ is the average value of MRD to identify the location that best estimate the average soil water content at different depths. Recently, Hu et al. (2009, 2010a, 2010b) calculated the absolute biased error,

$$ABE_{i,t} = \frac{\left|\delta_{i,t} - \bar{\delta}_i\right|}{1 + \bar{\delta}_i} \quad [2.9]$$

and mean absolute biased error,

$$MABE_i = \frac{\sum_{t=1}^{m} ABE_{i,t}}{m} \quad [2.10]$$

to identify time stable locations. This analysis provides the mean value in soil water storage within a desired error. However, the most widely accepted and used index is the SDRD, which calculate the uncertainties associated with measurement directly and can identify the location with least error in it.

Various authors have mentioned about the physical locations for the time stable sites. Grayson and Western (1998) identified the location of time stable sites or 'best' sites with respect to transect average soil water in areas that were neither convergent nor divergent. These locations tended to be located near the mid-slopes or in areas that had topographic aspects close to the average and were identified as the 'aspect neutral' part of the transect. Jacobs et al. (2004) and Vivoni et al. (2008) also documented that the locations that consistently maintained time stability were located at mid slopes or mid-elevation, respectively.

2.5 Factors Controlling the Time Stability of Spatial Patterns

At any given time, the water content in soil reflects the integration of all hydrologic processes. Therefore, the spatial pattern in soil water content reflect the influence of those factors on hydrologic processes and the response of these processes to climate, soil management practices, and the extraction of water by plants. However, there is no single factor or processes that control the spatial pattern of soil water in a field; rather a complex suite of environmental factors and processes work alone or in combination to determine the spatial pattern in soil water content. Various authors have argued that the soil properties have major control on this soil water content, while others indicated the topographic control is dominant. Vachaud et al. (1985) mentioned that a large extent of the spatial variability could be explained by the variability of soil texture. Mohanty and Skaggs (2001) found stronger time stability in sandy loam soil than silt loam, while Jacobs et al. (2004) reported weak time stability with highest sand content. With sand and clay content, Cosh et al. (2008) also mentioned bulk density as a control of soil water time stability. Starks et al. (2006) concluded that the soil parameters were more important in controlling time stability than the spatially variable rainfall. However, several studies have

reported topographical position or the local topography is important among the factors controlling time stability of soil water at transect scale (Kachanoski and de Jong, 1988; Western et al., 1999; Gómez-Plaza et al., 2000; Thierfelder et al., 2003; Brocca et al., 2007, 2009). Tomer and Anderson (1995) analyzed the variation in soil water storage across a sand plain hill-slope under grass and reported that among the important factors, terrain indices explained more than half of the spatial variability of soil water distribution. Different terrain indices have been used to represent the key hydrological processes controlling soil water distribution in a simplified but more realistic way. Western et al. (1999, 2002) summarized the effect of terrain indices on soil water variability studied over a variety of landscapes.

Gómez-Plaza et al. (2000) also showed the effect of vegetation on the time stability of the spatial pattern of soil water content. Soil water was highly variable along a transect with plant cover than two non-vegetated transect. Various authors also mentioned about the organic carbon (OC) content, which controls the soil distribution and its time stability. Hu et al. (2009, 2010a) reported that soil particle size and the organic matter were most important among the factors influencing time stability. da Silva et al. (2001) identified clay content and OC as better explanatory variable of time stability than topographic variables. The impact of the distribution of atmospheric forcing on soil water level has also been reported (Seyfried, 1998; Houser, 2000).

However, mutual and multiple influences from various controlling factors yielded contradictory findings (Famiglietti et al., 1998; Western et al., 1999). Tallon and Si (2004) did not find any strong correlation between temporally stable sites and soil properties or topographic indices suggesting the absence of single controlling factors. Choi et al. (2007) combined the results from several studies on grasslands and crops lands in Europe and USA and concluded that the rainfall and topography control the change in soil water variability under drying-wetting cycle, while soil parameters control the relative amplitude.

In identifying the time stable locations in a field, most of the studies have focussed on the surface soil water (Vachaud et al., 1985; Grayson and Western, 1998; Mohanty and Skaggs, 2001; Cosh et al., 2004; Brocca et al., 2009) and few have examined the deeper soil profile (Martínez-Fernández and Ceballos, 2005; Pachepsky et al., 2005; De Lannoy et al., 2007; Hu et al., 2009, 2010a). Fewer studies have explored the changes in time stability with depth (Hupet and Vanclooster, 2002; Martínez-Fernández and Ceballos, 2003). The dominant processes

operating at different layers of soil determined the hydrology of soil layers. For example, less root activity in deeper horizons yielded stronger time stability compared to surface (Cassel et al., 2000). Similarly, Comegna and Basile (1994) found a better time stable spatial structure in the top 90 cm of soil profile in a volcanic Visuvian sandy soil of large heterogeneity in terms of physical properties. However, Martínez-Fernández and Ceballos (2003) did not observe any specific pattern of stability with respect to depth. The changing pattern in water storage with depth was also reported by Tallon and Si (2004), Pachepsky et al. (2005), Guber et al. (2008), and Hu et al. (2009, 2010a). Though, Kamgar et al. (1993) could not identify the time stability of the soil water spatial pattern at the surface soil, time stability was found at the depth below 2.85 m. However, Grayson and Western (1998) reported that there were no significant effects of measurement depth between the measured data set.

Beside these factors, time stability of soil water storage also depends on initial soil water condition or the 'state'. The distinction between the 'wet' and 'dry' periods or the preferred states in soil water pattern has already been made (Kachanoski and de Jong, 1988; Grayson et al., 1997; Western and Blöschl, 1999). Martínez-Fernández and Ceballos (2003) reported increased time stability under recharge condition or 'wet' state and lowest under 'dry' state. The change in controlling factors with initial soil water condition has also been reported (Famiglietti et al., 1998). Grayson et al. (1997) separated the factors into 'local' and 'nonlocal' factors. The factors that vary locally (e.g. soil properties, micro-topography) are dominant in dry conditions (evapotranspiration > precipitation), while the factors that vary non-locally (e.g. drainage line due to catchment topography) are dominant in wet conditions (evapotranspiration < precipitation). High degree of spatial organization during 'wet' period was observed by Western and Blöschl (1999). Famiglietti et al. (1998) reported higher influence of porosity and hydraulic conductivity in wet conditions and elevation, aspect and clay content in dry condition. Various authors have reported high time stability associated with dry condition (Robinson and Dean, 1993), while others (Van Wesenbeeck, 1988; Zhang and Berndtsson, 1988; Gómez-Plaza et al., 2000; Qui et al., 2001; Hupet and Vanclooster, 2002) reported wet condition.

2.6 Issues with Time Stability of Spatial Pattern

The high degree of spatial variability is generally evolved from the combined action of soil physical, chemical and biological processes, which operates in different intensities and at different scales (Goovaerts, 1998; Entin et al., 2000). The scaling heterogeneity of factors makes the soil water storage highly scale dependent. For example, at small catchment and hill slope scale, factors like water routing processes (Dunne and Black, 1970; Beven and Kirkby, 1979; Moore et al., 1988a), differential radiation effects (Moore et al., 1993; Western et al., 1999), heterogeneity in soil (Hu et al., 1997; Famiglietti et al., 1998; Seyfried, 1998) and vegetation (Qui et al., 2001; Hupet and Vanclooster, 2002) affect soil water storage patterns on and within the landscape. Excess water at a particular location is observed to be important for runoff producing processes in many catchments (Dunne and Black, 1970; Anderson and Burt, 1978), which yields a systematic organization of soil water mainly associated with topographic convergence (Dunne et al., 1975; Anderson and Kneale, 1982; Moore et al., 1988a; Barling et al., 1994). In contrast, atmospheric, geologic, and climatic variability determine the organization of soil water over large area (Seyfried, 1998; Entin et al., 2000; Houser, 2000; Brocca et al., 2007; Schneider et al., 2008). The contribution of infiltration, runoff, and lateral redistribution of soil water make small-scale variability of utmost interest in hydrological studies at small and medium catchment or watershed.

The spatial scales of different factors and processes can be represented as the frequency components in the spatial series of soil water storage. Some processes vary frequently in space and are represented by high frequency components (small-scale processes), while others vary slowly and represented by low frequency components (large-scale processes) (Si, 2003). If the contribution of high frequency components to the total variation is different from that of low frequency components, soil water storage become highly variable with scale (Kachanoski and de Jong, 1988; Gómez-Plaza et al., 2000; Kim and Barros, 2002). The similarity in the scales of the spatial pattern of soil water storage over time was examined by Kachanoski and de Jong (1988), who termed the phenomena ‘temporal persistence’. The authors used spatial coherency analysis to examine the similarity in the scales of spatial patterns in soil water storage. The spatial coherency analysis is based on the spectral analysis (Jenkins and Watts, 1968; Kachanoski and de Jong, 1988), which approximates the spatial data series by a sum of sine and cosine functions.

Each function has an amplitude and a frequency or period. While the squared amplitude represents the variance contribution, the frequency component can be used to represent the spatial scale of ongoing processes (Webster, 1977; Shumway and Stoffer, 2000; Brillinger, 2001).

Sometimes, the spatial trend in the controlling factors can create gradually varying spatial pattern of soil water storage over distance. For example, the gradual effects of topography, lithology, parent material, climate, and vegetation (Van Wambeke and Dulal, 1978) can create a spatial trend is soil water storage. Therefore, the statistical parameters (mean and variance) of a spatial process may change with distance. This means that if we divide the spatial series into several segments, the mean and variance of a segment will be different from that of another. The non-uniform spatial mean(s) and/or variance(s) make a spatial series nonstationary. The nonstationarity in the spatial pattern of soil water storage has been reported by Kachanoski and de Jong (1988). Nonstationarity restricts the use of spectral analysis, which is based on the assumption of second order stationarity (i.e. the mean and the variance of the series are finite and constant). Wavelet analysis, an advanced mathematical technique, decomposes overall variations in a spatial series into different scales and locations and thus deals with nonstationarity. The similarity between two spatial series at different scales and locations can examined using wavelet coherency. Wavelet coherency has been used in soil science to examine the scale and location specific similarities between two soil properties (Si and Zeleke, 2005; Yates et al., 2007; Biswas et al., 2008). A review on the application of wavelet transform and wavelet coherency in soil science is added in the Appendix C. However, there is no information available on the similarity of the spatial pattern of nonstationary soil water storage. In this dissertation, wavelet coherency analysis has been used to examine the similarities between two nonstationary soil water series.

In addition, the effects from different processes controlling soil water storage as represented by the frequency components are non-additive and do not follow the principle of superposition (Yan and Gao, 2007) indicating the system to be nonlinear. For a linear system with input x and output y, the response to the sum of two inputs x_1 and x_2 equals the sum of the response to each input taken individually: $L(x_1 + x_2) = L(x_1) + L(x_2)$. Further, a linear system can be scaled by the magnitude (α) of the input x, where α is a scalar: $L(\alpha x) = \alpha L(x)$. Thus, a linear system follows the principle of superposition: $L(\alpha x_1 + \beta x_2) = \alpha L(x_1) + \beta L(x_2)$, where, β is

the magnitude of input x_2. However, in a nonlinear system, the target variables cannot be written as a linear sum of independent components of controlling factors or processes (Pai and Palazotto, 2008). For example, the response of soil water storage to *n* factors (x_i, i =1, 2, … , *n*) cannot be obtained by simply observing the response to one factor at a time and subsequently adding the individual observational results together. Therefore, the combined response, $S(x_1 + x_2 + \ldots + x_n)$, to the processes such as elevation, soil texture, … (x_1, x_2, … , x_n), will not be equal to the sum of individual response, $S(x_1) + S(x_2) + \ldots + S(x_n)$. This may be due to the change in the scale of processes with distance or location as represented by the oscillations that restricts the linear summation. Therefore, a nonlinear series was defined using the concept of sub- and super-cyclic variations in frequency (Huang et al., 1998; Kijewski-Correa and Kareem, 2006). The sub-cyclic variations are the change in frequency or scale that occurs within a single cycle of oscillations and the super-cyclic variations occur over the course of one or more cycle of oscillations present in the series. Therefore, the scale or frequency of a nonlinear spatial series will be locally unpredictable (Gautama et al., 2004) and therefore it is difficult to characterize variations in soil water storage. More often than not, soil water storage can be nonstationary and nonlinear together, which requires new method to characterize the variations in soil water storage. Hilbert-Huang transform is a relatively new method for time series analysis and can deal with nonstationarity and nonlinearity simultaneously. The method can be extended to examine the variations in spatial series.

Different characteristics of the spatial variability of soil water storage and its time stability needs to be taken care of in understanding the soil water distribution within landscape. The following results section deals with various characteristics of time stability of soil water storage spatial pattern in the hummocky regions of the PPR of North America.

3.0 SEASON AND DEPTH DEPENDENT TIME STABILITY AND BENCHMARKING OF SOIL WATER STORAGE IN A HUMMOCKY LANDSCAPE

3.1 Preface

In spite of high spatio-temporal variability, if a field is repeatedly surveyed for soil water content, some sites or points are consistently wetter or consistently drier than the field average. The similarity of the spatial pattern over time is termed as time stability, which can be used to determine the sampling strategy, define management units, and provide insight on risk assessment. There are contradictory statements about the dependence of time stability with different soil water content and depths from around the world. Is time stability the same at different seasons in the hummocky landscape of semi-arid Prairie pothole region? Is it the same at different layers of soil? The soil water content measured along a transect at the St. Denis National Wildlife Area over a four-year period is an excellent opportunity to explore the data at its basic level and fill in the knowledge gap.

3.2 Introduction

Soil water is the principal limiting factor in semi-arid agricultural production and a key element in environmental health. It is a key variable for describing many hydrological and climatic processes such as the partition of rainfall and snowmelt water into infiltration and runoff (Bronstert and Bárdossy, 1999; Raats, 2001; Wilson et al., 2004; Vereecken et al., 2007) or the distribution of mass and energy between soil and first layer of atmosphere (Famiglietti and Wood, 1994; Crow and Wood, 2002). Knowledge of soil water patterns over large areas is a prerequisite for better understanding evapotranspiration and runoff (Famiglietti and Wood, 1995), atmospheric variability (Delworth and Manabe, 1993), as well as improving hydrologic and climatic modelling (Western et al., 2002). However, understanding these processes is a major challenge in hydrology (Quinn, 2004) because the distribution of soil water is controlled by several factors and processes including soil properties, topography, vegetation, climatic processes, ground water, and water routing processes (Western and Blöschl, 1999; Gómez-Plaza et al., 2001; Tallon and Si, 2004). Moreover, the effect (individual or combined) of these factors and processes yield large spatio-temporal heterogeneity of soil water distribution in a field (Bell

et al., 1980; Munoz-Pardo et al., 1990; Seyfried, 1998; Gómez-Plaza et al., 2000; Lin et al., 2006; Brocca et al., 2009, 2010) thus making it challenging to measure the soil water over large areas.

A conventional way of determining soil water in a field is by measuring a number of randomly selected locations and averaging them over the field. The larger the number of samples measured, the more accurate the estimated average soil water. However, conventional sampling assumes that soil water content is randomly distributed in a field. Therefore, numerous samples are required to account for spatial variability and to obtain a desired level of accuracy and precision in soil water measurement. Fortunately, the factors controlling soil water exhibit non-random patterns in a field and the existing spatial patterns influence soil water fluxes giving rise to patterns in soil water and its storage (Kachanoski and de Jong, 1988; Grayson and Western, 1998). The similarity of this pattern over time was first analysed by Vachaud et al. (1985). They introduced this concept as 'time stability', which is defined as a time invariant association between spatial location and classical statistical measures of soil water, most often the mean (Grayson and Western, 1998). A large body of literature has used this concept to explain the temporal dynamics of soil water over a range of investigated areas (from few m^2 to 10^9 m^2), sampling schemes (random, grid, transect), sampling depths (5 cm to ~2 m), investigation periods (from few days to years), and land uses at different parts of the world. Time stability research has found that certain locations maintain their rank and consistently showed higher water content than others irrespective of dry or wet condition. Therefore, there will be a location that closely represents the field averaged soil water. Hence, the relative difference between the average soil water of that location and the field will be close to zero and the location can be used to represent the field averaged soil water at any time. The location is described as the benchmark location, which is time invariant. Grayson and Western (1998) identified this time stable location as catchment average soil moisture monitoring (CASMM) site. Identifying the benchmark location with field averaged soil water would greatly reduce the number of samples or observations needed to characterize a field.

In identifying the time stable benchmark location, the mean relative difference (MRD) and the standard deviation of the relative difference (SDRD) have been introduced by Vachaud et al. (1985). Various other indices have also been used to identify the time stable location. For

example, Jacobs et al. (2004) introduced root mean squared error (RMSE) of the relative difference and associated variance to identify the most time stable location. Guber et al. (2008) computed a new time stability index, T_{ik} on the width of 90% empirical tolerance interval of empirical probability distribution functions of relative soil water content (Guber et al., 2008) and used the root mean squared difference, D_{ik} to select the best locations. Hu et al. (2009, 2010a, 2010b) have reported mean absolute biased error (MABE) to identify time stable locations. However, the most widely accepted and used index is the SDRD and will be used in this study. Grayson and Western (1998) identified the location of time stable sites or 'best' sites with respect to transect average soil water in areas that were neither convergent nor divergent. These locations tended to be located near the mid-slopes or in areas that had topographic aspects close to the average and were identified as the 'aspect neutral' part of the transect. Jacobs et al. (2004) and Vivoni et al. (2008) also documented that the locations that consistently maintained time stability were located at mid slopes or mid-elevation, respectively.

Most of the efforts in identifying the time stable locations have focussed on the surface soil water (Vachaud et al., 1985; Grayson and Western, 1998; Mohanty and Skaggs, 2001; Cosh et al., 2004; Brocca et al., 2009) and few were directed to deeper soil profile (Martínez-Fernández and Ceballos, 2005; Pachepsky et al., 2005; De Lannoy et al., 2007; Hu et al., 2009, 2010a). Fewer studies have explored the changes in time stability with depth (Hupet and Vanclooster, 2002; Martínez-Fernández and Ceballos, 2003). To the best of our knowledge, there is no information on the time stability of the classified surface layer, root zone and total active soil profile. The surface layer is the soil management zone and is subject to climate forcing, the root zone is where the majority of plant roots are located and exhibits strong variability over time, and the total active soil profile is the zone below which seasonal changes are suppressed. The dominant processes operating at different layers of soil determine the hydrology of soil layers. For example, less root activity in deeper horizons created stronger time stability compared to surface layers (Cassel et al., 2000). Similarly, Comegna and Basile (1994) found a better time stable spatial structure in the top 90 cm of a volcanic Visuvian sandy soil profile of large heterogeneity in terms of physical properties. However, Martínez-Fernández and Ceballos (2003) did not observe any specific pattern of stability with respect to depth. Therefore,

knowledge of time stability at different layers of soil at different depths is necessary to understand the soil water dynamics better.

Researchers have made a distinction between wet and dry periods, or preferred states, in soil water patterns (Kachanoski and de Jong, 1988; Grayson et al., 1997; Western and Blöschl, 1999). Grayson et al. (1997) separated the factors in 'local' (e.g. soil properties and micro-topography) and 'nonlocal' factors (e.g., drainage lines due to catchment topography). The local controls dominate in dry conditions (evapotranspiration > precipitation), while nonlocal controls dominate in wet conditions (evapotranspiration < precipitation). Western and Blöschl (1999) and Western et al. (1999) reported high degrees of time stable spatial patterns during wet periods, while Martínez-Fernández and Ceballos (2003) found better stability during dry periods. Certain authors (Robinson and Dean, 1993; Famiglietti et al., 1998) have reported strong time stability in dry condition while others (Van Wesenbeeck et al., 1988; Zhang and Berndtsson, 1988; Gómez-Plaza et al., 2000; Qui et al., 2001; Hupet and Vanclooster, 2002) report them for wet conditions. Ultimately, there is no comprehensive information about how time stability persists within a season (intra-season) with similar moisture conditions, between seasons (inter-season) with different moisture condition, and between the same seasons of different years (inter-annual) with similar moisture conditions.

Time stability has been studied in different landscape conditions with varying slopes (0 to ~ 40 %). A comprehensive review of different study conditions were presented in a table by Brocca et al. (2009). Few studies have been carried out in rolling landscape and even fewer were completed in a hummocky landscape (Kachanoski and de Jong, 1988; Tallon and Si, 2004), which is a unique landscape with complex sequences of knolls and depressions. The depressions were formed during the last glacial retreat as also known as prairie potholes and the area is known as the prairie pothole region (PPR). The hydrology of the hummocky landscape in the PPR is also unique, as depressions generally have no permanent inlet or outlet and work as a micro-watershed (Brinson, 1993; Parsons et al., 2004). The PPR covers more than 775,000 km^2 of area in the Canadian Prairie region and provides various hydrological and ecological functions (National Wetlands Working Group, 1997). The area is known as the 'duck factory' of North America as the depressions provide 50 – 80% of nesting habitat for North America waterfowl population (LaBaugh et al., 1998). It acts as sink for agriculture-derived nutrients (Whigham and

Jordan, 2003) and storehouse of surface water, which can attenuate flood flows (Gleason and Tangen, 2008). Hence, in understanding the hydrology of this landscape, better information is necessary on the spatial pattern of soil water storage and its stability over time at different seasons and depths. Therefore, the objectives of this study were to a) examine the time stability of spatial patterns in soil water storage at different seasons and depths and b) identify the time stable location with field averaged soil water storage (benchmark location) in a hummocky landscape in semiarid climate.

3.3 Theory

In identifying benchmark locations, time stability analysis was performed following the method introduced by Vachaud et al. (1985). Briefly, if the soil water storage at i^{th} location and t^{th} date is $\theta_{i,t}$ and the mean water content is $\overline{\theta}_t$ at the same time, the difference (Δ) between individual determinations is

$$\Delta_{i,t} = \theta_{i,t} - \overline{\theta}_t \qquad [3.1]$$

The mean water content was calculated from

$$\overline{\theta}_t = \left(\frac{1}{n}\right)\sum_{i=1}^{n}\theta_{i,t} \qquad [3.2]$$

where n is the number of measurement locations (for this study n = 128). Then the relative difference, $\delta_{i,t}$ was calculated as

$$\delta_{i,t} = \frac{\Delta_{i,t}}{\overline{\theta}_t} \qquad [3.3]$$

The mean relative difference (MRD) was calculated as

$$\overline{\delta}_i = \frac{1}{m}\sum_{t=1}^{m}\delta_{i,t} \qquad [3.4]$$

where m is the number of sampling days (for this study, m = 20). SDRD, the standard deviation $\sigma(\delta_i)$ of relative differences ($\delta_{i,t}$) from the mean relative differences ($\overline{\delta}_i$) was calculated as

$$\sigma(\delta_i) = \sqrt{\frac{\sum\left(\delta_{i,t} - \overline{\delta}_i\right)^2}{m-1}} \qquad [3.5]$$

A location is considered as the benchmark location if its MRD is near zero with low SDRD. A large SDRD is an indication that the soil water storage at that location is not linearly related to the field average and therefore a poor predictor (Cosh et al., 2008).

The similarities of the spatial pattern of the soil water storage during different measurements were examined using Spearman rank correlation coefficients. Let, $R_{i,t}$ be the rank of variable $\theta_{i,t}$ at i^{th} location and t^{th} date and $R_{i,t'}$ the rank of identical variable at the same location but at different time t'. The Spearman's rank correlation coefficients were calculated as

$$r_s = 1 - \frac{6 \cdot \sum_{i=1}^{n} (R_{i,t} - R_{i,t'})^2}{n(n^2 - 1)} \qquad [3.6]$$

where n is the number of observations. A value of r_s =1 corresponded to identity of rank for any location, i.e., perfect time stability between dates t and t'. The closer r_s was to 1, the more stable the process was at that specific location (Vachaud et al., 1985).

3.4 Materials and Methods

3.4.1 Site Description

A sampling transect in the north-south direction was established at St. Denis National Wildlife Area (SDNWA) (52°12′ N latitude, 106°50′ W longitude), which is located approximately 40 km east of Saskatoon, Saskatchewan, Canada (Figure 3.1). The landscape of this area contains a very complex sequence of slopes originating from different sized rounded depressions to irregular complex knolls and knobs (Pennock, 2005), making the terrain hummocky with 10 to 15% slopes (Figure 3.1). Soils of this area are Dark Brown Chernozem (Mollisol in American system of soil classification) developed from moderately fine to fine textured, moderately calcareous, glacio-lacustrine deposits and modified glacial till (Saskatchewan Centre for Soil Research, 1989). The climate of this area is mainly semiarid with mean annual air temperature (at the Saskatoon airport) of 2°C with a monthly mean of -19°C in January and 18°C in July (AES, 1997). Snow generally covers the area for five to six months (November to April) and contributes approximately 30% of the total precipitation (Pomeroy et al., 2007). The 90-year mean annual precipitation in Saskatoon is 360 mm, of which 84 mm occurs in winter, mostly as snow (AES, 1997). The total precipitation of the area during the years

of 2006, 2007, 2008 and 2009 was 489 mm, 366 mm, 331 mm, and 402 mm, respectively (Figure 3.2; Environment Canada, 2010).

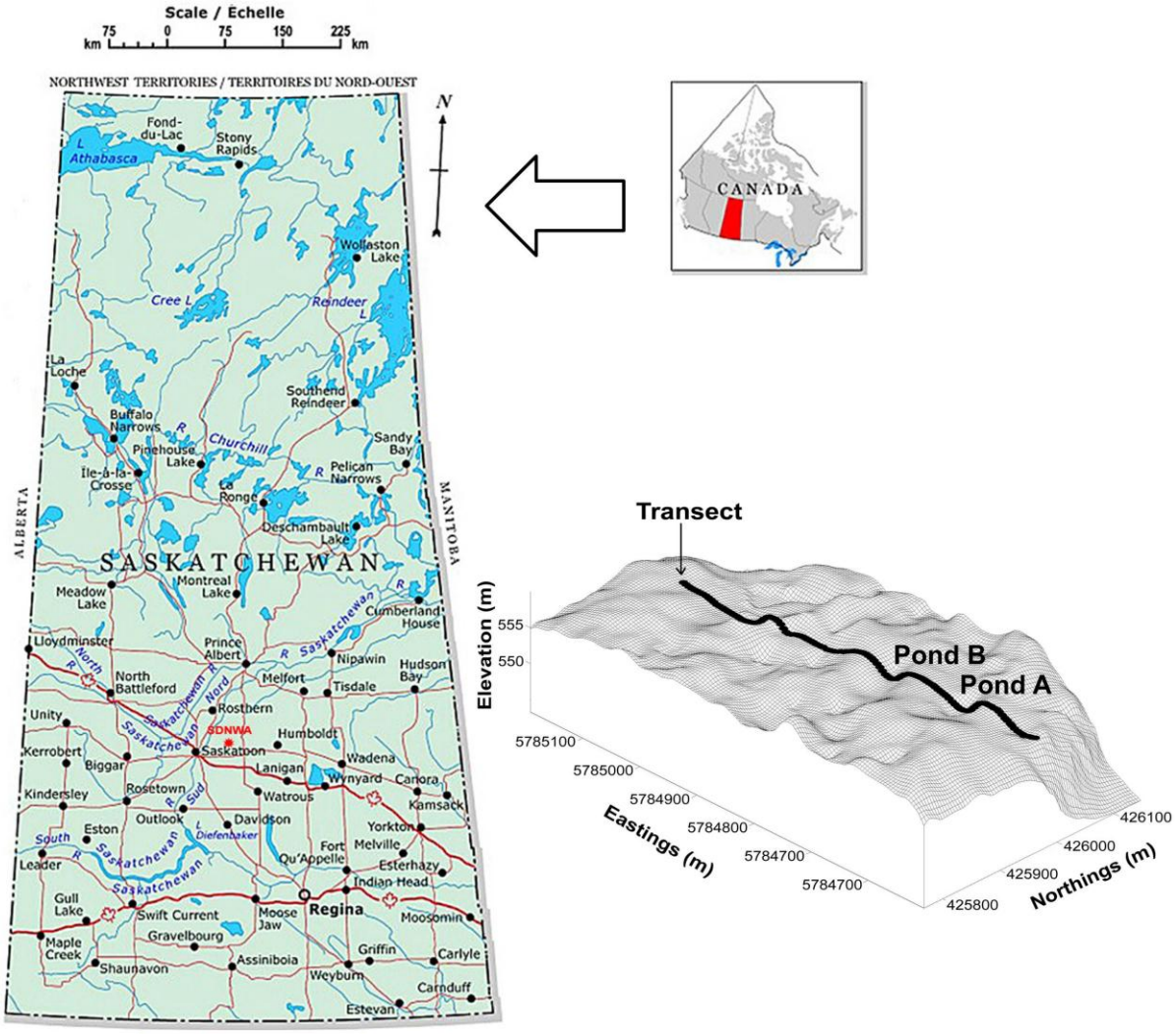

Figure 3.1. Geographic location of study site and the transect position on the hummocky landscape at St. Denis National Wildlife Area (SDNWA), Saskatchewan, Canada (Natural Resources Canada, 2001).

3.4.2 Data Collection

A 576 m transect with 128 equally spaced (4.5 m) points was established over several rounded knolls and seasonal depressions representing different landform cycles (Figure 3.1). Detailed information about the study site can be found at Yates et al. (2006a). Briefly, a topographic survey of this site was completed using Light Detection and Ranging (LiDAR)

survey of the study area at 5 m resolution. The vegetation of the site is mixed grass seeded in 2004 and allowed to grow every year. Each sample location was instrumented with 5 cm diameter and 200 cm long plastic (polyvinyl chloride; PVC) tubes using a truck-mounted hydraulic press. The open ends of the PVC tubes were kept closed with caps to prevent water entry from the top.

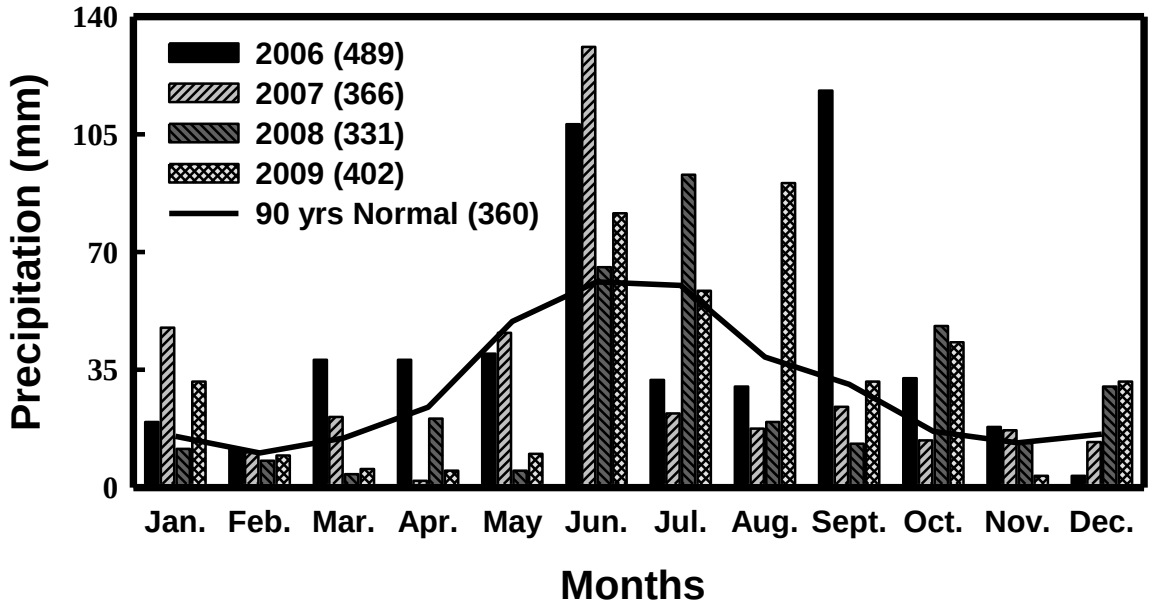

Figure 3.2. Monthly precipitation data for the years of 2006, 2007, 2008, and 2009 and 90 years average from Saskatoon International Airport (40 km west of study site)

These tubes were used as access tubes in measuring soil water by neutron probe in the field. A CPN 501 DR Depthprobe (CPN International Inc., Martinez, CA, USA) was used to measure the soil water every 20 cm from 20 cm to 140 cm. For calibration of the neutron probe, soil cores adjacent to access tubes were collected using a truck-mounted hydraulic press. The neutron count was recorded at each 10 cm depth interval using neutron probe in addition to the standard neutron count. The soil cores were immediately wrapped with plastic film to prevent water loss and subsequently transported to the laboratory. Volumetric water content of each 10 cm segment of soil core was determined using the gravimetric method and bulk density. The above procedure was repeated several times at different moisture conditions over three years (2007 – 2009) at different topographic locations. Volumetric soil water was compared with the neutron count ratio (neutron count / standard neutron count) and a final calibration equation was developed (Figure

3.3). The average soil water of the top 0 - 20 cm was measured using a vertically installed time domain reflectometry (TDR) probe and a metallic cable tester (Model 1502B, Tektronix, Beaverton, OR, USA). A standard calibration equation for TDR following Topp and Reynolds (1998) was used to calculate the soil water of surface soil.

Soil water was measured in the field 20 times over a four-year period (17 July 2007, 7 August 2007, 1 September 2007, 12 October 2007, 2 May 2008, 31 May 2008, 21 June 2008, 16 July 2008, 23 August 2008, 17 September 2008, 22 October 2008, 20 April 2009, 7 May 2009, 27 May 2009, 21 July 2009, 27 August 2009, 27 October 2009, 6 April 2010, 19 May 2010 and 14 June 2010). The soil water storage was calculated by multiplying the depth interval with water content calculated from the calibration relationships. Measured soil water storage was classified as surface layer water storage (0 - 20 cm depth), root zone water storage (0 - 60 cm depth) and total active soil profile water storage (0 - 120 cm depth).

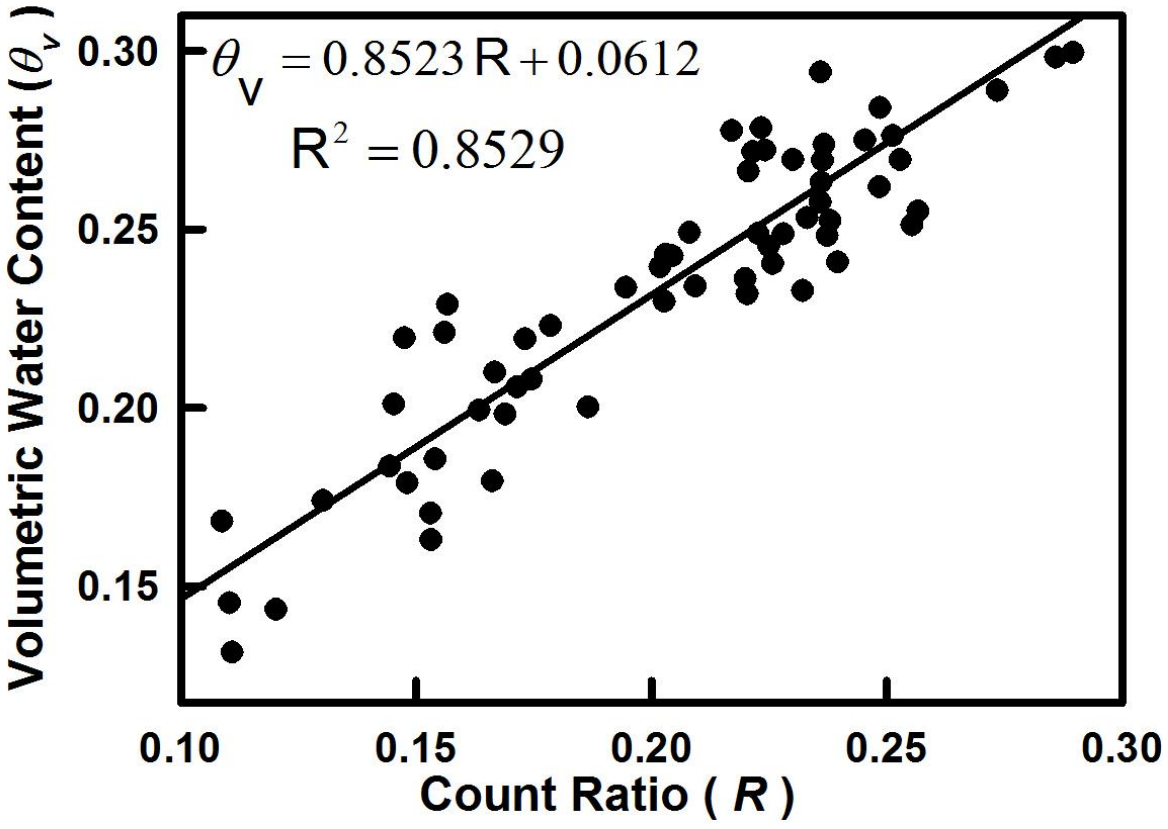

Figure 3.3. Site specific Neutron Moisture Meter calibration with the regression equation used for soil water calculation.

3.5 Results and Discussion

3.5.1 Soil Water Storage Spatial Pattern

The spatial distribution of soil water storage with field average in the surface layer for selected dates is presented in Figure 3.4. Note that the relative elevation is at the top. The average soil water storage in the surface layer over the entire measurement period was 5.25 cm. Soil water storage at 100 to 140 m (Pond A in Figure 3.1) and 225 to 250 m (Pond B in Figure 3.1) from the origin of the transect, which were located within depressions, were very high compared to other locations during the spring and the early part of the summer seasons (Figure 3.4). Generally the strong wind in the Prairie region redistributes snow in the landscape and within the depressions (Pomeroy and Gray, 1995; Elliot and Efetha, 1999; Fang and Pomeroy, 2007), which store more snow compared to surrounding uplands (Williams et al., 2008; Lungal, 2009). In addition, during early spring the frozen soil restricts the infiltration capacity (Gray et al., 1985; Winter and Rosenberry, 1995) resulting in redistribution of snowmelt water in the landscape. Depressions receive water from surrounding uplands and maintain a height of standing water (Woo and Rowsell, 1993; Hayashi et al., 1998; Lungal, 2009). In addition, knolls store less water due to drift accumulation in depressions and snowmelt runoff, thus yielding a wide range in soil water storage along the transect. A similar wide range in soil water storage in a non-level landscape was also reported by Flerchinger and Cooley (2000). Therefore, the spatial distribution of soil water storage in the surface layer almost mirrored (high topography low water storage and low topography high water storage) the spatial distribution of elevation during the spring and early part of the summer season (Figure 3.4). A similar spatial pattern was observed in other measurements completed within the spring or early summer.

Prior to vegetation maturity, the only source of water loss from the landscape was the evaporation from the bare field and the surface of standing water bodies and to a lesser extent, the groundwater interaction (Hayashi et al., 1998; van der Kamp et al., 2003). The loss of water through deep drainage in the hummocky landscape is as low as ~1 to 8% of the water lost annually (Hayashi et al., 1998) or 2 to 40 mm per year, the majority of which occurs through fractures and preferential flow paths (van der Kamp and Hayashi, 1998). Therefore, the main vector for water loss is evapotranspiration by growing vegetation. The large amount of water stored in the depression allowed the lush growth of grasses (particularly the aquatic species

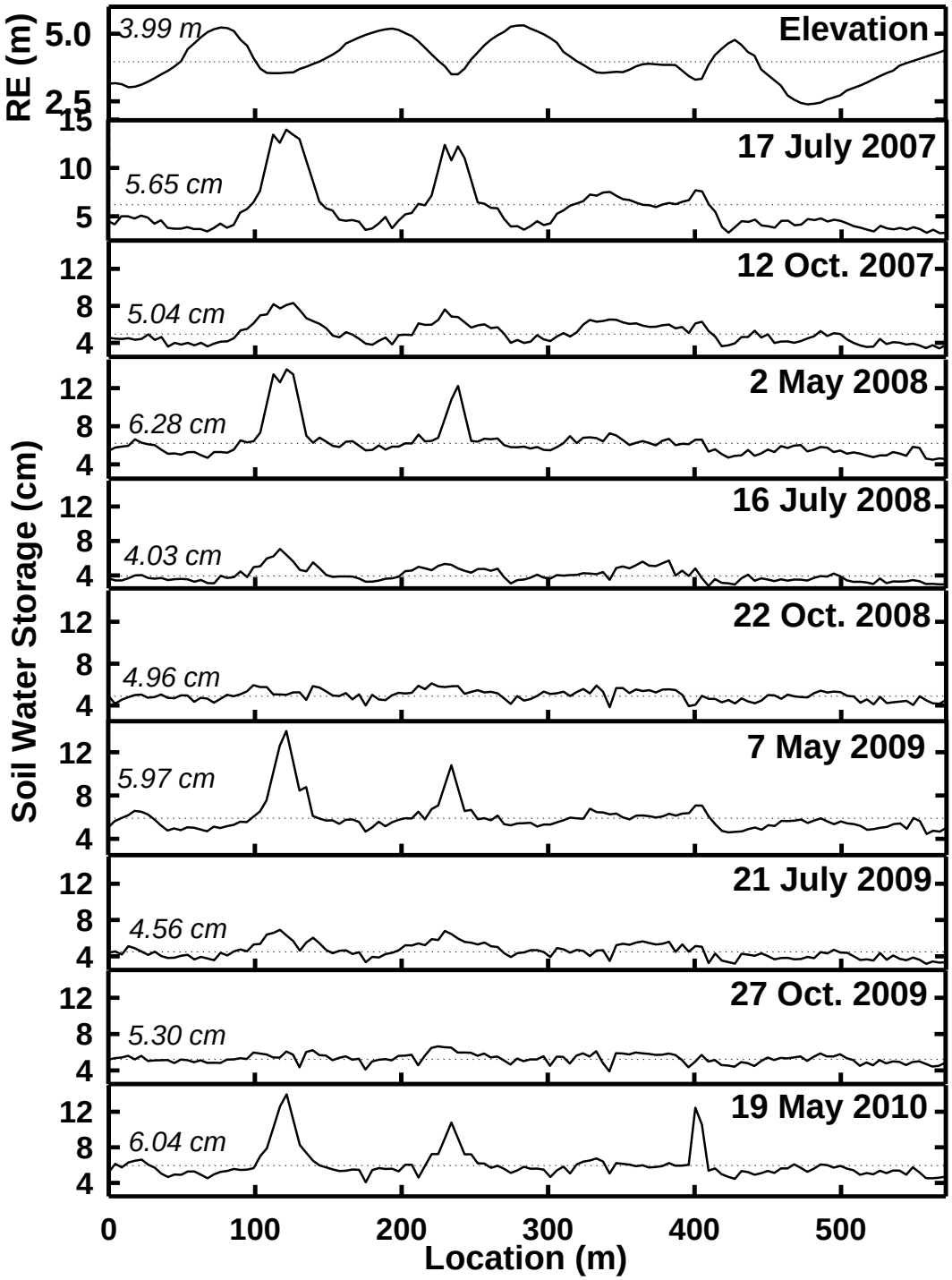

Figure 3.4. Spatial distribution of soil water storage for selected measurements at tillage layer (0 - 20 cm) along the transect over four years with the relative elevation at top. X-axis indicates distance along the transect (m); Y-axis indicates soil water storage (cm); RE indicates relative elevation (m); dotted line indicates average soil water storage of each date with the average value in *italics*.

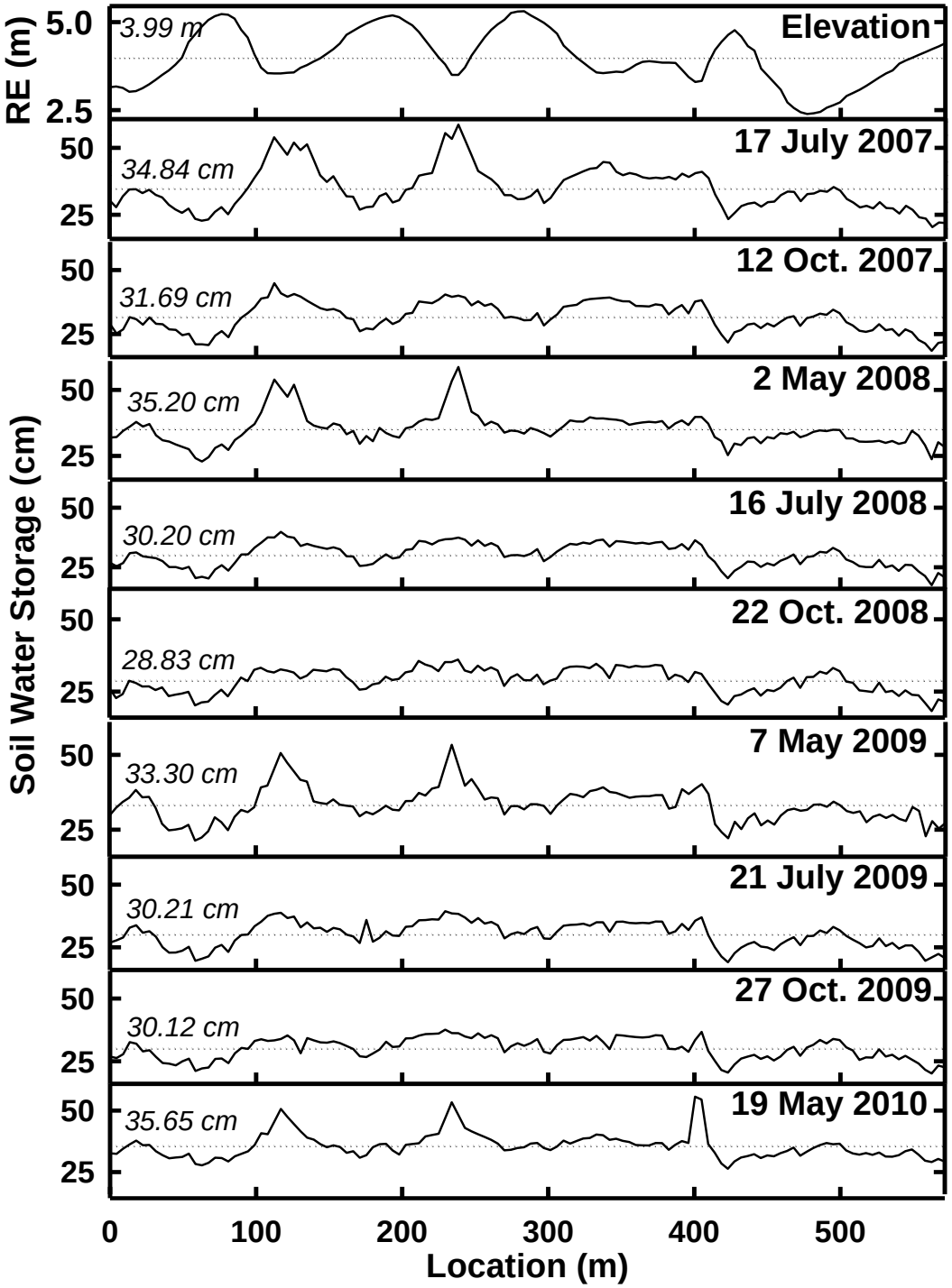

Figure 3.5. Spatial distribution of soil water storage for selected measurements at active root zone (0 - 120 cm) along the transect over four years with the relative elevation at top. X-axis indicates distance along the transect (m); Y-axis indicates soil water storage (cm); RE indicates relative elevation (m); dotted line indicates average soil water storage of each date with the average value in *italics.*

growing over 2 m in height in later summer), whereas, the small amount of water stored on knolls restricted plant growth and evapotranspiration. The high evapotranspiration of grass covers in depressions and low evapotranspiration on knolls during the summer and fall reduced the difference between the water content on the knolls and in the depressions. This variable water uptake weakened the topography-induced spatial pattern during the later summer and fall or in dry periods indicating a seasonal dependence of spatial pattern in the surface layer (Figure 3.4). Tallon and Si (2004) also reported a similar spatial pattern in soil water with elevation during a very dry year from a similar type of landscape. Though it changed over time within a year, the spatial pattern of a particular season was similar from one year to the next. For example, the spatial distribution during spring 2008 (2 May) was very similar to the spatial distribution during spring 2009 (7 May) and spring 2010 (19 May) (Figure 3.4). A similar trend in the spatial pattern was observed in other seasons of measurement (summer and fall). This may be because the hydrology of the study site is dominated by the distribution of snow (Gray et al., 1985; Pomeroy and Gray, 1995; Fang and Pomeroy, 2007) as the snowmelt water determines the spring spatial pattern in soil water storage. Therefore, in every spring, a similar pattern in soil water storage is demonstrated and later modified by the vegetation as the growing season progresses.

The average water storage over four years in the root zone and total active soil profile were 15.75 and 32.14 cm, respectively. The spatial patterns of water storage in the root zone and the total active soil profile were similar to the spatial pattern at the surface layer and thus mirrored the spatial pattern in elevation. Figure 3.5 shows the spatial distribution of soil water storage with field average in the total active soil profile for selected measurements. Unlike the surface layer, the pattern in root zone and total active soil profile persisted even in later summer and fall. The reason was that plants generally take up more than 70% of the water they need from the top 50% of the root zone (Feddes et al., 1978; Morris, 2006). Besides the intense root activity in the surface layer (Cassel et al., 2000), the more disturbed soil structure (Guber et al., 2003; Pachepsky et al., 2005) and the exposure to solar radiation, wind, and rainfall (Hu et al., 2010a) make the surface layer more dynamic. The dynamic behaviour of the surface layer exhausted the readily available water and equalized stored water over the transect during the latter part of the year. Therefore, the topographically induced spatial pattern was destroyed, while there were still patterns in the root zone and total active soil profile due to topography.

3.5.2 Time Stability of the Spatial Pattern

The similarity in the spatial pattern over time was examined using Spearman's rank correlation analysis. Table 3.1 showed the rank correlation coefficients between the measurement series for the surface layer. All the rank correlation coefficients were significant at $p < 0.0001$. The high rank correlation coefficient between measurement series indicated that a large number of measurement locations maintained their spatial ranks over time. In other words, the locations with high water storage relative to the field average at one location in any time maintained the high water storage relative to the field average in other times and vice versa. The greater the number of measurement locations that maintain the rank, more similar the spatial pattern is. The high rank correlation coefficients between the measurement series during 2007 clearly indicated the strong similarity in the spatial pattern of soil water storage. The correlation coefficients were comparable or larger than those reported elsewhere by Martínez-Fernández and Ceballos (2003), Mohanty and Skaggs (2001), Hu et al. (2009) and many others.

The time stability of the spatial pattern was observed throughout the measurement period. However, the degree of similarity changed over time as indicated by the magnitude of the rank correlations. Two measurement series during the early part of 2008 showed a strong correlation, as did the measurement series during the latter part of 2008 (intra-season) (Table 3.1). For example, the correlation coefficient was 0.96 between 31 May 2008 and 21 June 2008 (measurements from early part of 2008) and was 0.97 between 23 August 2008 and 17 September 2008 (measurements from latter part of 2008) (Table 3.1). Therefore, there was strong intra-season time stability. However, the change in the intensity of processes controlling soil water storage from one season to another might yield a weaker inter-season time stability compared to the intra-season time stability. The correlation coefficients between a measurement series of early 2008 and a measurement series of late 2008 were relatively low. This may be because similar processes are operating within a season and may have similar effects on soil water storage (Martínez-Fernández and Ceballos, 2003). For example, while evaporation is the dominant process of water loss during the spring and early summer, the strong transpirative demand of growing vegetation adds up during the later summer and fall and determines the soil water storage in the semi-arid climate (Miller, 1971; Parsons et al., 2004). Furthermore, the time stability depended on the time difference between the two measurements series as the effect of

Table 3.1: Spearman's rank correlation coefficients between the soil water storage measurements over three years in the surface layer.

	17 July 2007	7 Aug. 2007	1 Sept. 2007	12 Oct. 2007	2 May 2008	31 May 2008	21 June 2008	16 July 2008	23 Aug. 2008	17 Sept. 2008	22 Oct. 2008	20 April 2009	7 May 2009	27 May 2009	21 July 2009	27 Aug. 2009	27 Oct. 2009	6 April 2010	19 May 2010	14 June 2010
17 July 2007	1.00	0.95	0.95	0.95	0.88	0.89	0.87	0.84	0.66	0.64	0.64	0.81	0.88	0.86	0.81	0.75	0.65	0.57	0.80	0.86
7 Aug. 2007		1.00	0.94	0.94	0.83	0.83	0.81	0.83	0.69	0.68	0.67	0.73	0.82	0.79	0.77	0.72	0.65	0.48	0.74	0.81
1 Sept. 2007			1.00	0.98	0.85	0.87	0.86	0.85	0.68	0.66	0.67	0.75	0.84	0.83	0.83	0.77	0.67	0.48	0.77	0.82
12 Oct. 2007				1.00	0.85	0.87	0.87	0.87	0.70	0.68	0.68	0.75	0.82	0.81	0.82	0.76	0.66	0.48	0.76	0.82
2 May 2008					1.00	0.91	0.87	0.83	0.65	0.65	0.63	0.84	0.91	0.89	0.79	0.76	0.63	0.59	0.80	0.81
31 May 2008						1.00	0.96	0.89	0.69	0.66	0.68	0.80	0.88	0.94	0.85	0.82	0.68	0.59	0.83	0.81
21 June 2008							1.00	0.95	0.76	0.73	0.72	0.70	0.79	0.87	0.91	0.84	0.68	0.52	0.77	0.76
16 July 2008								1.00	0.87	0.83	0.77	0.67	0.76	0.83	0.93	0.86	0.72	0.48	0.74	0.74
23 Aug. 2008									1.00	0.97	0.82	0.48	0.57	0.64	0.80	0.79	0.71	0.29	0.56	0.57
17 Sept. 2008										1.00	0.83	0.46	0.56	0.61	0.77	0.76	0.70	0.27	0.54	0.56
22 Oct. 2008											1.00	0.49	0.58	0.64	0.73	0.76	0.78	0.34	0.57	0.58
20 April 2009												1.00	0.94	0.89	0.69	0.68	0.57	0.73	0.81	0.82
7 May 2009													1.00	0.93	0.75	0.76	0.64	0.69	0.86	0.89
27 May 2009														1.00	0.84	0.84	0.69	0.65	0.88	0.84
21 July 2009															1.00	0.92	0.76	0.51	0.78	0.74
27 Aug. 2009																1.00	0.87	0.47	0.81	0.75
27 Oct. 2009																	1.00	0.39	0.75	0.71
6 April 2010																		1.00	0.63	0.60
19 May 2010																			1.00	0.92
14 June 2010																				1.00

controlling processes may change gradually. For example, the correlation coefficient was 0.91 between 2 May 2008 and 31 May 2008, which gradually decreased to 0.63 between 2 May 2008 and 22 October 2008. The evapotranspirative demand of developing vegetation over time may change the soil water storage gradually. Therefore, the highest rank correlation coefficient was observed between the measurements taken close in time and gradually decreased with time. Similar trends in the rank correlation coefficients and thus the inter-season and intra-season time stability was observed in other years of measurements.

Strong correlation was also observed between the measurements from a particular season in one year and the measurements from the same season of other years (inter-annual time stability). For example, the correlation coefficient was 0.91 between 2 May 2008 and 7 May 2009. Similar high correlation was also observed between the measurements from spring, summer or fall of different years. This is because every year the redistribution of snow in winter and snowmelt water during spring creates a spatial pattern in soil water storage. The spatial pattern gradually changes with time with the development of vegetation. In later summer and fall, rainfall cannot meet the demand and the stored water in soil is utilized by plants. The more water that is stored in the soil, the better the plant growth and in turn, the more water from soil is utilized. Therefore, the spatial patterns established in the spring due to topography is weakened or diminished by vegetation in the surface layer.

The spatial patterns established in spring were weakened from wet state to dry state. Nevertheless, there was strong time stability of the spatial pattern that existed over the whole period of measurements. These results are in contrast with those of Gómez-Plaza et al. (2000) and Grayson and Western (1998), who found that the field scale or transect scale time stability did not exist as the spatial patterns were not consistent. However, in this study, the high Spearman rank correlation coefficients between measurements indicate strong time stability.

A similar trend in the time stability of the spatial series was also observed in the root zone and total active soil profile. The rank correlation coefficients of soil water storage in the root zone and total active soil profile were presented in Table 3.2 and Table 3.3, respectively. The high rank correlation coefficients (significant at $p < 0.0001$) suggested strong time stability of the spatial pattern of the soil water storage in the root zone and total active soil profile. A similar trend was also observed in intra-season, inter-season and inter-annual time stability.

Table 3.2: Spearman's rank correlation coefficients between the soil water storage measurements over three years in the root zone.

	17 July 2007	7 Aug. 2007	1 Sept. 2007	12 Oct. 2007	2 May 2008	31 May 2008	21 June 2008	16 July 2008	23 Aug. 2008	17 Sept. 2008	22 Oct. 2008	20 April 2009	7 May 2009	27 May 2009	21 July 2009	27 Aug. 2009	27 Oct. 2009	6 April 2010	19 May 2010	14 June 2010
17 July 2007	1.00	0.99	0.98	0.98	0.93	0.96	0.95	0.93	0.82	0.80	0.82	0.83	0.89	0.92	0.92	0.85	0.82	0.81	0.92	0.94
7 Aug. 2007		1.00	0.99	0.99	0.93	0.96	0.96	0.94	0.84	0.81	0.84	0.82	0.89	0.91	0.92	0.86	0.83	0.79	0.91	0.93
1 Sept. 2007			1.00	0.99	0.93	0.96	0.96	0.95	0.84	0.81	0.84	0.82	0.89	0.91	0.92	0.87	0.84	0.79	0.89	0.91
12 Oct. 2007				1.00	0.92	0.96	0.96	0.96	0.85	0.83	0.86	0.82	0.88	0.90	0.93	0.88	0.85	0.79	0.89	0.92
2 May 2008					1.00	0.95	0.92	0.90	0.80	0.77	0.79	0.89	0.94	0.94	0.90	0.84	0.79	0.83	0.91	0.90
31 May 2008						1.00	0.97	0.95	0.83	0.80	0.82	0.87	0.93	0.95	0.93	0.87	0.82	0.81	0.93	0.91
21 June 2008							1.00	0.98	0.87	0.85	0.87	0.83	0.89	0.93	0.96	0.91	0.87	0.82	0.91	0.90
16 July 2008								1.00	0.93	0.90	0.91	0.80	0.87	0.89	0.97	0.93	0.90	0.82	0.88	0.89
23 Aug. 2008									1.00	0.99	0.95	0.70	0.77	0.78	0.89	0.89	0.89	0.75	0.77	0.79
17 Sept. 2008										1.00	0.95	0.69	0.75	0.76	0.87	0.88	0.88	0.74	0.75	0.78
22 Oct. 2008											1.00	0.68	0.75	0.77	0.89	0.89	0.90	0.75	0.76	0.78
20 April 2009												1.00	0.96	0.94	0.83	0.77	0.70	0.87	0.87	0.85
7 May 2009													1.00	0.98	0.89	0.83	0.76	0.85	0.92	0.91
27 May 2009														1.00	0.92	0.86	0.79	0.86	0.94	0.92
21 July 2009															1.00	0.97	0.93	0.86	0.90	0.90
27 Aug. 2009																1.00	0.97	0.83	0.86	0.84
27 Oct. 2009																	1.00	0.79	0.81	0.81
6 April 2010																		1.00	0.83	0.80
19 May 2010																			1.00	0.96
14 June 2010																				1.00

Table 3.3: Spearman's rank correlation coefficients between the soil water storage measurements over three years in the total active soil profile.

	17 July 2007	7 Aug. 2007	1 Sept. 2007	12 Oct. 2007	2 May 2008	31 May 2008	21 June 2008	16 July 2008	23 Aug. 2008	17 Sept. 2008	22 Oct. 2008	20 April 2009	7 May 2009	27 May 2009	21 July 2009	27 Aug. 2009	27 Oct. 2009	6 April 2010	19 May 2010	14 June 2010
17 July 2007	1.00	0.99	0.98	0.98	0.95	0.98	0.98	0.96	0.89	0.86	0.87	0.87	0.92	0.94	0.91	0.90	0.86	0.87	0.93	0.94
7 Aug. 2007		1.00	0.99	0.99	0.95	0.97	0.98	0.97	0.91	0.88	0.89	0.86	0.91	0.93	0.92	0.91	0.88	0.86	0.93	0.94
1 Sept. 2007			1.00	1.00	0.95	0.97	0.98	0.97	0.91	0.89	0.90	0.85	0.91	0.93	0.92	0.92	0.88	0.86	0.92	0.94
12 Oct. 2007				1.00	0.95	0.97	0.98	0.98	0.92	0.90	0.91	0.85	0.91	0.93	0.93	0.92	0.89	0.86	0.93	0.94
2 May 2008					1.00	0.98	0.97	0.95	0.87	0.84	0.85	0.92	0.96	0.97	0.93	0.91	0.86	0.90	0.95	0.93
31 May 2008						1.00	0.99	0.97	0.89	0.85	0.86	0.90	0.95	0.97	0.93	0.91	0.86	0.88	0.94	0.94
21 June 2008							1.00	0.99	0.92	0.89	0.90	0.89	0.94	0.96	0.95	0.94	0.89	0.89	0.95	0.94
16 July 2008								1.00	0.96	0.93	0.94	0.87	0.92	0.94	0.96	0.96	0.93	0.90	0.93	0.94
23 Aug. 2008									1.00	0.99	0.99	0.80	0.85	0.87	0.92	0.95	0.95	0.86	0.87	0.88
17 Sept. 2008										1.00	0.99	0.77	0.83	0.84	0.90	0.94	0.95	0.84	0.85	0.86
22 Oct. 2008											1.00	0.77	0.83	0.84	0.90	0.94	0.96	0.85	0.84	0.86
20 April 2009												1.00	0.97	0.96	0.89	0.86	0.80	0.93	0.90	0.87
7 May 2009													1.00	0.99	0.93	0.92	0.86	0.92	0.95	0.92
27 May 2009														1.00	0.95	0.93	0.87	0.92	0.95	0.93
21 July 2009															1.00	0.97	0.93	0.91	0.92	0.90
27 Aug. 2009																1.00	0.98	0.92	0.92	0.90
27 Oct. 2009																	1.00	0.89	0.88	0.86
6 April 2010																		1.00	0.90	0.85
19 May 2010																			1.00	0.95
14 June 2010																				1.00

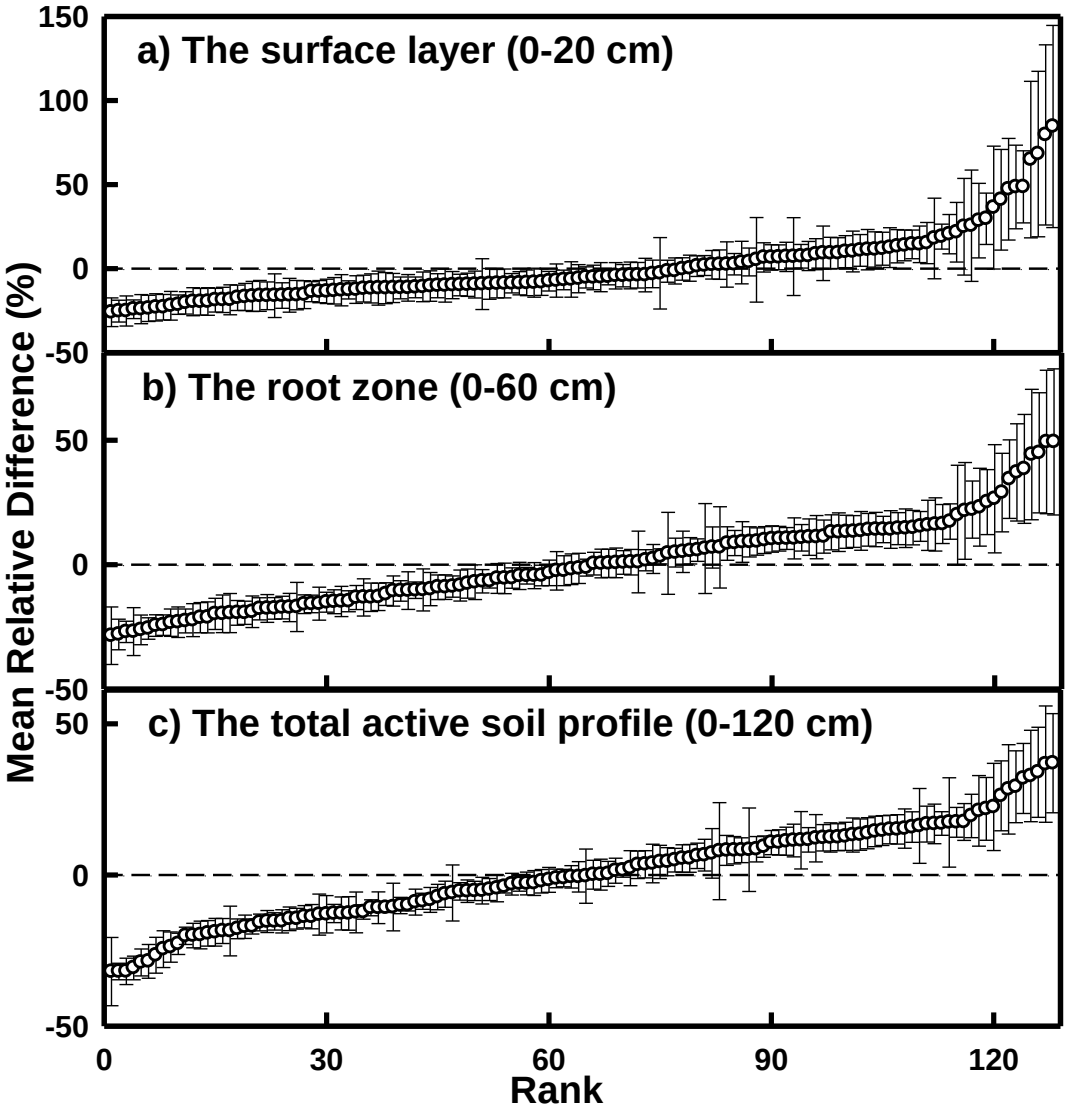

Figure 3.6. Ranked relative deviation from the mean soil water storage for a) the surface layer (0 - 20 cm), b) the root zone (0 - 60 cm), and c) the total active soil profile (0 - 120 cm).

However, the degree of similarity changed with depth as indicated by the change in the magnitude of the correlation coefficients (Table 3.2 and Table 3.3), which was generally in the order of the total active soil profile > the root zone > the surface layer suggesting the increase in similarity of the spatial pattern with the increase in depth. For example, the correlation coefficients between 31 May 2008 and 21 June 2008 in surface layer, root zone and total active soil profile were 0.96 (Table 3.1), 0.97 (Table 3.2) and 0.99 (Table 3.3), respectively. This may be attributed to lower root water uptake (Cassel et al., 2000), less meteorological effect (Hu et

al., 2010a) or a less disturbed soil structure (Guber et al., 2003; Pachepsky et al., 2005) in deeper soil layers. Guber et al. (2008) verified this between 0 – 60 cm depth using a new time stability index. The changing pattern in the water storage with depth was also reported by Martínez-Fernández and Ceballos (2003), Tallon and Si (2004), Pachepsky et al. (2005), Guber et al. (2008), and Hu et al. (2009, 2010a). However, Grayson and Western (1998) reported that there were no significant effects of measurement depth between the measured data set.

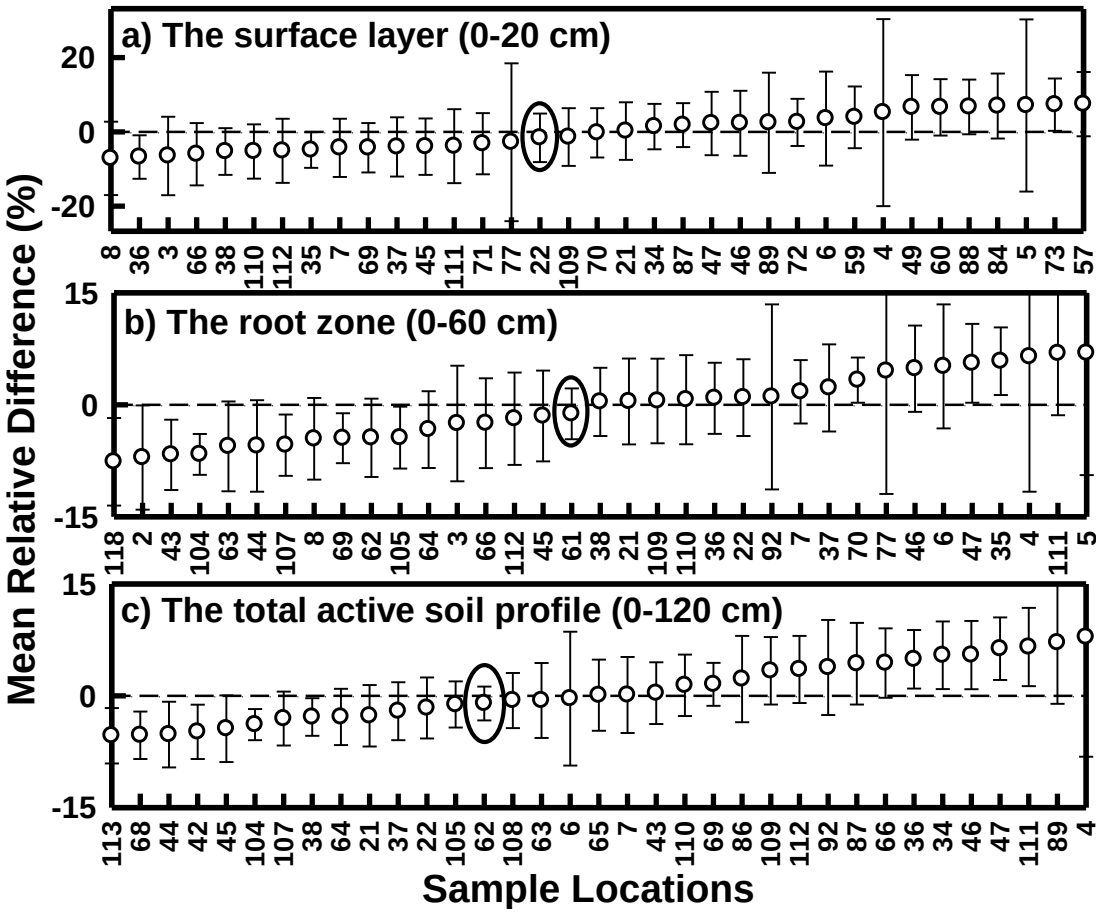

Figure 3.7. Zoomed ranked relative deviation from the mean soil water storage for a) the surface layer (0 - 20 cm), b) the root zone (0 - 60 cm), and c) the total active soil profile (0 - 120 cm). The error bars indicate the standard deviation of the mean relative difference. The points enclosed in eclipse represent the benchmark locations.

3.5.3 Identification of Benchmark Location

The stability of overall spatial pattern aids us in identifying the benchmark location. Figure 3.6 showed the rank of mean relative difference (MRD) and the standard deviation

associated with relative difference (SDRD) for a) the surface layer, b) the root zone, and c) the total active soil profile. The left and right ends of the horizontal axis represented the locations with much lower and higher water storage, respectively (Figure 3.6). The side with positive MRD indicated the locations that stored consistently higher water than the field average and the side with negative MRD indicated the locations with lower water content than field average. The location with the lowest absolute MRD and SDRD means that the value of soil water storage at this location was consistently close to the field average of soil water storage over time and was considered as benchmark location. A close view of the ranks of each location for a) the surface layer, b) the root zone and c) the total active soil profile was presented in Figure 3.7. The 22nd point on the transect showed the lowest MRD with smallest SDRD and was identified as the benchmark location for the surface layer. Similarly the benchmark locations for the root zone and total active soil profile were identified at 61st and 62nd points on the transect (Figure 3.7).

The benchmark location changed with the depth of measurement leading to the depth specific monitoring locations for the field. Tallon and Si (2004) reported substantial differences in the measurement depths and the benchmark locations, which were not adjacent in terms of spatial location. Martínez-Fernández and Ceballos (2003) and Guber et al. (2008) also reported different benchmark locations at different depths. However, this is not universal as Cassel et al. (2000) found the same benchmark locations for different depths. In this study, the surface layer benchmark location was different from the benchmark locations for the root zone and total active soil profile, which were located next to each other. The dynamic behaviour of the surface layer made the surface benchmark location slightly different from the benchmark locations of deep soil. This may be because the factors controlling the spatial pattern of soil water storage at the surface do not have as pronounced effect at greater depths (Cassel et al., 2000; Guber et al., 2003; Pachepsky et al., 2005; Hu et al., 2010a). However, the benchmark locations identified for different layers were located at mid-slope position. This aspect neutral or mid-slope position of benchmark location was also reported by Grayson and Western (1998), Jacobs et al. (2004) and Vivoni et al. (2008).

The performance of the benchmark location in representing field averaged soil water storage was evaluated following the procedure reported by Martínez-Fernández and Ceballos (2005). Figure 3.8 presented the scatter plot between field averaged soil water storage (except

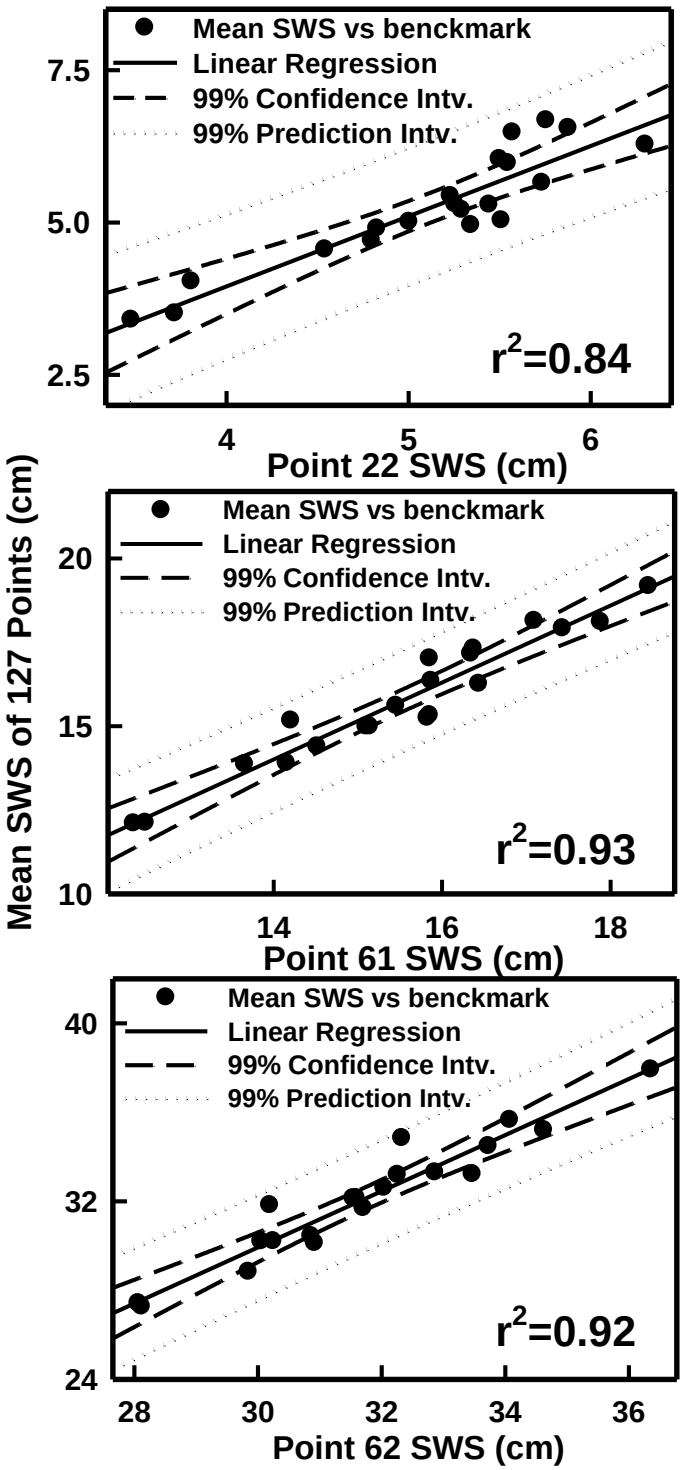

Figure 3.8. Suitability evaluations of benchmark locations with coefficient of determination value, 99 % confidence (dashed line) and prediction interval (dotted line) for the surface layer, the root zone and the total active soil profile. SWS indicates soil water storage (cm).

benchmark location) of the surface layer, the root zone and the total active soil profile and the average soil water storage of 22nd point, 61st point and 62nd point, respectively. The coefficient of determination (r^2) was 0.84 for surface layer, 0.93 for root zone and 0.92 for total active soil profile (Figure 3.8). This result was comparable with Martínez-Fernández and Ceballos (2005), which was 0.84 for REMEDHUS site and 0.92 for Rinconada site. In our study, this indicated that there would be around 16, 7, and 8 % error, respectively for surface layer, root zone, and total active soil profile if we predict the average soil water storage from the measurement of benchmark locations. Not surprisingly, the dynamic behaviour of the surface layer increased error in prediction.

This study was different from Tallon and Si (2004), which was based on soil water measurements taken from an undulating landscape during much drier years than the long-term normal. In dry years, vegetation utilized most water that was available to plants, leaving no difference in depressions or on knolls. Therefore, topographically introduced patterns did not exist in Tallon and Si (2004). However, the present study was conducted over years during which the total precipitation was almost equal to the long-term average with minor fluctuations. In these years, though the dynamic behaviour of the soil processes weakened the pattern in surface soil, the topographically induced spatial patterns still existed in deep soils. Thus, the topographically induced spatial pattern in soil water storage existed over the seasons and years.

3.6 Conclusions

Time stability analysis and Spearman's rank correlation coefficient were used to identify benchmark locations in a hummocky landscape and examine the time stability of spatial pattern of soil water storage. The analysis was carried out with soil water storage series measured over a four-year period at different depths. The spatial pattern of soil water storage was stable over time, yet the degree of the stability of the spatial pattern changed between different times of measurements. The spatial pattern of intra-season soil water storage was more stable than inter-season patterns. Furthermore, the inter-annual time stability of soil water storage was weaker than intra-season, but stronger than inter-season ones. The time stability of the spatial pattern aids us in identifying benchmark location with soil water storage representing the field average.

The benchmark locations varied with the depth of measurement. These locations can greatly improve the sampling efficiency by reducing the number of samples or observations for field averaged soil water storage monitoring over the conventional methods. Therefore, the benchmark locations can provide useful information for environmental monitoring.

4.0 SCALES AND LOCATIONS OF TIME STABILITY OF SOIL WATER STORAGE IN A HUMMOCKY LANDSCAPE

4.1 Preface

The previous chapter examined the intra-season, inter-season and inter-annual time stability of soil water storage collected from a hummocky landscape of Prairie pothole region. However, there is no information available about the scales and the characteristics of landscape that tend to have time stability or the locations of loss of the time stability. The scale as well as the landscape characteristics of time stability may lead to improve the prediction of soil water storage from the reduced number of monitoring sites, thus allowing improved runoff and stream flow prediction in scarcely gauged basins. Wavelet coherency can examine the similarity of two soil water spatial series at different scales and locations. Thus, we can get a clear picture on the scales and landscape characteristics of time stability.

4.2 Introduction

Soil water storage is one of the most important variables for understanding a large number of surface and sub-surface hydrological processes involved in a broad variety of natural processes (geomorphological, climatic, ecological) that act at different spatio-temporal scales (Entin et al., 2000). It has also been recognized as a key parameter of various environmental processes by hydrologists, meteorologists, and climate scientists. Knowledge of the behavior of soil water storage and its spatio-temporal distribution provides essential information for climatic and hydrological models (Beven, 2001; Western et al., 2002; Koster et al., 2004).

Soil water storage exhibits strong spatio-temporal variability and therefore a large number of sample points are required to obtain the accurate and precise field averaged soil water storage. Fortunately, the measurement, or the realization, of the processes controlling soil water storage in a field may show non-random spatial patterns resulting from the patterns of topographic, soil and vegetation factors. If a field or watershed is repeatedly surveyed for soil water storage, some sites or points store more water and are consistently wetter or less water and consistently drier than the field averaged soil water storage, creating a persistent spatial pattern in soil water storage over time. Vachaud et al. (1985) first introduced the phenomena as time

stability. They used Spearman's rank correlation to explain the similarity in the overall spatial patterns between two measurement series and the cumulative probability function of relative mean differences to examine the rank similarity of the individual locations over time. Various authors around the world have used the concept of time stability to explain the temporal dynamics of soil water storage over a range of investigated area, sampling scheme, sampling depth, investigation period, and land use (Vachaud et al., 1985; Kachanoski and de Jong, 1988; Martínez-Fernández and Ceballos, 2003; Tallon and Si, 2004; Cosh et al., 2008; Brocca et al., 2009). However, there is no information about time stability of the spatial patterns of soil water series from a season (intra-season), from different seasons (inter-season) and from particular season in different years (inter-annual). Information on the characteristics of the time stability at different depths is also scarce.

Although the approach by Vachaud et al. (1985) was attractive from the point of view of analytical simplicity, it missed the interactions between measurement locations, such as spatial autocorrelation (Kachanoski and de Jong, 1988). Given that soil water storage varies over a continuum of spatial and temporal scales (Entin et al., 2000; Brocca et al., 2010), Kachanoski and de Jong (1988) expanded the concept of time stability to account for spatial scale dependence. They used spatial coherency analysis as a method for examining the time persistence of spatial pattern as a function of spatial scale. Their results clearly showed the loss of time stability at small scales (< 40 m) during a recharge event resulting from topographic effects.

The method followed by Kachanoski and de Jong (1988) provided important insight into the scale dependence of time stability. However, the method does not allow identifying the characteristics of landscape that tend to have time stability or the locations of loss of the time stability. Spatial coherency analysis assumes the stationarity in the measured data series over space, hence may not capture localized features. More often than not, the measured data series are nonstationary and the variations at different scales may present at a location or time. After observing the presence of localized differences in the spatial pattern of recharge, Kachanoski and de Jong (1988) had to recheck the coherency analyses by comparing results from the whole and truncated transect. Even though this method may help in verifying losses of spatial patterns, its accuracy, especially in capturing the presence of localized patterns, was not guaranteed. This

implies the need to utilize a technique that does not require the assumption of stationarity and can analyze the changes in the spatial pattern at different scales and locations.

Wavelet coherency, based on the wavelet transform can deal with nonstationarity in the spatial series. It examines the correlation between spatial patterns of two variables at different scales and locations. Wavelet coherency has been used to identify the scale-location specific variations between two soil properties (Si and Zeleke, 2005; He et al., 2007; Yates et al., 2007; Biswas et al., 2008; Shu et al., 2008). There is no information available about the scale and location specific time stability of the spatial pattern of soil water storage. Therefore, our objective was to examine the scales and locations of time stability of soil-water storage patterns at different seasons and depths in a hummocky landscape. The overall similarity between the spatial patterns of soil water storage was examined using Spearman's rank correlation. Scales and locations of time stability between the spatial patterns of soil water storage were identified using wavelet coherency analysis.

4.3 Theory

4.3.1 Time Stability Analysis

Spearman's rank correlation coefficients were used to explain the similarity in the overall spatial pattern of soil water storage. Unlike Pearson correlation analysis, Spearman rank correlation explains the nonlinear association between two spatial series. If $R_{i,t}$ is the rank of the soil water storage $\theta_{i,j}$ observed at location *i* on time *t* and $R_{i,t'}$ is the rank of the soil water storage, at the same location, but on time t', then the Spearman's rank correlation coefficient r_s is calculated as

$$r_s = 1 - \frac{6 \cdot \sum_{i=1}^{n} (R_{i,t} - R_{i,t'})^2}{n(n^2 - 1)} \qquad [4.1]$$

A value of $r_s = 1$ corresponds to identify the rank for any location; i.e., perfect time stability of the spatial pattern between times *t* and t'. The closer the r_s is to 1, the more stable the spatial pattern (Vachaud et al., 1985).

4.3.2 Wavelet Coherency Analysis

Wavelet coherency analysis requires the calculation of wavelet coefficients for each of the two data series. Wavelet transform gives the wavelet coefficients at different scales and locations, the square of which represent the variances of the spatial series at that particular scale and location. A detail discussion of the methodology or the theory of wavelet transform and wavelet coherency is beyond the scope of this paper. The details of wavelet transform can be found in Farge (1992) and Kumar and Foufoula-Georgiou (1993, 1997) and the wavelet coherency can be found in Grinsted et al. (2004), Si and Zeleke (2005) and others. We will present only the basics regarding the wavelet transform and wavelet coherency analysis in this paper.

The continuous wavelet transform (CWT) of a soil water storage spatial series of length N (Y_i, $i = 1, 2, \cdots, N$) with equal incremental distance δx can be defined as the convolution of Y_i with the scaled and normalized wavelet (Torrence and Compo, 1998):

$$W_i^Y(s) = \sqrt{\frac{\delta x}{s}} \sum_{i=1}^{N} Y_j \psi\left[(j-i)\frac{\delta x}{s} \right] \qquad [4.2]$$

where $\psi[\ ]$ is the mother wavelet function and s represents scale. Wavelet coefficients, $W_i^Y(s)$ are expressed as $a + ib$ where a and b are the real and imaginary components of $W_i^Y(s)$. For the polar form of complex numbers, $W_i^Y(s) = \left|W_i^Y(s)\right|(\cos\theta + i\sin\theta)$, where $\theta = arc\tan\frac{b}{a}$, which is called the phase or argument of $W_i^Y(s)$ (Si and Zeleke, 2005). The wavelet power spectrum is defined as $\left|W_i^Y(s)\right|^2$ and the local phase can be defined from $W_i^Y(s)$. In extracting the local phase information, Morlet wavelet function is commonly used in continuous wavelet transform. Morlet wavelet can be represented as (Grinsted et al., 2004)

$$\psi(\eta) = \pi^{-1/4} e^{i\varpi\eta - 0.5\eta^2} \qquad [4.3]$$

where ω is dimensionless frequency and η is dimensionless space ($\eta = s/x$). The Morlet wavelet ($\omega = 6$) is good for feature extraction because it provides a good balance between space and frequency localization. The wavelet can be stretched in space (x) by varying its scale (s) (Si and Zeleke, 2005).

The cross-wavelet power spectrum between two soil water storage spatial series measured in two different dates *Y* and *Z* can be defined as

$$\left|W_i^{YZ}(s)\right| = \left|W_i^{Y}(s)\overline{W_i^{Z}(s)}\right| \quad [4.4]$$

where W_i^Y and W_i^Z are the wavelet coefficients of the spatial series *Y* and *Z*. $\overline{W_i^Z}$ is the complex conjugate of W_i^Z, the wavelet coefficients for soil water storage measurement series *Z*. While the cross wavelet spectra represent the covariance at a scale and location, the wavelet coherency is the correlation between two variables at each scale and location. Wavelet coherency between two soil water storage series can be defined as (Torrence and Webster, 1999)

$$R_i^2(s) = \frac{\left|S\left(s^{-1}W_i^{YZ}(s)\right)\right|^2}{S\left(s^{-1}\left|W_i^{Y}(s)\right|^2\right)S\left(s^{-1}\left|W_i^{Z}(s)\right|^2\right)} \quad [4.5]$$

where *S* is a smoothing operator and can be written as

$$S(W) = S_{\text{scale}}\left(S_{\text{space}}(W(s,\tau))\right) \quad [4.6]$$

where τ denotes the location and S_{scale} and S_{space} denote the smoothing along the wavelet scale axis and the spatial domain, respectively (Si and Zeleke, 2005). The smoothing function is the normalized real Morlet wavelet and has a similar footprint as the Morlet wavelet:

$$\frac{1}{s\sqrt{2\pi}}\exp\left(-\frac{\tau^2}{2s^2}\right) \quad [4.7]$$

Therefore, the smoothing along locations can be written as:

$$S_{space}(W(s,\tau)) = \sum_{k=1}^{N}\left(W(s,\tau)\cdot\frac{1}{s\sqrt{2\pi}}\exp\left(-\frac{(\tau-x_k)^2}{2s^2}\right)\right)\Bigg|_s \quad [4.8]$$

The Fourier transform of Equation 4.7 will be $\exp(-2\cdot s^2\omega^2)$, where ω is the frequency. Therefore, according to the convolution theorem, the Equation 4.8 can be implemented using Fast Fourier Transform (FFT) and Inverse Fast Fourier Transform (IFFT) and is written as

$$S_{space}(W(s,x)) = IFFT\left(FFT(W(s,\tau))\left(\exp(-2\cdot s^2\omega^2)\right)\right) \quad [4.9]$$

The smoothing along scales can be written as:

$$S_{scale}(W(s_k,x)) = \frac{1}{2m+1}\sum_{j=k-m}^{k+m}\left(S_{space}(W(s_j,x))\,\Pi(0.6s_j)\right)\Big|_x \quad [5.10]$$

where Π is the rectangle function, $\big|_x$ means at a fixed x value and j is the index for the scales. The factor of 0.6 is the empirically determined scale decorrelation length for the Morlet wavelet (Torrence and Compo, 1998; Si and Zeleke, 2005).

In testing the statistical significance, the wavelet coherency of the measured soil water storage was compared with that of the assumed background. In reality, we test the null hypothesis that there is no significant difference between the wavelet coherency of measured soil water storage and the assumed background. The significance testing for the wavelet coherency can be made against Gaussian white and red noises or permutation test (Pardo-Iguzquiza and Rodriguez-Tovar, 2000). For white noise, data points in the spatial data series are independently and identically distributed and not auto-correlated and can be used to test the null hypothesis for a statistical test in engineering applications (Si and Zeleke, 2005). The permutation test can destroy the cyclic and auto-correlated patterns in any spatial series by reordering at random (random permutation). A large number of permutations can yield complete random power spectra of original series (Pardo-Iguzquiza and Rodriguez-Tovar, 2000). However, soil properties are not completely random in a field and are generally autocorrelated (Nielsen et al. 1973; Trangmar et al., 1985; Isaaks and Srivastava, 1989; McBratney et al., 2000) and therefore, the white noise null hypothesis and the permutation test is not appropriate. With red noise, data values are similar between points next to each other, but are not similar further apart. Therefore, red noise is generally modeled as a univariate lag-1 auto regressive (AR1) process (Torrence and Compo, 1998; Si and Farrell, 2004). A simple model for the AR1 processes can be written as $x_n = \alpha x_{n-1} + z_n$, where α is the assumed lag-1 autocorrelation, $x_0 = 0$ and z_n is taken from Gaussian white noise. Following Gilman et al. (1963), the Fourier power spectrum of the previous model can be written as

$$P_q = \frac{1-\alpha^2}{1+\alpha^2-2\alpha\cos\left(2\pi q/N\right)} \qquad [4.11]$$

after normalization, where $q = 0 \ldots N/2$ is the frequency index (Torrence and Compo, 1998). The red noise-like behavior of soil properties is very common (Torrence and Compo, 1998; Nielsen and Wendroth, 2003; Grinsted et al., 2004; Si and Farrell, 2004) because in natural soils, the properties are very similar at two adjacent locations may be due to the mixing of mineral

properties. Therefore, small spatial variability is associated with small sampling interval and large spatial variability is associated with large sampling intervals (Isaaks and Srivastava, 1989). Therefore, if the measured soil water storage deviates from the red-noise like behavior, there must be some processes that alter the spatial pattern. Hence, we treated the red-noise like behavior as the background or the null hypothesis for the statistical test. However, if the soil water storage exhibit AR2 processes, we approximated the soil water storage with an AR1 process and the lag-1 autocorrelation coefficient was approximated by

$$r = \frac{r1 + \sqrt{r2}}{2} \qquad [4.12]$$

where $r1$ and $r2$ are lag-1 and lag-2 autocorrelation coefficients of soil water storage (Torrence and Compo, 1998; Si and Zeleke, 2005).

For a given AR1 process with lag-1 autocorrelation coefficient r, one thousand realizations of each of the soil water series were generated using Monte Carlo simulation. Similar to the measured soil water series, the wavelet coherencies of the simulated spatial series were calculated. Therefore, there were 1000 wavelet coherencies at each scale and location, which were subsequently sorted into increasing order. The 950^{th} wavelet coherency value at a scale and location gives the 95% confidence interval or the 5% significance level at that scale and location (Si and Zeleke, 2005). If the wavelet coherency between two-measured soil water series at a certain scale and location falls in the 95% confidence interval, we say that the wavelet coherency at this scale and location is not significantly different from the background red noise. Otherwise, the wavelet coherency is significantly different from the background red noise. In this significance test, we have tested the null hypothesis individually at each scale and location. Generally, there are a large number of wavelet coherencies between any two spatial series and therefore, a large number of hypotheses to be tested simultaneously. In this situation if the error is controlled at an individual level as if there was only one hypothesis for each of the any hypothesis, the test will be too permissive and the chances of error in identifying the significant difference will be high. This can be taken care of by controlling the family wise error rate. However, the tests controlling the family wise error rate such as Bonferroni adjusted p value (Westfall and Young, 1993), False Discovery Rate (Abramovich and Benjamini, 1996; Shen et al., 2002) are too conservative and very stringent in identifying the significant difference and are

also computation intensive (Si, 2008). Therefore, in our study, we have limited our scope in single hypothesis testing for the statistical significance.

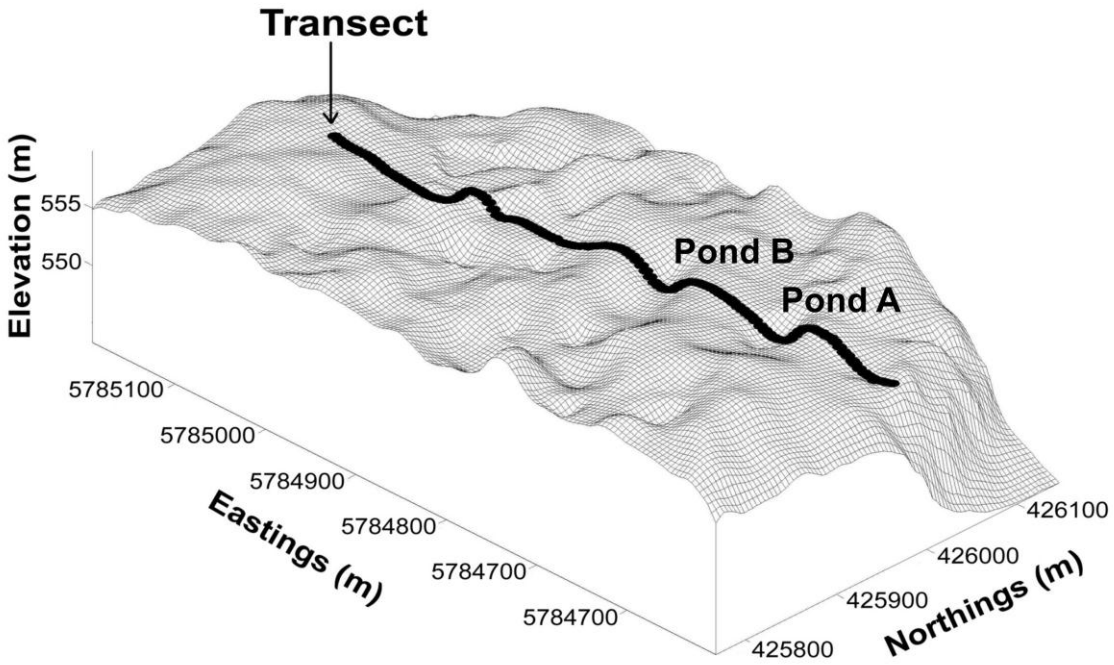

Figure 4.1. Transect position in the Hummocky landscape at St. Denis National Wildlife Area.

4.4 Materials and Methods:

4.4.1 Study Site

A field study was carried out at St. Denis National Wildlife Area (SDNWA) (52˚12′ N latitude, 106˚50′ W longitude) in central Saskatchewan, Canada. Detailed information about the study site is available in Yates et al. (2006a). In brief, the major landscape of the study area is hummocky with a complex sequence of slopes (10 to 15%) extending from rounded depressions to irregular complex knolls and knobs (Figure 4.1). This is the most common type of landscape covering more than 80% of area of the Canadian prairie region. The most common soil type of the study area is Dark Brown Chernozem, which is developed from moderately fine to fine textured, moderately calcareous, glacio-lacustrine deposits and modified glacial till (Saskatchewan Centre for Soil Research, 1989). The prevalent climate of the study area is semi-arid with the mean annual air temperature (at Saskatoon airport located at 40 km west of study site) is 2^{o}C with the monthly mean of -19^{o}C in January and 18^{o}C in July (AES, 1997). The study

area is generally covered by snow for five to six months (from November to April), contributing, and controlling the soil water dynamics of the area. Long-term (90-year) average precipitation for the area is 360 mm, of which 84 mm occurs in winter mostly as snow (AES, 1997). The total precipitation for the area during the years of 2006, 2007, 2008, and 2009 are 489 mm, 366 mm, 331 mm, and 402 mm, respectively (Figure 4.2). The study area received a record-breaking spring and summer rainfall during 2010.

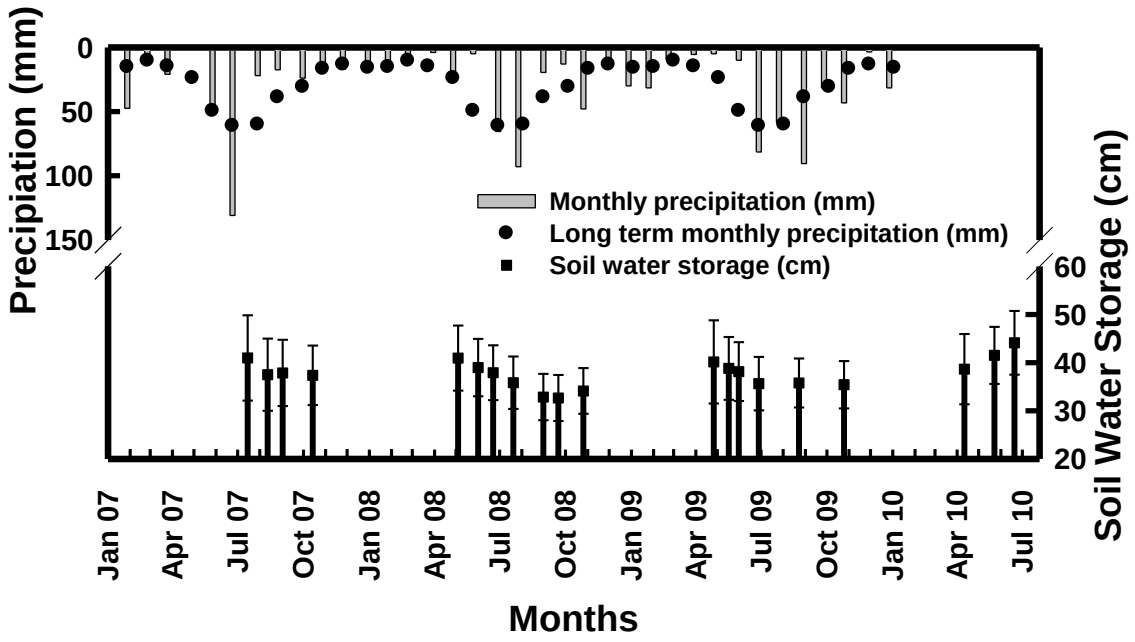

Figure 4.2. Average soil water storage with standard deviation of measurement and the average monthly and long-term average monthly precipitation at Saskatoon International Airport (40 km west of study site).

4.4.2 Data Collection

Soil water was measured along a 576 m transect extending north-south in the study area. The transect traversed several knolls and depressions representing different landform cycles with repetition (Yates et al., 2006a; Figure 4.1). A topographic survey of the study site was completed using Light Detection and Ranging (LiDAR) at 5 m resolution. Along the transect, the landform elements were marked as convex (CX), concave (CV), uncultivated wetland (UW) or cultivated wetland (CW). Convex elements were topographically high positions with positive profile curvature. Concave elements had negative curvature and uncultivated wetlands were seasonal depressions (Woo and Rowsell, 1993). There were 128 sampling points in the transect with a 4.5

m regular interval. Each point was installed with 5 cm diameter and 200 cm long PVC tube using a truck mounted hydraulic drill. These tubes were used for measuring soil water content using a neutron probe in the field. Soil water was measured at every 20 cm from 20 cm to 140 cm using the neutron probe (Model- CPN 501 DR Depthprobe, CPN International Inc., Martinez, CA, USA).

In calibrating the neutron probe at the study site, several similar holes were made adjacent to the neutron access tube using a truck mounted hydraulic drill. Soil samples were collected at every 10 cm depth interval to capture the small variations in soil water content with depth. The soil cores were immediately wrapped with plastic film to prevent water loss through evaporation. Water content in soil samples was determined using the gravimetric method. The volumetric soil water content was calculated from gravimetric water content and bulk density. The new holes were temporarily installed with similar PVC tubes for neutron measurement. A standard neutron count and the neutron count at every 10 cm depth interval were recorded. This procedure was completed at different locations along the transect several times over different years. The neutron count ratio (neutron count / standard neutron count) and the volumetric water content was compared to build a calibration equation, which is $\theta_v = 0.8523\ R + 0.0612$ with $n = 101$ and $r^2 = 0.86$, where R is the neutron count ratio. The calibration equation was used to calculate the soil water content at each 20 cm depth increment from the neutron counts. As the neutron probe measurement is prone to error for surface soil water measurement, the average soil-water content of the 0 to 20 cm soil layer was measured using a vertically installed time-domain reflectometry (TDR) probe and a metallic cable tester (Model 1502B, Tektronix, Beaverton, OR, USA). The TDR probes were inserted in soil as close as possible to the neutron access tube during each time of measurement. The probes were carefully inserted in soil at the locations as close as possible of last measurement and the measurements were considered as the fixed-point measurement over time. A standard calibration equation $\theta_v = 0.115\sqrt{k_a} - 0.176$ was used to calculate the average volumetric water content in the surface layer (0 – 20 cm). Where the dielectric constant, $k_a = \left[L_2/L\right]^2$, L_2 is the distance between the arrival of signal reflected from the probe-to-soil interface and the signal reflected from the end of the probe curves (measured from waveform) and L is the length of the TDR probe (Topp and Reynolds, 1998). Soil water content was measured 20 times over a four year (2007 - 2010) period covering

different environmental situations including spring snowmelt, summer and fall. The first measurement of each year was completed few days after the completion of snowmelt allowing the surface layer to thaw. Therefore, the TDR measured the liquid water content in the surface layer. Contrary, the neutron probe measurement is not affected by the frozen soil at deep layers. The soil water was measured at least after 2 to 3 days of any environmental events (e.g. rainfall) to ensure the quasi-steady state in soil water dynamics. The average soil water storage for surface (0 to 20 cm) and the whole soil profile (0 to 140 cm) was calculated by multiplying the volumetric water content with depth. The water storage of whole soil profile was calculated from the TDR and neutron probe measurements, which might have its own inaccuracies and errors associated with the instruments. However, in the time stability analysis we have compared the spatial patterns of soil water storage over time. In this, we assumed any error associated with a particular measurement is present in other measurements as the data were collected by a single person using same instruments. Therefore, the different measurement techniques might not have any possible effect in our data analysis and conclusion. The soil water storage of the surface and the whole soil profile were used in this study to examine the scale and location dependent spatial pattern and its stability over time.

4.4.3 Data Analysis

Exploratory analysis and the time stability analysis were completed in Microsoft Office Excel (Microsoft Corporation Inc.). Wavelet coherency analysis was completed using the MATLAB (The MathWorks Inc.) code written by Grinsted et al. (2004) and is available at URL http://www.pol.ac.uk/home/research/waveletcoherence/. The graphs were prepared in SigmaPlot (SysStat Software Inc.).

4.5 Results

4.5.1 Soil Water Storage Spatial Patterns

The water storage of the soil profile seemed to be inversely related to elevation along the transect (Figure 4.3). The locations from 100 m to 140 m (Pond A in Figure 4.1) and from 225 m to 250 m (Pond B in Figure 4.1) along the transect had very high water storage during spring, but less during late summer and fall. However, more soil water was stored in depressions than on

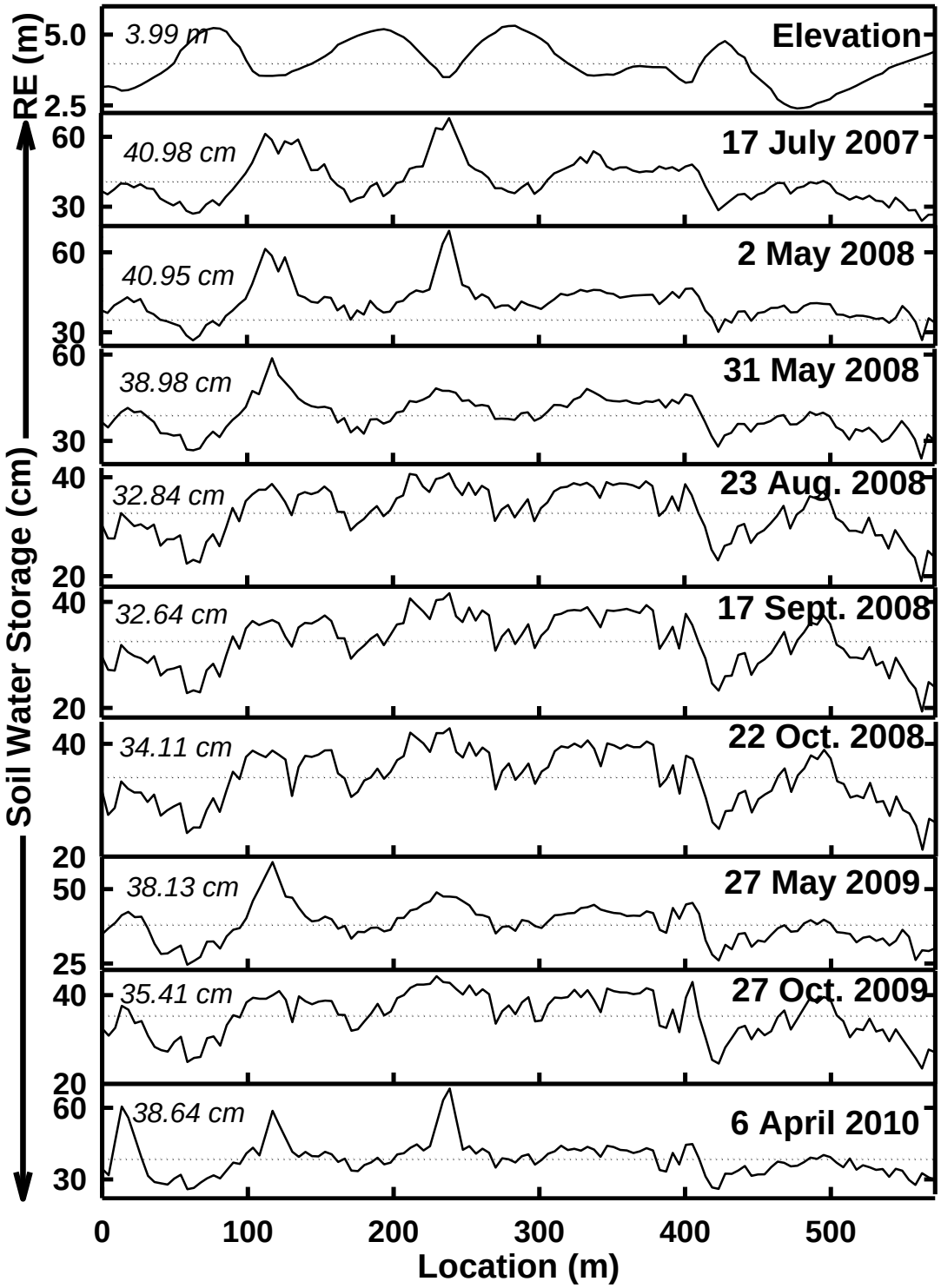

Figure 4.3. Spatial distribution of selected soil water storage series for the whole soil profile (0-140 cm) along the transect with a cross sectional view of the transect. Dotted line indicates the reference at average soil-water storage (cm) and RE indicates relative elevation (m).

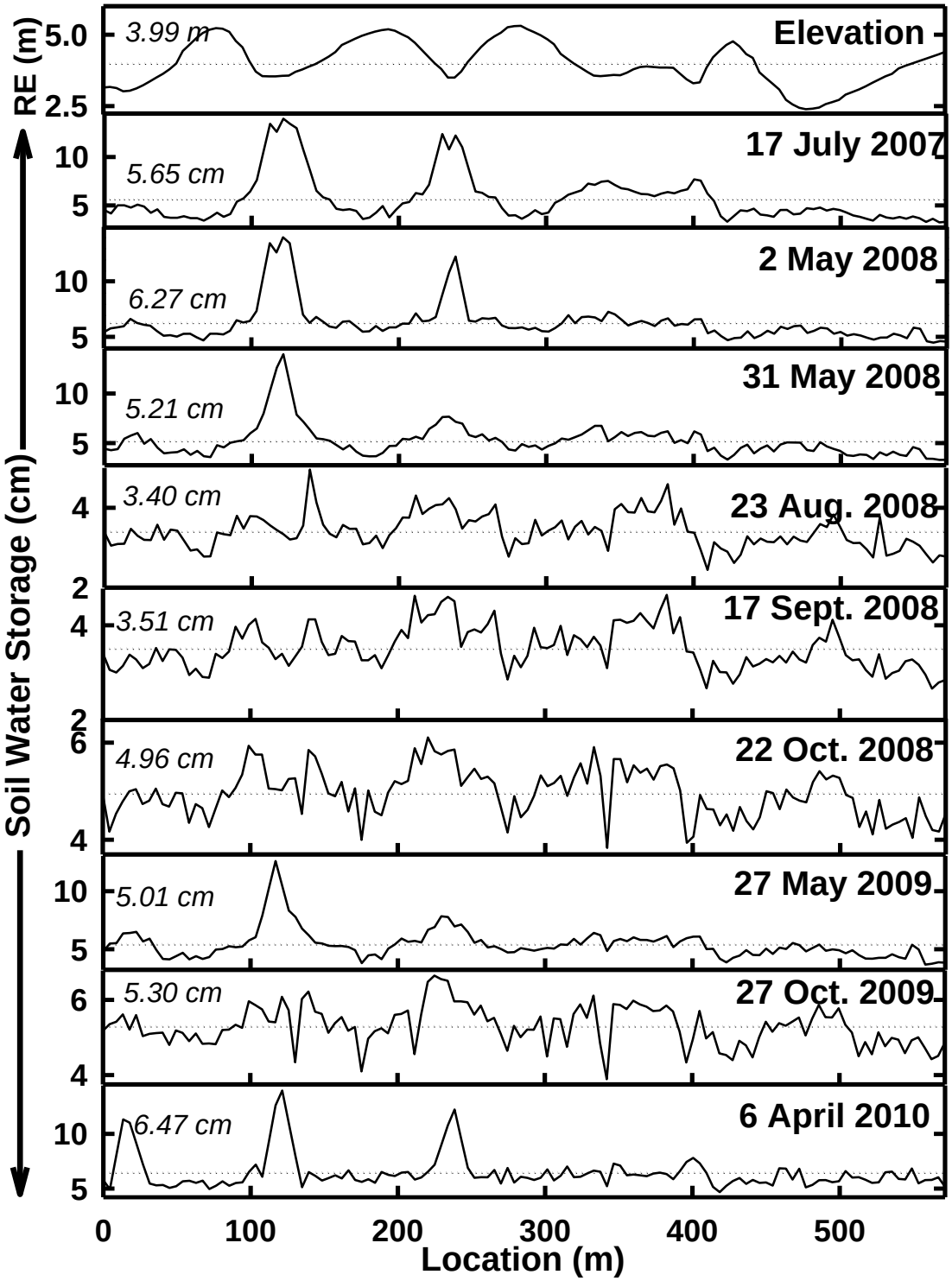

Figure 4.4. Spatial distribution of selected soil water storage series for the surface (0-20 cm) layer along the transect with a cross sectional view of the transect. The dotted line indicates the reference at average soil-water storage (cm) and RE indicates relative elevation.

knolls and the spatial pattern was maintained throughout the measurement period (Figure 4.3). The difference between the maximum and minimum soil water storage was higher during the spring or early part of the year (e.g., 41.1 cm for 2 May 2008) than in the fall (e.g., 21. 6 cm for 22 October 2008). The average soil-water storage for the whole soil profile was 41.0 cm on 17 July 2007, 41.0 cm on 2 May 2008 and 34.1 cm on 22 October 2008 (Figure 4.2). The coefficient of variation (CoV) was high during early spring measurements (e.g. 22 % on 20 April 2009) and gradually decreased in fall (e.g. 14 % on 27 October 2009). The overall spatial patterns were more similar among the soil water storage series measured close in time or within a season (intra-season) (e.g. 17 September 2008 and 22 October 2008) than among the soil water storage series measured further away in time or in different seasons (inter-season) (e.g. 2 May 2008 and 22 October 2008) within a year (Figure 4.3). A very similar spatial pattern in soil water storage was also observed between the measurements taken from a season of different years (inter-annual) (e.g. 31 May 2008 and 27 May 2009).

Similar to the whole soil profile, the soil water storage of the surface (0 - 20 cm) layer during spring and early summer was also inversely related to elevation along the transect (Figure 4.4). However, the relationship was weakened in late summer or fall. Furthermore, a strong upward peak in soil water storage (Figure 4.4) was observed during spring at the locations from 100 m to 140 m (Pond A in Figure 4.1) and from 225 m to 250 m (Pond B in Figure 4.1) along the transect. However, the peak was nearly reversed (downward) at the center of those locations during fall (Figure 4.4). The average soil-water storage for the surface soil layer was 5.7 cm on 17 July 2007, 6.3 cm on 2 May 2008 and 5.0 cm on 22 October 2008 (Figure 4.4). There was a higher CoV during spring (e.g. 30 % on 20 April 2009) than during fall (e.g. 10 % on 27 October 2009). The differences in maxima and minima of soil water storage were 9.5 cm for 2 May 2008 and 2.3 cm for 22 October 2008 (Figure 4.4).

4.5.2 Time Stability of Overall Spatial Patterns

High rank correlation coefficients between any two-measurement series indicated strong time stability in the spatial pattern of soil water storage in the surface and whole soil profile. The intra-season time stability was stronger than inter-season time stability (Table 4.1). For example, the correlation coefficient was 0.98 between 2 May 2008 and 31 May 2008 (spring) and was 0.99

Table 4.1. Spearman's rank correlation coefficients between the soil water storage measurements over three years for the whole soil profile (0-140 cm).

	17 July 2007	7 Aug. 2007	1 Sept. 2007	12 Oct. 2007	2 May 2008	31 May 2008	21 June 2008	16 July 2008	23 Aug. 2008	17 Sept. 2008	22 Oct. 2008	20 April 2009	7 May 2009	27 May 2009	21 July 2009	27 Aug. 2009	27 Oct. 2009	6 April 2010	19 May 2010	14 June 2010
17 July 2007	1.00	0.98	0.98	0.97	0.95	0.97	0.97	0.96	0.89	0.86	0.85	0.85	0.91	0.93	0.90	0.89	0.85	0.84	0.92	0.94
7 Aug. 2007		1.00	0.99	0.99	0.95	0.97	0.98	0.97	0.91	0.88	0.88	0.85	0.91	0.93	0.92	0.91	0.87	0.85	0.93	0.94
1 Sept. 2007			1.00	1.00	0.95	0.97	0.98	0.98	0.92	0.89	0.89	0.86	0.91	0.93	0.93	0.92	0.89	0.86	0.92	0.94
12 Oct. 2007				1.00	0.96	0.97	0.98	0.98	0.93	0.91	0.90	0.86	0.92	0.94	0.93	0.93	0.90	0.86	0.93	0.95
2 May 2008					1.00	0.98	0.97	0.96	0.89	0.86	0.85	0.92	0.96	0.97	0.94	0.92	0.87	0.90	0.95	0.94
31 May 2008						1.00	0.99	0.97	0.89	0.85	0.85	0.89	0.93	0.95	0.92	0.90	0.86	0.87	0.93	0.94
21 June 2008							1.00	0.99	0.92	0.89	0.89	0.89	0.94	0.96	0.95	0.93	0.89	0.88	0.94	0.95
16 July 2008								1.00	0.96	0.93	0.93	0.88	0.93	0.95	0.96	0.96	0.93	0.89	0.94	0.94
23 Aug. 2008									1.00	0.99	0.99	0.81	0.87	0.88	0.93	0.96	0.96	0.86	0.88	0.89
17 Sept. 2008										1.00	0.99	0.78	0.84	0.86	0.91	0.95	0.96	0.85	0.86	0.86
22 Oct. 2008											1.00	0.78	0.83	0.85	0.91	0.95	0.96	0.85	0.85	0.85
20 April 2009												1.00	0.97	0.96	0.90	0.88	0.82	0.93	0.90	0.86
7 May 2009													1.00	0.99	0.94	0.93	0.88	0.93	0.95	0.91
27 May 2009														1.00	0.96	0.94	0.89	0.93	0.96	0.92
21 July 2009															1.00	0.97	0.94	0.92	0.93	0.91
27 Aug. 2009																1.00	0.98	0.93	0.93	0.90
27 Oct. 2009																	1.00	0.90	0.89	0.87
6 April 2010																		1.00	0.90	0.85
19 May 2010																			1.00	0.95
14 June 2010																				1.00

between 23 August 2008 and 17 September 2008 (summer) for the whole soil profile. However, the correlation coefficient was only 0.89 between 2 May 2008 (spring) and 23 August 2008 (summer) and was 0.85 between 2 May 2008 (spring) and 22 October 2008 (fall) (Table 4.1). In fact, the correlation coefficient was high between the measurement series close in time and gradually decreased with increasing time difference between measurements. For example, the correlation coefficient was 0.99 between 31 May 2008 and 21 June 2008 and was 0.85 between 31 May 2008 and 22 October 2008 for the whole soil profile (Table 4.1). Furthermore, the inter-annual time stability was also strong. For example, the correlation coefficient was 0.95 between 31 May 2008 and 27 May 2009 and was 0.96 between 16 July 2008 and 21 July 2009 (Table 4.1). All the rank correlation coefficients are significant at $p < 0.0001$.

A similar trend in the correlation coefficients (intra-season, inter-season, and inter-annual) was observed in the surface soil layer. However, the magnitude of the correlation coefficients decreased. For example, the correlation coefficient was 0.97 between 23 August 2008 and 17 September 2008 (intra-season), 0.68 between 31 May 2008 and 22 October 2008 (inter-season), and 0.94 between 31 May 2008 and 27 May 2009 (inter-annual).

4.5.3 Scale-Location Specific Time Stability

Figure 4.5 shows typical examples of the wavelet coherency between different seasons (inter-season). The soil water measurement series of 2 May 2008, 23 August 2008, and 22 October 2008, respectively were used to represent spring, summer, and fall seasons. There were significant small-scale (< 18 m) correlations at the locations of 35 – 50 m, 230 – 300 m, 370 – 480 m and from 540 m to the end of the transect between spring and summer (Figure 4.5a) and spring and fall (Figure 4.5b) measurement series. The medium-scale correlation was only significant from the beginning of the transect to 150 m, 180 – 300 m, and from 350 m to the end of the transect (Figures 4.5a and 4.5b). There was large-scale (72 – 150 m) time stability between spring and summer (Figure 4.5a) and between spring and fall (Figure 4.5b) measurement series over the whole transect. Therefore, the scale-location specific correlations or time stability between spring and summer was very similar to that between spring and fall. However, the total area representing the significant correlation between spring and fall was low compared to the area between spring and summer at both medium and large scales. Remarkably, there were

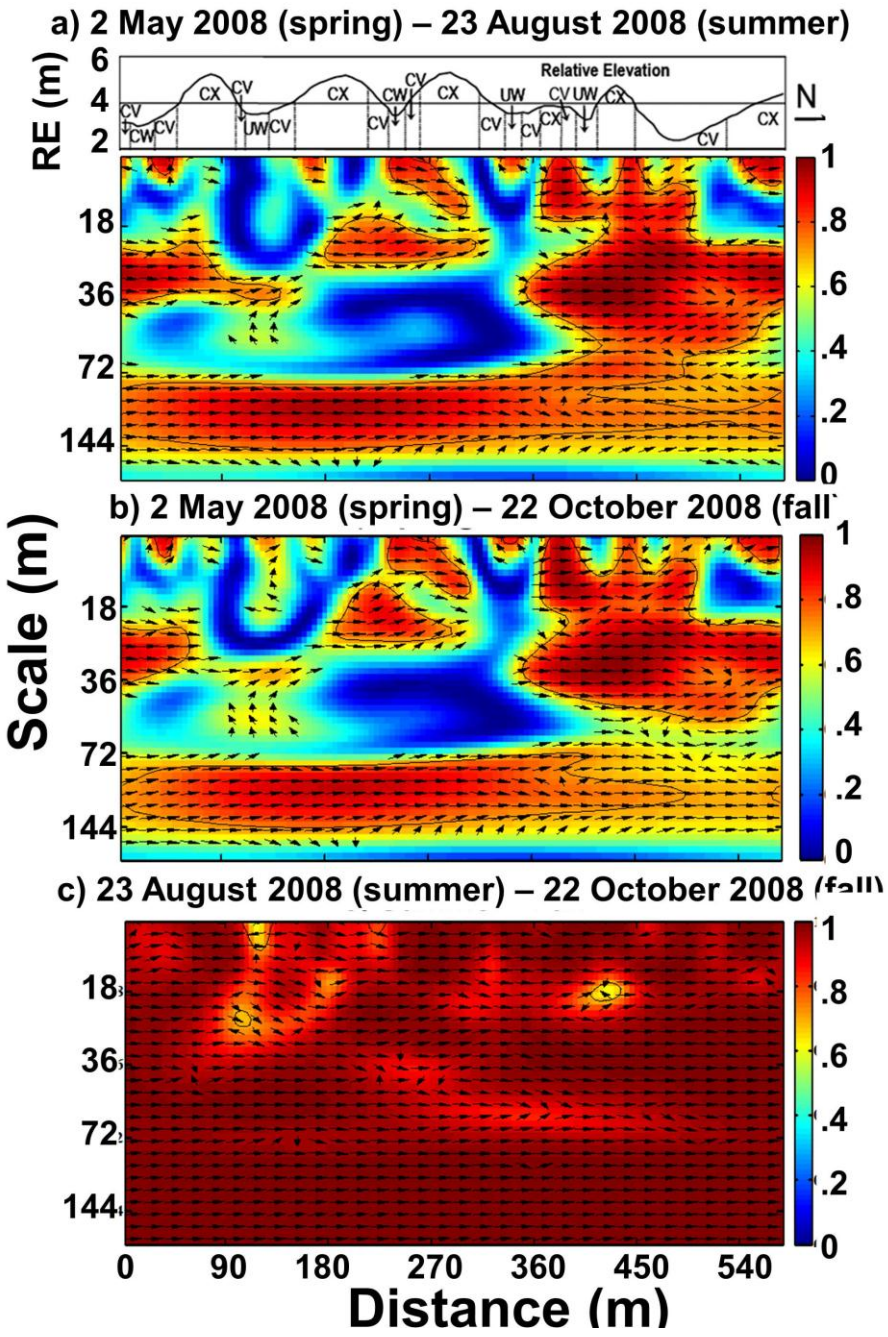

Figure 4.5. The inter-season wavelet coherencies between the soil water storage measured during a) spring (2 may 2008) and summer (23 August 2008), b) spring (2 May 2008) and fall (22 October 2008), and c) summer (23 August 2008) and fall (22 October 2008) for the whole soil profile. Cross sectional view of the transect with landform elements at the top. The X-axis indicates distance along the transect (m); the Y-axis indicates the scale (m); the solid black line indicates 5% significance level; the color bar indicates strength of correlation, and the direction of arrow indicates the phase relationship or type of correlation. CX stands for convex, CV stands for concave, CW stands for cultivated wetlands, and UW stands for uncultivated wetlands.

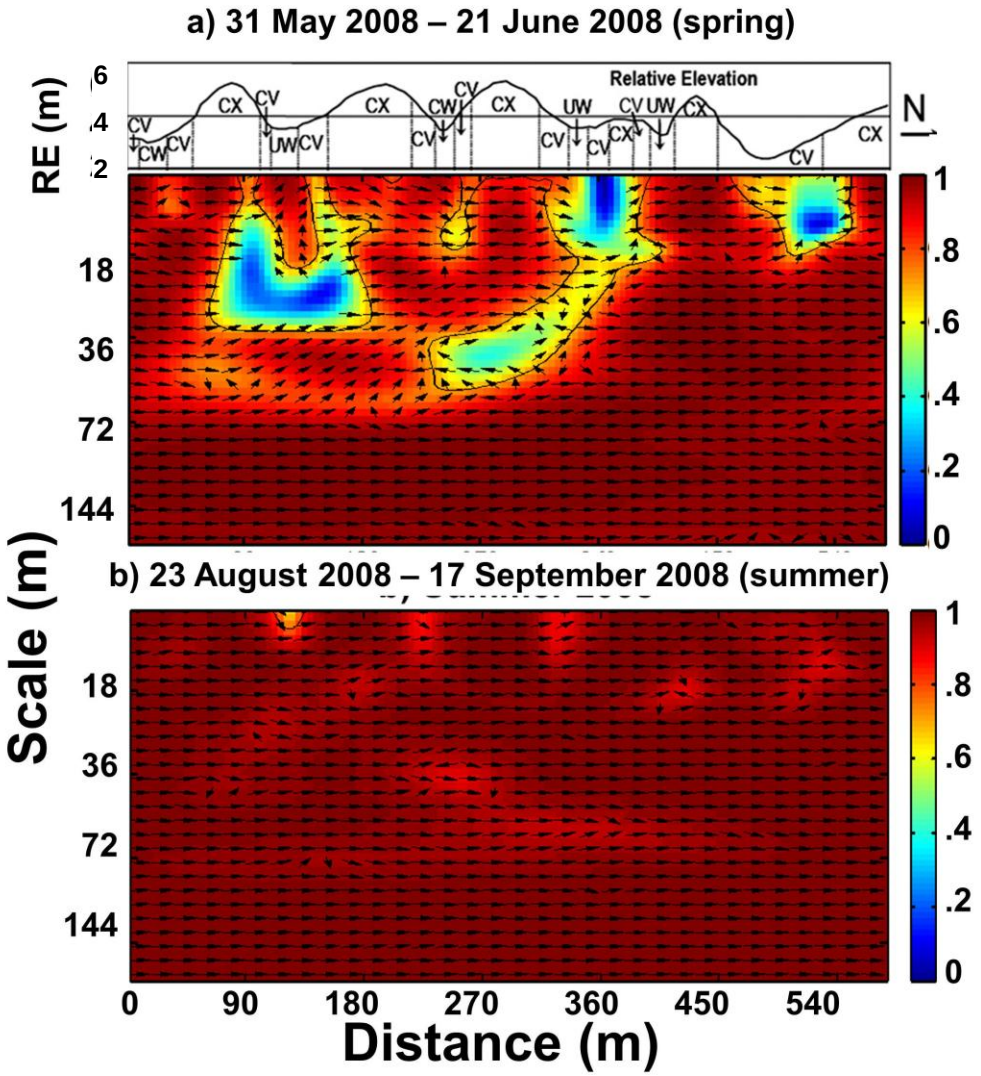

Figure 4.6. The intra-season wavelet coherencies between the soil water storage measured within a) spring (31 May and 21 June 2008) and b) summer (23 August and 17 September 2008) for the whole soil profile. Cross sectional view of the transect with landform elements at the top. The X-axis indicates distance along the transect (m); the Y-axis indicates the scale (m); the solid black line indicates 5% significance level; the color bar indicates strength of correlation, and the direction of arrow indicates the phase relationship or type of correlation. CX stands for convex, CV stands for concave, CW stands for cultivated wetlands, and UW stands for uncultivated wetlands.

strong coherent relationships at all scales and over the whole transect between summer and fall measurement series (Figure 4.5c).

The intra-season time stability (Figure 4.6) was different from the inter-season time stability (Figure 4.5). The soil water storage series of 31 May 2008 and 21 June 2008, and 23

August 2008 and 17 September 2008, respectively, were used to represent the spring and summer season time stability. There was a strong coherent relationship at all scales and almost all locations within spring measurement series (Figure 4.6a). Few non-significant correlations at very few places were also observed at small- and medium-scales. However, the summer season measurement series had very strong coherent relations at all scales and all locations (Figure 4.6b).

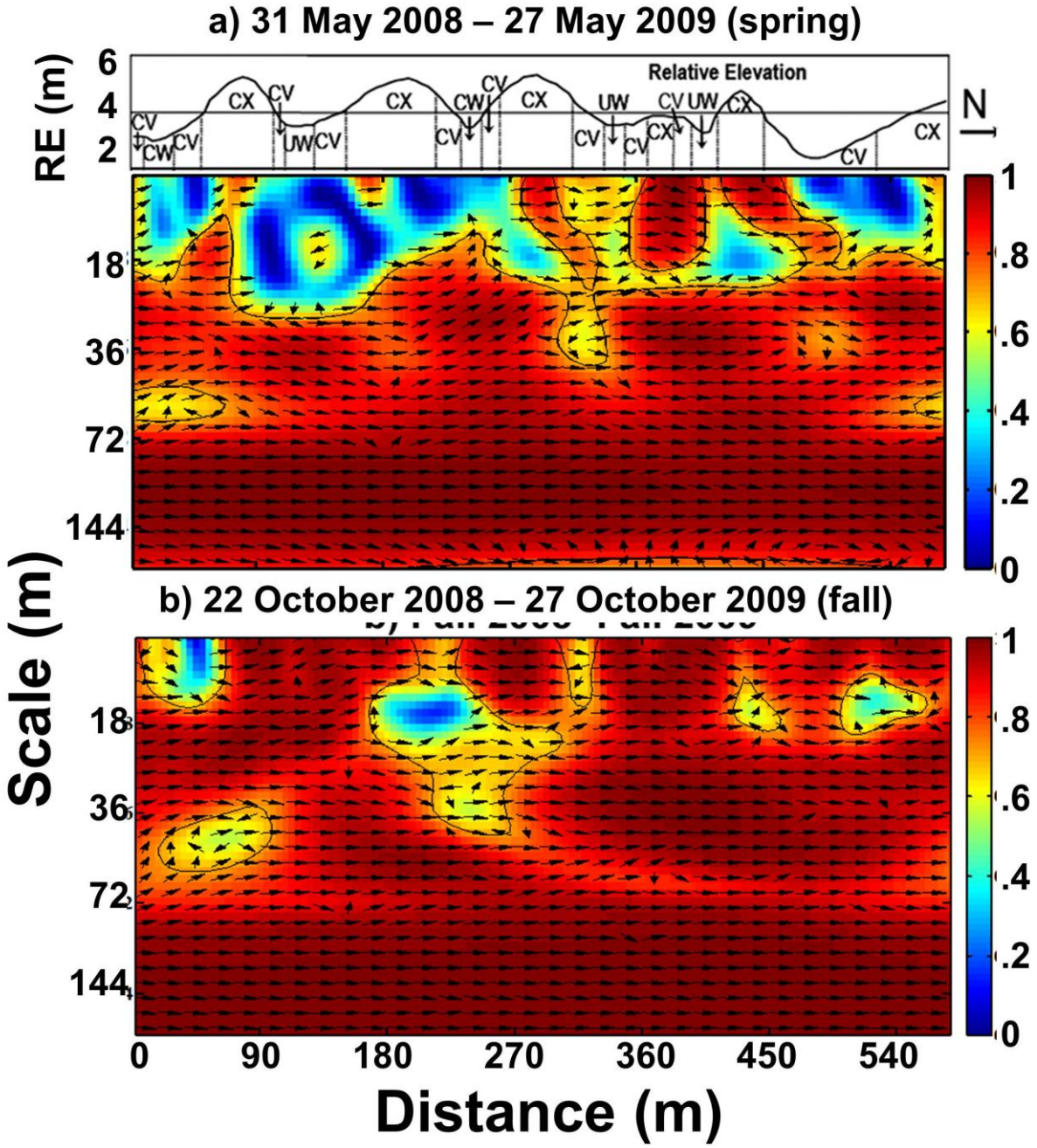

Figure 4.7. The intra-annual wavelet coherencies between the soil water storage measured during a) the spring (31 May) of 2008 and spring (27 May) of 2009 and b) the fall (22 October) of 2008 and fall (27 October) of 2009 for the whole soil profile. Cross sectional view of the transect with landform elements at the top. The X-axis indicates distance along the transect (m); the Y-axis indicates the scale (m); the solid black line indicates 5% significance level; the color bar indicates strength of correlation, and the direction of arrow indicates the phase relationship or type of correlation. CX stands for convex, CV stands for concave, CW stands for cultivated wetlands, and UW stands for uncultivated wetlands.

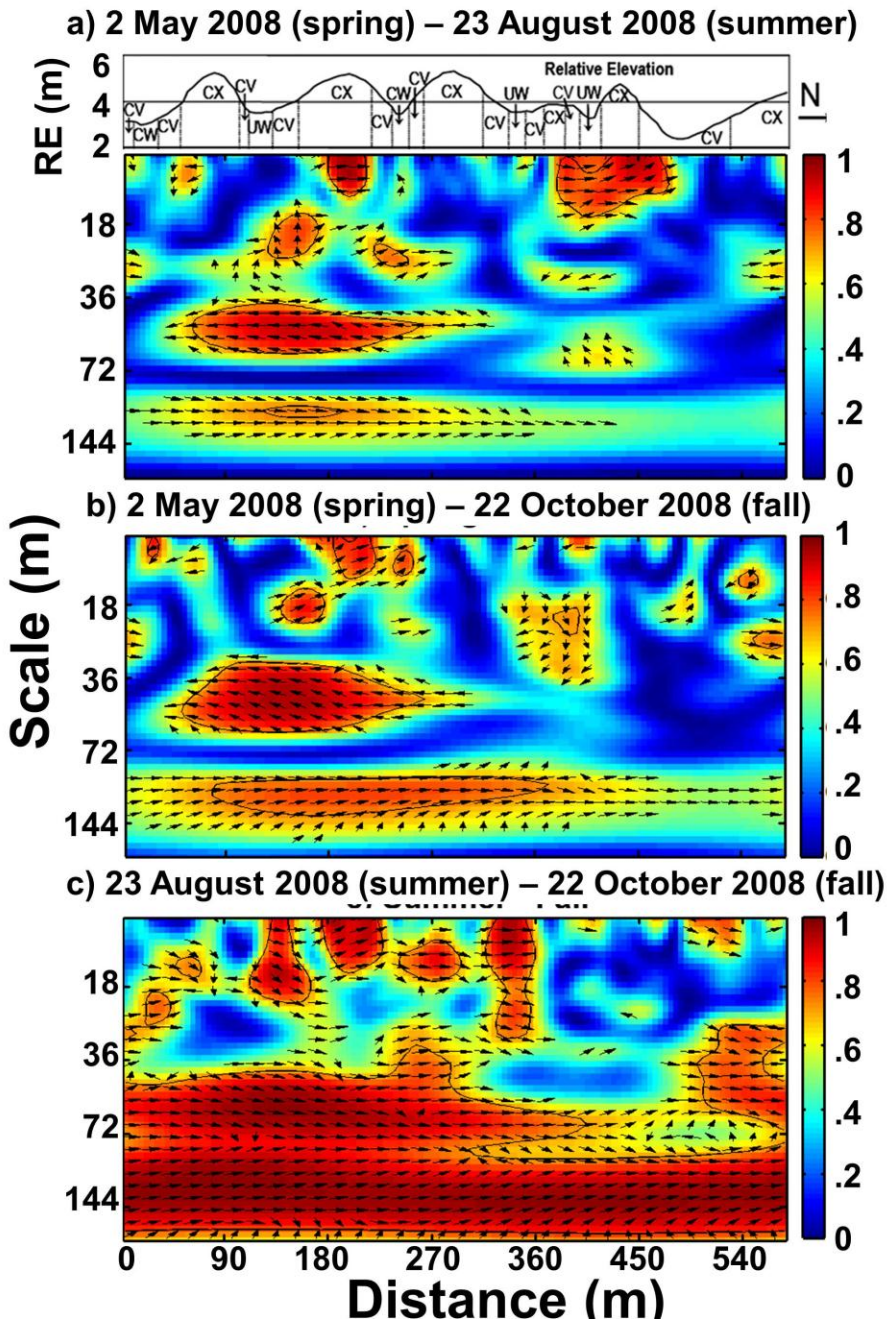

Figure 4.8. The inter-season wavelet coherencies between the soil water storage measured during a) spring (2 may 2008) and summer (23 August 2008), b) spring (2 May 2008) and fall (22 October 2008), and c) summer (23 August 2008) and fall (22 October 2008) for the surface (0 – 20 cm) soil layer. Cross sectional view of the transect with landform elements at the top. The X-axis indicates distance along the transect (m); the Y-axis indicates the scale (m); the solid black line indicates 5% significance level; the color bar indicates strength of correlation, and the direction of arrow indicates the phase relationship or type of correlation. CX stands for convex, CV stands for concave, CW stands for cultivated wetlands, and UW stands for uncultivated wetlands.

A strong inter-annual time stability was also observed (Figure 4.7) between measurement series from spring and fall of one year to the spring and fall of another year. There was strong medium- and large-scale time stability between the spring of 2008 and the spring of 2009 over the whole transect (Figure 4.7). However, the small-scale correlation was present only at the locations of 40 – 70 m, 280 – 340 m, 360 – 410 m, and 420 – 500 m along the transect (Figure 4.7a). Similarly, there was strong coherent relationship between fall of 2008 and fall of 2009 at all scales and almost all locations (Figure 4.7b). Very few places at small- and medium-scales were observed with non-significant correlation.

The type of relationship between any two spatial series was also examined from the wavelet coherency graph. The direction of arrows indicated the type of correlation. The right directed arrows indicated the 'in phase' relationship or positive correlation and the left directed arrows indicated the 'out of phase' relationship or negative correlation between the two spatial series. The intra-season, inter-season, and inter-annual time stability showed a positive correlation at almost all scales and locations with very little exception at some places with disoriented arrows indicating the random correlation.

The intra-season, inter-season, and inter-annual time stability for the surface soil (0 – 20 cm) was also examined using wavelet coherency (Figure 4.8). The strong coherency in soil water storage was observed at medium- and large-scales between summer and fall measurement series (Figure 4.8c), but not between spring and summer (Figure 4.8a), nor between spring and fall (Figure 4.8b). Strikingly, there were out of phase correlations at the medium scales at around 50 - 270 m along the transect between these seasons (Figures 4.8a and 4.8b). Coherency at all other scales and locations were in phase. In addition, very little small-scale time stability was also observed between seasons (Figure 4.8). As a result, the total area representing the significant correlations at all scales and locations for the surface layer (Figure 4.8) was smaller than that for the whole soil profile (Figure 4.5).

4.6 Discussion

The study area receives a considerable amount of precipitation during winter as snow. Strong wind creates an uneven distribution of snow in the landscape. While depressions receive snow, the snow blows off from knolls (Lungal, 2009). Therefore, drifting snow contributes to the

high water storage in depressions and low water storage on knolls during spring (Woo and Rowsell, 1993; Hayashi et al., 1998). Furthermore, in early spring, the snow melts resulting in a large amount of water within a short period. The frozen ground at that time does not allow water to enter into the soil and thus snowmelt water runs off to lower landscape positions. The high position receives less water and low position receives more water creating the spatial pattern of soil water storage similar to the shadow of elevation (Figure 4.3). The locations from 100 m to 140 m (Pond A in Figure 4.1) and from 225 m to 250 m (Pond B in Figure 4.1) along the transect were in depressions, thus received snowmelt water from surrounding and maintained a level of water during spring. Standing water in these depressions, created prolonged sharp peaks in the spatial pattern of soil water storage (Figure 4.3).

While the large amount of water stored in depressions enhanced plant growth, limited water storage on knolls restricted plant growth and actual evapotranspiration. Visual observation and measured leaf area index (unpublished data, 2011) clearly showed strong vegetation growth in depression and poor vegetation growth on knolls. The variable evapotranspiration demand during summer and fall reduced the difference in water storage between knolls and depressions. However, during spring, depressions may have stored more water than plants can take up and the difference in stored water was maintained even in fall for the whole soil profile. Therefore, topographically induced spatial patterns in soil water storage for the whole soil profile existed even in fall.

In the previous study, Biswas and Si (2011a) examined the time stability of the spatial pattern of soil water storage at different depth layers and at different seasons following Vachaud et al. (1985). The authors found strong time stability at the surface layer (0–20 cm), root zone (0–60 cm), and the total active soil profile (0–120 cm) at any time of the year. The observed time stability was used to identify benchmark locations or the locations with field averaged soil water storage. The benchmark location for the surface layer was little different from the root zone and the total active soil profile, which identified benchmark locations next to each other. While the benchmark location of the surface layer predicted the average soil water storage with 16% error, the benchmark locations at the root zone and total active soil profile predicted average soil water storage with 7 and 8% error, respectively (Biswas and Si, 2011a).

High rank correlation coefficients between any two-measurement series indicated strong time stability in the overall spatial patterns of soil water storage for the whole soil profile. Contrary to Gómez-Plaza et al. (2000) and Grayson and Western (1998), who did not find any field scale or transect scale time stability, the correlation coefficients from this study were comparable or even larger than those reported elsewhere (e.g. Martínez-Fernández and Ceballos, 2003; Mohanty and Skaggs, 2001; Hu et al., 2009).

The strong intra-season time stability of soil water storage may be due to similar processes operating within a season (Martínez-Fernández and Ceballos, 2003). The dominant processes operating in a season of one year (e.g., spring of 2008) may be similar to the dominant processes operating in that particular season of other years (e.g., spring of 2009 or 2010), which resulted in the inter-annual time stability. However, the dominant processes operating in different seasons within a year are different, leading to reduced inter-season time stability (Martínez-Fernández and Ceballos, 2003). Various authors have differentiated the preferred states in soil water spatial patterns (Kachanoski and de Jong, 1988; Grayson et al., 1997; Western and Blöschl, 1999), between wet season (Gómez-Plaza et al., 2000; Qui et al., 2001; Hupet and Vanclooster, 2002) and dry season (Robinson and Dean, 1993; Famiglietti et al., 1998). Our results clearly indicated strong intra-season and inter-annual time stability, no matter the soil is in wet or dry states. However, the degree of time stability changed with seasons or preferred states.

Wavelet coherency calculated the correlation between two soil water series at different scales and locations. Significant coherent relationships at any scale and location indicated the time stability of the spatial pattern of soil water storage at that scale and location. For example, the small-scale coherent relationship between spring and summer (Figure 4.5a) and between spring and fall (Figure 4.5b) at the locations of 35 – 50 m, 230 – 300 m, 370 – 480 m and from 540 m to the end of the transect, indicated the small-scale time stability at those locations. The small-scale time stability might have contributed from the localized variation in soil water storage and the measurement error. Non-significant relationships at other locations indicated the loss of time stability at the small scales. The loss of time stability or the change in the spatial pattern in soil water storage resulted from the change in hydrological processes operating at those scales and locations. The medium-scale correlations mainly represented the variations in

landform elements and micro-topography within a depression. The majority of the significant coherent relationships at medium-scale between spring and summer (Figure 4.5a) and between spring and fall (Figure 4.5b) were concentrated at the latter part of the transect. The large geographically low area at the end of the transect was not a real depression, rather it was the mid slope of a large depression (Figure 4.1) with less varying landform elements. Fewer landform elements within the depression might have contributed to the stronger similarity or time stability of the spatial pattern at those locations. Loss of time stability in other depressions was associated with variable vegetation growth in different landform elements as explained below. The change in the landform elements yielded the change in the hydrological processes, which determined the spatial pattern in soil water storage at the medium scales. However, the strong time stability in soil water storage at the scale of 90-100 m (Figure 4.4) can be attributed to the alternating knolls and depressions in the landscape. The large-scale alternating knolls and depressions in the landscape controlled the large-scale hydrological processes and thereby creating a very similar spatial pattern at any time of the year (Kachanoski and de Jong, 1988; Western et al., 1999).

Throughout the summer, vegetation gradually modified the spatial patterns of soil water storage formed during the spring. In the fall, vegetation had reduced evapotranspiration demand, leaving a spatial pattern very similar to that of summer. Therefore, the spatial patterns of soil water storage were very similar between summer and fall (Figure 4.5c) but less so between spring and fall (Figure 4.5b) (Martínez-Fernández and Ceballos, 2003).

The spatial pattern of soil water storage and its time stability for the surface soil layer was different from that of the whole soil profile (Cassel et al., 2000; Martínez-Fernández and Ceballos, 2003; Tallon and Si, 2004; Pachepsky et al., 2005; Guber et al., 2008; Hu et al., 2009). Generally, plants take up more than 70% of the water they need from the top 50% of the root zone (Feddes, 1978; Morris, 2006). Surface layers have highest root activity. Besides, the surface layers are subjected to atmospheric forcing and are very susceptible to change in any meteorological conditions (solar radiation, rainfall, wind effect) (Hu et al., 2010a), which make the surface layer very dynamic. The dynamic behavior of the surface layer equalized stored water over the transect during the latter part of the year, diminishing the topographically induced spatial pattern from spring (Figure 4.4; Tallon and Si, 2004), though there were still topographically induced spatial patterns in soil water storage for the whole profile (Figure 4.3).

The left directed arrow at the medium scale correlation between summer and fall and spring and fall measurement series showed time instability at those locations (Figures 4.8a and 4.8b). During spring, there was high soil water storage in depressions showing an upward peak in the spatial distribution. However, during summer and fall, the low water content in the middle of depressions and high water content just around it created a reverse peak in the spatial pattern of soil water storage (Figure 4.4). The large aquatic plants (growing more than 2 m high during late summer) at the middle of the depression pumped out more water from the surface layers than the grasses in surrounding riparian zone (Hayashi et al., 1998). The change in the processes contributed to the time instability at those locations.

The concept of time stability has been used to reduce a large measurement network to a few representative locations (Vachaud et al., 1985) and thus promising in reducing the cost, time, and labor associated with soil water measurement. The dominant scales and their associated locations of similar and dissimilar soil water spatial pattern over time can be determined from the scale and location specific relationship of the processes occurring between temporal measurements. The change in the similarity of the spatial patterns of soil water storage over time at different scales and locations is an indicative of the change in the hydrological processes operating at those scales and locations. Therefore, the analysis outcome can be used to identify the change in the sampling domain as controlled by the hydrological processes operating at different scales and locations delivering the maximum information with minimum sampling effort.

4.7 Conclusions

The spatio-temporal variability in the soil properties and the controlling factors make the spatial pattern of soil water storage and its time stability scale dependent. In this study, first we have examined the time stability of soil water storage overall spatial pattern using the Spearman's rank correlation proposed by Vachaud et al. (1985). Secondly, we used the wavelet coherency analysis to examine the time stability at different scales and locations.

High Spearman rank correlation coefficients indicated strong time stability in the spatial pattern of soil water storage. Stronger time stability was observed between the spatial series from a season (intra-season) compared to the time stability between season (inter-season). High time

stability was also observed between the measurement series from a particular season of different years (inter-annual). Wavelet coherency was used to identify the scales and locations of time stability. Stronger time stability at all scales and locations was observed between summer and fall, when the vegetation was present in field. However, the spatial pattern in spring was different from that of summer or fall. The large-scale (> 72 m) time stability was present over the whole transect. The medium-scale spatial patterns were time stable in large depressions that had fewer landform elements. However, the small-scale time stability was mostly random. Wavelet coherency analysis identified the change in the scales and locations of time stability with depth. The change in time stability at different scales and locations and at different depths indicated the change in the hydrological processes controlling the spatial pattern of soil water storage, which can be used to identify the change in sampling domain.

5.0 DEPTH PERSISTENCE OF THE SPATIAL PATTERN OF SOIL WATER STORAGE IN A HUMMOCKY LANDSCAPE

5.1 Preface

The similarity of the spatial pattern of soil water measured at different times was identified as the time stability. Is there any similarity between the spatial patterns of soil water measured at different depths at a particular time? The similarity between the spatial patterns of different depths may provide important information in understanding the hydrological processes operating at different layers of soil. For example, the surface soil water measurement is relatively easy. However, the similarity in the spatial pattern between the surface layer and subsurface layers will lead in understanding the deep layer hydrological processes from the surface measurement. The similarity at different depths is termed as depth persistence and is examined using the four-year soil water data collected from St. Denis National Wildlife Area.

5.2 Introduction

Soil water is a key determinant factor for infiltration, runoff, percolation, and evapotranspiration (Sivapalan, 1992). It also regulates the subsurface flow and migration of chemicals to environmentally sensitive areas such as surface water bodies and ground water. Soil water exhibits high spatio-temporal variability at different scales (Bell et al., 1980; Seyfried, 1998; Hupet and Vanclooster, 2002, 2005; Brocca et al., 2010), which makes the monitoring in large areas challenging. Information on soil water at different scales is required to improve hydrological and climatic modeling and prediction (Western et al., 2002; Koster et al., 2004).

Soil water is generally easier to measure in the surface soil than in the subsurface (Heathman et al., 2003). With the launch of several satellite instruments, remote sensing techniques showed promise in assisting hydrologists in describing and measuring surface soil-water for large areas (Brocca et al., 2009, 2010). However, plant roots, one of the most important factors regulating soil water storage, are not restricted to only surface layer. In addition, knowledge of surface soil water is often inadequate to understand hydrological processes. Therefore, information of soil water dynamics at different depths is necessary.

Soil water varies largely in space, depth, and time. However, if a field is surveyed repeatedly for soil water, some points may always be wetter and some would be drier than the field average. This means that the points within a field maintain their rank over time. Therefore, the spatial pattern of one measurement series will be similar to the spatial patterns of another. This phenomenon has been termed as time stability (Vachaud et al., 1985) of the spatial pattern of soil water. Time stability has been examined over a range of areas, sampling schemes, and sampling periods at different parts of the world. Similarity between the spatial patterns of soil water storage over time at different depths was also examined (Cassel et al., 2000; Pachepsky et al., 2005). However, information about the similarity or the persistence of the spatial pattern at different depths measured at a time is scarce. The persistence of the spatial pattern of soil water with depth may be termed as depth persistence.

The depth persistence can provide an opportunity to correlate the easy-to-measure surface soil water to the soil water at depth, and thus provide the necessary information in adopting the data assimilation techniques in integrating the remote sensing and soil water modeling (Jackson, 1993; Houser et al., 1998; Walker et al., 2001; Heathman et al., 2003). However, different factors and processes operating at different scales make the spatial pattern of soil water highly scale-dependent (Kachanoski and de Jong, 1988). Identifying the scales and the similarity of these scales of soil water at different depths can help build the scale-specific relationship between soil water contents of the surface and subsurface layers. Therefore, the objective of this study was to examine overall and scale-specific similarities of soil water spatial patterns at different depths. Spearman rank correlation analysis was conducted to measure the similarities between the overall spatial patterns at different depths and wavelet coherency was used to identify the scales of correlation in soil water series at any two different depths.

5.3 Materials and Methods

5.3.1 Site Description

The study site was located at St. Denis National Wildlife Area (SDNWA) in central Saskatchewan, Canada (52°12′ N latitude, 106°50′ W longitude). The landscape of this area is hummocky, which is characterized by a complex sequence of slopes extending from different-sized rounded depressions to irregular complex knolls and knobs (Pennock, 2005). This is the

dominant landscape type covering more than 80% of area in the Canadian prairie. The slopes of this area range from 10% to 15% (Figure 5.1). The soils of the area are mainly Dark Brown Chernozem (Mollisol in American system of soil classification) developed from moderately fine to fine-textured, moderately-calcareous, glacio-lacustrine deposits and modified glacial till (Saskatchewan Centre for Soil Research, 1989). Dominant climate of this area is semi-arid with mean annual air temperature (at the Saskatoon airport) of 2°C with a monthly mean of -19°C in January and 18°C in July (AES, 1997). Long-term (90 years) annual average precipitation of the study site is 360 mm, of which 84 mm occurs in winter months mostly as snow (AES, 1997). The vegetation of the site was mixed grass seeded by Ducks Unlimited Canada in 2004 and allowed to grow every year.

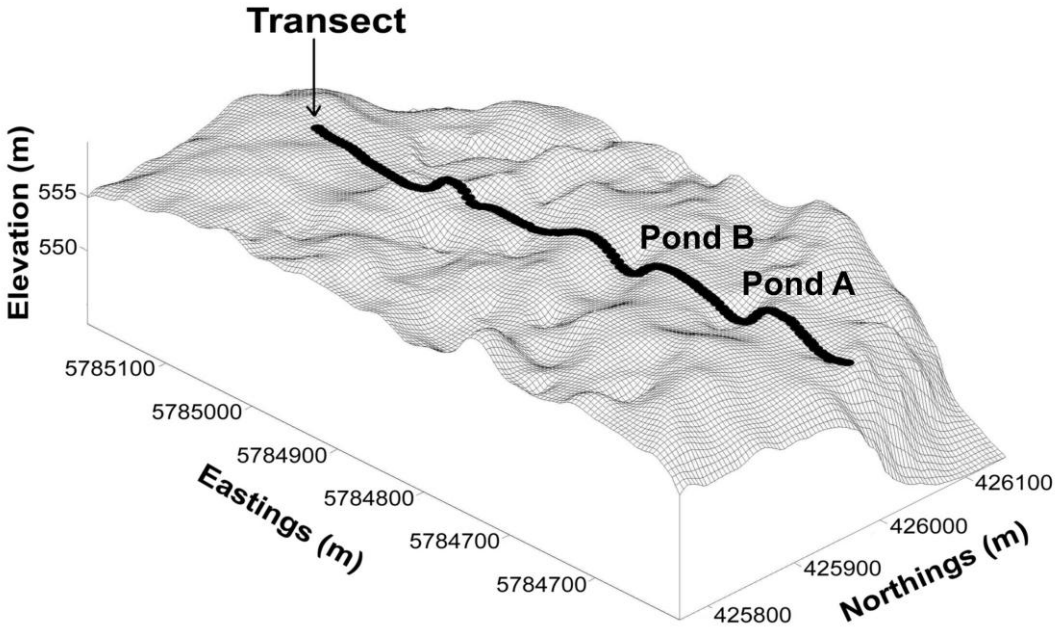

Figure 5.1. Transect position on the rolling landscape at St. Denis National Wildlife Area in central Saskatchewan, Canada.

5.3.2 Data Collection

A sampling transect of 128 points (576 m with regular interval of 4.5 m) was established in north-south direction over several rounded knolls and seasonal depressions representing different landform cycles (Figure 5.1). A topographic survey was completed using light detection and ranging (LiDAR) survey of the study area at a 5 m resolution. The digital elevation map (DEM) of the study area with transect position in the landscape is shown in Figure 5.1. Surface

soil water (0 to 20 cm) was measured using vertically installed time domain reflectometry (TDR) probe and a metallic cable tester (Model 1502B, Tektronix, Beaverton, OR, USA). A standard calibration equation, $\theta = 0.115\sqrt{k_a} - 0.176$ was used to calculate the volumetric water content in the surface layer (0 – 20 cm). Where the dielectric constant, $k_a = [L_2/L]^2$, L_2 is the distance between curves and the L is the length of the TDR probe (Topp and Reynolds, 1998). A CPN 501 DR Depthprobe (CPN International Inc., Martinez, CA, USA) was used to measure the soil water from 20 to 140 cm at 20-cm depth increments. The neutron probe was calibrated along the transect for several times over a three-year period (2007, 2008, and 2009) at different topographic locations and different moisture conditions. A truck mounted hydraulic drill was used to collect the core samples within 1 m radius of sampling locations. Volumetric water content was determined from the gravimetric water content and the bulk density. The neutron count at every 10 cm depth and the standard neutron count were recorded using the neutron probe. The procedure was completed for several times and a calibration equation was established from the volumetric water content and the neutron count ratio. The final calibration equation is $\theta_v = 0.8523\ R + 0.0612$ with $n = 101$ and $r^2 = 0.86$, where R is the ratio of neutron count to standard neutron count. The root mean squared error for the calibration equation is 0.016 $m^3\ m^{-3}$. Soil water was measured for 20 times (17 July 2007, 7 August 2007, 1 September 2007, 12 October 2007, 2 May 2008, 31 May 2008, 21 June 2008, 16 July 2008, 23 August 2008, 17 September 2008, 22 October 2008, 20 April 2009, 7 May 2009, 27 May 2009, 21 July 2009, 27 August 2009, 27 October 2009, 6 April 2010, 19 May 2010 and 14 June 2010) over a four-year period. The measurements were completed in different times during every year to represent different environmental events such as snowmelt, rainfall, or prolonged dry period. The measurements were completed after 2 to 3 days of the occurrence of different environmental events (e.g., rainfall) to ensure the quasi steady state in soil water storage The average water storage (in cm) was calculated for each 20 cm soil layer by multiplying the depth (20 cm) with soil water measured using the TDR and the neutron probe.

One of the important processes controlling the hydrology of the study area is snowmelt that takes place within a short period (Woo and Rowsell, 1993; Lungal, 2009). The snowmelt water fills up the depressions and increases the soil water content during early spring in the study area. In addition, the spring and the early summer rainfall also improves the water storage.

However, the only source of water loss during this period is evaporation from the bare ground and the surface of standing water and to a lesser extent, groundwater interaction (Hayashi et al., 1998; van der Kamp et al., 2003). The rate of water loss during this period is generally lower than that of water addition, which results in a net increase in soil water storage. Therefore, the spring and the early summer are considered as the 'recharge' period. However, with time, the vegetation establishes and utilizes the stored soil water. High evapotranspiration demand and the scanty precipitation during later summer and fall in the semi-arid climate deplete stored soil water and dry down the depressions. Even the vegetation around the depressions pulls water laterally and transpires to the atmosphere (Miller, 1971; Hayashi et al., 1998). As much as 70% of the infiltrated water under the depressions moves to local vegetation and is transpired thus drying up the depressions (Parsons et al., 2004). This period is generally considered as 'discharge' period. Though, the soil water storage was measured over four years (2007 – 2010), the space restriction of the manuscript only allowed us to present the data for only year (2008). Soil water storage was measured seven times in 2008. Based on the filling up and drying down the depressions and the overall soil water dynamics, the measurements were divided into two groups representing the recharge (4 measurements) and the discharge periods (3 measurements). Though, all the necessary analysis was performed for all measurements in all years, due to space restriction, we have only presented the details of two measurements, one from each period (2 May 2008 representing the recharge period and 23 August 2008 representing and the discharge period).

5.3.3 Data Analysis

Similarity of the overall spatial pattern of soil water storage was examined using Spearman's rank correlation analysis following Vachaud et al. (1985). Wavelet coherency analysis was completed using the MATLAB (The MathWorks Inc.) code written by Grinsted et al. (2004) and is available at URL: http://www.pol.ac.uk/home/research/waveletcoherence/. Theory of the wavelet coherency analysis is available elsewhere and beyond the scope of this paper. The detailed theory of wavelet coherency analysis can be found in Torrence and Compo (1998), Grinsted et al. (2004), and Si and Zeleke (2005).

5.4 Results

5.4.1 The Spatial Pattern of Soil Water Storage at Different Depths

There were two strong peaks in the spatial distribution of soil water storage at the surface 0 to 20 cm layer on a day (2 May 2008) during the recharge period (Figure 5.2). However, the height of the peak was lower in deeper soil layers (Figure 5.2). These peaks were concentrated at the locations of 100 to 140 m (Pond A in Figure 5.1) and 225 to 250 m (Pond B in Figure 5.1) from the origin of the transect. The soil water storage was 14.0 cm in the surface 0 to 20 cm layer at the 27^{th} point on the transect (Figure 5.2). The soil water storage was much higher than the average soil-water storage (6.3 cm) of that soil layer creating a wide range of storage (from 4.5 cm to 14.0 cm; Table 5.1). Average soil-water storage decreased from the surface (6.3 cm at the 0 to 20 cm layer) to the deepest layer (5.8 cm at 120 to 140 cm layer) on a day (2 May 2008) during the recharge period (Table 5.1). The coefficient of variation was the highest (28 %) in the surface layer (0 to 20 cm), and gradually decreased to 16 % at the deepest layer (120 to 140 cm). The standard deviation of soil water was the highest (1.7 cm) in the surface 0 to 20 cm layer and declined at deeper layers (Table 5.1). A similar trend was also observed at other day of measurements during the recharge period (Table 5.1).

The spatial distribution of soil water measurements on a day (23 August 2008) during the discharge period (Figure 5.3) was slightly different from that on a day (2 May 2008) during the recharge period (Figure 5.2). Depressions were dried up and the spatial distribution did not have strong peaks (high soil water storage). The average soil-water storage was 3.4 cm in the surface layer (0 to 20 cm) and gradually increased to the deepest layer (5.4 cm at 120 to 140 cm) on a day (23 August 2008) during the discharge period (Table 5.2). The difference between the maximum and minimum soil water contents was only 2.3 cm in the surface 0 to 20 cm layer (Table 5.2). CoV of soil water storage was 13 % in the surface (0 to 20 cm) layer and gradually increased to 19 % at the 80to 100 cm layer. Thereafter, the CoV decreased to 16 % at the deepest layer (120 to 140 cm) (Table 5.2). The standard deviation of soil water was the lowest in the surface 0 to 20 cm layer (0.43 cm) and gradually increased with depth (Table 5.2). A similar trend was observed for other measurements during the discharge period (Table 5.2).

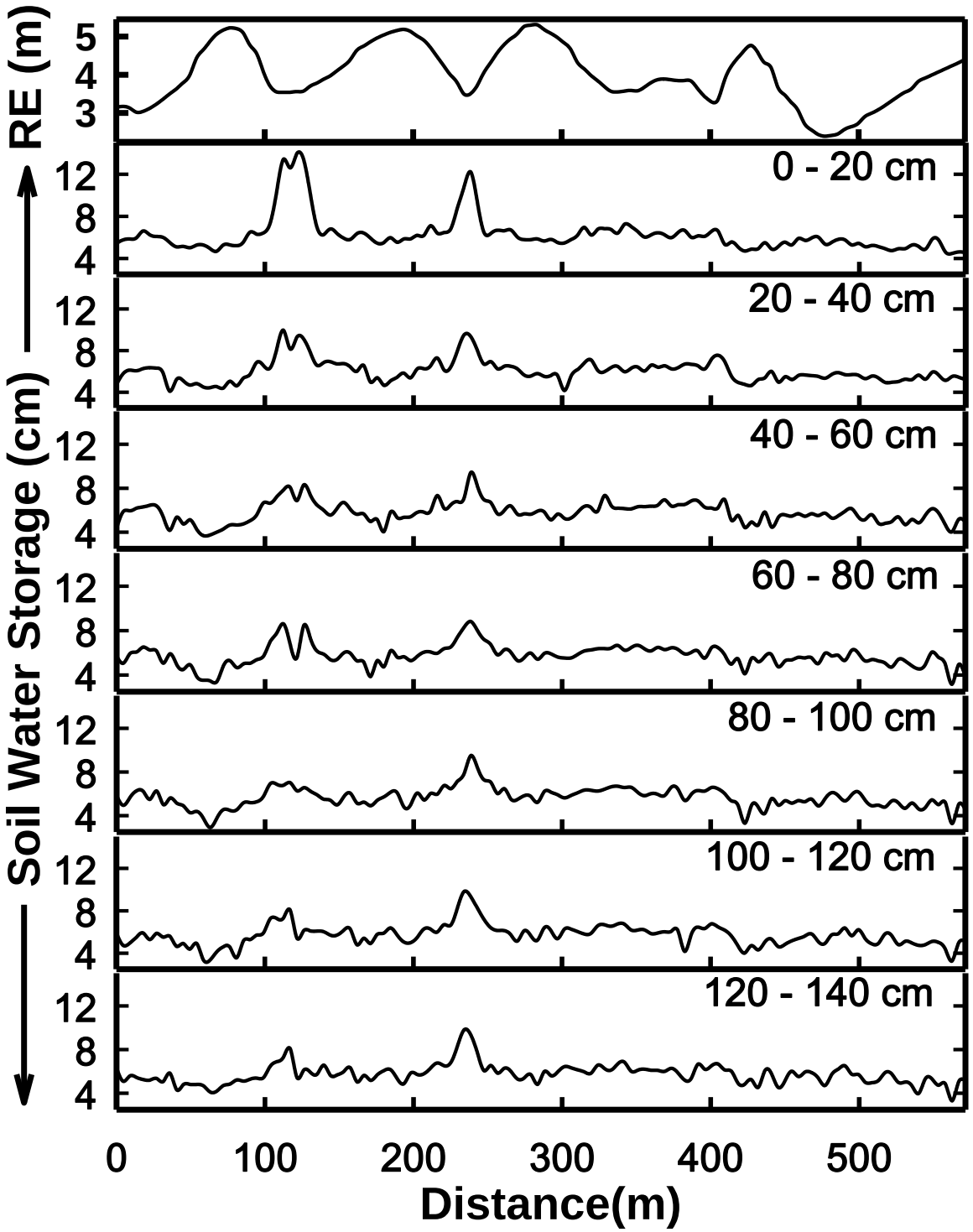

Figure 5.2. Spatial distribution of soil water storage at different depths on 2 May 2008 representing the recharge period with relative elevation (RE) at top. The X-axis indicates distance along the transect (m) and the Y-axis indicates soil water (cm).

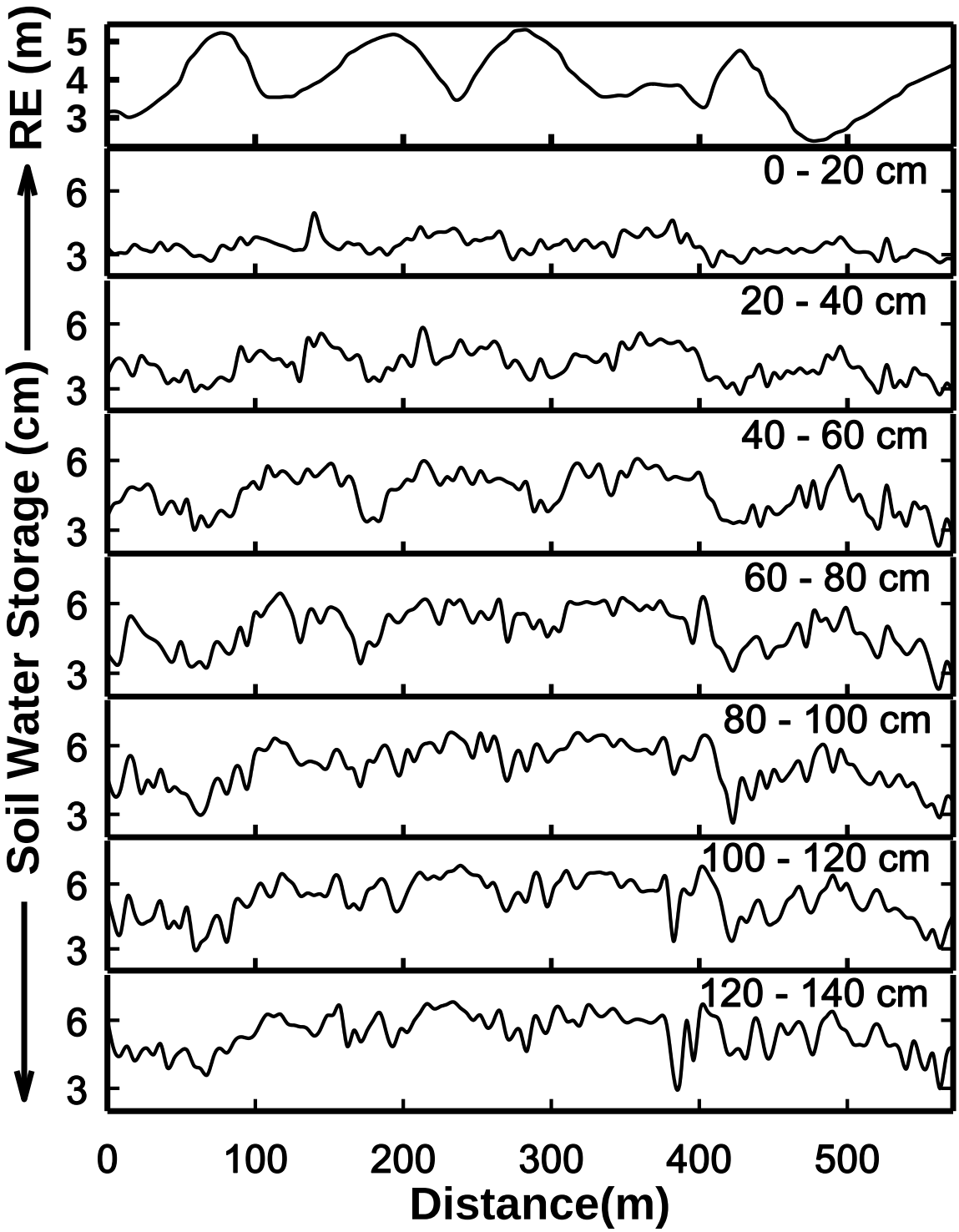

Figure 5.3. Spatial distribution of soil water storage at different depths on 23 August 2008 representing the discharge period with relative elevation (RE) at top. The X-axis indicates distance along the transect (m) and the Y-axis indicates soil water storage (cm).

Table 5.1. Descriptive statistics for measurement series from the recharge period at different depths

	Minimum (cm)	Maximum (cm)	Average (cm)	SD† (cm)	CoV‡ (%)
		2 May 2008			
0 to 20 cm	4.49	13.96	6.28	1.73	28
20 to 40 cm	4.09	9.96	6.03	1.08	18
40 to 60 cm	3.69	9.43	5.80	0.96	17
60 to 80 cm	3.16	8.83	5.74	0.97	17
80 to 100 cm	2.90	9.51	5.66	0.93	17
100 to 120 cm	3.26	9.81	5.70	1.02	18
120 to 140 cm	3.30	9.81	5.75	0.92	16
		31 May 2008			
0 to 20 cm	3.30	13.96	5.21	1.62	31
20 to 40 cm	1.54	9.28	5.51	1.00	18
40 to 60 cm	1.58	8.08	5.55	0.90	16
60 to 80 cm	3.00	6.85	5.58	0.81	15
80 to 100 cm	3.08	7.08	5.64	0.84	15
100 to 120 cm	3.22	8.08	5.70	0.87	15
120 to 140 cm	3.25	8.39	5.79	0.83	14
		21 June 2008			
0 to 20 cm	3.06	8.77	4.70	1.16	25
20 to 40 cm	3.43	7.84	5.25	0.96	18
40 to 60 cm	2.80	6.86	5.38	0.88	16
60 to 80 cm	2.77	6.78	5.52	0.84	15
80 to 100 cm	3.04	7.08	5.61	0.85	15
100 to 120 cm	3.28	7.73	5.69	0.86	15
120 to 140 cm	3.23	8.48	5.77	0.80	14
		16 July 2008			
0 to 20 cm	2.78	7.07	4.03	0.81	20
20 to 40 cm	3.06	6.78	4.77	0.94	20
40 to 60 cm	2.60	6.71	5.10	0.95	19
60 to 80 cm	2.56	6.75	5.30	0.91	17
80 to 100 cm	2.91	6.84	5.43	0.88	16
100 to 120 cm	3.17	6.98	5.56	0.87	16
120 to 140 cm	3.16	7.01	5.64	0.76	14

† SD- standard deviation, ‡ CoV- coefficient of variation

5.4.2 Similarity in the Overall Spatial Pattern of Soil Water Storage at Different Depths

Spearman rank correlation coefficients (r_s) between any two depths for any date were statistically significant ($p > 0.999$). The value of r_s was 0.84 between soil water storage of 0 to 20 cm and 20 to 40 cm layers and was 0.64 between 0 to 20 cm and 120 to 140 cm layers on a day (2 May 2008) during the recharge period (Table 5.3). The largest value of r_s was observed

between any two consecutive soil layers during the recharge period (Table 5.3), and gradually decreased with the increase in distance between soil layers. A similar trend in r_s was also observed for the other measurements during the recharge period (Table 5.3) and all measurements during the discharge period as well (Table 5.4). However, the value of r_s between any two layers during the discharge period (Table 5.4) was smaller than that during the recharge period (Table 5.3). For example, the value of r_s was 0.80 between 0 to 20 cm and 20 to 40 cm layers and was 0.48 between 0 to 20 cm and 120 to 140 cm layers on a day (23 August 2008) during the discharge period (Table 5.4). However, the value of r_s was 0.84 and 0.64 between the similar layers on a day (2 May 2008) during the recharge period (Table 5.3).

Table 5.2. Descriptive statistics for measurement series from the discharge period at different depths

	Minimum (cm)	Maximum (cm)	Average (cm)	SD† (cm)	CoV‡ (%)
		23 August 2008			
0 to 20 cm	2.44	4.96	3.40	0.43	13
20 to 40 cm	2.73	5.66	4.11	0.70	17
40 to 60 cm	2.37	6.02	4.59	0.86	18
60 to 80 cm	2.36	6.44	4.90	0.92	18
80 to 100 cm	2.63	6.56	5.12	0.92	19
100 to 120 cm	3.04	6.85	5.30	0.93	18
120 to 140 cm	2.99	6.81	5.42	0.84	16
		17 September 2008			
0 to 20 cm	2.66	4.64	3.51	0.45	13
20 to 40 cm	2.79	5.63	4.07	0.67	16
40 to 60 cm	2.49	5.91	4.55	0.83	18
60 to 80 cm	2.45	6.28	4.85	0.90	18
80 to 100 cm	2.63	6.59	5.05	0.91	18
100 to 120 cm	3.05	6.68	5.25	0.93	18
120 to 140 cm	2.96	6.91	5.37	0.86	16
		22 October 2008			
0 to 20 cm	3.83	6.11	4.96	0.50	10
20 to 40 cm	3.10	6.03	4.37	0.70	16
40 to 60 cm	2.52	5.92	4.53	0.84	18
60 to 80 cm	2.46	6.13	4.79	0.88	18
80 to 100 cm	2.63	6.55	5.00	0.90	18
100 to 120 cm	3.00	6.61	5.18	0.91	18
120 to 140 cm	1.22	6.73	5.28	0.93	18

† SD- standard deviation, ‡ CoV- coefficient of variation

Table 5.3. Spearman rank correlation coefficients (significant at < 0.001) between different depths during the recharge period

	0 to 20 cm	20 to 40 cm	40 to 60 cm	60 to 80 cm	80 to 100 cm	100 to 120 cm	120 to 140 cm
			2 May 2008				
0 to 20 cm	1.00	0.84	0.80	0.76	0.74	0.70	0.64
20 to 40 cm		1.00	0.86	0.74	0.71	0.65	0.59
40 to 60 cm			1.00	0.84	0.76	0.68	0.63
60 to 80 cm				1.00	0.89	0.79	0.74
80 to 100 cm					1.00	0.87	0.78
100 to 120 cm						1.00	0.89
120 to 140 cm							1.00
			31 May 2008				
0 to 20 cm	1.00	0.88	0.86	0.83	0.76	0.71	0.68
20 to 40 cm		1.00	0.92	0.85	0.82	0.76	0.73
40 to 60 cm			1.00	0.86	0.81	0.73	0.69
60 to 80 cm				1.00	0.89	0.80	0.75
80 to 100 cm					1.00	0.90	0.80
100 to 120 cm						1.00	0.89
120 to 140 cm							1.00
			21 June 2008				
0 to 20 cm	1.00	0.87	0.80	0.81	0.73	0.68	0.64
20 to 40 cm		1.00	0.88	0.87	0.81	0.75	0.73
40 to 60 cm			1.00	0.84	0.77	0.69	0.66
60 to 80 cm				1.00	0.90	0.81	0.75
80 to 100 cm					1.00	0.89	0.82
100 to 120 cm						1.00	0.88
120 to 140 cm							1.00
			16 July 2008				
0 to 20 cm	1.00	0.87	0.84	0.79	0.70	0.60	0.58
20 to 40 cm		1.00	0.92	0.85	0.76	0.67	0.63
40 to 60 cm			1.00	0.88	0.78	0.69	0.65
60 to 80 cm				1.00	0.89	0.79	0.73
80 to 100 cm					1.00	0.89	0.80
100 to 120 cm						1.00	0.87
120 to 140 cm							1.00

Table 5.4. Spearman rank correlation coefficients (significant at < 0.001) between different depths during the discharge period

	0 to 20 cm	20 to 40 cm	40 to 60 cm	60 to 80 cm	80 to 100 cm	100 to 120 cm	120 to 140 cm
			23 August 2008				
0 to 20 cm	1.00	0.80	0.74	0.65	0.55	0.49	0.48
20 to 40 cm		1.00	0.85	0.72	0.59	0.52	0.47
40 to 60 cm			1.00	0.84	0.69	0.61	0.54
60 to 80 cm				1.00	0.86	0.75	0.68
80 to 100 cm					1.00	0.89	0.78
100 to 120 cm						1.00	0.88
120 to 140 cm							1.00
			17 September 2008				
0 to 20 cm	1.00	0.81	0.73	0.68	0.60	0.55	0.53
20 to 40 cm		1.00	0.84	0.72	0.61	0.53	0.49
40 to 60 cm			1.00	0.82	0.66	0.59	0.52
60 to 80 cm				1.00	0.86	0.76	0.68
80 to 100 cm					1.00	0.88	0.78
100 to 120 cm						1.00	0.88
120 to 140 cm							1.00
			22 October 2008				
0 to 20 cm	1.00	0.72	0.69	0.64	0.56	0.48	0.48
20 to 40 cm		1.00	0.83	0.70	0.58	0.48	0.42
40 to 60 cm			1.00	0.83	0.67	0.58	0.49
60 to 80 cm				1.00	0.86	0.75	0.66
80 to 100 cm					1.00	0.87	0.78
100 to 120 cm						1.00	0.87
120 to 140 cm							1.00

5.4.3 Similarities in the Scales of Spatial Pattern at Different Depths

The scale-specific correlations between soil water at the surface layer and layers of different depth were examined using wavelet coherency analysis for the recharge period. The similarities among the coherency graphs between any two depths for all measurements were used to divide the scales into different groups; small (< 18 m), medium (18 to 72 m) and large (> 72 m) scales. There were very few locations that had significant correlation at small scales between soil water storage of 0 to 20 cm and 20 to 40 cm layers (Figure 5.4a), between 0 to 20 cm and 60 to 80 cm layers (Figure 5.4b), and between 0 to 20 cm and 120 to 140 cm layers (Figure 5.4c) on a day (2 May 2008) during the recharge period. The significant medium-scale correlations existed in the first half of the transect between the 0 to 20 and 20 to 40 cm layers, but reduced to

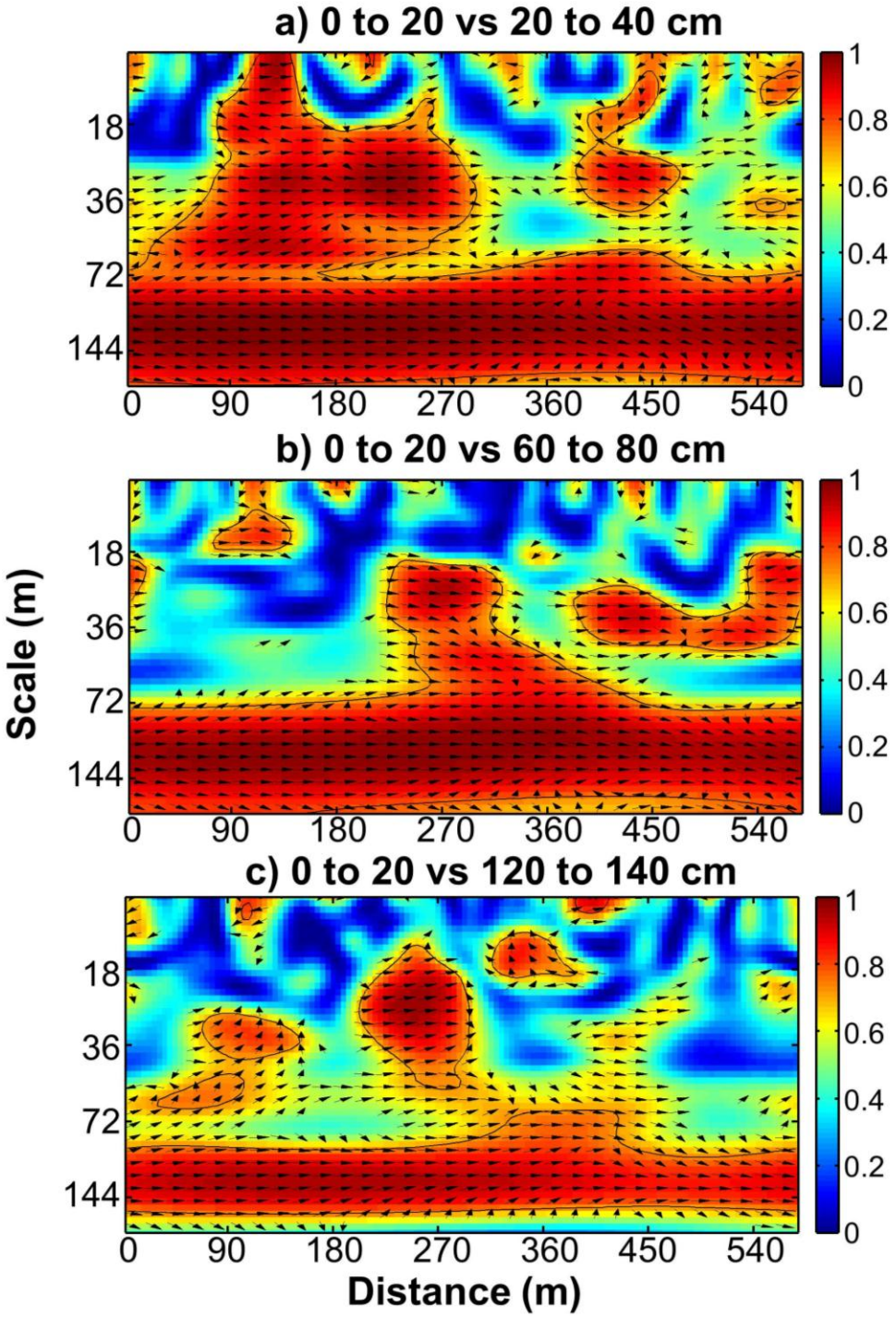

Figure 5.4. Wavelet coherency of soil water storage between a) 0 to 20 cm and 20 to 40 cm, b) 0 to 20 cm and 60 to 80 cm, and c) 0 to 20 cm and 120 to 140 cm depth layers measured on 2 May 2008 representing the recharge period. The X-axis indicates distance along the transect (m) and Y-axis indicates the scale (m). The color bar indicates the strength of the wavelet coefficients; the solid black line indicates 5% significance level; and the arrows indicate the phase relations.

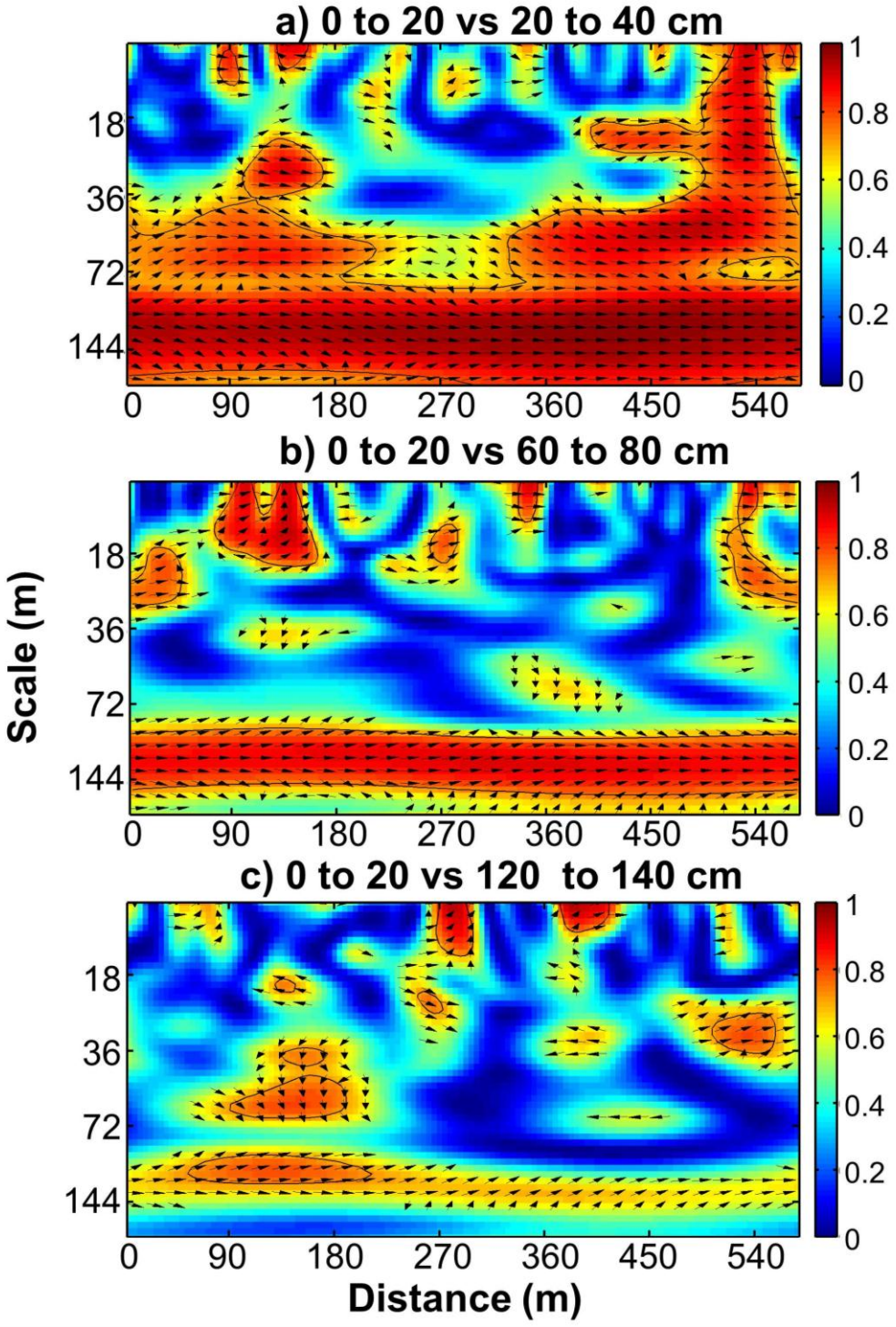

Figure 5.5. Wavelet coherency of soil water storage between a) 0 to 20 and 20 to 40 cm, b) 0 to 20 and 60 to 80 cm, and c) 0 to 20 and 120 to 140 cm depth layers measured on 23 August 2008 representing the discharge period. The X-axis indicates distance along the transect (m) and Y-axis indicates the scale (m). The color bar indicates the strength of the wavelet coefficients; the solid black line indicates 5% significance level; and the arrows indicate the phase relations.

a limited number of locations between the 0 to 20 cm and 60 to 80 or 120 to 140 cm layers (Figures 5.4a, 5.4b, and 5.4c). However, the large-scale spatial patterns were very similar between the surface 0 to 20 cm layer and any deeper layers (e.g., 20 to 40 or 80 to 100 or 120 to 140 cm) on 2 May 2008 during the recharge period (Figure 5.4).

On a day (23 August 2008) during the discharge period, however, there were only a few locations with significant correlations at small scales between the 0 to 20 cm and each of the 20 to 40, 60 to 80, and 120 to 140 cm layers (Figures 5.5a, 5.5b, and 5.5c). Significant correlations at the scale of 36 to 72 m were found across the transect between the 0 to 20 and 20 to 40 cm layers (Figure 5.5a). However, there were no significant correlations at the scale of 36 to 72 m between the 0 to 20 cm and 60 to 80 cm layers (Figure 5.5b) or were limited to few locations such as 90 to 200 m and 500 to 550 m between 0 to 20 cm and 120 to 140 cm layers on a day (23 August 2008) during the discharge period (Figure 5.5c). The significant correlations existed over the whole transect at the scales > 72 m between 0 to 20 cm and 20 to 40 cm layers (Figure 5.5a) and at the scale of 80 to 150 m between the 0 to 20 and 60 to 80 cm layers (Figure 5.5b) on a day (23 August 2008) during the discharge period. However, the significant correlations were found only at locations of 60 to 220 m between 0 to 20 cm and 120 to 140 cm layers (Figure 5.5c). Comparing Figure 5.4 to Figure 5.5, we observed that large-scale correlations in the recharge and the discharge periods were very similar between 0 - 20 cm and 20 - 40 cm layers (Figures 5.4a and 5.5a), and were slightly different between 0 to 20 cm and 60 to 80 or 120 to 140 cm layers. A similar trend in the spatial patterns of soil water storage at surface layer with deeper soil layers was also observed on other measurements during recharge and discharge periods.

An effort has also been made to understand the similarity between the scales of soil water storage at a particular depth between any two measurements. There were very few locations such as 180 to 210 m and 380 to 480 m that had statistically significant correlations at small scales among the 0 to 20 cm layer measurements (Figure 5.6a) of 2 May 2008 and 23 August 2008. However, the significant correlation was observed at small scales from 250 m to the end of the transect between the 60 to 80 cm layer measurements (Figure 5.6b) and almost all over the transect between the 100 to 120 cm layer measurements (Figure 5.6c) of 2 May 2008 and 23 August 2008. While, at the 0 to 20 cm layer (Figure 5.6a), the significant correlation at medium scales was concentrated only within the first half of the transect, it was mainly concentrated

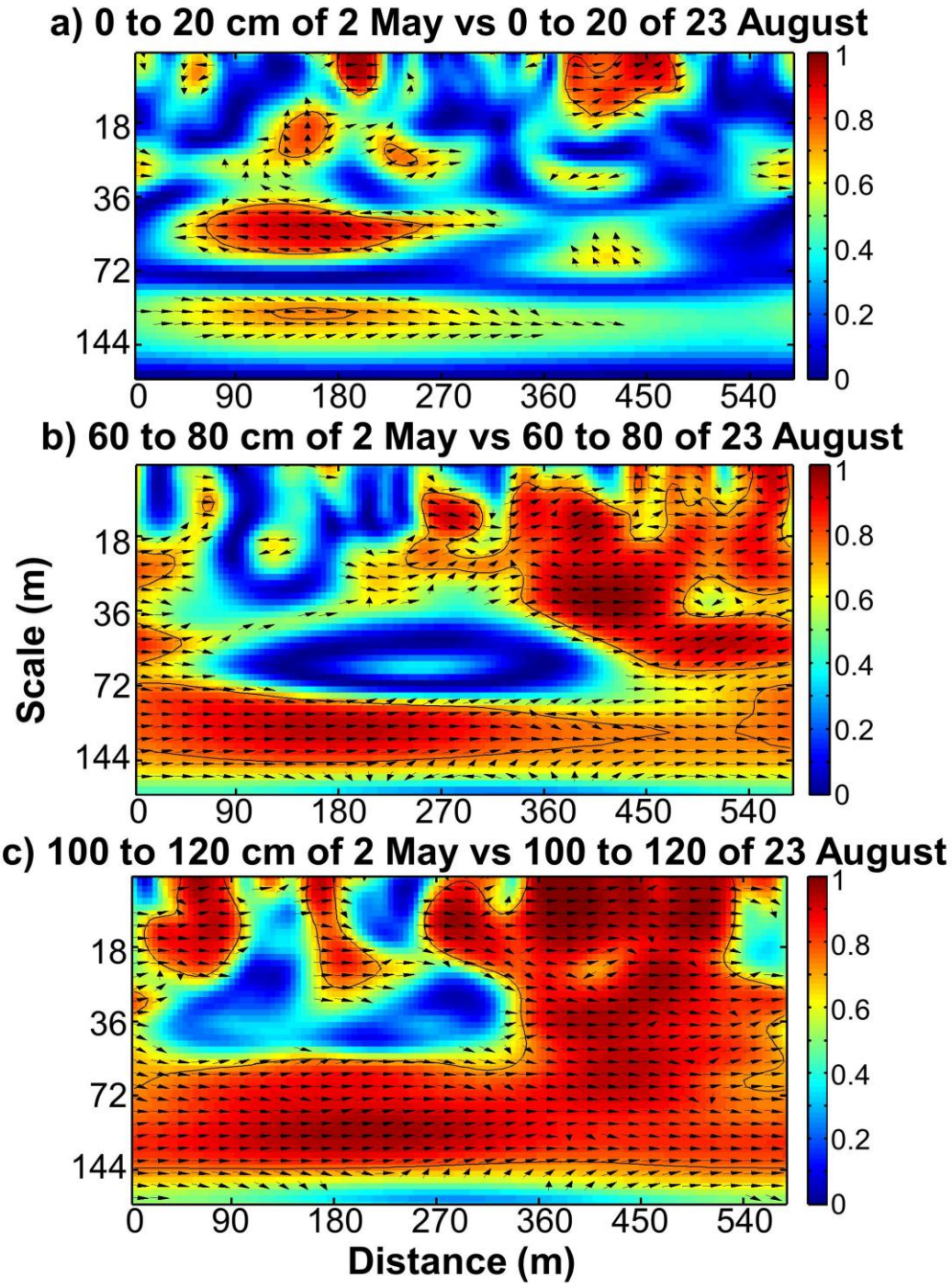

Figure 5.6. Wavelet coherency of soil water storage between a) 0 to 20 cm, b) 60 to 80 cm, and c) 100 to 120 cm between 2 May 2008 and 23 August 2008. The X-axis indicates distance along the transect (m) and Y-axis indicates the scale (m). The color bar indicates the strength of the wavelet coefficients; the solid black line indicates 5% significance level; and the arrows indicate the phase relations.

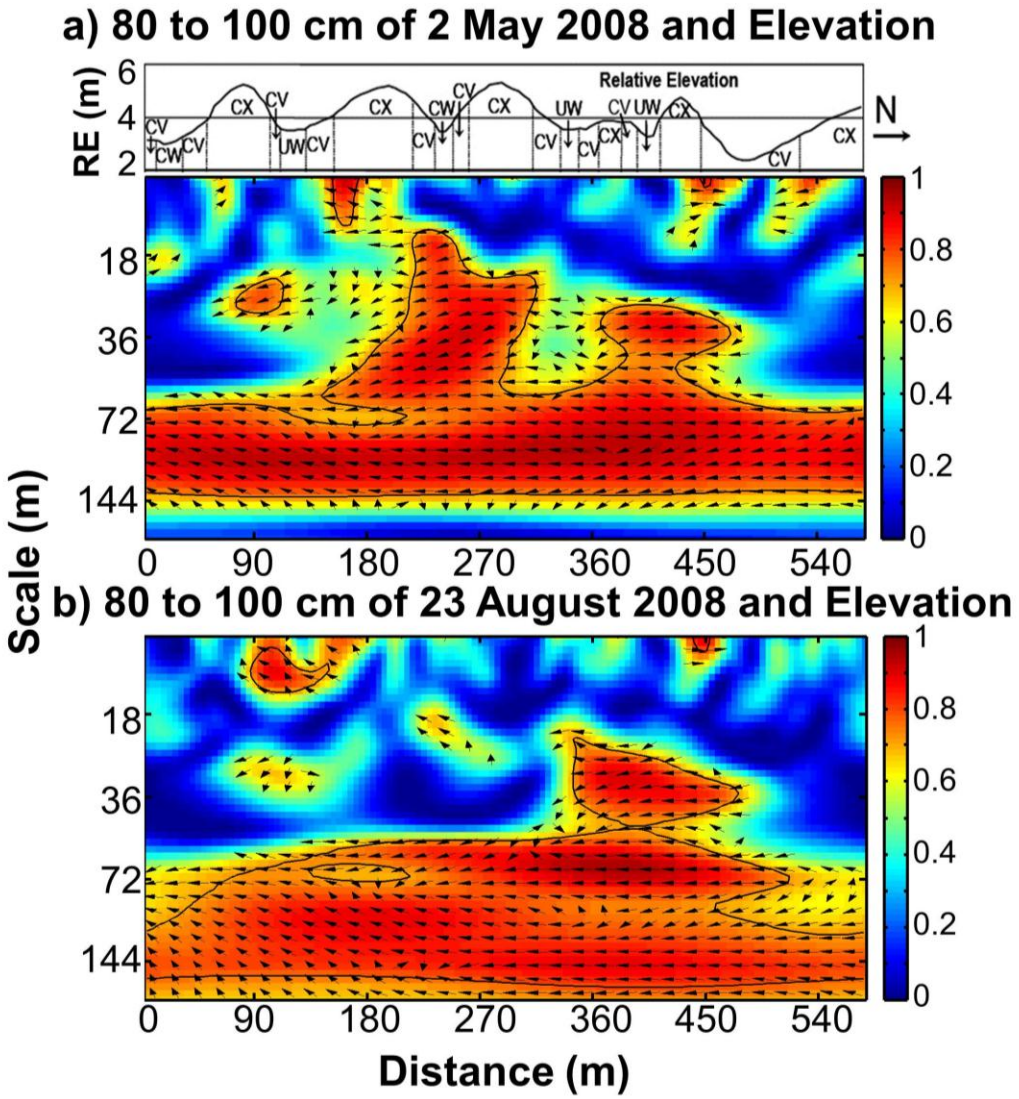

Figure 5.7. Wavelet coherency between a) soil water storage (80 to 100 cm) on 2 May 2008 and relative elevation (RE) and b) soil water storage (80 to 100 cm) on 23 August 2008 and relative elevation. The graph of relative elevation shows different landform elements; CV stands for concave, CX stands for convex, UW stands for uncultivated wetlands, and CW stands for cultivated wetlands. The X-axis indicates distance along the transect (m) and Y-axis indicates the scale (m). The color bar indicates the strength of the wavelet coefficients; the solid black line indicates 5% significance level; and the arrows indicate the phase relations.

within the second half of the transect at the 60 to 80 (Figure 5.6b) and 100 to 120 cm (Figure 5.6c) layers. A similar trend was observed at large scales for the 0 to 20 cm layer (Figure 5.6a). However, the significant correlation was present all over the transect at the 60 to 80 (Figure 5.6b) and 100 to 120 cm (Figure 5.6c) layers.

The difference in wavelet coherency between different depths in the recharge or discharge periods was also examined in terms of area of significant correlation. The total area representing significant correlations at different scales gradually decreased with the increase of distance between surface layer and subsurface layers for both recharge and discharge period (Figures 5.4 and 5.5). Similarly, the total area representing significant correlations was also lower for the day during the recharge period compared to the discharge period. However, an increase in the total area of significant correlation between the layers from different measurements was observed with the increase of depth (Figure 5.6). In addition, the type of correlation was also examined from the wavelet coherency spectra.

The right directed arrows within the significant area indicated the 'in phase' relationship or positive correlation between any two depths (Figures 5.4 and 5.5). However, left directed arrows at the medium scale between the 0 to 20 cm layer of 2 May 2008 and 23 August 2008 indicated the 'out of phase' relationship or negative correlation (Figure 5.6). A similar 'out of phase' relationship was observed between soil water storage and elevation at both the recharge and discharge periods (Figure 5.7).

5.5 Discussion

In the study area, approximately 30% of the annual precipitation occurs as snow during winter (Pomeroy et al., 2007). Strong wind in the prairie region redistributes snow from knolls to depressions, creating an uneven distribution in the landscape (Pomeroy and Gray, 1995; Fang and Pomeroy, 2007; Lungal, 2009). Fast snowmelt during early spring contributes a large amount of water within a short period. However, the frozen ground at that time does not allow much water to enter the soil and snowmelt water runs off to depressions (Gray et al., 1985; Woo and Rowsell, 1993; Hayashi et al., 1998). In our study, the locations of 100 to 140 m (Pond A in Figure 5.1) and 225 to 250 m (Pond B in Figure 5.1) along the transect were located in two depressions. There was much higher soil water storage in depressions than on knolls, creating a wide range of soil water storage in the landscape for all depths during the recharge period (Figure 5.2; Flerchinger and Cooley, 2000).

However, generally the soil-water storage capacity decreases with the increase in bulk density and the decrease in soil organic matter from the surface to deep layers. In our study, as

such the soil water storage at the surface layer was much higher than that at deeper layers during the recharge period (Table 5.1). In addition, soil water at the surface had stronger variability than in the subsurface which may be a result of highly variable organic matter content at the surface (CoV = 41%). The topography resulted in differences in exposure to solar radiation, wind, local rainfall distribution, enhancing the variability of surface soil water (Hu et al., 2010a). Therefore, there were higher CoV values of soil water storage in the surface soil than soil at deeper layer during the recharge period (Table 5.1). In addition, deeper soil layers are less influenced by the meteorological conditions, creating 'inertia' in soil water dynamics (Martínez-Fernández and Ceballos, 2003). Therefore, standard deviation and variability in soil water were smaller at depth than at surface.

A large amount of water was stored in local depressions, allowing plants to grow much faster than those growing on knolls. Leaf area index (unpublished data) and visual observation clearly suggested biomass production on knolls was much smaller than that in depressions. Increased evapotranspiration demand from vegetation in depressions reduced the difference (small range) in soil water storage along the transect. Plants generally take up more than 70% of the water they need from the top 50% of the root zone (Feddes et al., 1978; Morris, 2006). The intense root activity in the surface layer depleted stored water irrespective of landscape positions and equalized soil water over the transect. Therefore, there was a small CoV and SD in soil water measurements in the surface layer compared to the CoV at depth during later summer and fall. However, as the most active roots are located within a meter of the soil surface (Hu et al., 2009; Si and de Jong, 2007), the variability in the soil water measurement at the deepest layer during the discharge period (Table 5.2) was very similar to the variability at the deepest layer during the recharge period (Table 5.1).

High rank correlation coefficients between soil water measurement series at any two depths indicated strong depth persistence in the overall spatial patterns during any time. This may be due to less heterogeneity between soil layers, which could not completely de-couple the surface hydrology from the subsurface ones. However, the correlation coefficients between the surface layer and subsurface layers gradually decreased with the increase of distance between them. For example, the soil water storage in the layer (20 to 40 cm) close to the soil surface layer showed the highest correlation and the soil water storage in the layer (120 to 140 cm) far from

the surface layer yielded the lowest correlation with soil water in the surface layer (0 to 20 cm). Similar results were also reported in the literature (Martínez-Fernández and Ceballos, 2003; Tallon and Si, 2004; Pachepsky et al., 2005; Guber et al., 2008; Hu et al., 2009). This is because the impact of soil water processes such as runoff, evapotranspiration controlling the spatial patterns of soil water storage at the surface layer gradually decreased with increase in depth and therefore providing a smooth change in the control of soil water dynamics. For example, deeper layers had less response to the changes in meteorological conditions (Hu et al., 2010a), less root activity (Cassel et al., 2000) or less disturbed soil structure (Guber et al., 2003; Pachepsky et al., 2005).

Similarly, particular processes (such as runoff) operating in the recharge periods may be in different intensity from that in the discharge period, resulting in reduced Spearman rank correlation between soil water of two depths from the recharge period to the discharge period (Tables 5.3 and 5.4). This is different from Grayson et al. (1997) who indicated different major controls of soil water storage in different seasons.

Significant coherent relationships between soil water contents at different depths at a scale and location indicated the depth persistence of the spatial pattern of soil water storage at that scale and location. Significant coherency at medium-scales may be attributed to the variations in landform elements and micro-topography within depressions. The significant medium-scale correlations at these locations were associated with more variation in landform elements (Figure 5.7). However, strong depth persistence at large scales (> 72 m) may be a result of alternating knolls and depressions (Biswas and Si, 2011b). The correlation between elevation and 80 to 100 cm layers of 2 May 2008 and 23 August 2008 clearly showed the large-scale dependence of soil water on elevation (Figure 5.7). The decrease in the total area of significant coherency and its intensity at different scales from the surface to subsurface layers and from recharge to the discharge period indicated the reduction in the degree of depth persistence. The degree of persistence changed with depth and season, indicating the change in the intensity of controls; however, the scale of dominant variation remained the same, regardless of depth and season. The strong evapotranspiration demand yielded much change in the relationship between the surface layer and subsurface layers during the discharge period. The maximum change in the relationship also occurred in the surface layer from recharge to discharge period. However, with

depth, the total area of significant relationship was much larger with the maximum at the deepest layer, which indicated strong similarity in the processes operating at depth (largest area of significant correlation at deepest layer in Figure 5.6). Greater the depth, more stable the hydrological dynamics is. Therefore, the maximum similarity in the spatial pattern of large scales at the deepest layer indicated the similarity in the hydrological processes operating at the scale > 72 m, which may be controlled by topography (Figure 5.7). However, the medium scale spatial pattern of the most dynamic surface layer (0 to 20 cm) even reversed from the recharge to discharge period (left directed arrow at medium scale between 0 to 20 cm of 2 May 2008 and 23 August 2008). This may be due to the exposure of surface layer to atmosphere and the lush growth of aquatic vegetation (growing more than 2 m in height) within the depressions during later summer and thus pumping out the water at its maximum.

The persistence in the spatial patterns of soil water storage between the surface layers and deeper layers can be used to correlate the easy-to-measure surface soil water to the soil water of subsurface layers. This can improve the understanding of soil water dynamics of subsurface layers from the surface measurements. The persistence of the spatial pattern at large-scales can be used to improve the prediction of soil water storage at depth, thus is promising in reducing the cost and resources. In this study, the soil water was measured at different depths along a transect for different time representing two-dimensional spatial field. However, the soil water dynamics is not confined to two dimensions and therefore future study is necessary to understand the soil water variation in three dimensions over time.

5.6 Conclusions

Soil water is characterized by high spatio-temporal variability, which makes the monitoring of soil water in a large area challenging. Measurement of soil water at the land surface is easier than that at depth. During the recharge period, soil water was highly variable in the surface layer. The variation gradually decreased with increasing soil depth. However, during the discharge period, the variation of soil water storage was minimal at the surface layer probably due to intense root water uptake in the surface layer. The variation in soil water gradually increased up to the depth of one meter, and decreased subsequently. The overall spatial pattern of the surface layer was very similar to the layers closest to the surface and gradually

decreased with the increase in distance between the layers. The large-scale (> 72 m) spatial pattern of the surface layer was persistent in the subsurface layers during the recharge period. However, the degree of persistence at large scales reduced during the discharge period indicating the change in the intensity of the control. The soil water spatial pattern at the small and medium scale changed with depth during the recharge and discharge periods. The correlation between the spatial patterns of soil-water at the surface layer and subsurface layers benefited from the persistence of the large-scale patterns, but reduced from inconsistent spatial patterns at small and medium scales. The scale information of soil water variations at different depths helps determine if the easy-to-measure surface soil water can be used to estimate soil water at depth and understand the landscape hydrological dynamics.

6.0 FACTORS CONTROLLING SOIL WATER STORAGE IN THE HUMMOCKY LANDSCAPE OF THE PRAIRIE POTHOLE REGION OF NORTH AMERICA

6.1 Preface

The spatial variability soil water is mainly affected by physical properties such as soil texture, vegetation, and topography in natural catchment or agricultural land. Contradictory findings available on the dominant control of soil water storage in different situation. The mutual influence and multiple controls have also been reported. Comprehensive information on the controls of soil water storage is scarce in the prairie pothole region of North America, which contains a unique hummocky landscape. This chapter examines the correlation between soil water storage and various controlling factors using Pearson correlation analysis in the hummocky landscape.

6.2 Introduction

The "prairie pothole region" (PPR), the largest wetland landscape in North America, encompasses approximately 775,000 km^2 from the north-central United States to south-central Canada and contains around 5 to 60 wetlands per km^2 (National Wetlands Working Group, 1997). These wetlands, commonly termed potholes, provide important hydrological and ecological functions, such as supporting nesting for various birds (Ogaard et al., 1981; Johnson et al., 2005), acting as a sink for agriculturally-derived nutrients (van der Valk, 1989; Whigham and Jordan, 2003), and storing surface water, which can attenuate flood flows (Hubbard and Linder, 1986; Gleason and Tangen, 2008). Therefore, understanding the factors controlling the distribution of water in the pothole landscape is important, which can infer about the ground water fluctuations, runoff generation, and the changes in stream-flow volume.

The wetlands and the knolls in the landscape that formed during the Pleistocene glacier retreat created a unique hummocky topography in the PPR (Huel, 2000). In addition to various static and dynamic factors, topography plays an important role in redistributing incoming water in this type of landscape, thus forming a unique spatial pattern (Woo and Rowsell, 1993; Hayashi et al., 1998). Moreover, the spatial pattern of soil water from snow-dominated precipitation is largely dictated by the variability of snow accumulation and melt in the landscape (Woo and

Rowsell, 1993; Litaor et al., 2008; Lungal, 2009). For example, the potholes receive water through runoff from the melting of snow that accumulates in uplands and wetland areas during winter and from precipitation during summer. However, the water loss from the closed basins is almost entirely by the evapotranspiration and to a lesser extent the deep infiltration or ground water interaction (Hayashi et al., 1998; van der Kamp et al., 1999). The contribution of infiltration, runoff, and lateral redistribution make the soil water highly variable within the pothole landscape and of utmost interest in hydrological studies in small- and medium-scale catchments or watersheds.

Much research has been devoted in understanding the dynamics of soil water over time and space at different climatic conditions and landscapes. There are different factors and processes that work alone or in combination to control the spatial variability of soil water. Various authors have suggested that soil properties are the major control on soil water variability (Vachaud et al., 1985; Mohanty and Skaggs, 2001; Starks et al., 2006; Cosh et al., 2008), while others have indicated that the main control is topography (Famiglietti et al., 1998; Western et al., 1999; Thierfelder et al., 2003; Brocca et al., 2007, 2009). While soil properties control the entry and vertical movement of water in the soil, topography controls the lateral redistribution of surface and subsurface flow and generated runoff in the landscape (Beven and Kirkby, 1979; Brocca et al., 2007). Various terrain indices characterizing topography have been used to represent different key hydrological processes controlling soil water distribution in the landscape because of their variable effects (Western et al., 1999). For example, the surface slope influences the hydraulic gradient driving any surface and subsurface flows when the groundwater has a similar slope to the ground surface (Western et al., 1999). However, while the surface slope and aspect together can influence both rainfall input and radiation flux (Sharon, 1980), the convergence index can measure the local convergence or divergence of lateral flow (Western et al., 1999). These factors have variable effect in controlling soil water storage and sometimes the combined effect can be more than 50 percent of the total variability (Tomer and Anderson, 1995). Therefore, it is necessary to identify the most important terrain indices controlling the distribution of soil water in the PPR.

The effect of different terrain indices as well as the soil properties can be different in different initial or antecedent soil-water conditions (Grayson et al., 1997; Western et al., 1999;

McNamara et al., 2005). For example, in wet situations, where precipitation exceeds evapotranspiration, hill slopes are hydraulically connected and lateral redistribution (surface and subsurface) can occur according to different terrain indices. However, when evapotranspiration exceeds precipitation, hill slopes are not hydraulically connected and vertical fluxes dominate. Grayson et al. (1997) divided the factors controlling spatial pattern of soil water at these situations into nonlocal and local factors, respectively. They also mentioned high water content in topographic convergence areas during the transition period from dry to wet.

However, Tallon and Si (2004) did not find any strong correlation between soil water spatial patterns and soil properties or terrain indices suggesting the absence of a single controlling factor. Therefore, the controls of spatial distribution of soil water can be a combinations of static (e.g., topography, soil variables) and dynamic (e.g., antecedent moisture) variables (Reynolds, 1970). The interaction among the controlling factors may contribute to the combined control from different factors. Choi et al. (2007) combined the results from several studies on grasslands and croplands in Europe and USA and concluded that the rainfall and topography control the change in soil water variability under drying-wetting cycle, while soil parameters control the relative amplitude.

The influences of different factors (e.g., soil, vegetation, topography, and precipitation) on soil water has been extensively investigated in different landscapes and environments (Vachaud et al., 1985; Famiglietti et al., 1998; Gómez-Plaza et al., 2001; Western et al., 2004; Brocca et al., 2007). Hydrology for an independent pothole was also studied (Hayashi et al., 1998). However, very few studies have documented the controlling factors of soil water in the unique hummocky landscapes (Kachanoski and de Jong, 1988; Tallon and Si, 2004), which contains a very complex sequence of slopes originating from the rounded depressions to complex knolls (Pennock, 2005) and therefore creating challenge in understanding hydrological processes within this area. Comprehensive comparison of relative roles of different soil factors (e.g., soil properties, bulk density, depth of different horizons, depth of carbonate layer, etc.) and terrain indices (elevation, wetness index, convergence index, slope, flow connectivity etc.) in controlling soil water distribution in the hummocky landscape are rare.

Understanding the spatial distribution of soil water storage and its dominant controlling factors in the hummocky landscape would allow a better assessment of wetland functions in the

landscape and improved accuracy of hydrological models that predict the water balance, including stream-flow in watersheds within the PPR (Fang and Pomeroy, 2007). The relative roles of different factors in controlling the spatial patterns of soil water storage in different seasons can provide information on temporal evolution of different vertical and lateral hydrological processes occurring at different initial soil water condition. This would provide a better understanding of dominant hydrological, ecological, and biogeochemical processes in the PPR, as most of these processes are related to the soil water content. Therefore, the objective of this study was to understand the controls of soil water storage in the hummocky landscape of PPR over different times with different soil water condition.

6.3 Materials and Methods

The St. Denis National Wildlife Area (SDNWA) in central Saskatchewan, Canada (52°12′ N, 106°50′ W) is a typical hummocky landscape of the North American PPR. It contains 216 wetlands distributed over an area of 3.84 km^2 (Hogan and Conly, 2002). A sampling transect of 576 m long extending north-south direction was established with 128 sampling points over several knolls and depressions in the SDNWA. The soil of this area is mainly Dark Brown Chernozem developed from moderately fine to fine-textured, moderately-calcareous, glacio-lacustrine deposits and modified glacial till (Saskatchewan Centre for Soil Research, 1989). The climate of the study area is semi-arid in nature with long-term (90 years) average precipitation 360 mm of which 84 mm occurs in winter months mostly as snow (AES, 1997). The study area received total precipitation of 366 mm, 331 mm, and 402 mm, respectively during the year of 2007, 2008, and 2009. The average annual air temperature (at Saskatoon airport, 40 km west of study site) is 2°C with monthly average of -19°C in January and 18°C in July (AES, 1997).

Surface soil water (0 to 20 cm) was measured using vertically installed time domain reflectometry (TDR) probe and a metallic cable tester (Model 1502B, Tektronix, Beaverton, OR, USA). A standard calibration equation (Topp and Reynolds, 1998) was used to determine the soil water content from the TDR recordings. Soil water content at 20 to 140 cm depth was measured using a neutron probe (Model CPN 501 DR Depthprobe, CPN International Inc., Martinez, CA, USA) with the vertical depth interval of 20 cm. For neutron probe soil-water measurement, sample points were installed with 5 cm diameter and 200 cm long plastic tubes (PVC) using a

truck mounted hydraulic drill. The open end of the PVC tubes were kept closed using cap to prevent the entry of water in the tube, which was used as neutron access tube for measuring soil water. The bulk density (BD) at depths and locations along the transect was measured during the installation of neutron access tubes. The neutron probe was calibrated using soil cores taken at different depths from the proximity of neutron access tubes using a truck mounted hydraulic drill. The soil cores of 10 cm height were subsequently wrapped in polythene film and transported to laboratory for measuring bulk density and gravimetric soil water. The volumetric soil water was calculated from the gravimetric soil water and bulk density and compared with neutron count ratio. This procedure was repeated for different landscape positions at different moisture conditions during 2007, 2008, and 2009. The final calibration equation is $\theta_v = 0.8523\ R + 0.0612$ with $n = 101$ and $r^2 = 0.86$, where R is the ratio of neutron count to standard neutron count.

Soil water was measured in different environmental situation (e.g., spring snowmelt, drying summer, dried fall) for 20 times over a four year period (17 July 2007, 7 August 2007, 1 September 2007, 12 October 2007, 2 May 2008, 31 May 2008, 21 June 2008, 16 July 2008, 23 August 2008, 17 September 2008, 22 October 2008, 20 April 2009, 7 May 2009, 27 May 2009, 21 July 2009, 27 August 2009, 27 October 2009, 6 April 2010, 19 May 2010 and 14 June 2010). The measurements were completed at least after 2 to 3 days of any environmental event to make sure that the quasi steady state of soil water dynamics was reached. Soil water storage up to 140 cm was determined by multiplying the depth with water content calculated form the neutron probe calibration relationship and the TDR measurement.

The topographic survey of the study site was completed using Light Detection and Ranging (LiDAR) at 5 m resolution. The digital elevation map of the study site was prepared from LiDAR survey data using SURFER (Golden Software Inc., Golden, CO, USA) software. The geographic location of sample points and elevation was noted using Trimble Pro XRS Global Positioning System (Trimble Navigation, Sunnyvale, CA, USA). Different terrain indices for every sample points were calculated using open source Geographic Information System (GIS) software named System for Automated Geoscientific Analyses (SAGA) (available online at http://www.saga-gis.org/en/index.html). The terrain indices included wetness index, catchment area, convergence index, curvature, aspect, gradient, slope, slope length, solar radiation, and flow

connectivity. The horizon identification and the soil classification were completed at each sample point following Canadian System of Soil Classification (Soil Classification working group, 1998). The depth of A and C horizon was measured from the surface in centimeter. The depth of calcium carbonate ($CaCO_3$) layer from surface was determined from the dilute hydrochloric acid (HCl) test. The particle size distribution of surface soil samples was characterized using HORIBA LA-950 Laser diffraction particle-size analyzer (HORIBA Scientific Inc., Edison, NJ, USA). The organic carbon (OC) of surface soil was determined using LECO-C6235 carbon determinator (LECO Corp., St. Joseph, MI, USA). The dominant vegetation of the study site was mixed grass seeded by Duck Unlimited Canada in 2004. The leaf area index (LAI) was measured using LI-COR LAI-2000 plant Canopy Analyzer (Li-COR Biosciences, Lincoln, NE, USA) for two times in 2007.

The association between soil water storage and the controlling factors were examined using Pearson correlation analysis. The correlation among the controlling factors was also examined. Principle component analysis (PCA) was carried out on the correlation matrix between soil water storage of a particular day and the controlling factors using STATISTICA software (StatSoft Inc.) for each day of measurement. The correlation of controlling factors with principle component 1 and 2 were plotted and presented for selected dates along with the 'scree plot', which shows the percent variance contribution and the eigenvalue of each principle components.

6.4 Results and Discussion

The average soil-water storage (SWS) varied greatly over the measurement time. For example, the average SWS was 40.1 cm on 20 April 2009, which gradually decreased to 35.4 cm on 27 October 2009. The standard deviation (SD) and the coefficient of variation (CoV) of soil water storage along the transect also varied similarly with that of average SWS. For example, there was large SD (e.g., 8.65 cm on 20 April 2009) and CoV (e.g., 21.5% on 20 April 2009) during spring with high average SWS and gradually decreased with the decrease in average SWS during fall (e.g., SD = 4.92 cm and CoV = 13.9% on 27 October 2009). Therefore, there was a positive correlation between average SWS and SD (correlation coefficient, $r = 0.74$) or SWS and CoV ($r = 0.54$). The correlation was in agreement with various others (Famiglietti et al., 1998;

Martínez-Fernández and Ceballos, 2003; Western et al., 2004; Williams et al., 2008) who found a positive correlation between soil water variability and average soil water. This may be partially due to the effect of soil heterogeneity, which maximizes the soil water variability after a large input (e.g., rainfall and snowmelt; Reynolds, 1970). However, after an extended drying period, the effect of soil heterogeneity is minimized and the variance declined (Reynolds, 1970; Famiglietti et al., 1998).

The range of soil water storage along the transect was the highest during spring. For example, the maximum water storage was 68.5 cm and the minimum water storage was 25.1 cm on 20 April 2009 creating a wide range of 43.4 cm. In the PPR, the strong wind redistributes snow across large areas and within potholes (Pomeroy and Gray, 1995; Elliot and Efetha, 1999; Fang and Pomeroy, 2009), which store more snow compared to surrounding uplands (Williams et al., 2008; Lungal, 2009). The snow melts in spring and the water redistributes in the landscape. During the initial stages of snowmelt, water transported over frozen soil, which restricts the infiltration capacity and thus majority of the snowmelt water reached the potholes (Gray et al., 1985; Winter and Rosenberry, 1995). As a result, the potholes remain saturated or ponded in the early spring (Woo and Rowsell, 1993; Hayashi et al., 1998, 2003; Lungal, 2009).

However, the range in the soil water storage decreased during the latter part of the year. For example, the range was only 20.8 cm on 27 October 2009 with the maximum and minimum of 45.2 and 23.4 cm, respectively. In the PPR, when snowmelt is exhausted, the water levels of the potholes fluctuate mainly due to evapotranspiration, and to a lesser extent, groundwater interaction (Hayashi et al., 1998; van der Kamp et al., 2003). This is because the potholes are being situated on low permeability glacial tills, which allow groundwater recharge of 2 to 40 mm of water per year, mainly through fractures and preferential flow paths (van der Kamp and Hayashi, 1998). Hayashi et al. (1998) estimated that only ~1 to 8% of the water lost annually from a prairie pothole goes towards recharging the groundwater aquifer. Even the photosynthetically active vegetation around the potholes pulls water laterally during summer months and transpires it to the atmosphere (Miller, 1971). As much as 70% of water that infiltrates under wetlands is transpired by local vegetation (Parsons et al., 2004). The combined effect of transpiring vegetation and open water evaporation dries up standing water in the pothole during summer and fall and thus reduces the range in SWS and variability as well. This is

Table 6.1. Pearson correlation coefficients (*r*) between soil water series over four years and different controlling factors

	17-Jul-07	7-Aug-07	1-Sep-07	12-Oct-07	2-May-08	31-May-08	21-Jun-08	16-Jul-08	23-Aug-08	17-Sep-08	22-Oct-08	20-Apr-09	7-May-09	27-May-09	21-Jul-09	27-Aug-09	27-Oct-09	6-Apr-10	19-May-10	14-Jun-10
Sand (%)	**-0.60**†	**-0.60**	**-0.62**	**-0.64**	**-0.59**	**-0.61**	**-0.66**	**-0.68**	**-0.70**	**-0.70**	**-0.69**	**-0.57**	**-0.65**	**-0.65**	**-0.72**	**-0.73**	**-0.71**	**-0.62**	**-0.59**	**-0.61**
Silt (%)	**0.35**	**0.32**	**0.35**	**0.38**	**0.35**	**0.35**	**0.40**	**0.43**	**0.46**	**0.47**	**0.46**	**0.31**	**0.36**	**0.39**	**0.45**	**0.48**	**0.47**	**0.39**	**0.33**	**0.36**
Clay (%)	**0.48**	**0.51**	**0.51**	**0.50**	**0.47**	**0.50**	**0.50**	**0.50**	**0.49**	**0.48**	**0.47**	**0.48**	**0.54**	**0.52**	**0.54**	**0.51**	**0.49**	**0.46**	**0.50**	**0.48**
OC§ (%)	**0.71**	**0.71**	**0.72**	**0.68**	**0.72**	**0.74**	**0.67**	**0.63**	**0.51**	**0.47**	**0.47**	**0.71**	**0.74**	**0.75**	**0.59**	**0.53**	**0.47**	**0.57**	**0.68**	**0.71**
Rel. Ele.¶ (m)	**-0.24**	**-0.23**	*-0.22*‡	*-0.21*	**-0.24**	**-0.23**	*-0.20*	*-0.18*	-0.14	-0.12	-0.12	**-0.29**	**-0.24**	**-0.24**	-0.15	-0.13	-0.12	**-0.24**	**-0.23**	**-0.24**
Wetness Index	**0.65**	**0.63**	**0.61**	**0.59**	**0.61**	**0.66**	**0.63**	**0.60**	**0.51**	**0.48**	**0.47**	**0.65**	**0.67**	**0.65**	**0.58**	**0.54**	**0.50**	**0.59**	**0.59**	**0.59**
Catchment Area	**0.25**	**0.27**	**0.28**	**0.25**	*0.19*	**0.27**	**0.24**	**0.24**	*0.20*	*0.19*	*0.20*	*0.17*	**0.24**	**0.23**	*0.19*	*0.18*	0.17	0.17	*0.19*	0.17
Convergence Index	**-0.54**	**-0.52**	**-0.50**	**-0.46**	**-0.52**	**-0.58**	**-0.52**	**-0.47**	**-0.34**	**-0.30**	**-0.29**	**-0.60**	**-0.57**	**-0.55**	**-0.45**	**-0.38**	**-0.32**	**-0.50**	**-0.53**	**-0.51**
Curvature	*-0.19*	*-0.20*	*-0.18*	*-0.18*	*-0.18*	*-0.22*	*-0.20*	*-0.17*	-0.16	-0.15	-0.15	-0.17	*-0.19*	*-0.21*	-0.17	-0.15	-0.14	-0.15	-0.17	-0.16
Aspect	**0.26**	**0.28**	**0.30**	**0.30**	**0.27**	**0.32**	**0.34**	**0.33**	**0.33**	**0.33**	**0.35**	**0.25**	**0.30**	**0.35**	**0.38**	**0.38**	**0.35**	**0.26**	**0.26**	**0.28**
Gradient	*-0.20*	*-0.21*	**-0.23**	**-0.26**	*-0.20*	-0.15	*-0.20*	**-0.24**	**-0.31**	**-0.34**	**-0.34**	-0.06	-0.17	-0.15	*-0.22*	**-0.27**	**-0.31**	-0.07	*-0.21*	**-0.27**
Slope	**-0.52**	**-0.49**	**-0.47**	**-0.45**	**-0.50**	**-0.51**	**-0.49**	**-0.48**	**-0.43**	**-0.41**	**-0.40**	**-0.55**	**-0.56**	**-0.54**	**-0.51**	**-0.48**	**-0.44**	**-0.50**	**-0.51**	**-0.52**
Slope Length	0.16	0.15	0.12	0.12	*0.19*	*0.18*	0.15	0.13	0.09	0.09	0.08	**0.31**	**0.26**	**0.23**	0.15	0.14	0.12	**0.29**	**0.25**	*0.22*
Solar Radiation Flow	-0.06	-0.10	-0.14	-0.16	-0.09	-0.15	-0.17	-0.16	-0.16	-0.16	*-0.18*	-0.07	-0.09	-0.14	-0.16	-0.17	*-0.18*	-0.10	-0.04	-0.04
Connectivity	**0.44**	**0.43**	**0.41**	**0.39**	**0.45**	**0.48**	**0.44**	**0.41**	**0.33**	**0.29**	**0.27**	**0.60**	**0.52**	**0.49**	**0.43**	**0.39**	**0.34**	**0.52**	**0.55**	**0.49**
CaCO3 depth (cm)	**0.68**	**0.60**	**0.58**	**0.54**	**0.72**	**0.63**	**0.56**	**0.50**	**0.36**	**0.31**	**0.31**	**0.79**	**0.70**	**0.67**	**0.51**	**0.44**	**0.36**	**0.62**	**0.72**	**0.73**
A Horizon (cm)	**0.46**	**0.44**	**0.42**	**0.39**	**0.47**	**0.46**	**0.40**	**0.33**	*0.22*	*0.18*	*0.19*	**0.49**	**0.47**	**0.47**	**0.31**	**0.24**	*0.19*	**0.33**	**0.48**	**0.49**
C Horizon (cm)	**0.62**	**0.53**	**0.52**	**0.47**	**0.67**	**0.59**	**0.51**	**0.45**	**0.33**	**0.29**	**0.30**	**0.69**	**0.64**	**0.61**	**0.45**	**0.40**	**0.34**	**0.61**	**0.63**	**0.63**
BD# (20 cm)	**-0.43**	**-0.40**	**-0.40**	**-0.37**	**-0.49**	**-0.42**	**-0.37**	**-0.34**	**-0.24**	*-0.22*	*-0.22*	**-0.56**	**-0.50**	**-0.50**	**-0.36**	**-0.31**	**-0.26**	**-0.43**	**-0.50**	**-0.48**
LAI!! (26 Jul 2007)	-0.14	*-0.19*	*-0.20*	*-0.21*	-0.10	-0.14	-0.18	*-0.21*	**-0.25**	**-0.26**	**-0.28**	-0.04	-0.09	-0.12	*-0.21*	**-0.25**	**-0.28**	-0.05	*-0.20*	-0.18
LAI (30 Aug 2007)	-0.08	-0.02	-0.07	-0.10	-0.16	-0.02	-0.08	-0.13	*-0.22*	**-0.25**	**-0.25**	-0.07	-0.11	-0.05	*-0.19*	*-0.22*	**-0.25**	-0.17	-0.13	-0.16

† **Bold**- significant at $p = 0.01$; ‡ *Italics*- significant at $p = 0.05$

§ OC- organic carbon, ¶ Rel. Ele. – relative elevation, # BD- bulk density, !! LAI- leaf area index

consistent with Flerchinger and Cooley (2000), who reported a similar trend in SWS in a non-level landscape.

The spatial series of soil water storage over time were correlated with different terrain indices, soil properties, and vegetation to understand the relative influence of different factors controlling SWS and how the influence changes with time on a hummocky landscape of the PPR. There is no single factor that can explain the spatial pattern of SWS in the region; rather they are influenced by multiple factors that exert an interactive effect (Table 6.1). In our study, sand was negatively correlated to SWS (correlation coefficient, r = -0.73 (maximum) and -0.57 (minimum); Table 6.1) and provided one of the best explanations for the spatial pattern in SWS at different times. Various other authors also reported strong correlation between soil water storage and sand (Reynolds, 1970; Vachaud et al., 1985; Mohanty and Skaggs, 2001; Jacobs et al., 2004; Starks et al., 2006; Cosh et al., 2008). However, soil water storage was positively correlated with silt and clay at different times (Table 6.1). The negative correlation between SWS and sand (Table 6.1) may be a result of the high infiltration capacity of sand. The high infiltration capacity favors the entry of water in soil or the vertical fluxes of water and the rapid drying out of the surface moisture (Vachaud et al., 1985; Gomez-Plaza et al., 2001; Pan and Wang, 2009). On the other hand, silt and clay favors the water storage capacity of soil by preventing the deep percolation of surface soil water and thus increasing the SWS.

While the BD of surface soil was negatively correlated (r = -0.56 (maximum) and -0.22 (minimum)), the depth of $CaCO_3$ (r = 0.72 (maximum) and 0.31 (minimum)) and C-horizon (r = 0.67 (maximum) and 0.29 (minimum)) were positively correlated with soil water storage at different times (Table 6.1). Generally, the soil with high BD has a large proportion of macro-pores, which holds less water and is more water conductive compared to the soil with low BD and yields a negative correlation with soil water storage. Presence of $CaCO_3$ layer and the C-horizon favors SWS by slowing down percolation (Miller et al., 1985). Cosh et al. (2008) reported that the soil characteristics, such as bulk density, sand, and clay content are responsible for more than 50% of the variations in soil water.

Though the variability in LAI was not at all correlated with the SWS at any time (Table 6.1), the long-term effect of vegetation growth as expressed through the presence of OC (r = 0.75 (maximum) and 0.47 (minimum)) was strongly correlated with SWS (Table 6.1). Hu et al. (2009,

2010a) reported a strong correlation between soil water and organic matter. The OC modifies soil BD, soil structure, and porosity, which affect the soil water holding capacity (retention) and soil hydraulic conductivity (transmission) (Hawley et al., 1983; Jacobs et al., 2004). Therefore, high OC in the A-horizon favored water storage yielding a positive correlation between soil water storage and the depth of A-horizon (Table 6.1).

Correlations between SWS and various terrain indices are shown in Table 6.1. There was negative correlation (r = -0.56 (maximum) and -0.40 (minimum)) between SWS and slope, a primary terrain index, at different times. The negative correlation results from the favored partition of the lateral flow on steep sites after rainfall or snowmelt (Moore et al., 1988b; Nyberg, 1996; Western et al., 1999; Gómez-Plaza et al., 2001). Contrary to slope, the direction of slope or the aspect was positively correlated with soil water storage (Table 6.1). This is because, aspect influences rainfall input, wind speed, and radiation influx (Sharon, 1980), which controls the available energy for evapotranspiration and snowmelt and favors the water storage (Blöschl et al., 2001). The convergence index, a measure of local convergence or divergence, was negatively (r = -0.60 (maximum) and -0.29 (minimum); Table 6.1) correlated with soil water storage as it controls the lateral flow path of snowmelt water in the hummocky landscape (Western et a., 1999). On contrary, there was a positive correlation (r = 0.60 (maximum) and 0.27 (minimum); Table 6.1) between flow connectivity and the soil water storage. The points with high connectivity received water from other points and contributed to high water storage. There was weak to moderate positive correlation between the catchment area and soil water storage (r = 0.28 (maximum) and 0.17 (minimum); Table 6.1). Famiglietti et al. (1998) also reported a weak correlation between the soil water at surface layer and the catchment area as the thin surface layer quickly saturates after any significant precipitation event. A weak correlation between soil water and the catchment area has also been reported by Moore et al. (1988b) and Nyberg (1996).

However, there was strong positive correlation (r = 0.67 (maximum) and 0.47 (minimum); Table 6.1) between soil water storage at different times and the wetness index, a compound terrain index calculated from the catchment area and the local surface gradient (Beven and Kirkby, 1979). The wetness index predicts the zones of surface saturation (Beven and Kirkby, 1979). The lateral flow towards the depression points contributed to high water storage

Table 6.2: Pearson correlation coefficients (*r*) among the controlling factors

Variables	Sand (%)	Silt (%)	Clay (%)	OC (%)	Rel. Ele. (m)	Wetness Index	Catchment Area	Convergence Index	Curvature	Aspect	Gradient	Slope	Slope Length	Solar Radiation	Flow Connectivity	CaCO3 depth (cm)	A Horizon (cm)	C Horizon (cm)	BD (20 cm)	LAI (26 Jul 2007)	LAI (30 Aug 2007)
Sand (%)	1.00	**-0.77**†	**-0.55**	**-0.46**	*-0.18*‡	**-0.35**	-0.14	0.18	0.02	**-0.48**	*0.21*	**0.52**	-0.02	-0.04	-0.16	*-0.25*	-0.07	-0.17	**0.42**	*0.24*	**0.29**
Silt (%)		1.00	-0.10	*0.21*	0.13	*0.20*	0.11	-0.07	-0.05	**0.34**	-0.13	**-0.33**	0.07	0.06	0.06	0.09	0.00	0.04	**-0.34**	-0.16	**-0.24**
Clay (%)			1.00	**0.44**	0.11	**0.28**	0.08	-0.19	0.03	**0.31**	-0.16	**-0.39**	-0.07	-0.02	0.17	**0.28**	0.11	*0.21*	*-0.20*	-0.16	-0.13
OC§ (%)				1.00	**-0.33**	**0.68**	**0.38**	**-0.59**	*-0.22*	*0.20*	-0.07	**-0.55**	*0.21*	0.00	**0.38**	**0.72**	**0.64**	**0.61**	**-0.61**	0.09	*0.23*
Rel. Ele.¶ (m)					1.00	**-0.57**	**-0.28**	**0.56**	**0.37**	**0.46**	**-0.28**	0.15	**-0.64**	**-0.07**	**-0.45**	**-0.39**	**-0.35**	**-0.44**	0.12	**-0.36**	**-0.42**
Wetness Index						1.00	**0.46**	**-0.76**	**-0.24**	-0.05	0.08	**-0.76**	**0.50**	0.09	**0.62**	**0.57**	**0.48**	**0.55**	**-0.40**	**0.26**	**0.25**
Catchment Area							1.00	**-0.34**	-0.03	-0.05	0.03	**-0.24**	*0.21*	0.00	0.16	0.12	0.19	0.16	*-0.21*	0.11	**0.26**
Convergence Index								1.00	**0.46**	0.05	*-0.22*	**0.37**	**-0.55**	-0.02	**-0.78**	**-0.65**	**-0.58**	**-0.62**	**0.34**	-0.19	**-0.33**
Curvature									1.00	0.06	-0.11	0.03	**-0.37**	-0.04	**-0.39**	**-0.30**	**-0.42**	**-0.36**	0.02	-0.17	**-0.26**
Aspect										1.00	-0.04	*-0.20*	**-0.29**	**-0.38**	-0.09	0.07	0.00	-0.01	-0.19	**-0.36**	-0.09
Gradient											1.00	0.00	0.15	0.16	0.16	0.05	0.02	0.08	0.11	*0.23*	**0.44**
Slope												1.00	*-0.19*	**-0.27**	**-0.34**	**-0.41**	**-0.30**	**-0.35**	**0.42**	-0.15	-0.08
Slope Length													1.00	0.18	**0.57**	**0.38**	**0.36**	**0.36**	**-0.24**	**0.28**	**0.27**
Solar Radiation														1.00	0.15	0.09	0.04	0.07	0.01	*0.20*	0.03
Flow Connectivity															1.00	**0.62**	**0.44**	**0.57**	*-0.21*	0.13	**0.27**
CaCO3 depth (cm)																1.00	**0.74**	**0.89**	**-0.59**	*0.22*	*0.19*
A Horizon (cm)																	1.00	**0.71**	**-0.46**	**0.24**	**0.33**
C Horizon (cm)																		1.00	**-0.46**	**0.31**	0.19
BD# (20 cm)																			1.00	-0.10	-0.08
LAI!! (26 Jul 2007)																				1.00	**0.47**
LAI (30 Aug 2007)																					1.00

† **Bold**- significant at $p = 0.01$; ‡ *Italics*- significant at $p = 0.05$

§ OC- organic carbon, ¶ Rel. Ele. – relative elevation, # BD- bulk density, !! LAI- leaf area index

and showed a positive correlation between wetness index and SWS in the PPR (Table 6.1). Various other authors have also reported a strong correlation between soil water storage and the wetness index (Burt and Butcher, 1985; Moore et al., 1988b; Nyberg, 1996).

There was very weak correlation between relative elevation and soil water storage at different times (r = -0.29 (maximum) and -0.12 (minimum); Table 6.1). A very low correlation between soil water at different moisture condition and relative elevation was also reported by Zhao et al. (2010) from grazed semi-arid steppe environment. Relative elevation is an easy-to-measure surrogate for a number of terrain and soil attributes and is known to influence the lateral redistribution of soil water. Generally, the low topographic locations or potholes store more water and high topographic locations or knolls store less water. However, the low correlation in this study may be due to closed hydrological system of pothole wetlands, which receives water from corresponding uplands (knolls) irrespective of their elevation. For example, the elevation of one depression can be higher than the elevation of one knoll corresponding to another depression. Therefore, the water stored in depressions has been contributed from other locations. However, the Pearson correlation coefficient, which is scale and location independent analysis, only measures the linear association between SWS and a factor at measurement scale. Therefore, the high SWS in depressions contributed from surroundings may not be explained through Pearson correlation analysis and a more comprehensive investigation is needed to understand the effect of different factors such as elevation operating at different scales other than measurement in controlling SWS.

The strong correlation between SWS and different soil factors as well as terrain indices indicated a combined influence from the controlling factors. However, some of the soil properties were also correlated with different terrain indices. For example, OC and the depth of $CaCO_3$ were correlated with wetness index (r = 0.68 and 0.57, respectively), convergence index (r = -0.59 and -0.65, respectively), flow connectivity (r = 0.38 and 0.62, respectively), slope (r = -0.55 and -0.41, respectively) and relative elevation (r = -0.33 and -0.39, respectively; Table 6.2). A similar correlation was observed between depth of A-horizon and C-horizon with various terrain indices such as relative elevation, wetness index, convergence index, slope etc. (Table 6.2). This is because; the topography controls the redistribution of soil in the hummocky landscape and thus the soil properties (Bedard-Haughn and Pennock, 2002). For example, the

knolls are dominated by low vegetative cover and shallow soils. Therefore, the correlation between soil water storage and these soil properties also reflects the controls from topography. An obvious strong correlation among various soil properties as well as terrain indices was also observed (Table 6.2). The correlation among the controlling factors makes the identification of dominant controlling factor more difficult.

The Principle component analysis (PCA) was performed to convert the set of correlated variables in to a set of uncorrelated variables called principle components (PCs). The correlation between the controlling factors and the PCs for selected dates is presented in Figure 6.1. For 2 May 2008 measurements (Figure 6.1a), PC1 explained 31 % and PC2 explained 17 % of the total variation. Different terrain indices and the soil properties that were correlated with terrain indices had high correlation with PC1. For example, there was high correlation between PC1 and wetness index (r = -0.80), convergence index (r = -0.84), relative elevation (r = 0.68), flow connectivity (r = -0.76), slope length (r = -0.63), $CaCO_3$ layer (r = -0.82), depth of C-horizon (r = -0.81) and A horizon (r = -0.71) on 2 May 2008 (Figure 6.1a). Other soil properties such as sand (r = -0.91), silt (r = -0.65), clay (r = -0.58) were correlated with PC2 (Figure 6.1a). This means that the soil properties, which control the entry and transmission of water in soil, can form a group, while the terrain indices, which control the surface and subsurface redistribution of water, can form another group. The first group control soil water locally and is consider as the 'local' control and the latter group control soil water nonlocally and is considered as 'nonlocal' control (Grayson et al., 1997). The aspect, which had high correlation with PC2 (r = -0.62), control the local energy balance and determine the snowmelt and evapotranspiration and thus the soil water storage. However, the first two PCs can only explain less than half of the total variation. Rest PCs combined represent the remaining variations (Figure 6.1d). Therefore, there is no single dominating group of factors that can explain a major portion of total variation. This indicated a combined influence on soil water storage from different controlling factors. However, among these groups, the group that represents the terrain indices is better than other groups. A very similar correlation between PCs and the controlling factors were observed on other measurements such as on 23 August 2008 (Figure 6.1b) and 22 October 2008 (Figure 6.1c). However, a slight change in the magnitude of the percent variance contribution was observed among PCs. For example, the variance explanation by PC1 was decreased slightly from

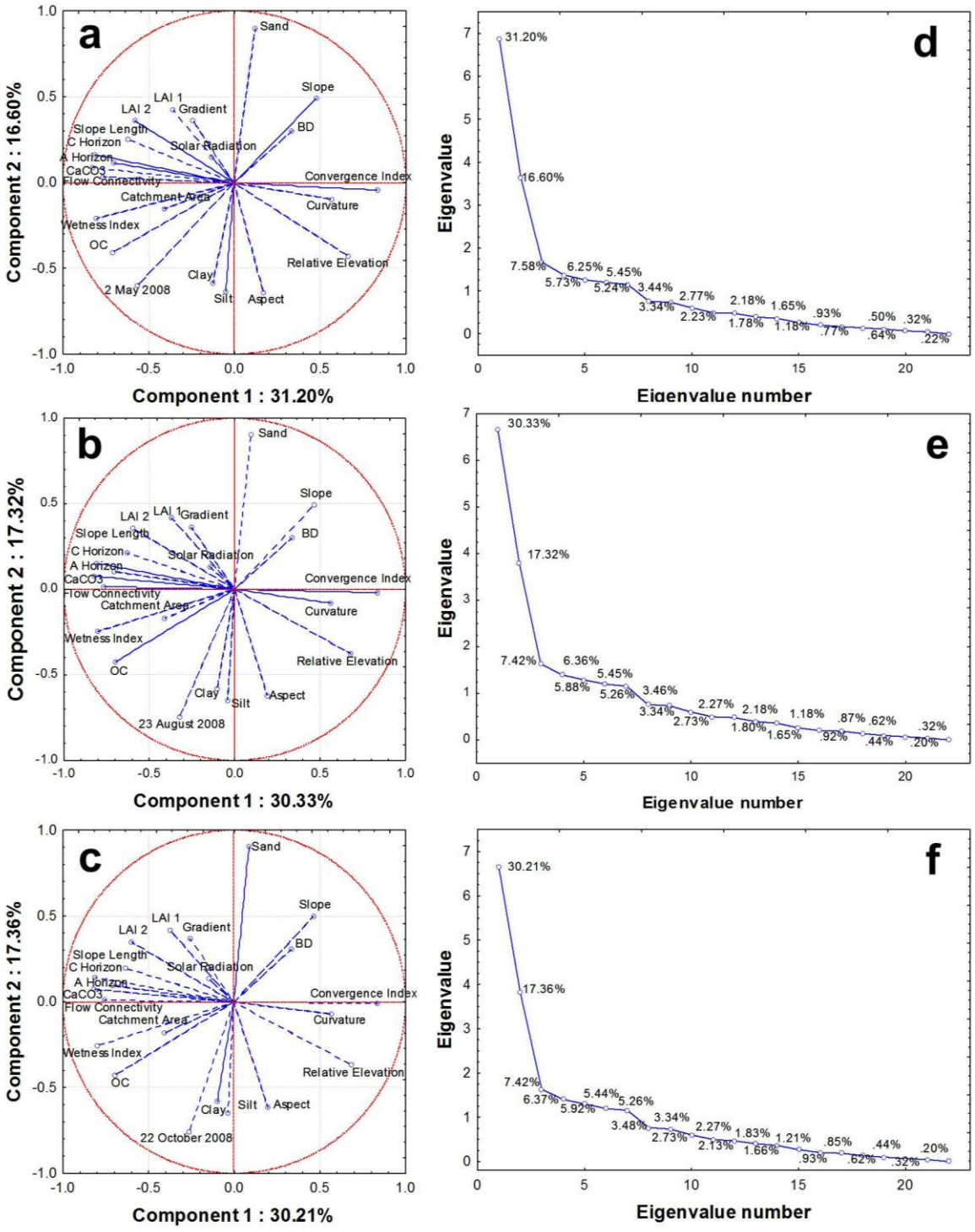

Figure 6.1. Correlation between controlling factors and the principle components (component 1 and 2) for a) 2 May 2008, b) 23 August 2008, and c) 22 October 2008. The scree plots show the percent contribution and associated eigenvalues of different principle components (or eigenvalue numbers) for d) 2 May 2008, e) 23 August 2008, and f) 22 October 2008.

2 May 2008 to 23 August 2008 and further to 22 October 2008 (Figures 6.1d, 6.1e, and 6.1f). However, a slight increase in the percent contribution was observed for PC2 from the wet to the dry conditions.

The average soil water content also affected the dependence of SWS on topographic and soil factors (Grayson et al., 1997). For example, the value of *r* between soil water storage and sand was the lowest during the spring (e.g. -0.57 on 20 April 2009) and gradually increased towards later part of the year (e.g. 0.71 on 27 October 2009; Table 6.1). A similar increasing trend was observed in the correlation between soil water storage and silt. However, a decreasing trend was observed between soil water storage and other soil properties and the terrain indices as well. For example, the value of *r* was 0.71 on 20 April 2009 and was 0.47 on 27 October 2009 between soil water storage and OC (Table 6.1). Similarly, the value of *r* was 0.65 on 20 April 2009 and was 0.50 on 27 October 2009 between soil water storage and the wetness index.

During spring, the snow melts and contributes a large amount of water within short period (Gray et al., 1985; van der Kamp et al., 2003). The soil property determines the infiltration capacity or the entry of water in the soil. When the input rate of water is more than the infiltration rate, the excess water redistributes in the landscape as infiltration excess runoff (Horton, 1933). At the same time, the saturated pores are well connected, which may create some subsurface lateral flow along the topography (Grayson et al., 1997). However, the possibility of subsurface flow is less in soils of the PPR because of its fine texture. Therefore, in wet condition, different terrain indices control the redistribution of water mostly through surface lateral flow and to a lesser extent through subsurface lateral flow. A high correlation between the PC1 and the terrain indices were also observed during wet condition (e.g. 2 May 2008; Figure 6.1a). However, in semi-arid climate of the PPR, the combined losses of water from evaporation and transpiration are between 3 to 5 mm per day (Winter and Rosenberry, 1997; Parkhurst et al., 1998), which is approximately double the average daily summer precipitation (Price, 1993; Parkhurst et al., 1998). The high evaporative demand during drier period creates a soil water situation well below saturation. Therefore, the possibility of runoff will be very less. In addition, the unsaturated condition rarely allows the macro-pore flow connectivity and therefore the subsurface lateral redistribution (Grayson et al., 1997). Hence, the factors that control infiltration had increased effect on SWS during the dry period, while the factors that control the lateral

redistribution had a decreased effect. The slight change in the magnitude of the variance contribution from PCs may be due to the slight change in the degree of controls from the factors, but not the complete switch of controls from a factor to another. This contradicts the findings of Grayson et al. (1997), who suggested the switching on or off of controlling factors at different soil water conditions. In this study, the effect of terrain indices that control the redistribution of soil water in the landscape was always correlated with PC1 (Figure 6.1), which explains the maximum variation irrespective of soil water condition. This indicates a stronger topographic control on soil water storage than that from soil texture at any time of the year. In the study area, topography plays a major role in redistributing water during the spring and the effect of which is persistent during later summer or fall.

From the above discussion, it is obvious that the soil factors control the SWS most in the hummocky landscape by modifying the infiltration capacity of soil. The presence of $CaCO_3$ layer and the C-horizon depth in the PPR also have a major role in controlling the water transmission through soil and thus the storage. However, in wet periods, different terrain indices play a major role in redistributing soil water in the landscape by generating surface lateral flow (Grayson et al., 1997). The effect of the redistribution carries over to dry periods. Among the terrain indices, wetness index play a major role in controlling soil water in the PPR. Other terrain indices, such as slope, convergence index and flow connectivity have important contribution in controlling SWS. Therefore, the observation on soil properties in addition to various terrain indices will provide a better understanding on SWS in the hummocky landscape of the PPR.

Knowledge of these factors is useful to improve the prediction of soil water in the hummocky landscape in semi-arid areas. The relationship between soil water storage and different landscape properties provides the insight about various important ongoing hydrological and ecological processes. The spatial variations in the more static controlling factors can be used to predict the spatial pattern of soil water storage. The consistent correlation with only a slight change in magnitude between the controlling factors and the soil water storage can help catchment managers to identify the management units in a more cost effective manner for precision management of crop biomass production and the environment.

6.5 Conclusions

In this study, a simple correlation analysis was performed between a number of soil water storage series measured over a four year period and different controlling factors along a transect from the hummocky landscape of the Prairie pothole region of North America. The correlation indicated the strong association of soil water storage with soil properties and terrain indices, simultaneously. Soil properties, such as soil texture control the infiltration and the transmission of water in the soil. The bulk density, depth of A and C horizon, and the presence of $CaCO_3$ layer in soil also control the transmission of water in the soil and thus the storage. Different terrain indices such as wetness index, slope, convergence index, and flow connectivity also exhibited association with soil water storage. The wetness index was the measure of the zones of surface saturation and was strongly correlated with soil water during wet period. The redistribution of infiltration excess runoff during wet period yield stronger correlation with terrain indices compared to dry period. While slope controlled the infiltration, drainage, and runoff, the local convergence or divergence of any location controlled the lateral flow path of snowmelt water in the hummocky landscape. The principle component analysis of these factors could not identify a dominant group of factors that control soil water storage. Therefore, a combined observation of soil properties and the terrain indices are required to explain the soil water storage in the Hummocky landscape of the Prairie pothole region of North America.

7.0 IDENTIFYING SCALE SPECIFIC CONTROLS OF SOIL WATER STORAGE IN A HUMMOCKY LANDSCAPE USING WAVELET COHERENCY

7.1 Preface

High spatio-temporal variability of soil water is contributed from different hydrological and soil processes operating in different intensities and at different scales. Pearson correlation analysis examines the linear correlation between soil water storage and controlling factors only at the measurement scale. However, the scale of processes controlling soil water storage may not be same with the scale of measurement. Moreover, a factor can have variable relationship (positive or negative) over scales. In addition, one scale process can be dominant at one location while another can be at another location. This chapter examines the correlation between soil water storage and its controlling factors at different scales and locations in a hummocky landscape using wavelet coherency.

7.2 Introduction

Soil water is the key variable for a number of surface and subsurface hydrological, geomorphological, ecological, and climatic processes operating in different intensities at different spatio-temporal scales (Entin et al., 2000), making the soil water highly variable in space and time (Bell et al., 1980; Seyfried, 1998; Hupet and Vanclooster, 2002, 2005; Brocca et al., 2010). For example, at a small watershed scale, the spatial and temporal variability of soil water can be high due to heterogeneity in soil, vegetation, and topography. Whereas, the large-scale soil water dynamics are controlled by atmospheric, geologic, and climatic variability (Seyfried, 1998; Entin et al., 2000; Brocca et al., 2009; Schneider et al., 2008).

In past years, a lot of research has been dedicated in understanding the soil water dynamics over time and space and its dominant control (Vachaud et al., 1985; Grayson et al., 1997; Famiglietti et al., 1998; Gómez-Plaza et al., 2001; Cosh et al., 2008; Brocca et al., 2010). Vachaud et al. (1985) first examined the nature of spatial structure from the spatial distribution of soil water storage and observed the similarity over time, and identified this phenomenon as time stability. The authors mentioned soil texture as the main control of time stability. Thereafter, various other authors also reported soil properties (e.g., particle size, bulk density,

organic carbon) that control time stability (Mohanty and Skaggs, 2001; Jacobs et al., 2004; Starks et al., 2006; Cosh et al., 2008; Hu et al., 2009). At the same time, various others identified topographic position or local topography as the major control of time stability (Grayson et al., 1997; Famiglietti et al., 1998; Gómez-Plaza et al., 2000; Thierfelder et al., 2003, Brocca et al., 2007, 2009). Sometimes the terrain indices explain more than half of the spatial variability of soil water distribution (Tomer and Anderson, 1995; Western et al., 1999).

However, Tallon and Si (2004) did not find any strong correlation between spatial distribution of soil water and soil properties or topographic indices suggesting the absence of single controlling factors in a non-level landscape. It was identified that the topography and rainfall control the change in soil water variability under drying-wetting cycle, while soil parameters control its relative magnitude (Choi et al., 2007).

In addition, the initial soil water content also regulates the time stability of soil water storage spatial pattern. Famiglietti et al. (1998) observed that the influence of factors on soil water changed with the initial soil water content. Under wet conditions, variations in soil properties (porosity, hydraulic conductivity) control soil water variability. However, under dry conditions, relative elevation, aspect, and clay content controlled surface soil water content (Famiglietti et al, 1998). Researcher has made a distinction between wet and dry periods or preferred states in soil water spatial patterns (Kachanoski and de Jong, 1988; Grayson et al., 1997; Western and Blöschl, 1999). While, Western and Blöschl (1999) reported that the high degree of time stability was present during wet period (Gómez-Plaza et al., 2000; Hupet and Vanclooster, 2002), Martínez-Fernández and Ceballos (2003) reported strong time stability during dry periods (Robinson and Dean, 1993; Famiglietti et al., 1998). Furthermore, Grayson et al. (1997) classified the controlling factors into two groups and reported the dominance of ‘local’ factors (e.g. soil properties, micro-topography) in dry conditions (evapotranspiration > precipitation) and ‘nonlocal’ factors (e.g. drainage line due to catchment topography) in wet conditions (evapotranspiration < precipitation).

In identifying the important controlling factors of soil water distribution and its time stability, Pearson correlation analysis is the most commonly used method. However, this analysis loses the location and scale information. It can examine the linear relationship (dependence) between soil water and its controlling factors only at the measurement scale. The highest

correlation coefficient between the spatial pattern of a controlling factor and soil water storage indicates the strongest linear dependence of soil water storage on that particular factor. Therefore, the factor is identified as the dominant control of soil water storage.

However, the scale of the processes controlling soil water storage may not always be at the scale of the measurements (Blöschl and Sivapalan, 1995) making it difficult to identify the control. In addition, a factor can have variable correlation (positive or negative) over scales and locations that may neutralize each other over the entire measurement area and scales, which may mislead the result.

Wavelet coherency, an advanced mathematical technique, is a measure of correlation between two spatial series at different scales and locations. It has widely been used to examine the scale-location specific correlation between two variables in different fields of science including soil science (Si and Zeleke, 2005; He et al., 2007; Yates et al., 2007; Biswas et al., 2008, Furon et al., 2008; Shu et al., 2008). Wavelet coherency has also been used to correlate soil water with drought variability (Tang and Piechota, 2009), and precipitation (Wu et al., 2002; Parent et al., 2006). However, there is no information on the use of wavelet coherency to examine the scale-location specific controls of soil water. Therefore, the objective of this study was to identify the scale-specific controls of soil water storage using wavelet coherency. Pearson correlation analysis was used to calculate the linear correlation between soil water storage and controlling factors at measurement scale. Wavelet coherency analysis was used to examine the correlation between soil water and its controlling factors at different scales and locations over different seasons.

7.3 Theory

7.3.1 Wavelet Coherency Analysis

Theory of the wavelet transform and wavelet coherency analysis is well established in literature. We only present the basics regarding wavelet coherency analysis in this manuscript. Detailed theory on wavelet transform can be found in Farge (1992) and Kumar and Foufoula-Georgiou (1993, 1997) and the wavelet coherency can be found in Grinsted et al. (2004), Si and Zeleke (2005) and others and is beyond the scope of this paper.

Wavelet coherency is calculated using wavelet spectra and wavelet cross spectra, which is calculated from the wavelet coefficients after wavelet transform. There are two types of wavelet transform, discrete wavelet transform (DWT) and continuous wavelet transform (CWT). Wavelet coherency in both frequency and spatial domain is readily available using CWT but not using DWT (Shu et al., 2008). The CWT for a spatial series of length N (Y_i, i = 1, 2, · · ·, N) with equal incremental distance δx, can be defined as the convolution of Y_i with the scaled and normalized wavelet, which is implemented using the fast Fourier transform (Torrence and Compo, 1998).

$$W_i^Y(s) = \sqrt{\frac{\delta x}{s}} \sum_{j=1}^{N} Y_j \psi\left[(j-i)\frac{\delta x}{s}\right] \qquad [7.1]$$

where $\psi[\ ]$ is the mother wavelet function, s is the scale, $W_i^Y(s)$ is the wavelet coefficients, which are expressed as $a + ib$ where a and b are the real and imaginary components of $W_i^Y(s)$, respectively. Similar to the Fourier power spectrum, the wavelet power spectrum is defined as $\left|W_i^Y(s)\right|^2$ and the local phase can be defined from $W_i^Y(s)$.

The mother wavelet, a standard mathematical function, is a small wave that grows and decays over a small distance. There are a number of mother wavelets. For example, Haar, Mexican hat, Meyer and Morlet wavelet. Among these, Morlet wavelet is a complex symmetric function that retains the real and imaginary component of wavelet coefficients. Therefore, in extracting the local phase information, Morlet wavelet is commonly used in CWT. Morlet wavelet can be represented as (Grinsted et al., 2004)

$$\psi(\eta) = \pi^{-1/4} e^{i\varpi\eta - 0.5\eta^2} \qquad [7.2]$$

where ω is dimensionless frequency and η is dimensionless space ($\eta = s/x$). The Morlet wavelet ($\omega = 6$) is good for feature extraction because it provides a good balance between space and frequency localization and is used in this study.

The cross wavelet power spectrum of two spatial series for example soil water storage (X) and controlling factor (Y) can be defined as

$$\left|W_i^{XY}(s)\right| = \left|W_i^X(s)\overline{W_i^Y(s)}\right| \qquad [7.3]$$

where W_i^X and W_i^Y are the wavelet coefficients of the spatial series *X* and *Y*. $\overline{W_i^Y}$ is the complex conjugate of W_i^Y.

The wavelet coherence of the two spatial series (*X* and *Y*) can be defined as (Torrence and Webster, 1999; Grinsted et al., 2004)

$$R_i^2(s) = \frac{\left|S\left(s^{-1}W_i^{XY}(s)\right)\right|^2}{S\left(s^{-1}\left|W_i^X(s)\right|^2\right)S\left(s^{-1}\left|W_i^Y(s)\right|^2\right)} \quad [7.4]$$

where *S* is a smoothing operator and can be written as

$$S(W) = S_{\text{scale}}\left(S_{\text{space}}(W(s,\tau))\right) \quad [7.5]$$

where τ denotes the location and S_{scale} and S_{space} denote the smoothing along the wavelet scale axis and the spatial domain, respectively (Si and Zeleke, 2005). The smoothing function or the normalized real Morlet wavelet has a footprint similar to the Morlet wavelet. Therefore, the smoothing along locations can be written as

$$S_{space}(W(s,\tau)) = \sum_{k=1}^{N}\left(W(s,\tau)\cdot\frac{1}{s\sqrt{2\pi}}\exp\left(-\frac{(\tau-x_k)^2}{2s^2}\right)\right)\Bigg|_s \quad [7.6]$$

where $\frac{1}{s\sqrt{2\pi}}\exp\left(-\frac{\tau^2}{2s^2}\right)$ is a smoothing function, and the Fourier transform is of this smoothing function is $\exp(-2s^2\omega^2)$, where ω is the frequency (Si and Zeleke, 2005). According to the convolution theorem, the Equation 7.6 can be implemented using Fast Fourier Transform (FFT) and Inverse Fast Fourier Transform (IFFT) and is written as

$$S_{space}(W(s,x)) = IFFT\left(FFT(W(s,\tau))\left(\exp(-2\cdot s^2\omega^2)\right)\right) \quad [7.7]$$

Therefore, the smoothing along scales can be written as

$$S_{scale}(W(s_k,x)) = \frac{1}{2m+1}\sum_{j=k-m}^{k+m}\left(S_{space}(W(s_j,x))\Pi(0.6s_j)\right)\Big|_x \quad [7.8]$$

where Π is the rectangle function, $\big|_x$ means at a fixed *x* value and *j* is the index for the scales. The factor of 0.6 is the empirically determined scale decorrelation length for the Morlet wavelet (Torrence and Compo, 1998; Si and Zeleke, 2005).

7.3.2 Significance Testing

The significance testing for the wavelet coherency can be made against Gaussian white and red noises (Pardo-Iguzquiza and Rodriguez-Tovar, 2000). For a white noise, data points in the spatial data series are independently and identically distributed and not auto-correlated, whereas in red noise, data values are similar between points next to each other, but are not similar further apart. Therefore, red noise is generally modeled as a univariate lag-1 auto regressive (AR1) process (Torrence and Compo, 1998; Si and Farrell, 2004). The red noise-like behavior of soil property is very common (Torrence and Compo, 1998; Neilson and Wendroth, 2003; Grinsted et al., 2004; Si and Farrell, 2004). Therefore, our null hypothesis is that the wavelet coherency at a scale and location between two soil water measurement series is not different from that between two red noises, each of which has the mean, variance and lag-1 autocorrelation coefficient (r) of one of two soil water data series (Si and Zeleke, 2005).

For testing the statistical significance of wavelet coherency, one thousand (1000) realizations of a pair of spatial series (each having the r value from one of the two spatial soil water storage series to be tested), were generated and wavelet coherency of each realization at each scale and location was calculated. Therefore, 1000 wavelet coherency values were generated at each scale and location and subsequently sorted in ascending order. The 950^{th} wavelet coherency value at a scale and location gives the 95% confidence level or the 5% significance level at that scale and location (Si and Zeleke, 2005).

The correlation shows whether and how strongly two variables are related to each other. It measures the overall relationship between two variables only at the scales they were measured. On contrary, wavelet coherency measures the relationship between two variables as a function of frequency or scales and locations. The relationship between two variables can be different at different scales and locations. For example, the relationship can be positive at some places and negative at some other places. The opposite relationship can neutralize each other showing a weak overall relationship. The phase information in the wavelet coherency analysis can identify different types of relationships at different scales and locations. Therefore, the information on local relationship between two variables can lead to better performance of the predictive relationship. For example, the relationship at different scale and location can improve the performance of pedo-transfer functions in predicting various dynamic soil properties using more

stable and easily measured soil properties. However, wavelet coherency is generally calculated at the scales equivalent to the minimum length of two-sample interval. Therefore, the relationship at the scale of measurement or the local scale is missing. On contrary, the correlation analysis takes into consideration the overall correlation, which includes the local scale relationship.

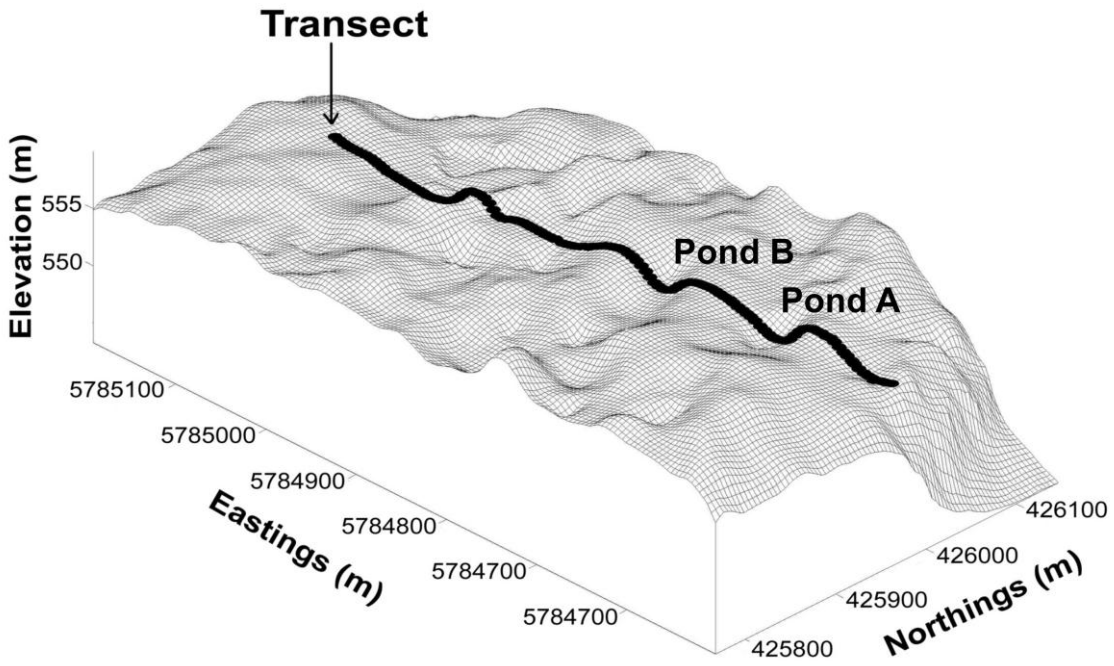

Figure 7.1. Transect position in the Hummocky landscape of St. Denis National Wildlife Area, Saskatchewan.

7.4 Materials and Methods

7.4.1 Study Site

A field experiment was conducted at St. Denis National Wildlife Area (52°12′ N latitude, 106°50′ W longitude), which is located approximately 40 km east of Saskatoon, Saskatchewan, Canada. The landscape of this area is hummocky with a complex sequence of slopes (10 to 15 %) extending from different sized rounded depressions to irregular complex knolls and knobs (Figure 7.1) (Pennock, 2005). This is the most common type of landscape covering > 80 percent of the area of Canadian Prairies. Soils of this area are mainly dark brown Chernozem developed from moderately fine to fine-textured, moderately-calcareous, glacio-lacustrine deposits and modified glacial till (Saskatchewan Centre for Soil Research, 1989). The climate of the study site

is semi-arid with mean annual air temperature (at the Saskatoon airport) of 2^{o}C and the monthly mean of -19^{o}C in January and 18^{o}C in July (AES, 1997). Long-term (90 years) annual average precipitation of the study site is 360 mm, of which 84 mm occurs in winter months mostly as snow (AES, 1997). The total precipitation of the area was 366 mm, 331 mm, and 402 mm, respectively during the year of 2007, 2008, and 2009. The study area also received a record-breaking spring and summer rainfall during 2010.

7.4.2 Data Collection

Soil water was measured along a transect of 576 m (128 points with 4.5 m regular interval) established in North-South direction over several rounded knolls and seasonal depressions (Woo and Rowsell, 1993) representing different landform cycles (Figure 7.1). Vertically installed time domain reflectometry (TDR) probe (using metallic cable tester of Model 1502B, Tektronix, Beaverton, OR, USA) and neutron probe (CPN 501 DR Depthprobe, CPN International Inc., Martinez, CA, USA) were used to measure the soil water storage at 0 to 20 cm and 20 to 140 cm, respectively. Neutron probe measurements were completed at each 20 cm depth interval. A standard calibration equation $\theta = 0.115\sqrt{k_a} - 0.176$ was used to calculate the volumetric soil water content from the TDR measurements. Where the dielectric constant $k_a = [L_2/L]^2$, L_2 is the distance between curves and the L is the length of the TDR probe (Topp and Reynolds, 1998). Neutron probe was calibrated against the volumetric water content (calculated from gravimetric water content and bulk density) along the transect for several times over a three-year period (2007, 2008, and 2009) at different topographic positions and different moisture conditions. Soil water storage was calculated by multiplying the volumetric water content with depth (20 cm). Total soil water storage of the whole soil profile (up to 140 cm) was calculated by adding the soil water storage of each layer together. Soil water storage was measured for 20 occasions over a four-year period (2007 to 2010) at different environmental conditions to represent different types of distribution pattern of soil water at different seasons. A topographic survey of this site was completed using light detection and ranging (LiDAR) survey of the study area at 5 m resolution. The vegetation of the site was mixed grass seeded by Ducks Unlimited Canada in 2004 and allowed to grow every year. The organic carbon (OC) of surface soil was determined using LECO-C6235 carbon determinator (LECO Corp., St. Joseph, MI,

USA). The particle size distribution of surface soil was characterized using HORIBA LA-950 Laser diffraction particle-size analyzer (HORIBA Scientific Inc., Edison, NJ, USA).

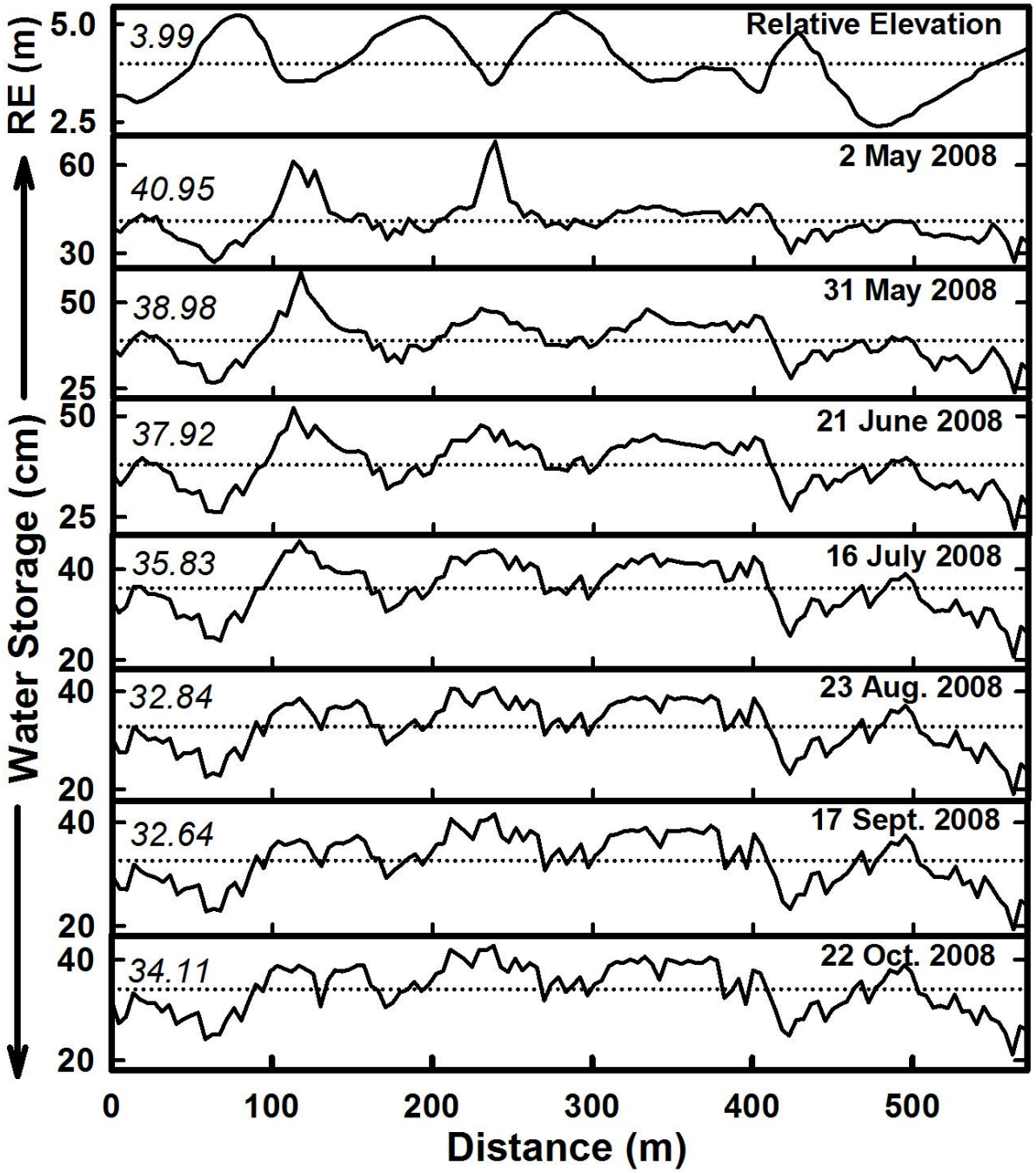

Figure 7.2. Spatial distribution of water storage (cm) for the whole soil profile (0-140 cm) measured in 2008 and relative elevation (m) along the transect with the average value in *italics*. X-axis indicates distance along the transect (m).

7.4.3 Data Analysis

Exploratory data analysis was completed in Microsoft Office Excel (Microsoft Corporation Inc.). Graphs were prepared in SigmaPlot (SysStat Software Inc.). The wavelet coherency was completed using the MATLAB (The MathWorks Inc.) code written by Grinsted et al. (2004) and is available at URL: http://www.pol.ac.uk/home/research/waveletcoherence/.

One of the important processes controlling the hydrology of the study area is snowmelt during spring. It contributes a lot of water within a very short time and increase the soil water storage. In the summer the vegetation develops and grows until early fall. Rainfall cannot meet strong evapotranspirative demand of growing vegetation and the stored water is being utilized. Later in the fall, the vegetation dies and some amount of fall rainfall increase the soil water storage slightly. Soil water storage was measured for 20 occasions covering these seasons. Though, the necessary data analysis was performed for all measurements, the result of wavelet coherency between controlling factors and one soil water storage from each season is presented in the manuscript. The measurement on 2 May 2008, 23 August 2008, and 22 October 2008 was considered as the representative of spring, summer, and fall season measurement, respectively.

7.5 Results and Discussion

7.5.1 Spatial Pattern of Soil Water Storage

Figure 7.2 presented the spatial distribution of selected soil-water storage series for the whole soil profile (0-140 cm). During early spring (2 May 2008), the locations from 100 to 140 m (Pond A in Figure 7.1) and 225 to 250 m (Pond B in Figure 7.1) along the transect stored more water compared to other locations (Figure 7.2). These locations were situated within depressions. Generally, the study area receives a considerable amount of precipitation (around 30% of the annual precipitation; Pomeroy et al., 2007) during winter as snow. The uneven distribution of snow in the prairie landscape (Pomeroy and Gray, 1995; Elliot and Efetha, 1999; Fang and Pomeroy, 2009; Lungal, 2009) and rapid snowmelt during early spring contributed high water storage in depression than that on knolls (Woo and Rowsell, 1993; Hayashi et al., 1998). The frozen soil surface during snowmelt in early spring and the divergent characteristics of rounded knolls did not allow sufficient time for water to infiltrate into the soil.

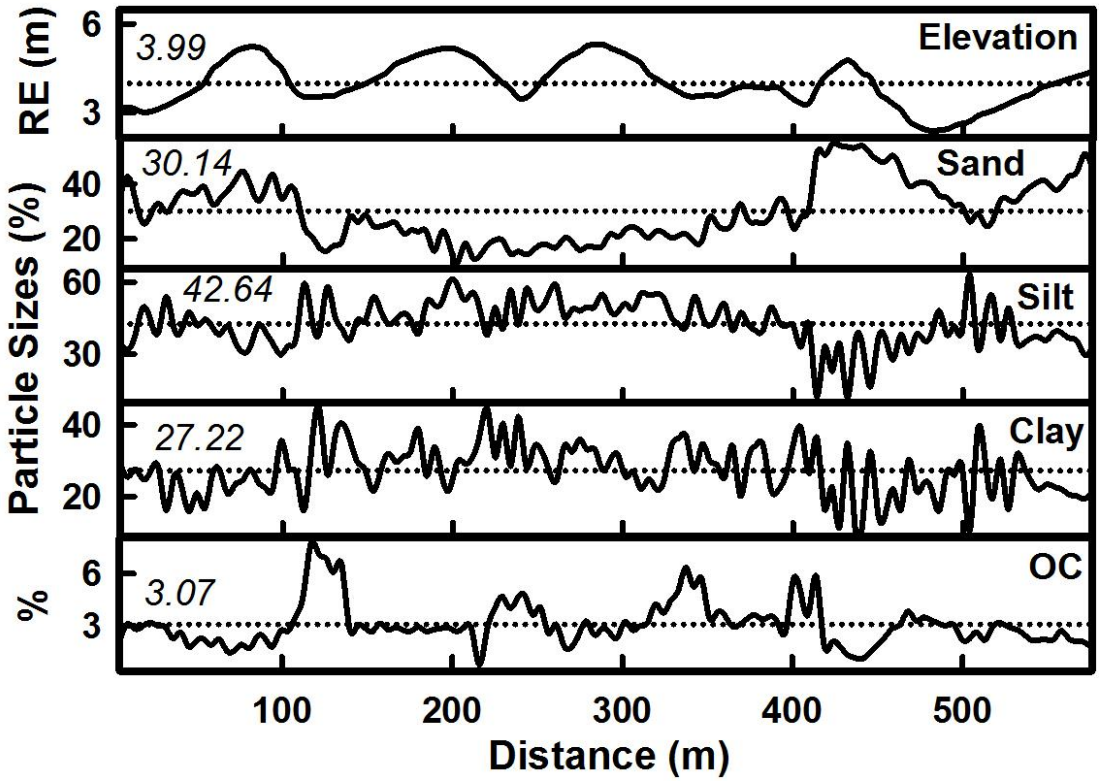

Figure 7.3. Spatial distribution of soil water storage controlling factors along the transect. X-axis indicates distance along the transect (m). Particle sizes and OC for the surface soil layer (0-20 cm).

Therefore, the excess amount of water redistributes in the landscape and creates a wide range of soil water storage (Gray et al., 1985; Winter and Rosenberry, 1995; Flerchinger and Cooley, 2000) between knolls and depressions. High water storage in depressions and low water storage on knolls created a spatial pattern inverse to the spatial pattern of elevation (Figure 7.2).

Vegetation generally establishes during early summer and grows until fall. The major source of water loss during this time was evapotranspiration and to a lesser extent, groundwater interaction (Hayashi et al., 1998; van der Kamp et al., 2003) resulting very similar spatial patterns in soil water storage during summer (e.g., 23 August 2008) and fall (e.g., 22 October 2008) (Figure 7.2). The better vegetation in depressions than that on knolls (leaf area index and visual observation; unpublished data) reduced the difference in water storage between those locations. However, the depressions stored more water during spring than plant can take up during summer and fall. Therefore, the topographically induced spatial pattern in soil water

storage was maintained but with a reduced degree (Figure 7.2). Similar snowmelt processes during spring and evapotranspirative demand of plants during summer and fall created similar spatial patterns of soil water storage over years. However, the spatial patterns of soil water at different season were not very comparable to the spatial patterns of sand, silt, clay, and organic carbon (Figures 7.2 and 7.3).

7.5.2 Soil Water Storage Controlling Factors

7.5.2.1 Pearson Correlation Analysis

Table 7.1 reported the correlation coefficients (*r*) between all soil-water storage series and the five different factors. The value of *r* was high (maximum = 0.74 and minimum = 0.47) and statistically significant between soil water storage and organic carbon (OC) during spring and gradually decreased during fall of each year (Table 7.1). The value of *r* between the average soil water storage over four years and OC was 0.70. A similar high correlation with OC was also reported elsewhere (Gómez-Plaza et al., 2000; da Silva et al., 2001; Hu et al., 2010). OC contributes to better soil structure and thus the water storage is higher (Chang, 1968; Pachepsky et al., 2005). The value of *r* was high and significant between soil water storage and different particle size fractions during spring (e.g. sand: maximum = -0.73, minimum = -0.57; clay: maximum = 0.54, minimum = 0.47; Table 7.1). The value of *r* was -0.68 and 0.53 between average soil water storage over four years and sand and clay, respectively. Various other studies also indicated high correlation between soil water and soil texture (Vachaud et al., 1985; Mohanty and Skaggs, 2001; Jacobs et al., 2004; Starks et al., 2006; Cosh et al., 2008). While, the value of *r* gradually increased for sand and silt from spring to fall, it remained almost constant for clay. The particle sizes control the infiltration capacity and permeability of water. The high infiltration capacity favors the infiltration of water in soil and the rapid drying out of the surface soil water (Vachaud et al., 1985; Gómez-Plaza et al., 2001; Pan and Wang, 2009) regulating the soil water storage. In spite of visual similarity between the spatial pattern of soil water storage and elevation, weak or no significant linear correlation was observed (e.g. value of *r*, maximum = -0.29, minimum = -0.12; Table 7.1). In a recent study, Zhao et al. (2010) also reported a low correlation between soil water storage and elevation form a grazed semi-arid steppe environment.

Table 7.1. Linear correlation coefficients (*r*) between soil water storage over three years and its controlling factors.

Measurement	Elevation	Sand	Silt	Clay	OC
17 July 2007	-0.24**	-0.60**	0.35**	0.48**	0.71**
7 August 2007	-0.23**	-0.60**	0.32**	0.51**	0.71**
1 September 2007	-0.22*	-0.62**	0.35**	0.51**	0.72**
12 October 2007	-0.21*	-0.64**	0.38**	0.50**	0.68**
2 May 2008	-0.24**	-0.59**	0.35**	0.47**	0.72**
31 May 2008	-0.23**	-0.61**	0.35**	0.50**	0.74**
21 June 2008	-0.20*	-0.66**	0.40**	0.50**	0.67**
16 July 2008	-0.18*	-0.68**	0.43**	0.50**	0.63**
23 August 2008	-0.14	-0.70**	0.46**	0.49**	0.51**
17 September 2008	-0.12	-0.70**	0.47**	0.48**	0.47**
22 October 2008	-0.12	-0.69**	0.46**	0.47**	0.47**
20 April 2009	-0.29**	-0.57**	0.31**	0.48**	0.71**
7 May 2009	-0.24**	-0.65**	0.36**	0.54**	0.74**
27 May 2009	-0.24**	-0.65**	0.39**	0.52**	0.75**
21 July 2009	-0.15	-0.72**	0.45**	0.54**	0.59**
27 August 2009	-0.13	-0.73**	0.48**	0.51**	0.53**
27 October 2009	-0.12	-0.71**	0.47**	0.49**	0.47**
6 April 2010	-0.24**	-0.62**	0.40**	0.50**	0.57**
19 May 2010	-0.22*	-0.60**	0.33**	0.50**	0.68**
14 June 2010	-0.24**	-0.68**	0.36**	0.48**	0.71**
Average (4 yrs.)	-0.22**	-0.68**	0.41**	0.53**	0.70**

* Significant at $p < 0.05$ level of probability

** Significant at $p < 0.01$ level of probability

7.5.2.2 Wavelet Coherency Analysis

The scale and location specific correlation between soil water storage at different seasons and the controlling factors was examined using wavelet coherency. Based on the dominant coherencies between soil water storage and controlling factors, three dominant scales of coherencies were identified. Up to 15 m, 15 to 70 m, and 70 to 150 m were identified as the

Table 7.2. Average, maximum, minimum, and standard deviation of wavelet coherency at different scales between soil water storage of whole soil profile (0-140 cm) and different controlling factors over seasons.

Coherency	Scale	Average	Maximum	Minimum	Standard deviation
Spring-Elevation	<15 m	0.31	0.95	0.00	0.24
	15-70 m	0.55	0.93	0.00	0.26
	70-150 m	0.80	0.96	0.40	0.15
Spring-Sand	<15 m	0.24	0.85	0.00	0.19
	15-70 m	0.45	0.90	0.00	0.25
	70-150 m	0.37	0.70	0.01	0.14
Spring-OC	<15 m	0.36	0.88	0.00	0.22
	15-70 m	0.48	0.95	0.00	0.27
	70-150 m	0.86	0.98	0.60	0.09
Summer-Elevation	<15 m	0.38	0.92	0.00	0.26
	15-70 m	0.33	0.91	0.00	0.22
	70-150 m	0.82	0.94	0.51	0.09
Summer-Sand	<15 m	0.37	0.90	0.00	0.25
	15-70 m	0.36	0.90	0.00	0.23
	70-150 m	0.65	0.90	0.01	0.24
Summer-OC	<15 m	0.43	0.88	0.00	0.24
	15-70 m	0.35	0.80	0.00	0.22
	70-150 m	0.70	0.89	0.14	0.18
Fall-Elevation	<15 m	0.37	0.89	0.00	0.23
	15-70 m	0.30	0.89	0.00	0.21
	70-150 m	0.78	0.92	0.41	0.11
Fall-Sand	<15 m	0.38	0.90	0.00	0.24
	15-70 m	0.34	0.88	0.00	0.22
	70-150 m	0.63	0.91	0.00	0.27
Fall-OC	<15 m	0.43	0.90	0.00	0.24
	15-70 m	0.33	0.84	0.00	0.23
	70-150 m	0.65	0.86	0.18	0.19

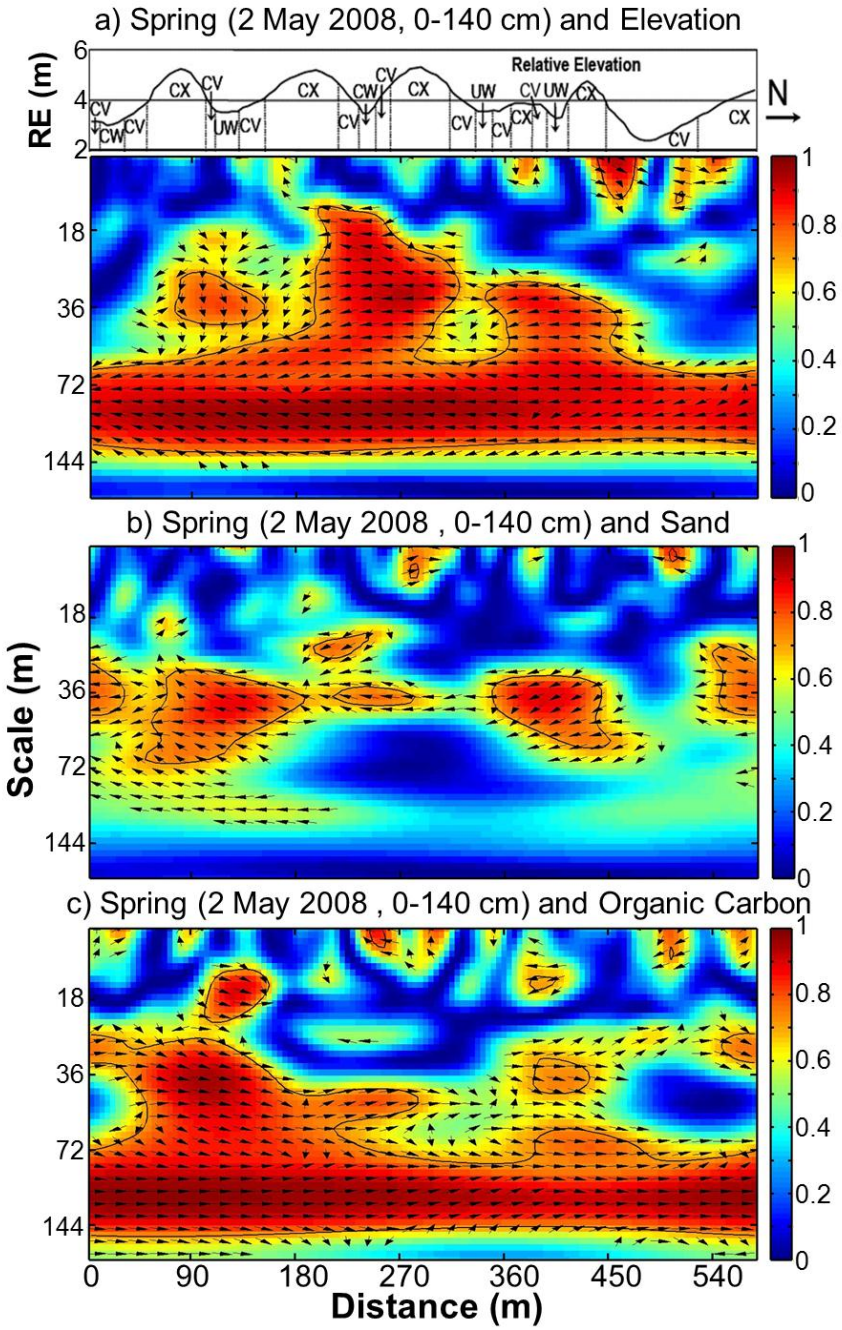

Figure 7.4. Wavelet coherency between soil water storage for whole soil profile (0-140 cm) measured on 2 May 2008 and a) relative elevation, b) sand, and c) organic carbon are shown. X-axis indicates distance along the transect in meter, Y-axis indicates scale in meter, solid black line indicates 5% significance level, color bar indicates strength of correlation, and the direction of arrow indicate phase information or the type of correlation (right directed- 'in phase' or positive; left directed- 'out of phase' or negative). The cross sectional view of relative elevation with different landform elements is shown at top. CX indicates convex, CV indicates concave, CW indicates cultivated wetlands and UW indicates uncultivated wetlands.

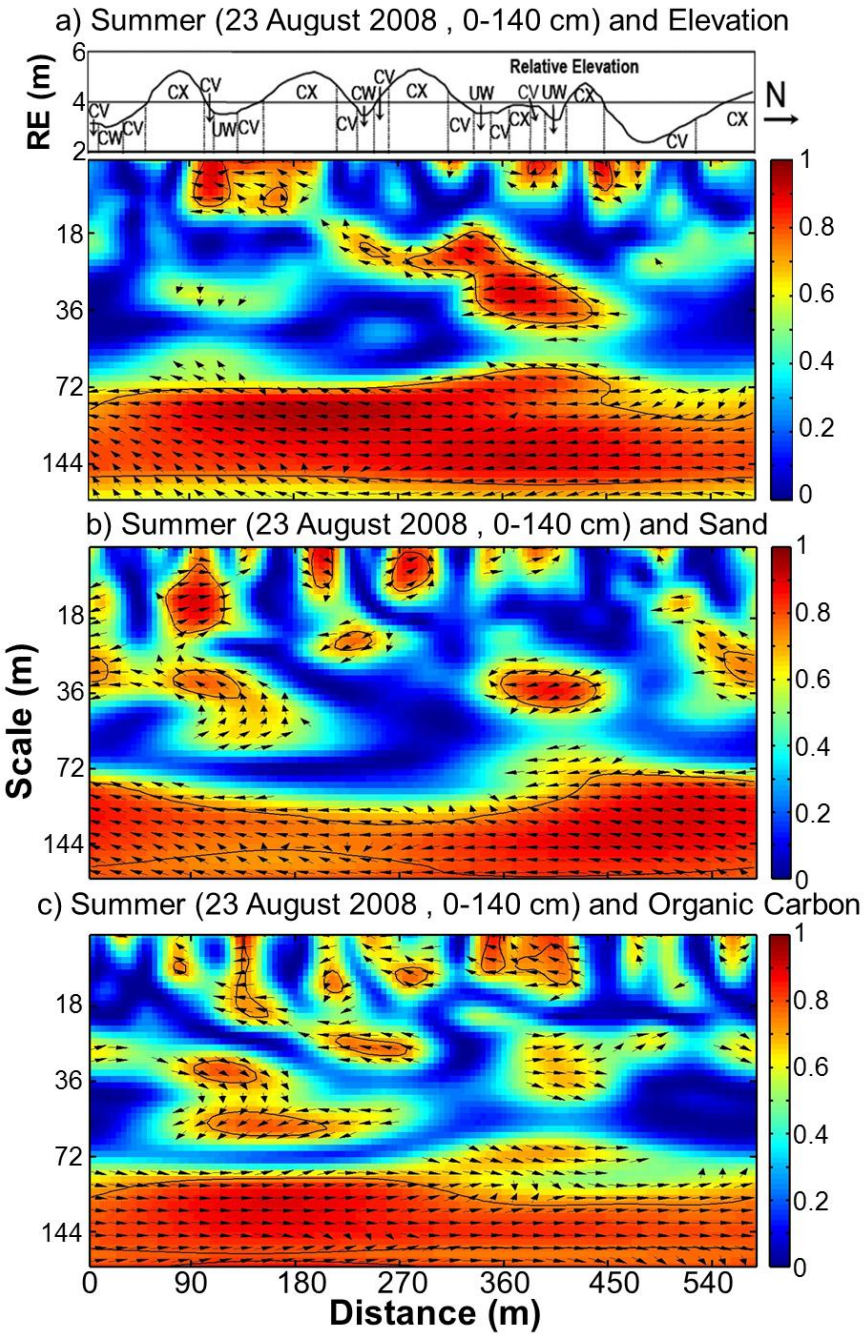

Figure 7.5. Wavelet coherency between soil water storage for whole soil profile (0-140 cm) measured on 23 August 2008 and a) relative elevation, b) sand, and c) organic carbon are shown. X-axis indicates distance along the transect in meter, Y-axis indicates scale in meter, solid black line indicates 5% significance level, color bar indicates strength of correlation, and the direction of arrow indicate phase information or the type of correlation (right directed- 'in phase' or positive; left directed- 'out of phase' or negative). The cross sectional view of relative elevation with different landform elements is shown at top. CX indicates convex, CV indicates concave, CW indicates cultivated wetlands and UW indicates uncultivated wetlands.

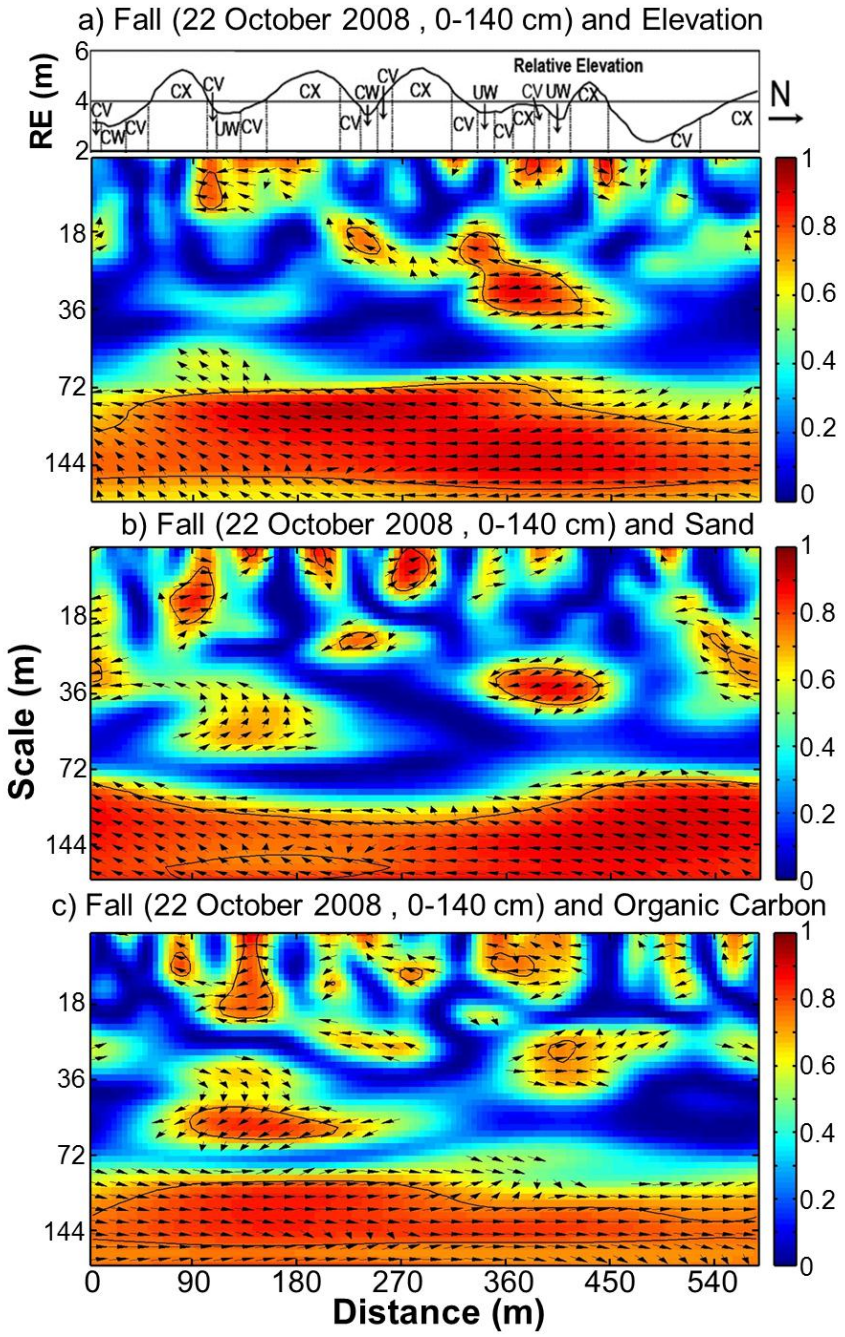

Figure 7.6. Wavelet coherency between soil water storage for whole soil profile (0-140 cm) measured on 22 October 2008 and a) relative elevation, b) sand, and c) organic carbon are shown. X-axis indicates distance along the transect in meter, Y-axis indicates scale in meter, solid black line indicates 5% significance level, color bar indicates strength of correlation, and the direction of arrow indicate phase information or the type of correlation (right directed- 'in phase' or positive; left directed- 'out of phase' or negative). The cross sectional view of relative elevation with different landform elements is shown at top. CX indicates convex, CV indicates concave, CW indicates cultivated wetlands and UW indicates uncultivated wetlands.

small, medium, and large scale, respectively (Figures 7.4, 7.5, and 7.6). The average coherency at small-scale (<15 m) was 0.31 between spring soil water storage (2 May 2008) and elevation with the maximum of 0.95, minimum of 0 and the standard deviation (SD) of 0.24 (Table 7.2) for the whole soil profile (0-140 cm). Similarly, the small-scale average coherency between spring soil water storage and sand and OC was 0.24 (SD = 0.19) and 0.36 (SD = 0.22), respectively (Table 7.2). There were very few locations that had significant coherency at small scales between spring soil water storage and elevation (Figure 7.4a), sand (Figure 7.4b), and OC (Figure 7.4c). These significant coherencies were not associated with any particular landscape position and may be attributed to the localized variations in soil water storage. The medium scale (15 to 70 m) average coherency was 0.55 (SD = 0.26), 0.45 (SD = 0.25), and 0.48 (SD = 0.27) between spring soil water storage and elevation, sand, and OC (Table 7.2). The coherencies were significant at the locations of 80 to 160 m, 190 to 320 m, and 340 to 450 m along the transect between spring soil water storage and elevation (Figure 7.4a). The medium scale coherencies were significant at 0 to 40 m, 60 to 280 m, 350 to 450 m and 540 m to the end of the transect (Figure 7.4b) and at 0 to 280 m, 380 to 470 m and 550 m to the end of the transect (Figure 7.4c) between soil water storage of the whole soil profile and sand and OC, respectively. The medium scale correlations may be attributed to the variations in micro-topography and landform elements (e.g., convex, concave, cultivated, and uncultivated wetlands) within depressions (Kachanoski and de Jong, 1988). The average coherency was 0.80 (SD = 0.15), 0.37 (SD = 0.14), and 0.86 (SD = 0.09) between spring soil water storage and elevation, sand, and OC, respectively at large scales (70 to 150 m; Table 7.2). There were significant coherencies at all locations between spring soil-water storage and elevation (Figure 7.4a) or OC (Figure 7.4c). The large-scale significant coherencies might have contributed from the alternating knolls and depressions along the transect (Kachanoski and de Jong, 1988). However, there were no significant coherencies at large scale between spring soil water storage and sand (Figure 7.4b). This was also true for silt and clay.

There was very similar wavelet coherency between the soil water storage during summer and fall with elevation (Figures 7.5a and 7.6a), sand (Figures 7.5b and 7.6b), and OC (Figures 7.5c and 7.6c). The small-scale average coherency was 0.38 (SD = 0.26), 0.37 (SD = 0.25), and 0.43 (SD = 0.24) and 0.37 (SD = 0.23), 0.38 (SD = 0.24), and 0.43 (SD = 0.24) between

elevation, sand, and OC and soil water storage during summer and fall, respectively (Table 7.2). The medium scale average coherency was 0.33 (SD = 0.22), 0.36 (SD = 0.23), and 0.35 (SD = 0.22) and 0.30 (SD = 0.21), 0.34 (SD = 0.22), and 0.33 (SD = 0.23) between controlling factors and above mentioned soil water storage of two seasons, respectively. There were very few locations that had significant coherencies at small and medium scales between soil-water storage during summer and fall and elevation (Figures 7.5a and 7.6a), sand (Figures 7.5b and 7.6b), and OC (Figures 7.5c, and 7.6c). However, the large-scale average coherency was 0.82 (SD = 0.09), 0.65 (SD = 0.24), and 0.70 (SD = 0.18) and 0.78 (SD = 0.11), 0.63 (SD = 0.27), and 0.65 (SD = 0.19) between elevation, sand, and OC and soil water storage during summer and fall, respectively (Table 7.2). The large-scale coherencies were significant at almost all locations between soil water storage during summer and fall and all controlling factors (Figures 7.5 and 7.6).

The wavelet coherencies were calculated at scales between 9 to 200 m for all locations along the transect. The minimum scale was equal to the length of two-sample interval. There were total of 54 scales at each of the 128 locations. Therefore, the total number of wavelet coherency was 6912. Among these, total number of locations that had significant coherency at different scales can be used to compare the relative dominance of different controlling factors on soil water storage at different seasons. In the contour plot, one significant coherency at a particular scale and location represents significant correlation in a unit area. Consequently, the total area of significant coherency can be used as a proxy of strength of correlations between two variables. Total area of significant relationship was compared between different controlling factors and soil water storage of one season and between a controlling factor and soil water storage of different seasons. Total area of significant relationship between soil water storage and different controlling factors was in the order of elevation > OC > sand during spring (Figure 7.4) and in the order of elevation > sand > OC during summer and fall (Figures 7.5 and 7.6). This indicated elevation as the dominant controlling factor of soil water storage (Famiglietti et al., 1998; Western and Blöschl, 1999; Gómez-Plaza et al., 2000; Hupet and Vanclooster, 2002) irrespective of season. While, there was decrease in the total area of significant correlation from spring through summer to fall between soil water storage and elevation or OC, there was an increase in the total significant area between soil water storage and sand (Figures 7.4, 7.5, and

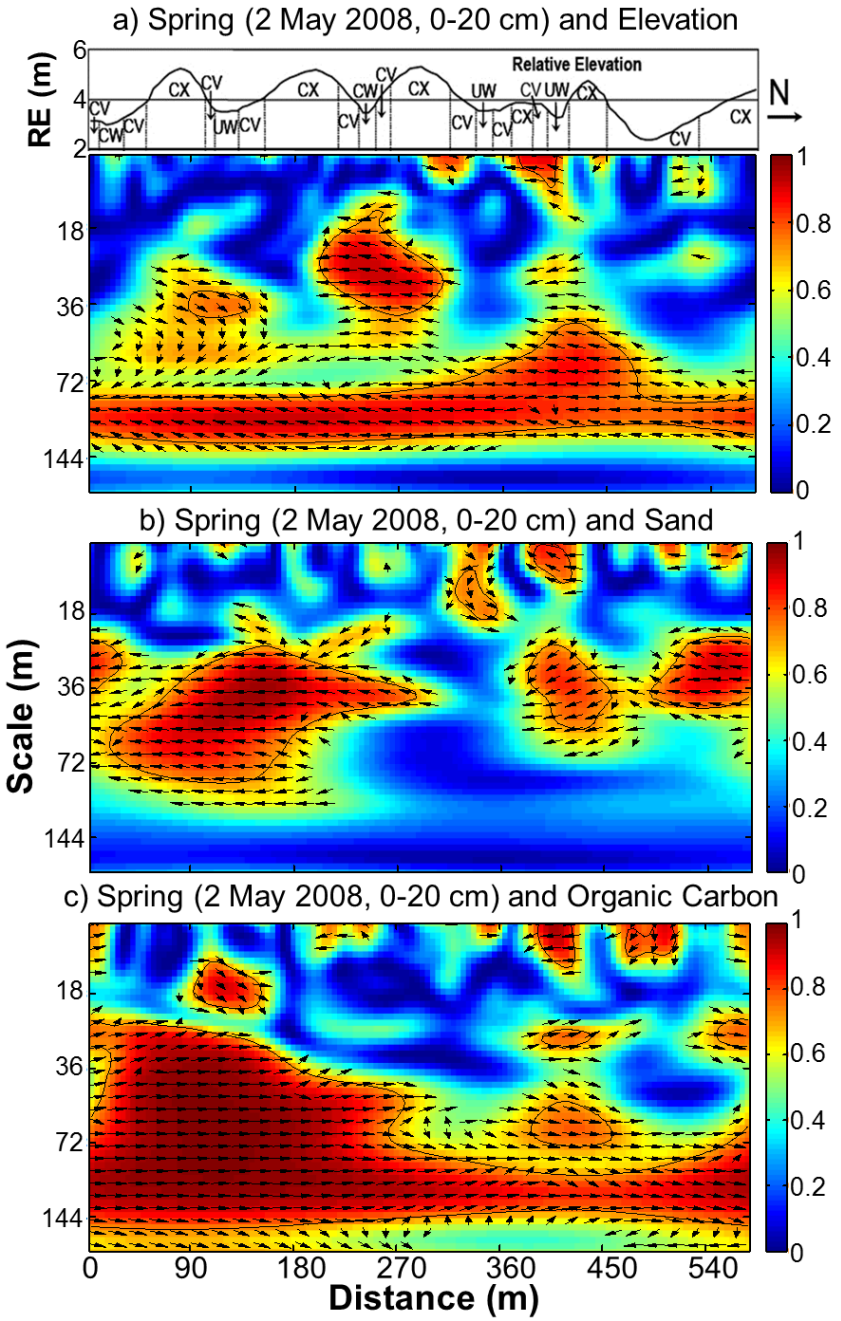

Figure 7.7. Wavelet coherency between soil water storage for the surface layer (0-20 cm) measured on 2 May 2008 and a) relative elevation, b) sand, and c) organic carbon are shown. X-axis indicates distance along the transect in meter, Y-axis indicates scale in meter, solid black line indicates 5% significance level, color bar indicates strength of correlation, and the direction of arrow indicate phase information or the type of correlation (right directed- 'in phase' or positive; left directed- 'out of phase' or negative). The cross sectional view of relative elevation with different landform elements is shown at top. CX indicates convex, CV indicates concave, CW indicates cultivated wetlands and UW indicates uncultivated wetlands.

7.6). This indicated the decrease in the intensity of control from elevation and OC and increase in the intensity of control from sand over seasons but not switching of controls from one factor to another. This result contradicted the result of Grayson et al. (1997), who indicated the change in the control of soil water storage over seasons. In our study, snowmelt runoff created a strong spatial pattern in soil water storage with elevation during spring that persisted even at the end of the fall indicating the persistence of control from elevation.

The comparison of the total area of significant relationships between scales explained relative dominance of scales. The large scale was the dominant scale as the area of significant relationship was the highest between soil water storage of all seasons and elevation or OC (Figures 7.4, 7.5, and 7.6). This clearly indicated that the alternating knolls and depressions in the landscape had major control on soil water storage. While, sand had the maximum large-scale contribution during summer (Figure 7.5b) and fall (Figure 7.5c), the medium scale contributed the maximum during spring (Figure 7.4b). This may be due to the variations in soil texture between landform elements and the differential exposure of landform elements to solar radiation and wind that modify the water loss by evaporation during spring.

The relationship between soil water storage at the surface layer (0-20 cm) and various controlling factors at different scales and locations were also examined using wavelet coherency. The surface soil water storage at different seasons also had a very similar relationship at different scales to that of whole soil profile. For example, the average small-scale coherency was 0.27 (SD = 0.22), 0.33 (SD = 0.23), and 0.38 (SD = 0.25) between spring surface soil water storage and elevation, sand, and OC, respectively. There were only few locations with significant coherency at small scales between soil water storage and controlling factors (Figure 7.7). The medium-scale average coherency was 0.44 (SD = 0.24), 0.53 (SD = 0.25), and 0.51 (SD = 0.29) between surface soil water storage and elevation, sand, and OC, respectively. The medium-scale coherencies between soil water storage and elevation were located within depressions with more variations in landform elements (Figure 7.7b). However, the medium scale coherencies between soil water storage and OC were located within first half of the transect (Figure 7.7c). The average large-scale coherency was 0.68 (SD = 0.17), 0.33 (SD = 0.18), and 0.84 (SD = 0.11) between spring surface soil water storage and elevation, sand, and OC, respectively. However, the total area of significant relationships was the highest between soil water storage and OC (Figure 7.7c).

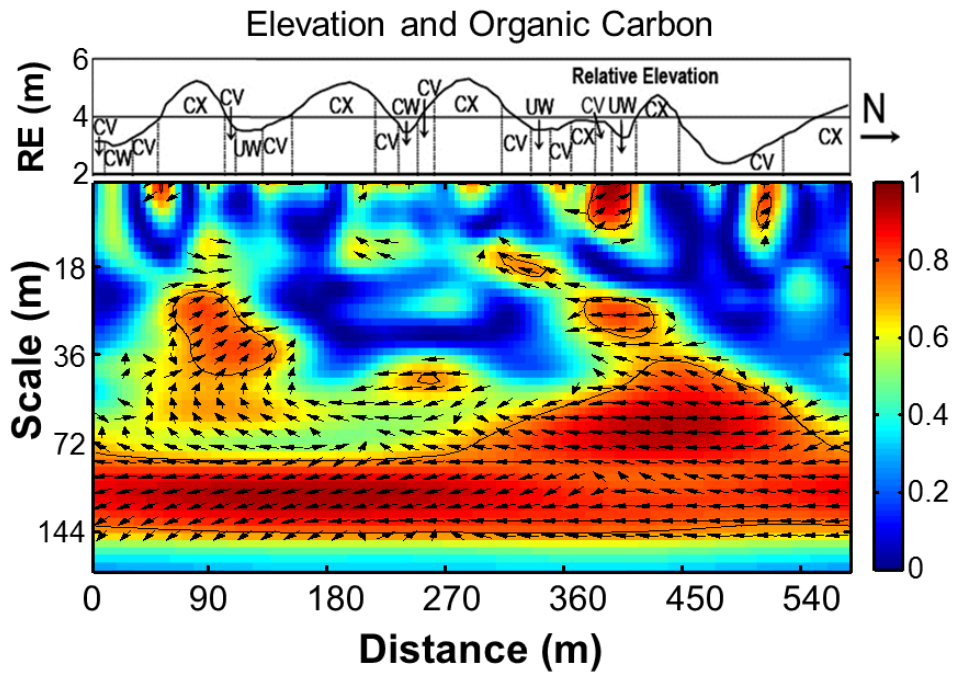

Figure 7.8. Wavelet coherency between elevation and organic carbon along the transect was shown. X-axis indicates distance along the transect in meter, Y-axis indicates scale in meter, solid black line indicates 5% significance level, color bar indicates strength of correlation, and the direction of arrow indicate phase information or the type of correlation (right directed- 'in phase' or positive; left directed- 'out of phase' or negative). The cross sectional view of relative elevation with different landform elements is shown at top. CX indicates convex, CV indicates concave, CW indicates cultivated wetlands and UW indicates uncultivated wetlands.

OC modifies the bulk density, soil structure, and porosity, which affect the soil water holding capacity and soil hydraulic conductivity (Hawley et al., 1983; Jacobs et al., 2004). Generally, OC in the surface soil is higher compared to deep layers. Organic carbon, which reflects the long-term history of soil water storage, was strongly correlated with relative elevation. Organic carbon indicates the long-term footprint of soil water storage and vegetation growth in the landscape. As the elevation has a major control on soil water storage in the landscape, the variations in OC was very similar to the variations in elevation (Figure 7.8). The average coherency was 0.45 and 0.80 between elevation and OC at medium- and large-scales, respectively. The large-scale variations were contributed form alternating knolls and depressions and were present all over the transect (Figure 7.8). Therefore, the similarity in the relationship between soil water storage and elevation and OC may be a representative of control from elevation. However, there were no significant coherencies at large scales between soil water storage and sand (Figure 7.7b). A very similar

relationship was observed between surface soil water storage during summer and fall and different other controlling factors.

The type of correlation was determined from the phase relationships; 'in phase' or right directed arrow indicated positive correlation and 'out phase' or left directed arrow indicated negative correlation. While the elevation and sand were negatively correlated (phase anti-locked or out of phase) to soil water storage, OC was positively correlated (phase locked or in phase) at large scales (Figures 7.4, 7.5, and 7.6). The organized arrow at medium scales also indicated a positive correlation between soil water storage and organic carbon while negative relationship between soil water storage and elevation and sand. However, the small-scale relationships were mostly random between soil water storage and controlling factors (Figures 7.4, 7.5, and 7.6).

Knowledge on the controls of soil water storage at different scales is useful in improving the scale specific prediction of soil water storage in the hummocky landscape of the prairie pothole region. The change in the dominant control of soil water storage at different scale is an indicative of the change in the hydrological processes operating at those scales. The transformation of information from one scale to another is also possible from the scale specific relationship between soil water storage and different controlling factors. The relationship at different scales has important implications for the pedo-transfer functions. The persistence of the controls from different factors over seasons can help catchment managers to identify the management units in a more cost effective manner for precision management of crop biomass production and the environment.

In this study, we have only considered five different factors to understand the scale specific control of soil water storage. Elevation is the most easily measured and commonly used index to represent topography. However, there are different other topographic indices such as wetness index, contributing area, slope, curvature etc., which was reported to control soil water distribution (Grayson et al., 1997; Grayson and Western, 1998; Famiglietti et al., 1998; Western et al., 1999; Thierfelder et al., 2003; Brocca et al., 2007, 2009). Future work is necessary to understand the scale specific controls from different topographic indices on soil water storage.

7.5 Conclusions

Soil water is characterized by high spatio-temporal variability contributing from the different factors and processes working alone or in combination. In studying the soil water dynamics, it is necessary to understand the controls behind the variability. Various authors have used Pearson correlation analysis to identify the important controls from the linear dependence between soil water storage and controlling factors. Pearson correlation is space and scale invariant and identifies the correlation at the measurement scale. However, factors can vary at different scales controlling soil water storage variably over scales, which cannot be identified from traditional correlation analysis. Wavelet coherency was used to examine scale and location specific correlation between soil water storage and controlling factors at different seasons.

In spite of low Pearson correlation coefficient, wavelet coherency showed strong correlation between soil water storage and elevation at different scales and locations. There was persistent significant correlation at large scales (> 70 m) between soil water storage and elevation or OC at locations. However, there was significant correlation at large scales between soil water storage and sand only during summer and fall but not during spring. The dominant scale of variations was the large scale, which was attributed to the alternating knolls and depressions along the transect. While, the relationship was persistent, the magnitude of correlation changed over seasons indicating changes in the degree of control. Elevation controlled the water redistribution process (e.g., runoff) in the landscape in spring, establishing a spatial pattern that was persistent during other seasons.

This study clearly indicated that the importance of nonlocal controls (e.g., elevation) (Grayson et al., 1997) on soil water storage in the Canadian Prairies. The scale at which elevation was the major control was >70 m. Pearson correlation coefficient, which measures linear correlation at measurement scales (point scale), was not able to identify this relationship. Wavelet coherency analysis successfully unraveled this scale- and location-dependent relationship, thus should be an essential tool for spatial analysis.

8.0 IDENTIFYING EFFECTS OF LOCAL AND NONLOCAL FACTORS OF SOIL WATER STORAGE USING CYCLICAL CORRELATION ANALYSIS

8.1 Preface

There are various factors governing the spatial and temporal variability of soil water storage including soil properties, topography, and vegetation. Some factors act locally, while others act non-locally, which means that a factor measured at one place has effect on soil water storage of another place. Therefore, there is a lag between the origin of the factor and its response in soil water storage. This chapter examines the effect of local and nonlocal factors on soil water storage using cyclical correlation analysis.

8.2 Introduction

The distribution of soil water in space and time has important hydrologic applications. However, high spatio-temporal variability of soil water is a major challenge in hydrology (Quinn, 2004) as the distribution of soil water in the landscape is the response of many factors and processes acting in different intensities over a variety of scales (Goovaerts, 1998; Entin et al., 2000). While some factors have very localized effects on soil water storage, others act non-locally, which means that the soil water storage of one location is controlled by factors from other locations (Grayson et al., 1997). The correlation of soil water storage with controlling factors at the measurement scale could only explain the localized influence from those factors. However, understanding the nature of nonlocal controls and its dominant scale would explain the relationship between soil water storage and its controlling factors better and improve the prediction.

Numerous studies have been conducted to identify the main controls of spatial and temporal dynamics of soil water storage. The main controls include a) soil properties (Vachaud et al., 1985; Zhang and Berndtsson, 1988; Fitzjohn et al., 1998), (b) topography (Burt and Butcher, 1985; Moore et al., 1988b; Western et al., 1999; Gómez-Plaza et al., 2001) and (c) vegetation (Sharma et al., 1980; Hawley et al., 1983; Seghieri et al., 1997; Bromley et al., 1997; Rodríguez-Iturbe et al., 1999). The findings from different studies are sometimes contradictory

because the interaction between various factors on soil water storage may be site-dependent (Famiglietti et al., 1998; Tallon and Si, 2004; Choi et al., 2007).

The spatial variability of soil water storage at small catchment and hill-slope scales is determined by the water routing processes (Beven and Kirkby, 1979; Moore et al., 1988b), differential radiation effect (Moore et al., 1993; Western et al., 1999), heterogeneity in soil (Hu et al., 1997; Famiglietti et al., 1998) and vegetation (Qui et al., 2001; Hupet and Vanclooster, 2002). Furthermore, all these factors are somewhat dependent upon terrain characteristics; therefore, terrain often explains more than half of the variations in the spatial distribution of soil water storage (Tomer and Anderson, 1995; Western et al., 1999, 2002, 2004). Often the remaining variance is either random or associated with other factors such as soil properties. The patchy or spatially correlated deviation from the topographic signal in soil water usually suggests the effect of the variation in soil properties on soil water (da Silva et al., 2001; Wilson et al., 2004).

The effects are also known to be dependent on the general soil water condition because the different processes control the soil water storage under different conditions (Grayson et al., 1997). When precipitation exceeds evapotranspiration or in dry state, the spatial pattern of soil water storage is determined by the dominant vertical flux. Soil properties and local terrain determine the entry and transmission of water in soil mostly as vertical fluxes and the factors are denoted as 'local' factors (Grayson et al., 1997). However, with the increase of water content, the hydraulic conductivity increases nonlinearly (Grayson et al., 1992). At saturation or near saturation, the macro-pore flow may generate and contribute to the lateral redistribution of subsurface soil water in addition to the surface runoff. In this situation, different terrain properties provide organization in the spatial pattern of soil water storage in the landscape. These factors were identified as the 'nonlocal' factors (Grayson et al., 1997). Moreover, if the infiltration capacity of the soil decreases by any reason such as frozen ground (Gray et al., 1985), the surface lateral redistribution or runoff will dominate and determine the soil water storage spatial pattern in the landscape. Therefore, one location in the landscape will have the influence on soil water content of another location. For example, high soil water storage in a low topographic position has contribution from the high topographic positions. Therefore, there is a lag in distance between the origin of the controlling factors and its response for soil water

content, which can be considered as the scale of nonlocal effects. Characterization of the nonlocal effects from different controlling factors and their lags/leads or scales can better explain the relationship between soil water content and the controlling factors, which may improve the prediction.

Therefore, the objective of this study was to examine effects of local and nonlocal controls of soil water storage in the hummocky landscape of North America using cyclical correlation analysis. Pearson correlation analysis explains the linear association between two variables only at the scale of measurement. Therefore, the correlation can explain the localized effect of any factor on soil water storage. However, the correlation between the soil water storage and the controlling factors separated by certain distance or lag between them can explain the nonlocal effect of that factor on soil water storage.

8.3 Materials and Methods

A field study was conducted at St. Denis National Wildlife Area (52°12′ N latitude, 106°50′ W longitude), Saskatchewan, Canada. Detailed description on study site, soil water measurements, measurement instrument calibration, controlling factors measurements can be found in Biswas et al. (2011). We limited our scope in presenting any details on site description and data collection in this manuscript. Briefly, soil water storage was measured up to 140 cm depth for 20 times over a four-year period along a 128 point transect (576 m long) developed over several knoll-depression cycles in the hummocky landscape study area using time domain reflectometry and neutron probe. Various soil properties such as particle sizes (sand, silt, and clay), bulk density (BD), depth of A and C horizon, and depth of $CaCO_3$ layer from the surface were measured along the transect and terrain indices such as relative elevation, wetness index, catchment area, convergence index, curvature, aspect, gradient, slope, slope length, solar radiation, and flow connectivity were calculated form a digital elevation map of the study area (Biswas et al., 2011).

Pearson correlation coefficients between soil water storage and controlling factors were calculated at the scale of measurement as well as at different lag or lead distance by shifting the spatial series of soil water storage back and forth (by multiples of sampling interval) with respect to fixed spatial series of controlling factors (Kydland and Prescott, 1990; Oladosu, 2009). The

coefficient at zero lag/lead indicated the Pearson correlation coefficient at the measurement scale. Though the necessary calculation was performed between all 20 measurements completed at different environmental situations over four-years and different controlling factors, the results of only two measurements were presented in the manuscript to demonstrate the use of cyclical correlation analysis in identifying the local and nonlocal effects of various controlling factors. Generally, the study area receives approximately 30% of the annual precipitation as snow (Pomeroy et al., 2007), which melts within short time during early spring season. The snowmelt water and the spring season rainfall increase soil water storage in the landscape and the soil is considered to be in 'wet state'. However, once the vegetation is developed, the little rainfall during summer season could not meet strong evapotranspirative demand of growing plants. Therefore, the stored water is depleted in later summer and fall season and the soil is considered to be in 'dry state'. The relationship between one measurement from each condition (7 May 2009 and 27 August 2009 representing the wet and dry state, respectively) and seven selected controlling factors are presented in the manuscript.

8.4 Results

There was high soil water storage in the depressions and low soil water storage on the knolls. The variable water storage yielded a spatial pattern that was inverse to the spatial pattern in relative elevation. However, there was very low correlation between soil water storage and relative elevation at the measurement scale (coefficient of determination, $r^2 = 0.06$ on 7 May 2009 and 0.02 on 27 August 2009; Table 8.1). Unlike relative elevation, there was strong to moderate correlation between soil water storage and other topographic indices such as wetness index ($r^2 = 0.45$), and convergence index ($r^2 = 0.33$) at the measurement scale on 7 May 2009 (Table 8.1). However, the correlation decreased gradually at the later part of the year. For example, the value of r^2 was 0.29, and 0.19 between soil water storage and wetness index, and convergence index, respectively on 27 August 2009 (Table 8.1). There was strong to moderate correlation between soil water storage and various soil properties such as sand ($r^2 = 0.42$), silt ($r^2 = 0.13$), OC ($r^2 = 0.54$), and depth of $CaCO_3$ layer ($r^2 = 0.49$) at the measurement scale on 7 May 2009 (Table 8.1). Unlike the terrain indices, the correlation between soil water storage and sand and silt was increased during the latter part of the year or in

Table 8.1. Coefficients of determination (r^2) between soil water storage and different controlling factors at various lags and leads

Lag/Lead (m)	Relative Elevation		Sand		Silt		OC†		Convergence Index		Wetness Index		$CaCO_3$	
	7 May	27 Aug	7 May	27 Aug	7 May	27 Aug	7 May	27 Aug	7 May	27 Aug	7 May	27 Aug	7 May	27 Aug
-90	0.00	0.00	0.07	0.15	0.08	0.08	0.00	0.00	0.03	0.02	0.00	0.00	0.04	0.06
-81	0.06	0.06	0.04	0.11	0.06	0.07	0.02	0.01	0.00	0.00	0.06	0.06	0.00	0.02
-72	0.17	0.17	0.03	0.06	0.02	0.03	0.02	0.01	0.03	0.04	0.14	0.14	0.02	0.00
-63	0.27	0.27	0.03	0.05	0.02	0.04	0.02	0.02	0.12	0.12	0.19	0.22	0.05	0.02
-54	0.29	0.26	0.03	0.05	0.03	0.04	0.04	0.03	0.27	0.20	0.21	0.24	0.09	0.05
-45	0.22	0.17	0.03	0.07	0.02	0.05	0.03	0.01	0.31	0.17	0.14	0.13	0.11	0.05
-36	0.10	0.07	0.09	0.16	0.05	0.10	0.00	0.01	0.17	0.09	0.07	0.03	0.05	0.01
-27	0.02	0.01	0.11	0.21	0.05	0.09	0.01	0.05	0.04	0.02	0.01	0.00	0.01	0.00
-18	0.00	0.00	0.17	0.28	0.04	0.13	0.08	0.09	0.01	0.00	0.03	0.03	0.01	0.00
-9	0.04	0.02	0.32	0.42	0.13	0.21	0.36	0.20	0.15	0.04	0.25	0.16	0.22	0.05
0	0.06	0.02	0.42	0.53	0.13	0.23	0.54	0.28	0.33	0.15	0.45	0.29	0.49	0.19
9	0.01	0.00	0.33	0.47	0.13	0.20	0.36	0.31	0.23	0.16	0.33	0.27	0.35	0.18
18	0.02	0.05	0.19	0.37	0.10	0.18	0.09	0.18	0.11	0.11	0.15	0.20	0.07	0.08
27	0.17	0.18	0.15	0.29	0.07	0.13	0.00	0.04	0.01	0.03	0.03	0.10	0.00	0.02
36	0.38	0.34	0.09	0.14	0.04	0.07	0.01	0.00	0.00	0.00	0.00	0.01	0.02	0.00
45	0.50	0.47	0.04	0.06	0.02	0.05	0.05	0.02	0.04	0.01	0.06	0.01	0.09	0.06
54	0.50	0.53	0.01	0.01	0.01	0.01	0.07	0.06	0.08	0.06	0.12	0.07	0.10	0.07
63	0.37	0.49	0.00	0.00	0.00	0.00	0.06	0.06	0.11	0.09	0.14	0.10	0.06	0.07
72	0.20	0.37	0.00	0.00	0.01	0.00	0.03	0.03	0.07	0.03	0.10	0.06	0.05	0.06
81	0.06	0.19	0.00	0.00	0.01	0.00	0.00	0.00	0.04	0.02	0.03	0.02	0.02	0.01
90	0.00	0.07	0.01	0.00	0.00	0.00	0.01	0.01	0.01	0.01	0.00	0.00	0.00	0.00

† organic carbon

dry state. The change in the correlation was gradual from wet to the dry state (Table 8.1). A similar trend in the correlation was also observed in other years of measurements.

The r^2 value between soil water storage on 7 May 2009 and relative elevation increased to 0.50 at the lead of 54 m (Table 8.1). Similarly, the r^2 value increased to 0.53 at 54 m lead on 27 August 2009 (Table 8.1). However, the value of r^2 gradually decreased with the increase of lag/lead between soil water storage at any time and sand or silt. The r^2 values for 27 August 2009 were comparatively higher than that of 7 May 2009 (Table 8.1). However, a little different trend in the correlation was observed between soil water storage at any time and OC, convergence index, wetness index, or depth of $CaCO_3$. The highest correlation was observed without any shift and gradually decreased with the increase in lag/lead. However, a slight elevated correlation was observed at 54 m lag/lead between soil water storage and OC, convergence index, wetness index, or $CaCO_3$ and gradually decreased thereafter. The value of r^2 was higher on 7 May 2009 than that on 27 August 2009 (Table 8.1).

The inter-correlation among the factors was also observed. For example, the relative elevation was moderately correlated with some soil properties including OC ($r^2 = 0.11$) and depth of $CaCO_3$ layer ($r^2 = 0.15$). These soil properties were also correlated with other topographic indices. An obvious strong correlation was also observed between relative elevation and other terrain indices such as wetness index ($r^2 = 0.33$) and convergence index ($r^2 = 0.31$). There was also moderate to strong correlation among the soil properties.

8.5 Discussion

In the study area, the snowfall contributes more than 30 % of the annual precipitation (Pomeroy et al., 2007). The strong wind of prairie region redistributes snow across the landscape and within depressions (Pomeroy and Gray, 1995; Elliot and Efetha, 1999; Fang and Pomeroy, 2009). Generally, the depressions receive and store more snow compared to the surrounding uplands (Williams et al., 2008; Lungal, 2009). In addition, the frozen ground during snowmelt restricts the infiltration capacity (Gray, 1985; Winter and Rosenberry, 1995) and the infiltration excess snowmelt water is redistributed in the landscape. The depressions receive water from the surroundings and store more water compared to the knolls (Woo and Rowsell, 1993; Hayashi et al., 1998, 2003; Lungal, 2009) and therefore creating a spatial pattern inverse to that of relative

elevation. Generally, the location with high elevation contributes the water storage to some other locations with low elevation. However, the low correlation between soil water storage and the relative elevation may be because the correlation explained the relationship only at the scale of measurement.

However, the cyclical correlation analysis identified strong correlation between soil water storage and controlling factors at a scale different from the scale of measurement. The correlation between the spatial series of soil water storage and the controlling factors was improved after physically shifting the spatial series. For example, the value of r^2 was 0.06 between soil water storage and the relative elevation at the scale of measurement on 7 May 2009, which was improved to 0.50 after shifting the soil water series by 54 m (Table 8.1). In the hummocky landscape of the study area, water from the knolls runs down to the depressions and contributes to high storage in depressions. Therefore, the distance between the origin of the controlling factor and its response in improving soil water storage will be the difference between the knolls and depressions or the length of the slopes. In fact, the average length of the slopes in the study area was around 50 to 55 m. This can be explained with a simple theoretical example. A sine and a cosine wave with opposite phase are orthogonal to each other and therefore, the correlation is zero. However, if we shift the sine wave by half of the period or change the phase by 90°, the correlation between the waves will be unity. Moreover, if we compare a spatial series with any sine or cosine wave, a full period will have two slopes. Therefore, the length of one slope will be equivalent to the half of the period, which in this case was identified at 54 m.

Sine wave will have unity correlation in either forward or backward shifting. The improvement of the correlation between soil water storage and the relative elevation was observed in forward and backward shifting. However, the magnitude of correlation was slightly different. This may be due to the effect of north-facing and south-facing slopes. In our study area, the south facing slopes are longer than north facing slopes, therefore providing better correlation in forward shifting than that of backward shifting.

The wetness index, a compound terrain index, is calculated from the catchment area and the local surface gradient (Beven and Kirkby, 1979). The catchment area by definition is a nonlocal factor and the effect from this nonlocal factor is already being included in the wetness index calculation. Therefore, the strong correlation between soil water storage and wetness index

at the measurement scale explains local effect in soil water storage contributing from other nonlocal factors. In addition, the strong correlation at the lag/lead of 54 indicated the nonlocal effect from the wetness index. Moreover, the wetness index was also correlated with relative elevation, which had nonlocal effect at 54 m scale. Therefore, the wetness index had some local effect as well as nonlocal effect in controlling soil water storage.

The gradual decrease in the correlation with increasing lag/lead between soil water storage and sand or silt indicated that their effect is confined more locally or at the measurement scale (Grayson et al., 1997). However, the cyclical correlation between soil water storage and other soil properties such as OC or depth of $CaCO_3$ layer showed slight different trend than that of sand or silt. The strong correlation at the measurement scale explained the local effect form these factors. However, the slight elevated correlation at the lag/lead of 54 m may be due to the effect of elevation on these factors (Bedard-Haughn and Pennock, 2002). A similar trend in cyclical correlation was also observed in convergence index, which measures the local convergence of divergence. The elevated correlation at the lag/lead at 54 m scale may be due to the strong association with relative elevation.

A similar trend in local and nonlocal effect was also observed for the dry period. However, the magnitude of correlations was lower between soil water storage and different controlling factors except sand and silt. Sand and silt controlled the soil water storage only locally (Grayson et al., 1997). During the dry period, the summer precipitation could not meet the increased evapotranspirative demand of vegetation and deplete the stored water in soil. In the semi-arid climate of prairie, the average water loss from evaporation and transpiration can go as high as 3 to 5 mm per day (Rosenberry and Winter, 1997; Parkhurst et al., 1998), which can be approximately double the average daily summer precipitation (Price, 1993; Parkhurst et al., 1998). Therefore, after a prolonged drying period, any rainfall will infiltrate in the soil and the chance of lateral redistribution will be less (Grayson et al., 1997). Hence, the effect on soil water storage from factors that had nonlocal effects during the spring weakened in dry period in the fall.

While the correlation analysis reveals the relationship only at the measurement scale and explains the local effect of different controlling factors, the cyclical correlation analysis examines the relationship at multiple scales. The strong correlation at a scale different from the

measurement scale pointed towards the nonlocal effects from different controlling factors. The information on the scales of significant correlation can be used to improve the relationship between soil water storage and various controlling factors. The relationship clearly improved the prediction in soil water storage from the factors that have nonlocal effects.

8.6 Conclusions

High spatio-temporal variability of soil water is contributed from different factors and processes that operate in different intensities and at different scales. While some factors have localized effect on soil water storage, other factors act non-locally, which mean a factor measured in one location have effect on soil water storage at another location. Therefore, there is a lag in distance between the origin of the factor and the response in soil water storage. Effect of these nonlocal factors can be characterized by examining the lags or scales of their variations.

In this study, we have examined the effect of local and nonlocal controls on soil water storage using Pearson correlation analysis. Soil properties such as sand, silt, OC, depth of $CaCO_3$ layer, and topographic indices such as wetness index, and convergence index showed strong correlation with soil water storage during any spring measurement (soil is in wet state). Though the soil water storage spatial pattern was almost inverse to that of relative elevation, the correlation was negligible at the scale of measurement. However, the correlation was improved by more than eight folds at a lag of 54 m. As the high topographic position (knolls) contributed soil water to the low topographic positions (depressions), the length of the slope was identified as the lag in their effect. In fact, the average length of the slopes was around 50 to 55 m in the landscape. Some soil properties such as OC and depth of $CaCO_3$ also showed moderate correlation at the lag of around 54 m, which may be due to the correlation between those factors and relative elevation. The topographic indices were also correlated with relative elevation. These correlations were stronger in spring season or wet state and gradually decreased in fall or dry state of soil water condition. The correlation between soil water storage and controlling factors at scales other than measurement examined the nonlocal effects of those factors on soil water storage. Identifying the nonlocal effects of various factors improved the prediction of soil water storage.

9.0 REVEALING THE CONTROLS OF SOIL WATER STORAGE AT DIFFERENT SCALES IN A HUMMOCKY LANDSCAPE

9.1 Preface

Soil water storage is controlled by topography, soil texture, vegetation, water routing processes and depth to water table. Interaction between these factors may give rise to scale dependent nonstationary and nonlinear patterns in soil water storage. In revealing the controls of soil water storage, available methods either assume the spatial series to be stationary or linear or both together. This chapter uses the newly introduced Hilbert-Huang transform to identify the dominant scales of variations associated with nonstationary and nonlinear soil water spatial series and delineate dominant controls at those scales using the data collected from St. Denis National Wildlife Area.

9.2 Introduction

Soil water is the primary limiting factor in semi-arid ecosystems as it controls the transpiration demand of plant community. It also shapes environmental health by affecting transport of sediment, toxins, and chemicals to environmentally sensitive areas such as surface water bodies and ground water (Sun, 1986; Loague et al., 1989). In addition, the amount of water stored in soil controls the near surface hydrological processes. For example, it influences partitioning of rainfall and snowmelt into infiltration and runoff and incoming radiation into latent and sensible heat (Gómez-Plaza et al., 2000; Mohanty et al., 2000).

Soil water storage is not controlled by a single factor, rather a complex suite of environmental factors and processes work independently or in combination to determine soil water storage. Among these factors topography, soil properties (such as soil texture), water routing processes, depth to water table, meteorological conditions, geology and vegetation (Braud et al., 1995; Western and Blöschl, 1999; Gómez-Plaza et al., 2001) are important. The effects of these factors are not uniform in space, creating strong heterogeneity in soil water. Moreover, the spatial heterogeneity in soil water exhibits spatial continuity, meaning that two points close in space have more similar soil water values than those far apart. Furthermore, soil water storage can also vary gradually over distance, forming a spatial trend.

The statistical parameters (mean and variance) of a spatial process may change with distance. This means that if we chop up the spatial series into several segments, the mean and variance of a segment will be different from that of another. The non-uniform spatial mean(s) and/or variance(s) make a spatial series nonstationary. Moreover, the spatial series of soil water storage is composed of different frequency components, which can be representative of different scale processes. Some processes vary frequently in space and are represented by high frequency components (small-scale processes), while others vary slowly and represented by low frequency components (large-scale processes) (Si, 2003). If the contribution of high frequency components to the total variation is different from that of low frequency components, soil water storage become highly variable with scale (Kachanoski and de Jong, 1988; Gómez-Plaza et al., 2000; Kim and Barros, 2002).

For a linear system with input x and output y, the response to the sum of two inputs x_1 and x_2 equals the sum of the response to each input taken individually: $L(x_1 + x_2) = L(x_1) + L(x_2)$. Further, a linear system can be scaled by the magnitude (α) of the input x, where α is a scalar: $L(\alpha x) = \alpha L(x)$. Thus, the linear system enjoys the principle of superposition: $L(\alpha x_1 + \beta x_2) = \alpha L(x_1) + \beta L(x_2)$, where, β is the magnitude of input x_2. However in nature, the effects from different processes as represented by different frequency components are non-additive and do not follow the principle of superposition (Yan and Gao, 2007) indicating the system to be nonlinear. Alternatively, in a nonlinear system, the target variables cannot be written as a linear sum of independent components of controlling factors or processes (Pai and Palazotto, 2008). For example, the response of soil water storage to the n factors (x_i, i =1, 2, …, n) cannot be obtained by simply observing the response to one factor at a time and subsequently adding the individual observational results together. Therefore, the combined response, $S(x_1 + x_2 + \ldots + x_n)$, to the processes such as elevation, soil texture, … (x_1, x_2, …, x_n), will not be equal to the sum of individual response, $S(x_1) + S(x_2) + \ldots + S(x_n)$. This may be due to the change in the scale of processes with distance or location as represented by the oscillations that restricts the linear summation. Therefore, a nonlinear series was defined using the concept of sub- and super-cyclic variations in frequency (Huang et al., 1998; Kijewski-Correa and Kareem, 2006). The sub-cyclic variations are the change in frequency or scale that occurs within a single cycle of oscillations and the super-cyclic variations occur over the course of one or more cycle of oscillations present

in the series. Therefore, the scale or frequency of a nonlinear spatial series will be locally unpredictable (Gautama et al., 2004).

During the last decades, wavelets have been used to analyze the spatial heterogeneity of stationary or nonstationary soil properties (Lark and Webster, 1999; Si, 2003; Lark et al., 2004; Yates et al., 2006b; Biswas et al., 2008; Watkins et al., 2009). However, this analysis assumes the system to be linear (Huang et al., 1998). To the best of our knowledge, there is no instance of the use of any method that deals with nonstationary and nonlinear spatial heterogeneity together in soil science.

Hilbert-Huang Transform (HHT) is a new method that can deal with both nonlinear and nonstationary spatial series (Huang et al., 1998). Although it was originally used for time series analysis, it can be extended to spatial data analysis. HHT is a two-step method. The first step is Empirical Mode Decomposition (EMD) and the second step is Hilbert Spectral Analysis (HSA). In transforming the data, HHT does not consider any mathematical function in the analysis (such as trigonometric functions in Fourier analysis and mother wavelets in wavelet analysis); rather it identifies the hidden trends directly from the data (Huang et al., 1998; Huang and Wu, 2008). Similar to a time series, different frequency components of a soil physical property can operate simultaneously at a location creating intrinsic oscillations in the spatial distribution of the soil property. The EMD decomposes the overall spatial pattern into a finite and often small number of intrinsic modes, which are known as Intrinsic Mode Functions (IMFs). These IMFs represent the characteristic scales of the variability in the soil physical property. In the second step of HHT, the Hilbert transform is applied to each IMF and the instantaneous energy and frequency are obtained. Instantaneous frequency is the localized frequency in a spatial domain and addresses the nonlinearity (Huang et al., 1998).

The adaptivity of HHT makes it applicable to nonlinear and nonstationary data series (Huang et al., 1998). The superiority of the analysis technique in addressing nonlinear and nonstationary series has made it useful in different fields of science. A detail review of the application of HHT in geophysical studies can be found in Huang and Wu (2008).

Therefore, the objectives of this study were to 1) identify the dominant scale of variation of nonstationary and nonlinear soil water storage and 2) delineate the dominant controls of soil water storage at those scales in a hummocky landscape using HHT. The soil-water storage series

were decomposed into different IMFs using EMD according to their characteristic scales. Multiple regression analysis was used to make a scale specific inference about soil water storage from other soil variables and landscape properties.

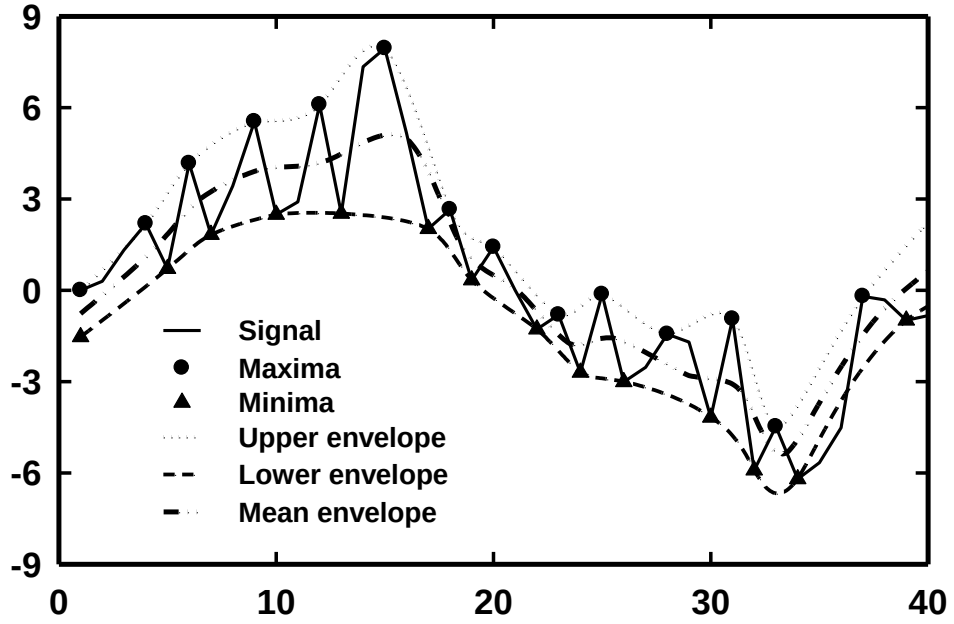

Figure 9.1. Mamixa, minima, upper envelope, lower envelope and mean envelope of a signal.

9.3 Materials and Methods

9.3.1 Theory

9.3.1.1 Empirical Mode Decomposition

EMD separates the variation in a spatial series according to their characteristics scales. Unlike previous methods, EMD works directly in the spatial domain with the basis derived from the data. This decomposition is based on a simple assumption that at a given space, there may be different simple oscillatory modes of significantly different frequencies superimposing one another (Huang et al., 1998). In a natural system, the overall variability is controlled by a number of processes occurring together in different intensities at different scales (Goovaerts, 1998). The processes with similar scales are separated into different mode functions (IMFs). In defining the IMFs, it should satisfy the following conditions: 1) the mode may or may not be linear and the number of extrema and zero crossings must either equal or differ at most by one. While, extrema

indicates smallest (minima) or largest (maxima) value that a function can take (Figure 9.1), zero crossing indicates the point where function changes its sign; 2) the oscillation will be symmetric with respect to the local mean; that is, at any data point the mean value of the envelopes defined by local maxima and local minima is zero. The upper envelope and lower envelope are respectively created by joining all the maxima and the minima through spline interpolation (Figure 9.1). According to these definitions, IMFs can be obtained after decomposing any function through a sifting process. For example an input, $Y(x)$ as a function of distance *x* can be decomposed into different IMFs by following the steps below.

1. An upper envelope (UE) and lower envelope (LE) can be created after finding the local maxima and local minima, respectively and joining them using a cubic spline line (Figure 9.1). These envelopes will encompass all data points. The mean of the envelope, $m_1 = (UE + LE)/2$, is calculated locally and subtracted from the data, $Y(x)$. The first prototype (h_1) is represented as $h_1(x) = Y(x) - m_1(x)$, which is a function of space. This prototype will be an IMF by construction provided h_1 satisfies the definition of an IMF. However, changing a local zero from a rectangular to curvilinear coordinate system may introduce new extrema and requires sifting processes (Huang et al., 1998).
2. The first prototype is treated as data in the next iteration, then $h_1(x) - m_{11}(x) = h_{11}(x)$. The sifting process has to be repeated to extract the signal satisfying the definition of an IMF. After *k* times of iterations, $h_{1(k-1)}(x) - m_{1k}(x) = h_{1k}(x)$, the local envelope symmetry condition is satisfied and $h_{1k}(x)$ is defined as the first IMF named C_1 as a function of space, $C_1(x) = h_{1k}(x)$.
3. This approximate symmetry of local envelopes in the sifting process is called stoppage criterion. Huang et al. (1998) defined this stoppage criterion based on a Cauchy type of convergence test, which is the normalized squared difference between two successive sifting operations and is given as

$$SD_k = \frac{\sum_{x=0}^{X} |h_{k-1}(x) - h_k(x)|^2}{\sum_{x=0}^{X} h_{k-1}^2(x)} \qquad [9.1]$$

where *X* represents maximum of *x*. When the SD value is smaller than a predetermined value (usually set between 0.2 and 0.3), the iteration has to stop to guarantee that the IMF components retain enough physical sense of both amplitude and frequency modulations.

4. The first IMF contains the finest scale or the shortest period oscillations in the signal and can be extracted from the data as $Y(x)-C_1(x)=r_1(x)$. This residue is then treated as new data for the longer period variations and subjected to the sifting steps as described earlier. If the sifting is carried out for subsequent $r_j(x)$'s, where *j* = 1, 2, 3, …, *n* and the result can be written as

$$r_1(x)-C_2(x)=r_2(x), \ldots, r_{n-1}(x)-C_n(x)=r_n(x) \quad [9.2]$$

5. where, $C_n(x)$ are the IMFs and $r_n(x)$ are the residues.

The decomposition process is carried out until the residue, $r_n(x)$ is left with only one extremum or the residue becomes a monotonic function. This final residue represents the underlying trend in the data (Huang et al., 1998). The signal is the sum of all empirical modes and final residue and can be written as

$$Y(x)=\sum_{j=1}^{n} C_j(x)+r_n(x) \quad [9.3]$$

Therefore, the total variance of a spatial series can be represented as the sum of variances of IMFs and residue. The variance (σ^2) of the spatial series, IMFs and residues were calculated as

$$\sigma^2=\frac{1}{N}\sum_{i=1}^{N}(x_i-\mu)^2 \quad [9.4]$$

where $\mu=\frac{1}{N}\sum_{i=1}^{N}x_i$, *N* is the number of data points in the spatial series, IMFs and residues.

Therefore, the percent variance contribution (%) of each IMF can be calculated as

% = [Variance of an IMF / {(Σ variances of all IMFs) + residue}] × 100.

Each IMF contributes a certain percent of total variations, which can determine the relative importance of IMFs and thus the different scale processes (Oladosu, 2009). The average scale of an IMF can be calculated by counting the average number of oscillations present in that IMF. For example, there were around 17 complete cycles or oscillations in IMF 2 over the transect length. Therefore, the average scale of IMF 2 will be (576/17) around 34 m. The oscillations were

identified using the MATLAB function '*extrema*'. However, due to the nonlinearity, the periods or scales will be unpredictable locally. In this situation, the instantaneous scales can provide the range of scales representing by an IMF and can be calculated from the instantaneous frequency using Hilbert transform.

9.3.1.2 Hilbert Spectral Analysis

Once the IMFs are calculated, Hilbert transform can be carried out for each IMF. For example, the first IMF, $C_1(x)$, which is a function of space can have its Hilbert transform,

$$D_1(x) = \frac{1}{\pi} P \int_{-\infty}^{\infty} \frac{C_1(\tau)}{x-\tau} d\tau \qquad [9.5]$$

where *P* is the Cauchy principle value and τ is the sample location. The Hilbert transform, $D_1(x)$, of the function, $C_1(x)$, produces an analytical function,

$$Z_1(x) = C_1(x) + iD_1(x) = a(x)e^{i\theta(x)} \qquad [9.6]$$

where $i = \sqrt{-1}$, *a* is the instantaneous amplitude, $a(x) = \sqrt{\left(C_1^{\,2} + D_1^{\,2}\right)}$, and θ is the instantaneous phase function, $\theta(x) = \tan^{-1}\left(\frac{D_1}{C_1}\right)$. The instantaneous frequency can be simply calculated as $\omega(x) = \frac{d\theta(x)}{dx}$. Then the data can be expressed as

$$Y(x) = \sum_{j=1}^{n} a_j(x) e^{i\int_{\tau=0}^{x} \omega_j(\tau) d\tau} \qquad [9.7]$$

Although we can obtain the Hilbert transform for any function of class L^p [$L(\infty, -\infty)$], the phase of the transformed function is sometimes limited in producing physically meaningful instantaneous frequency. Decomposition of any function into IMFs improves the chance of getting physically meaningful instantaneous frequencies (Huang and Shen, 2005). However, one of the limitations of the transform is that it cannot satisfy the Bedrosian theorem, which states that the Hilbert transform of the product of a low-pass and a high-pass signal with non-overlapping spectra is given by the product of the low-pass signal and the Hilbert transform of the high-pass signal (Bedrosian, 1963). For example, the Hilbert transform for the product of two functions, $f(t)$ the envelope function and $h(t)$ the phase function can be written as H [$f(t)$ $h(t)$] =

$f(t)$ H [$h(t)$] only if the Fourier spectra for $f(t)$ and $h(t)$ are totally disjoint in frequency space and the range of the spectrum of $h(t)$ is higher than that of $f(t)$. According to the Bedrosian theorem, this can be true if the amplitude is varying so slowly that the frequency spectra of the envelope and the IMFs are disjoint. However, this condition is seldom satisfied in nature. Therefore, Huang (2005) proposed the normalized Hilbert transform to overcome the problem. The normalization is given by an iterative process.

As the IMFs are used as the data, the envelope $e_1(x)$, can be defined by a spline through the interpolation of the extrema points of the absolute value of j^{th} IMF, $C_j(x)$. We can normalize the IMF after dividing it by the envelope. Then we can write the iterative process;

$$f_1(x) = C_j(x)/e_1(x),\ f_2(x) = f_1(x)/e_2(x), till\ f_n(x) = f_{n-1}(x)/e_n(x), \quad [9.8]$$

when $e_n(x)$ is unity and $e_i(x)$ is obtained from $f_{i-1}(x)$ and from interpolation process (Huang and Milkereit, 2009). Then the IMFs are expressed as

$$C_j(x) = a_j(x)\cos\left(\int_{\tau=0}^{x} \omega_j(\tau)d\tau\right) \quad [9.9]$$

and the original data is expressed as the instantaneous amplitude and frequency modulated signal,

$$Y(x) = \sum_{i=1}^{n} a_j(x)\cos\left(\int_{\tau=0}^{x} \omega_j(\tau)d\tau\right) + r_n(x). \quad [9.10]$$

As the amplitude and the frequency is a function of space, the amplitude (or energy, the square of amplitude) can be represented as a joint function of space and frequency $H(\omega, x)$. This space-frequency-energy [x, $\omega(x)$, $a(x)$] distribution can be viewed in a 3D space as Hilbert spectra, which can provide a clear picture of scale and location specific variations presenting in any spatial series. The energy was plotted at a relative scale.

The EMD separates scale specific processes and HSA calculates their energy and frequency at each location at each scale. The frequencies that vary locally are extracted directly from the data. In the wavelet analyses, the resulting scales will be the multiple of the mathematical function with lowest scale equivalent to the frequency of the function. Whereas HHT examines possible frequencies at each location instantaneously and thus considers the nonlinearity. The scale separation through EMD addresses the nonstationarity and the instantaneous frequency in HSA addresses the nonlinearity.

9.3.2 Site Description

A field experiment was conducted at St. Denis National Wildlife Area, (SDNWA) (52°12′ N latitude, 106°50′ W longitude), which is located approximately 40 km east of Saskatoon, Saskatchewan, Canada (Figure 9.2). Soils of this area are mapped within the Wyandotte Association, which are Dark Brown Chernozemic (Mollisols in American System of Soil Classification) soils developed from moderately fine to fine textured, moderately calcareous, clayey glacio-lacustrine deposits and modified glacial till (Acton and Ellis, 1978). The landscape of this area contains a very complex sequence of slopes extending from different size rounded depressions to irregular to complex knolls and knobs (Pennock et al., 1987) with 10-15% slopes (Figure 9.2). This area has mainly a semi-arid climate with a mean annual air temperature (Saskatoon airport) of 2°C, and the monthly mean of -19°C in January and 18°C in July. The 90-year mean annual precipitation at Saskatoon is 360 mm, of which 84 mm occurs in winter mostly as snow (AES, 1997). The total precipitation in the years of 2006, 2007, 2008, 2009 were 489 mm, 366 mm, 331 mm, and 402 mm, respectively (Environment Canada, 2010).

9.3.3 Data Collection

A sampling transect, extending north-south, was established over several rounded knolls and depressions representing different landform cycles including three vegetated depressions (Figure 9.2; Yates et al., 2006a). The transect was 576 m long with 128 sampling points at 4.5 m interval. Detailed information about the study site is available in Yates et al. (2006a). Briefly, the topographic survey of this site was completed using light detection and ranging (LiDAR) survey and a Trimble Pro XRS, Global Positioning System (Trimble Navigation, Sunnyvale, CA). The vegetation of the site is mixed grass seeded by Ducks Unlimited Canada in 2004. At each sampling point, plastic (Polyvinyl Chloride, PVC) tubes of 5 cm diameter and 200 cm long were installed using a truck mounted hydraulic drill. These tubes were used as access tubes for measuring soil water content using the neutron probe. A CPN 501 DR Depthprobe (CPN International Inc., Martinez, CA, USA) was used to measure the soil moisture from 20 cm to 140 cm at a depth increment of 20 cm. The neutron probe was calibrated for the study site following the standard calibration procedure for three years (2007, 2008, and 2009), in different moisture conditions and at select topographic locations. All the measurements were considered in

developing the calibration equation and the soil water contents were calculated from the neutron count ratio. The average soil water content from 0 to 20 cm depth was measured through a vertically-installed time domain reflectometry probe using a metallic cable tester (model 1502B, Tektronix, Beaverton, OR, USA). The soil water storage was calculated by multiplying the depth with volumetric moisture content calculated from the calibration relationship. Field moisture measurements were recorded 16 times (17 July, 2007; 7 August, 2007;1 September, 2007; 12 October, 2007; 2 May, 2008; 31 May, 2008; 21 June, 2008;16 July, 2008; 23 August, 2008; 17 September, 2008; 22 October, 2008; 20 April, 2009; 7 May, 2009; 27 May, 2009; 21 July, 2009; 27 August, 2009) over a three year period.

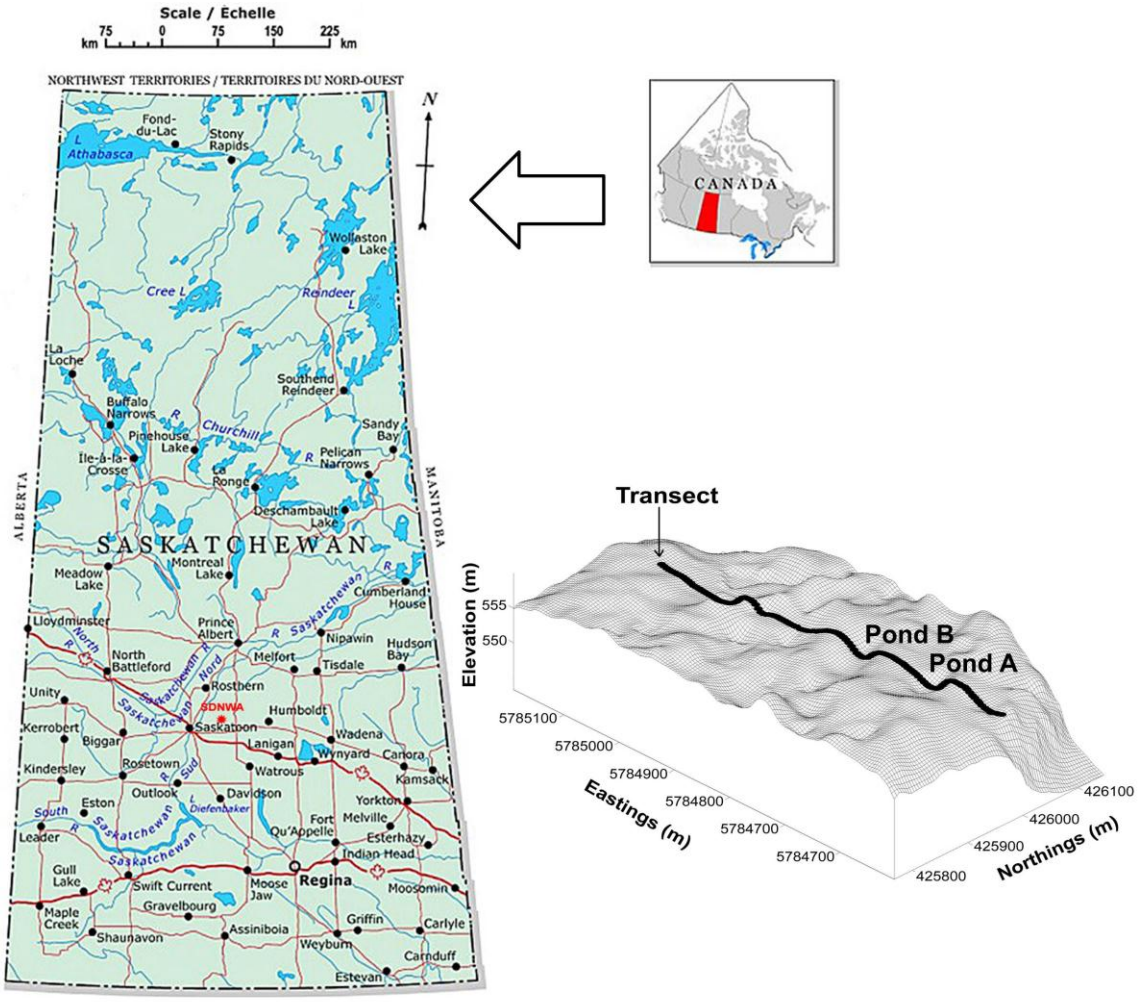

Figure 9.2. Geographic location of study site and the transect position on rolling landscape at St. Denis National Wildlife Area (SDNWA), Saskatchewan, Canada (Natural Resources Canada, 2001).

Spring was considered as a recharge period since snowmelt and rainfall increased water storage. High evapotranspiration demand during summer depleted the stored water, thus summer was considered as a discharge period. The 16 measurements can be divided into two groups, representing two periods. Although the necessary analysis was performed for all the data series, the space restriction allowed the presentation of the results of one typical measurement from each group in this manuscript (recharge period- 2nd May 2008 and discharge period- 23rd August 2008) to demonstrate the HHT. Bulk density was measured (up to 140 cm at a depth increment of 20 cm) during installation of neutron access tube. Organic carbon (OC) of surface soil (0 to 20 cm) was determined using LECO-C6235 carbon determinator (LECO Corp., St. Joseph, MI, USA). The particle size distribution of surface soils was characterized using HORIBA LA-950 Laser diffraction particle-size analyser (HORIBA Scientific Inc., Edison, NJ, USA).

9.3.4 Data Analysis

Exploratory data analysis for the soil-water storage series was carried out using classical statistical tools in SigmaPlot 11 (Systat Software Inc.) and Microsoft Office Excel 2007 (Microsoft Inc.) software. The linear relationship among soil water storage series, controlling factors, and different IMFs were determined using Pearson correlation coefficients (r).

The IMFs were separated and instantaneous frequencies were calculated using a MATLAB (MathSoft Inc.) program modified from the original program written by Dr. Wu. The original program is available at http://rcada.ncu.edu.tw/research1_clip_program.htm. The percent variance contribution of each IMF was calculated from the variance of IMFs, residue and the total variance of the spatial series. The instantaneous frequency was converted to period (1/frequency), which was further converted to the spatial scale after multiplying the period with the sampling interval (4.5 m). The Hilbert spectrum was calculated and represented in a contour plot of space-frequency-energy. The plot was obtained after a Gaussian weighted filter using a MATLAB program modified from the original program written by Dr. Huang (Huang and Milkereit, 2009).

The normality in soil-water storage series, IMFs, and the controlling factors were examined through skewness and kurtosis values and a quantile-quantile (q-q) plot. The variance inflation factor (VIF) was used to examine the collinearity between the controlling factors using

SPSS software (SPSS Inc.). The VIF value for different factors was < 2 indicating the absence of multi-collinearity between controlling factors. The relationships between different IMFs of soil water storage and controlling factors were developed following forward stepwise multiple regression using SPSS software. In the forward stepwise regression, the variables were added to the regression model one at a time and the analysis of variance was performed for the model. A factor was added to the regression equation when the value of $p = 0.05$ and was taken out at $p = 0.10$. The normality of residuals of the regression analysis was examined through histogram. The constant variance assumption was checked by plotting the residuals against the predicted values following Myers (1990). The independence of the errors was examined by semivariances plotted against the distance between samples (lag distance) (called semivariogram).

9.4 Results and Discussion

The average soil-water storage varied over the measurement period. The difference in the water content between the recharge and discharge period was > 0.06 $cm^3\ cm^{-3}$ (40.95 cm / 140 cm = 0.29 $cm^3\ cm^{-3}$ for recharge period and 32.84 cm / 140 cm = 0.23 $cm^3\ cm^{-3}$ for discharge period). The high evapotranspiration demand in the semiarid climate of the study area left less water stored in the soil profile during the discharge period. Drifting snow and uneven distribution of snowmelt water in the hummocky landscape (Figure 9.2) resulted in a wide range of stored water during the recharge period (Figure 9.3; Hayashi et al., 1998; Lungal, 2009). For example, the range of soil water storage on 2 May 2008 was 41.11 cm (maximum = 68.08 cm; minimum = 26.97 cm). Similar trends in stored water were also reported by Flerchinger and Cooley (2000) in a non-level landscape. In spite of the large range, the skewness values were close to zero indicating that all the soil water storage series were likely normally distributed.

There was enhanced growth of vegetation in depressions compared to that on knolls, which removed more water from the depressions than that from the knolls during the growing season. The different growth of vegetation made soil-water storage much more uniform in the landscape in late summer or at the end of the growing season. However, the amount of water stored in the depressions in spring was so high that despite plant water uptake during a growing season, consistently higher water storage in depressions occurred throughout the season. Linear correlation between different factors and the water storage was presented in Figure 9.4. Organic

carbon showed the highest correlation (r = 0.72 significant at p = 0.05) with the water storage series during the recharge period, while sand showed the highest correlation (r = -0.70 significant at p = 0.05) during the discharge period. Similar correlation was also observed for measurements taken at other dates (data not shown) and by da Silva et al. (2001).

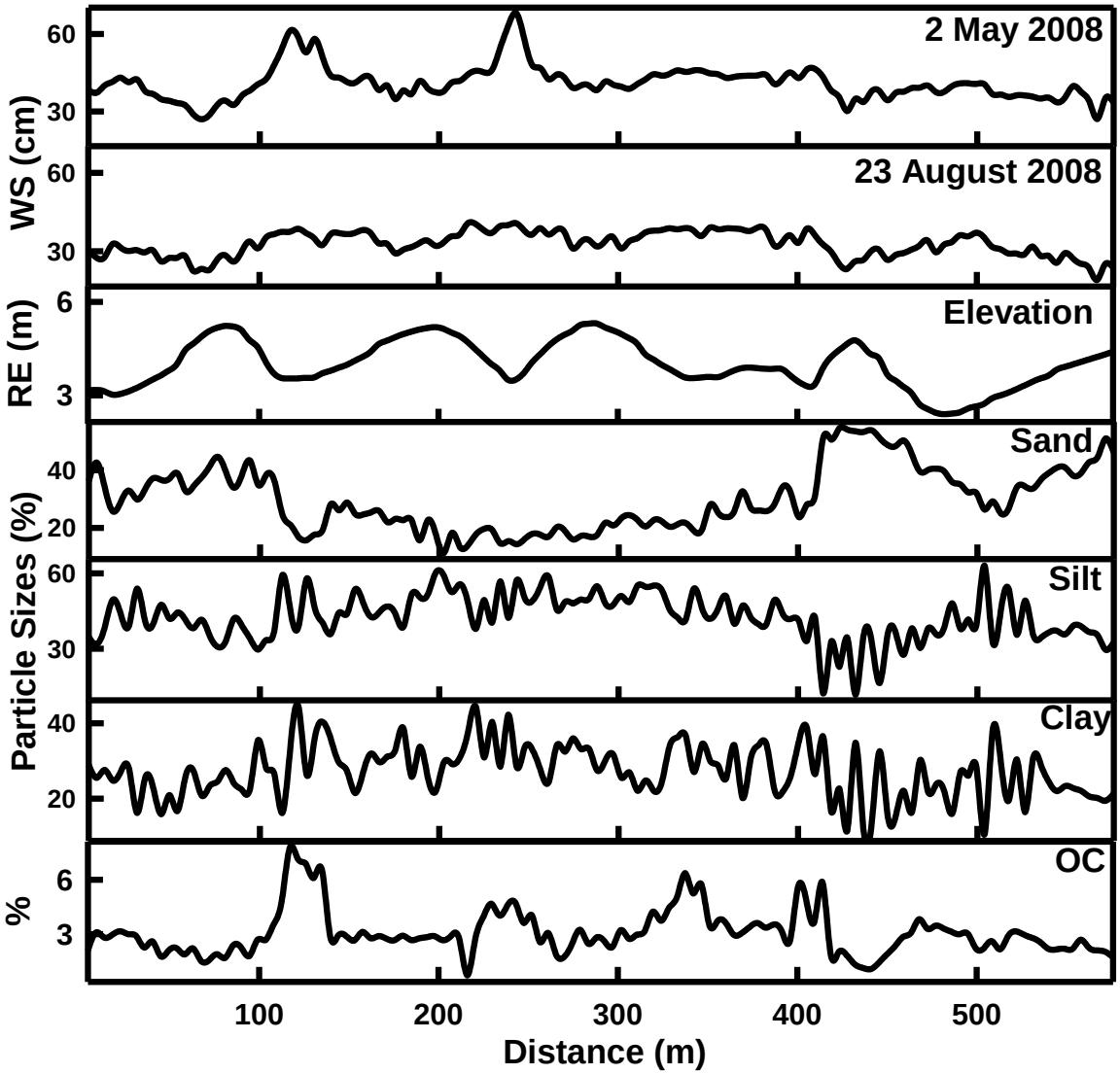

Figure 9.3. Spatial distribution of soil water storage and its controlling factors along the transect. RE indicates the Relative Elevation (m) and the WS indicates the Water Storage (cm). Horizontal axis is the distance between a sampling location and the origin of the transect.

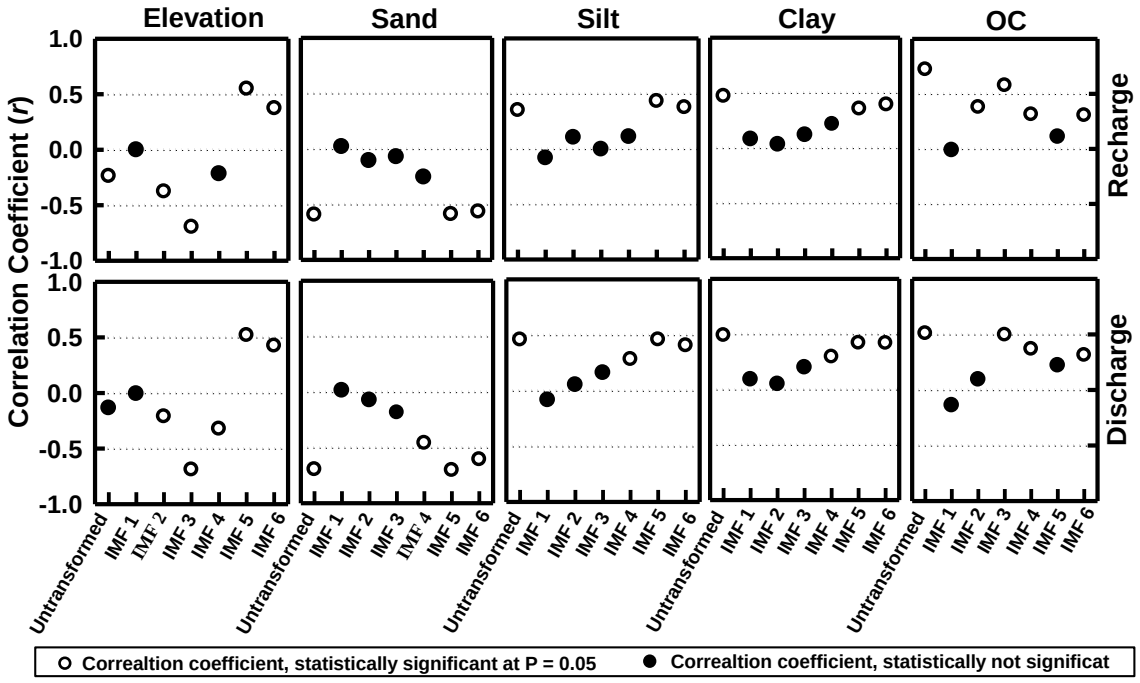

Figure 9.4. Correlation coefficient between controlling factors and IMFs of soil water storage. While open circle indicates the statistically significant at $p = 0.05$, solid circle indicates statistically insignificant. Dotted line indicates the grids on Y-axis.

Though visually the soil-water storage pattern was related to elevation (Figure 9.3), the correlation between water storage and elevation at the measurement scale was not as strong as expected ($r = -0.24$ significant at $p = 0.05$ for recharge period and $r = -0.14$ for discharge period) (Figure 9.4). This may be because the correlation only explained the association between soil water storage and its controlling factors at one scale, the measurement scale, which may not be same at other scales (Kachanoski and de Jong, 1988).

9.4.1 Empirical Mode Decomposition

In order to examine the correlation at different scales, the soil water spatial series were separated into six different modes of oscillations using the empirical mode decomposition. IMF 1 through IMF 6 were presented in Figures 9.5 and 9.6 for the recharge (2 May 2008) and the discharge period (23 August 2008), respectively. The residues after extracting all IMFs still

showed quite high variations (average of around 15 to 20% of total variation). The IMFs with lower numerical numbers extracted higher frequency oscillations, whereas IMFs with higher numerical numbers extracted lower frequency oscillations, which can be representative of smaller and larger scale processes, respectively (Si, 2003). The IMF 1 might represent localized variations at approximately 5 to 10 m scale during the recharge period (Figure 9.5). However, there was no significant correlation between the controlling factors and IMF 1 (Figure 9.4) and the variance contribution of IMF 1 towards the total variation was very small (about 6%). These localized variations at small scales might be associated with the random processes operating in the landscape.

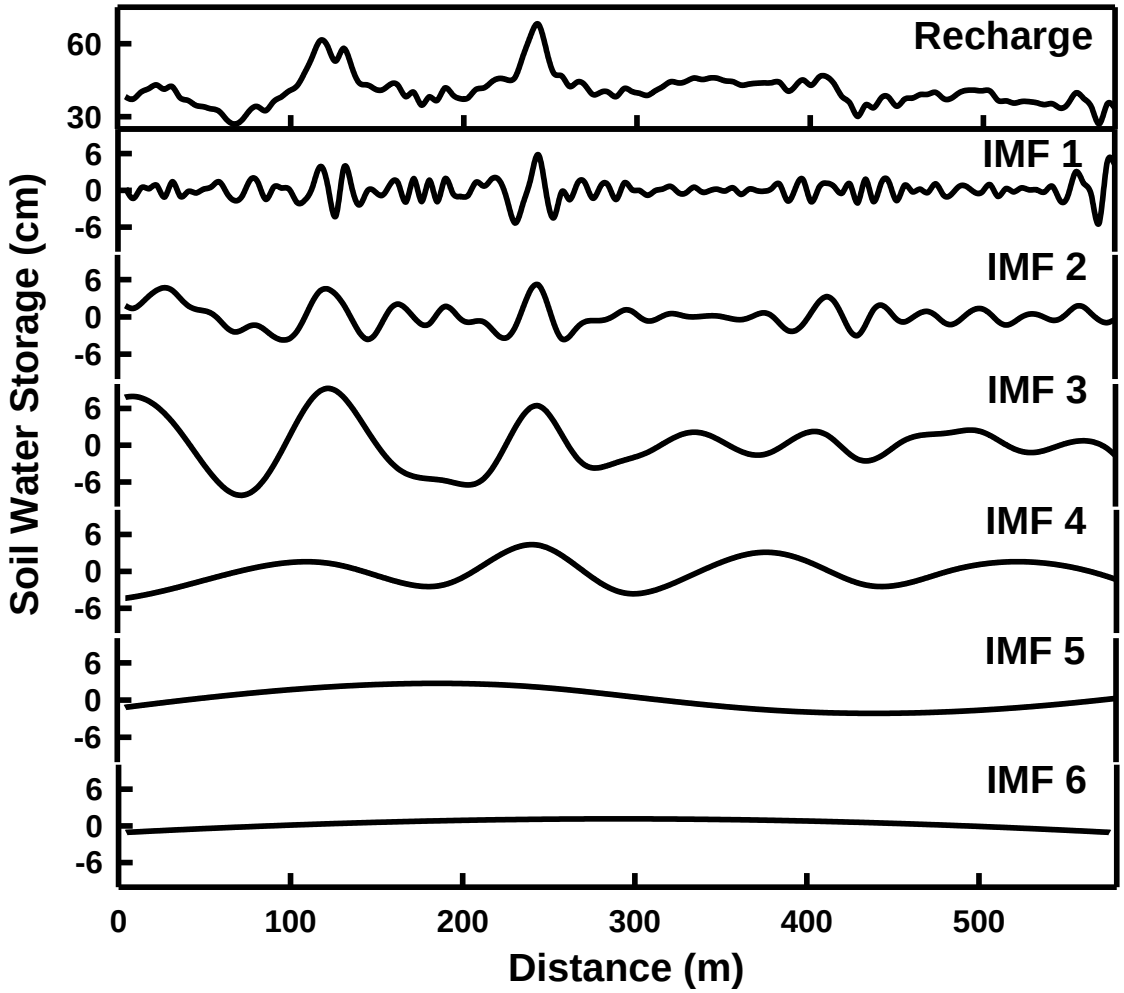

Figure 9.5. IMFs and soil-water storage series (top) of recharge period (2nd May 2008). Horizontal axis is the distance between a sampling location and the origin of the transect. The vertical solid bar in Y-axis shows the scale of IMFs.

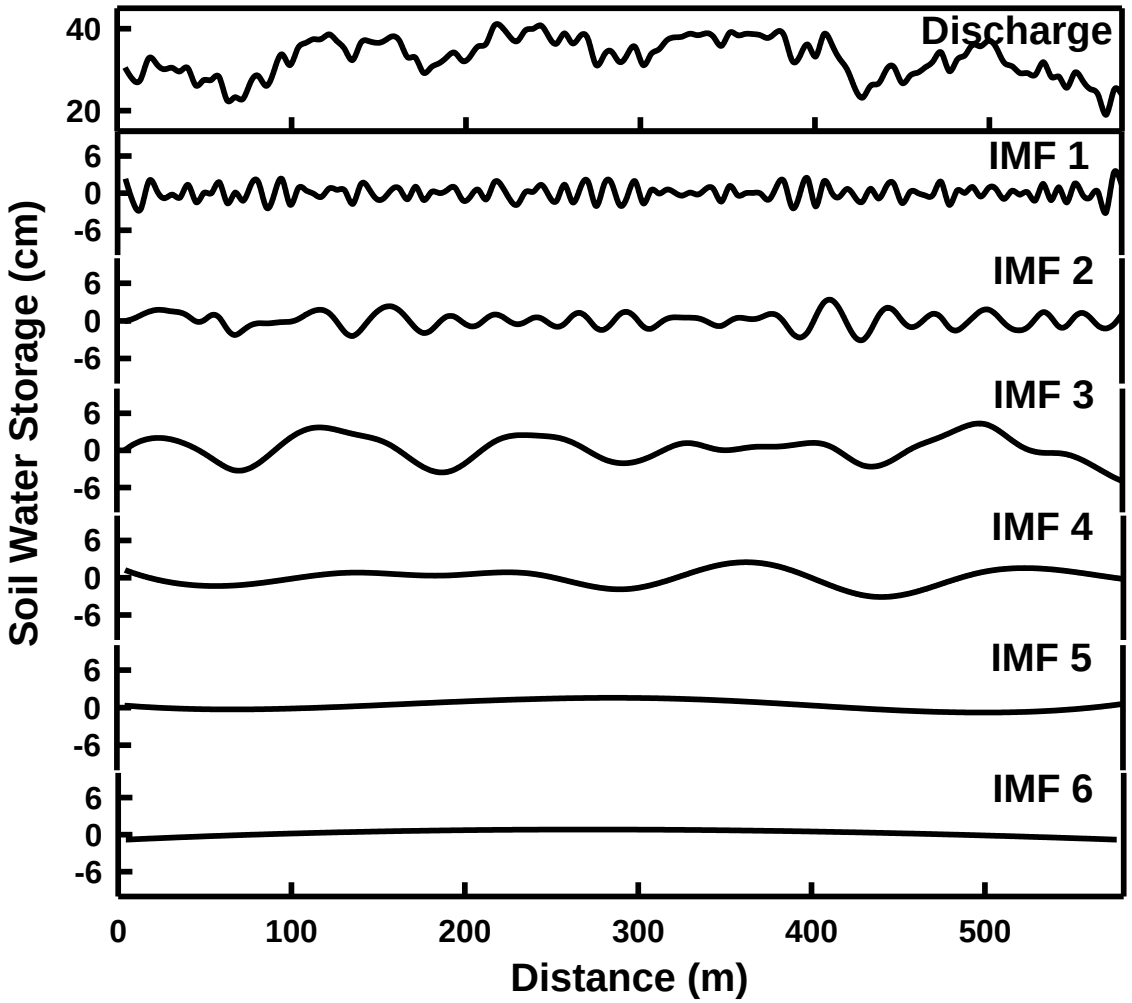

Figure 9.6. IMFs and soil-water storage series (top) of discharge period (23rd August 2008). Horizontal axis is the distance between a sampling location and the origin of the transect. The vertical solid bar in Y-axis shows the scale of IMFs.

The IMF 2 represented the variations at the scale of 30 to 40 m (Figure 9.5) for the recharge period. However, the variance contribution of IMF 2 towards the total variations was around 10 percent. The value of *r* was -0.38 between IMF 2 and elevation and 0.38 between IMF 2 and OC (both values were significant at $p = 0.05$) (Figure 9.4). Among the factors, IMF 2 had the highest correlation with elevation and OC indicating the strongest association between soil water storage with elevation and OC at the scales of 30 to 40 m. The variations in micro-topography and the landform elements might attribute to the variations at the scales of 30 to 40 m. Furthermore, the variation in OC content in a field is a reflection of the long-term variation in

soil water storage, and consequently might be reflective of historical topography, micro-topography or the landform elements in that field. High water storage in topographically low lands supports better vegetation than that on high lands, which contributes more OC deposition in the depressions than that on knolls (Gómez-Plaza et al., 2001).

The variations at the scales of 80 to 100 m were separated into IMF 3, which was strongly correlated with elevation (r = -0.7 significant at p = 0.05) (Figure 9.4). The variance contribution of IMF 3 was 41% towards the total variation in the soil water storage during the recharge period. The highest contribution of IMF 3 towards total variation and the strongest correlation with elevation clearly indicated the strongest association between elevation and soil water storage at the scale of 80 to 100 m in the recharge period.

While IMF 5 was correlated with sand (r = 0.59 significant at p = 0.05) and elevation (r = 0.52 significant at p = 0.05), IMF 6 was correlated with almost all factors. The correlation at these large scales (IMF 5 and 6) indicated an association between soil texture and topography and soil water storage. However, the variation represented by these IMFs combined was less than 10% of the total variation.

Similar to the recharge period, the IMFs extracted from the water storage series during the discharge period showed similar types of correlations with these factors (Figure 9.6). However, the magnitude of the correlation with these factors had changed from recharge to discharge periods. While correlations at the measurement scale between soil water storage and soil texture increased (e.g., r = -0.59 during recharge period to r = -0.70 during discharge period between soil water storage and sand), correlations between elevation and soil water storage decreased (e.g., r = -0.24 during recharge period to r = -0.14 during discharge period) (Figure 9.4). IMF 1 had no significant correlations with any controlling factors, while IMF 2 had significant correlations only with elevation (r = -0.21) (Figure 9.4). However, the IMF 2 accounted for a small variation (around 10%). Similar to the recharge period, IMF 3 of the discharge period was strongly correlated to elevation (r = -0.69) and OC (r = 0.58). IMF 5 was correlated to sand (r = -0.70) and elevation (r = 0.52) and IMF 6 showed a moderate correlation to all factors during the discharge period (Figure 9.4). However, IMF 3 alone explained the major variations in the dataset (over 41% of total variation), while IMF 5 and IMF 6 combined explained less than 7% of total variations. IMF 4 contributed 12% to the total variation and had a

moderate correlation with all the factors. The correlation coefficients between IMF 4 and other controlling factors (Figure 9.4) suggested a combined association with different factors. Similar type correlations were also observed between other soil water measurements during the recharge and discharge period and controlling factors. Even though one measurement from each moisture condition (recharge and discharge) was presented in this paper, the results were very typical of other measurements at hummocky landscapes.

Table 9.1. Percent contribution of IMF 3 towards total variation and its correlation with elevation over the whole measurement period.

Measurement date	Percent Contribution	Correlation** with Elevation
17 July 2007	47.45	-0.69
7 Aug. 2007	51.52	-0.66
1 Sept. 2007	44.84	-0.70
12 Oct. 2007	43.84	-0.61
2 May 2008	41.37	-0.71
31 May 2008	39.77	-0.67
21 June 2008	40.30	-0.62
16 July 2008	40.01	-0.65
23 Aug. 2008	41.03	-0.72
17 Sept. 2008	41.36	-0.69
22 Oct. 2008	37.23	-0.66
20 April 2009	43.29	-0.72
7 May 2009	39.28	-0.68
27 May 2009	38.59	-0.70
21 July 2009	37.23	-0.65
27 Aug. 2009	37.12	-0.66

** Significant at $p < 0.01$ level of probability

Besides these controlling factors, the leaf area index (LAI) was measured during the discharge period (unpublished data) to understand the effect of vegetation. There was weak correlation between LAI and different IMFs during the discharge period. However, a moderate correlation was observed between elevation and LAI (r = -0.42 significant at p = 0.05) as the

vegetation growth depends on the availability of water and thus on topography. The presence of vegetation during the discharge period and the absence of vegetation during recharge period make the vegetation a dynamic controlling factor in the hummocky landscape of semi-arid climate. Therefore, in our study, we only considered the static controlling factors of soil water storage, including elevation, soil texture and organic carbon.

The correlation between soil water storage and elevation at the measurement scale was smaller than that between soil water storage and other factors (OC, sand) (Figure 9.4). However, there were strong correlations between elevation and soil water storage at a different scale (Figure 9.4). With increases in scales, the correlation between soil water storage and elevation increased initially and then decreased. In addition, the sign of correlation between them also changed with scale. IMF 2, IMF 3 and IMF 4 were negatively correlated, but IMF 5 and IMF 6 were positively correlated to elevation. The change in the sign of correlation over scales might have neutralized the effects from different scales, which led to a low linear correlation at the measurement scale.

Although the trend of the correlation between different factors and soil water storage at different scales were persistent throughout the measurement period, the magnitude of the correlation changed over time. This indicated a change in the degree of association between the controlling factors and soil water storage in the hummocky landscape over seasons, but not the switch of controls from one factor to another. This contradicts the findings of Grayson et al. (1997), who found local controls like vegetation and soil texture are the dominating controls during dry conditions when evapotranspiration is greater than precipitation. During wet periods or moisture surplus conditions when the precipitation is greater than evapotranspiration, the nonlocal controls (i.e. topography) dominate redistribution of water (Grayson et al., 1997; Gómez-Plaza et al., 2001). The persistence in the correlation was also observed between the different IMFs of soil water storage and the controlling factors. For example, IMF 3 was correlated with elevation and contributed the highest compared to the other IMFs for all measurements (Table 9.1). This indicated the strongest association between soil water storage and elevation in this hummocky landscape irrespective of measurement period. This may be due to the effect of water redistribution by elevation during recharge period. Depressions accumulated so much water during recharge period that the effect persisted throughout the

discharge period. However, a small change in the magnitude of correlation was observed over time at different scales.

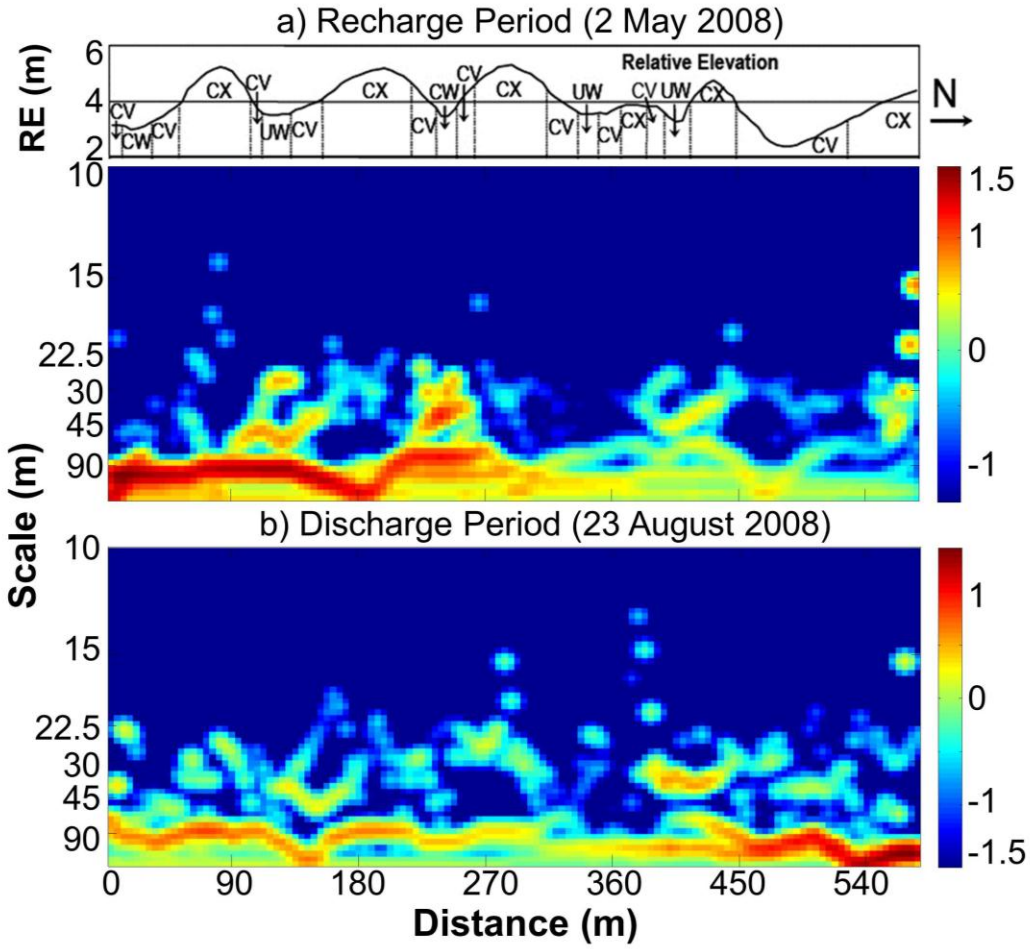

Figure 9.7. Hilbert Spectrum of soil water storage of a) recharge period (2nd May 2008) and b) discharge period (23 August 2008) with relative elevation (RE) at top. Horizontal axis is the distance between a sampling location and the origin of the transect (m).Vertical axis represents the instantaneous spatial scale (m). The color scale at the right side of the graph indicated the magnitude of the relative variations. CX stands for convex, CV stands for concave, CW stands for cultivated wetlands, and UW stands for uncultivated wetlands.

9.4.2 Hilbert Spectral Analysis

While the EMD and the correlation analysis indicated the possible association of soil water variations at different scales with controlling factors, the HHT spectra clearly identified the scales and locations of those variations. The scale-location specific variations in soil water storage during the recharge and discharge period were presented Figure 9.7. The spatial

distribution of elevation with different landform elements was also presented in Figure 9.7. There was strong variability (maximum relative red color intensity value up to 1.7 unit) at the scales of 80 m or larger in the first half of the transect, which may be attributed to the variations due to alternating knolls and depressions or topographic setting (Figure 9.7a). Previously, EMD and the correlation analysis indicated the possible association between the soil water variations at the scales of 80 to 100 m and elevation. However, the variation was not very strong (maximum relative yellow color intensity value up to only 0.9 unit) at the latter half of the transect. There were some weak to moderate variations (maximum relative light blue to yellow color intensity up to 1.4 unit) at the scales of 25 to 80 m at the locations of 125 m, 250 m, and 410 m along the transect. These variations might be attributed to the variations in landform elements within the depressions (Figure 9.7a). In spring, different landform elements receive the sunlight and the wind differently, modifying the evaporation from soil surface. In addition, very few weak variations (maximum relative light blue color intensity up to 0.1) were also observed at the scales < 25 m representing the localized variations in soil water storage (Figure 9.7a). Similar types of variation were observed in the Hilbert spectra of soil water storage during the discharge period (Figure 9.7b). However, the variation at the scale of 25 m to 80 m was less intense (maximum relative light blue to yellow color intensity up to 0.5 units) during the discharge period than that of the recharge period (Figure 9.7b). This may be due to the presence of vegetation that could have reduced the variations in soil water storage contributing at landform elements. Due to high evapotranspirative demand in semi-arid climate, vegetation pumps out water from the soil and reduces the variation in soil water storage. In addition, the intensity of the red color also reduced at large scales (maximum relative color intensity value up to 1.4 units) indicating the change in the degree of association between elevation and soil water storage at two different seasons (Figure 9.7).

9.4.3 Regression Analysis

At the measurement scale, OC, sand and elevation were the major predictive variables during the recharge period (Table 9.2). The interactions between OC and elevation and between the sand and elevation were also considered in the predictive model. The model was statistically significant at $p = 0.05$. However, for IMF 1, no factors were significant and the regression

equation was presented only by the intercept (Table 9.2). For IMF 2 and 3, the predictive variables were elevation, OC and the interaction between them. However, for IMF 4, the only predictive variable was OC. On the contrary, the regression model for IMF 5 and 6 included almost all factors as predictors (Table 9.2). However, the importance of predictive models for different IMFs can be different. For example, IMF 2 and IMF 3 represent major variations in the spatial series of soil water storage and the majority of the overall prediction is contributed from these IMFs. Elevation was the major predictor for these IMFs and therefore was considered as the major controlling factor for soil water storage in the hummocky landscape irrespective of recharge or discharge period. Similarly, the IMF 5 and 6 explained little variation compared to other IMFs and the regression model will contribute little in predicting the overall soil water storage.

Soil water storage at the measurement scale was predicted from different IMFs using the regression relationship. As the different IMFs represented a different portion of the overall variations in the spatial series, the predicted values for each IMF were added together to obtain the overall prediction. After the regression, the residuals between the actual and predicted soil water storage at the measurement scale and the different IMF regressions were tested for normality, equality of variances and autocorrelation. The plot of cumulative probability distribution of observed and expected frequency (Figure 9.8A for the recharge period and 9.8B for the discharge period) and the histogram (Figure 9.8C for the recharge period and 9.8D for the discharge period) clearly indicated the normality in the residuals for both the recharge and discharge periods at the measurement scale. Similarly, the residuals were plotted against the predicted value of soil water storage. The residuals were scattered around zero indicating the homogeneity of variance (Figure 9.8E for the recharge period and 9.8F for the discharge period) (Myers, 1990). In addition, the semivariances of the residuals were calculated and plotted as a semivariogram. A theoretical linear plateau model was fitted to the semivariogram. The presence of low autocorrelation range indicates the residuals are independent of each other (Figure 9.8G for the recharge period and 9.8H for the discharge period).

Table 9.2. Predictive relationship of soil water storage for untransformed data and different IMFs of recharge and discharge periods. 'F' indicates the *F* statistics for the accepted models.

	Model†	F*	Adjusted R^2
	Recharge		
Untransformed	45.16 + 2.67 OC – 0.24 Sand – 1.28 Ele + 0.19 OC × Ele + 0.11 Sand × Ele	68.83	0.65
IMF 1	Intercept only	N/A	
IMF 2	5.22 + 1.29 Ele – 2.87 OC + 0.27 Ele × OC	21.63	0.59
IMF 3	9.89 + 2.01 Ele + 1.88 OC + 0.18 Ele × OC	21.27	0.74
IMF 4	6.41+ 0.93 OC	15.85	0.61
IMF 5	2.41 + 0.18 Sand + 1.21 Ele + 0.87 OC – 0.24 Clay + 0.08 Silt + 0.14 Ele × OC + 0.07 Ele × Clay	39.52	0.67
IMF 6	1.58 - 0.21 Sand + 1.01 OC + 1.27 Ele + 0.14 Silt – 0.31 Sand × Ele + 0.38 Ele × OC	26.79	0.70
	Discharge		
Untransformed	33.41 + 1.09 OC – 0.28 Sand - 1.72 Ele + 0.08 OC × Ele + 0.09 Sand × Ele	55.16	0.61
IMF 1	Intercept only	N/A	
IMF 2	4.39 + 1.23 Ele – 2.06 OC + 0.17 Ele × OC	19.59	0.58
IMF 3	7.83 + 1.87 Ele + 1.98 OC + 0.11 Ele × OC	17.71	0.71
IMF 4	5.28 + 0.87 OC	12.04	0.56
IMF 5	1.87 + 0.19 Sand + 0.87 Ele + 0.56 OC – 0.27 Clay + 0.10 Silt + 0.17 Ele × OC + 0.06 Ele × Clay	31.98	0.62
IMF 6	1.27 – 0.14 Sand + 0.87 OC + 1.27 Ele + 0.08 Silt – 0.35 Sand × Ele + 0.51 Ele × OC	24.05	0.65

† OC- Organic Carbon, Ele- Elevation. N/A- Not Applicable

* Significant at $p < 0.05$ level of probability; ** significant at $p < 0.01$ level of probability

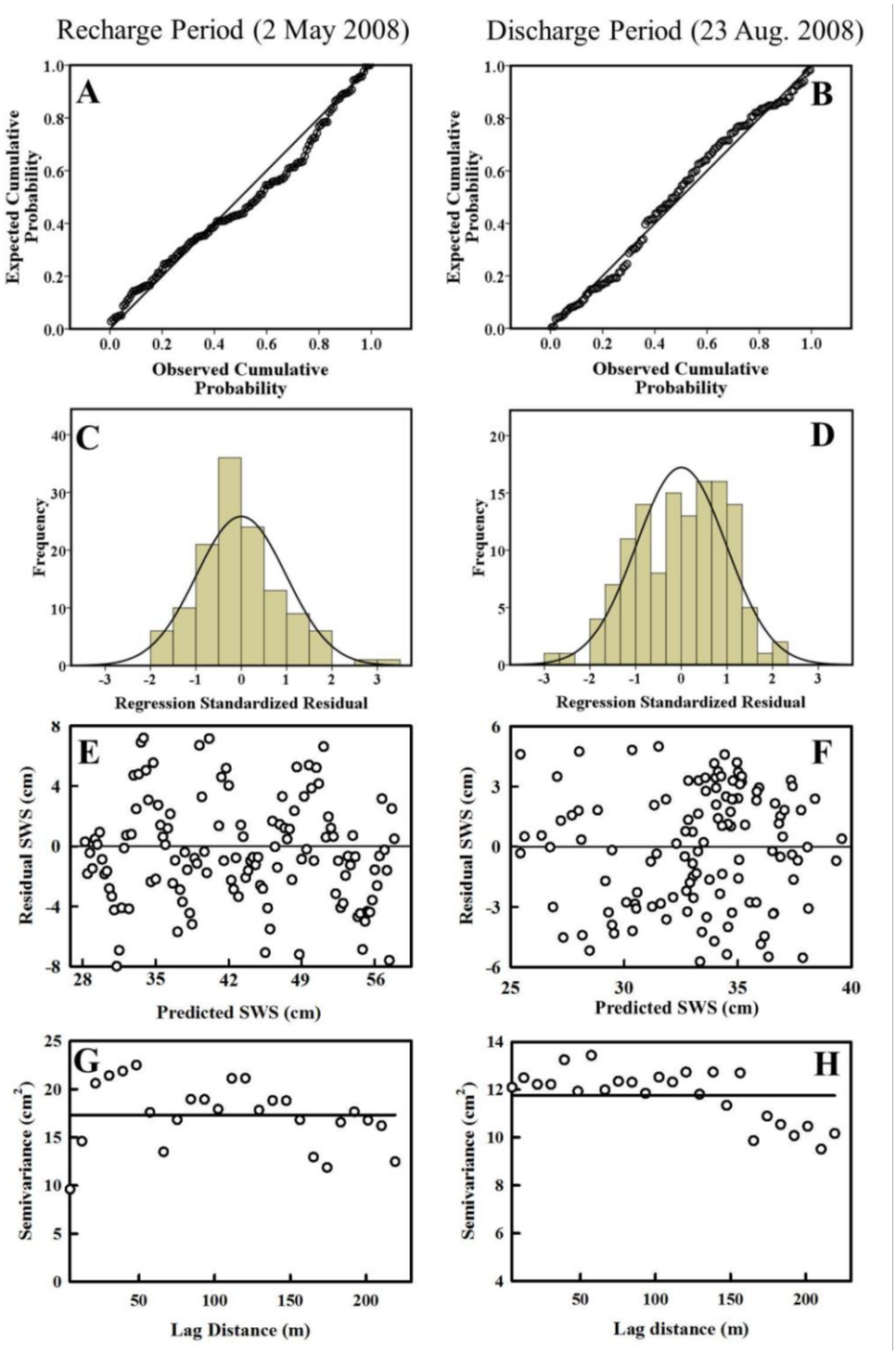

Figure 9.8. The observed cumulative probability vs. expected cumulative probability plot of residuals during the A) recharge and B) discharge period; the histogram of standardized residuals during the C) recharge and D) discharge period; the residual vs. the predicted soil water storage during the E) recharge and F) discharge period; and the semivariogram of regression residuals of the G) recharge and H) discharge period.

The predicted soil water storage at the measurement scale was compared with the measured soil water storage during the recharge and discharge period. Similarly, the overall prediction after combining the individual IMF predictions was also compared with the measured soil water storage for both periods. The coefficients of determination (r^2) between the measured soil water storage and predicted soil water storage at the measurement scale were between 0.57 and 0.66. However, the values of r^2 were between 0.65 and 0.76 between measured soil-water storage series and the prediction of soil water storage based on multiple linear regression of different IMFs. The sum of the predictions from individual scales provided improved prediction over the prediction at the measurement scale.

9.5 Conclusions

In this study, Hilbert Huang transform (HHT) was used to delineate the scale specific controls of soil water storage in a hummocky landscape. Empirical mode decomposition separated the overall variation from soil water storage into six different mode functions (also called IMFs) according to the scale of occurrence. IMF 1 represented the variations at very small scale that might be attributed to the localized variations in soil water storage. However, the contribution of variation of IMF 1 towards the overall variation in soil water storage was small (<6%). IMF 2 and IMF 3 separated 10 and 41%, respectively of the overall variations. The variations separated in IMF 2 and 3 were associated with elevation and OC. The high contribution towards the total variation and the strong correlation of IMF 3 with elevation indicated the strong association between soil water storage and elevation at the scale of 80 to 100 m. The IMF 4 was associated with OC, which might reflect the long-term effects of soil water storage that have been modified by the effect of topographic setting or elevation. Very large-scale variations separated in IMF 5 and 6 were associated with all the factors. However, the variance contributions from these IMFs towards the overall variance were very small. Based on the variance contribution and the predictive relationship between different IMFs and controlling factors, elevation was found to have the strongest association with soil water storage in the rolling landscape irrespective of the recharge or discharge period. IMFs decomposed through HHT were physically meaningful and provided improved prediction of soil water storage from topography, soil texture, and organic carbon in the hummocky landscape. The HHT was used to

identify the controls of soil water storage measured along a transect over multiple times in the hummocky landscape of Prairie pothole region of North America. In future studies, the method can be used to delineate the controls in other types of landscapes, which would greatly improve the understanding about the controls of soil water storage.

10.0 SYNTHESIS AND CONCLUSIONS

Knowledge on the spatial and temporal variability of soil water is an imperative for improving the understanding of various hydrological processes such as evapotranspiration, runoff, and precipitation and the prediction of various hydrologic, climatic and land surface process models. However, there is high spatio-temporal variability in soil water contributing from various controlling factors and processes operating in different intensities and at different scales. Fortunately, the effects of controlling factors on soil water are not completely unpredictable (random) in field and the spatial organization (or patterns) in the controlling factors reflected in the spatial pattern of soil water. The similarity of the spatial patterns over time was described as the 'time stability' and identification and understanding of this time stability provides useful assessment of, and insights into, the complex spatial and temporal variability of soil water.

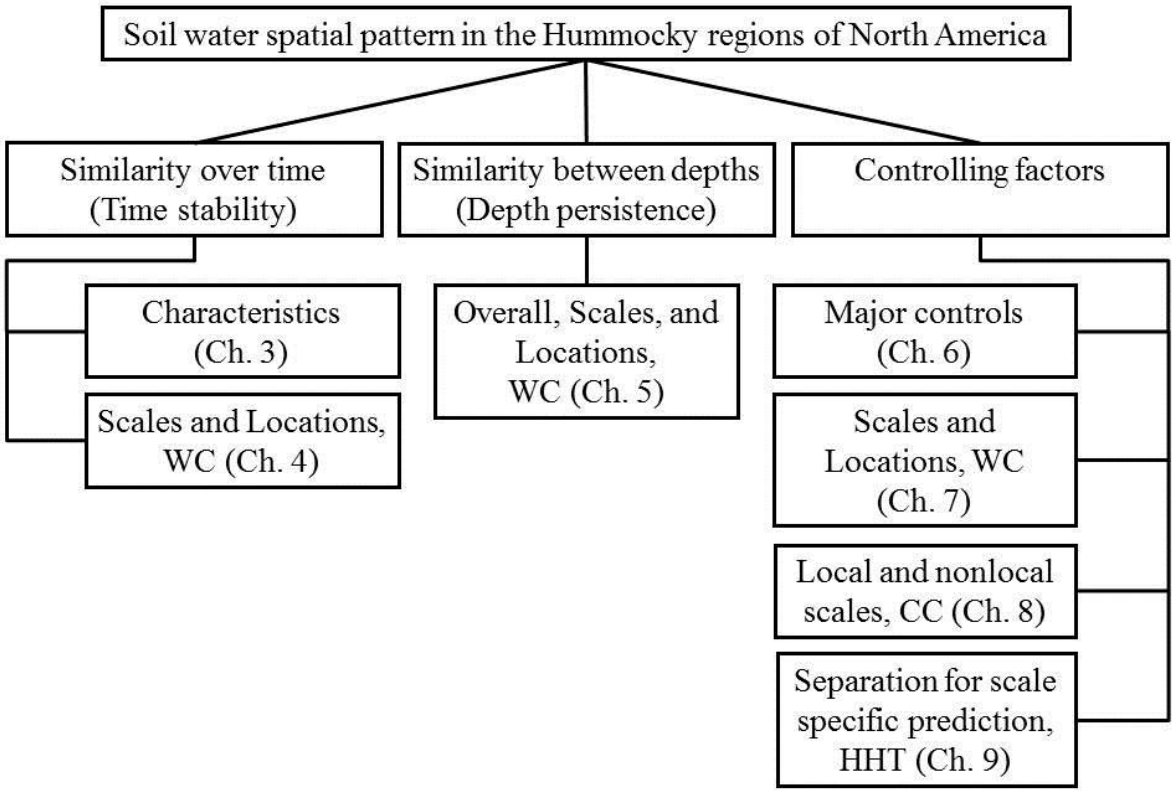

Figure 10.1. A roadmap of chapters of this dissertation indicating the main theme and the core methodology used in the chapter. Ch. indicates chapter, WC indicates wavelet coherency, CC indicates cyclical correlation, and HHT indicates Hilbert-Huang transform.

In the past, hydrologists and soil scientists have integrated many techniques to understand the spatial pattern of soil water, its dominant controlling factors, and the similarity over time. The research that comprises this dissertation sought to understand the issues regarding the spatial distribution of soil water. To do so, state-of-the-art methodologies are introduced for analyzing the similarity of the spatial patterns of soil water over time and depths and its dominant controlling factors in the hummocky landscapes of the prairie pothole region of North America. A roadmap of different chapters of this dissertation addressing different issues regarding the spatial distribution of soil water storage is shown in Figure 10.1.

10.1 Methodological Development

The scale dependence of the controlling factors makes the spatial pattern of soil water and its time stability highly scale dependent. Previously the scale dependence of time stability was analyzed using the spatial coherency (Kachanoski and de Jong, 1988), which is based on spectral analysis. The spectral analysis is useful in extracting the scale information of any spatial processes. However, this analysis deals with global state and loses spatial information. Moreover, this analysis assumes the spatial series to be stationary meaning that the average and the variance of the series are finite and constant. More often than not, trends in controlling factors make the spatial field nonstationary, and thus the spatial pattern of soil water is often nonstationary (Kachanoski and de Jong, 1988). Moreover, different scale processes can operate together in field resulting scale localization. Nonstationarity and the localized scale information restrict the spatial coherency analysis and calls for new method. Wavelet analysis can examine the scales and locations of variations in nonstationary spatial series and is introduced in this dissertation. In Chapter 4, I examined the scale and location dependence of the nonstationary soil water and its time stability using wavelet coherency, which is first in reference. This early work provided the basis for interpretation of scale dependent time stability of nonstationary soil water series measured within a season (intra-season), within the same season over different years (inter-annual) and between seasons (inter-season).

Wavelet coherency can examine the similarity between two spatial series at different scales and locations. This analysis has been used in examining the scale- and location-specific similarity between two soil properties by various authors (Si and Zeleke, 2005; Yates et al.,

2007; Biswas et al., 2008; Furon et al., 2008; Shu et al., 2008). Appendix E provides a detailed review on the application of wavelet analysis and wavelet coherency in examining the scale and location specific variability of various soil properties. However, I have used this method for the first time to examine the landscape characteristics of intra-season, inter-season and inter-annual time stability. I have also used this method in Chapter 5 to examine the scale and location specific similarity between the soil water spatial patterns at the surface layer to that of subsurface layers measured at a point of time, as well as to identify the scale- and location-specific controls of soil water storage in Chapter 7 of this dissertation.

While the spatial trend in controlling factors makes the spatial field nonstationary, the mutual and multiple influences from different factors make the system nonlinear. In this situation, the overall response to soil water storage as controlled by a number of factors (e.g., topography, soil texture) cannot be explained by simply measuring the effect of one factor at a time and subsequently adding the individual observation. Moreover, the complex relationship between different factors at multiple scales makes the identification of dominant controls complicated using the available methodology. I have introduced Hilbert-Huang transform (HHT) in the field of soil science and hydrology to examine and explore the complex relationship. HHT is a new spatial analysis method that deals with nonstationary and nonlinear spatial heterogeneity together (Biswas et al., 2009; Biswas and Si, 2011d). In Chapter 9, I have used this method to reveal the controls of soil water storage at different scales.

HHT is a two-step method. In the first step, empirical mode decomposition (EMD) separated the overall variation in the spatial pattern into a finite and often small number of intrinsic mode functions (IMFs). The IMFs represented the characteristic scales of variability in soil water. As a new method, I have compared the EMD with well-established discrete wavelet transform based multi-resolution analysis (MRA) in separating out the scale specific variability in Appendix A. The EMD separated the variations accurately at the scales it was present compared to the MRA that separated the variations in a predefined range of scales. In addition, separating the amount of variation present at a scale was exact in EMD compared to the MRA. In the second step of HHT, the Hilbert spectral analysis (HSA) identified the scale and location specific variability in soil water. The HSA that is based on Hilbert transform (HT) calculated the instantaneous frequency and energy as a function of space. The variations in soil water were

viewed as a function of locations (space) and scales (frequencies). In Appendix B, I have compared the HHT with well-established continuous wavelet transform (CWT) in examining the location- and scale-specific variability in nonstationary and nonlinear soil water. While the CWT identified a range of frequency band for a particular frequency present in the signal, HHT identified the frequency exactly. In addition, CWT is biased to the large-scale variations and identified different frequency components with different emphasis compared to the HHT that provided an equal representation of different scale processes. Moreover, the HHT identified the variations from nonstationary as well as nonlinear spatial series while CWT is good for only nonstationary spatial series.

These methodologies provided the baseline for examining the scale- and location-specific spatial variability. These techniques were then applied to understand the soil water variability in the landscape as well as to process and interpret data in comprehending the underlying variability of hydrological processes. These techniques were also used in identifying the dominant controls of soil water storage in the landscape.

10.2 Characteristics of Spatial Patterns of Soil Water Storage

Soil water storage is highly variable in space and time. However, if a field is repeatedly surveyed for soil water storage, there will be some locations always stored more or less water compared to the field average. Therefore, the locations maintain their rank and the spatial pattern will be similar over time. The similarity of the spatial pattern of soil water storage was first examined by Vachaud et al. (1985) and termed the phenomenon time stability. The time stability has been examined by various scientists at different parts of the world. Contradictory findings have been reported about the presence of time stability at different landscapes and climates. The wet or dry condition on time stability has also been reported. Chapter 3 examined the similarity of the spatial pattern of soil water storage within a season, within the same season over different years, and between seasons in the hummocky landscape of the prairie pothole region of North America. Based on the data collected from this study, I proposed the intra-season, inter-annual and inter-season time stability, respectively for the above-mentioned situations, which helped to explain the contradictory conclusion regarding when the time stability is strong, when the time stability is weak.

The spatial pattern of soil water storage was stable over time throughout the study period irrespective of average soil water condition. However, the intra-season time stability was stronger than inter-annual time stability, which was stronger than inter-season time stability. During the recharge period, a set of processes without vegetation determine the spatial pattern, whereas, the vegetation determine the spatial pattern during later part of the year or during the discharge period. The similar processes within a season yielded more similar spatial pattern than between seasons. However, as the processes repeat over years, strong inter-annual time stability was also observed.

The time stability was lost at different scales (Chapter 4). For example, the intra-season and inter-annual time stability was lost at the scales < 18 m during spring and early summer or the recharge period. The loss of time stability at these scales during spring may be attributed to the random variations in soil water measurement as well as the differential evaporation effects from local factors (e.g. surface roughness, soil texture). These variations were not associated with any particular landscape characteristics. On the contrary, the spatial patterns were almost identical at all locations during summer and fall or the discharge period, which indicated similar hydrological processes at scales < 18 m between summer and fall. Unfortunately, the variations at small scales were not strong enough to alter the spatial patterns at large scales, which resulted in strong large-scale time stability. While, the similar spatial pattern between summer and fall yielded strong inter-season time stability, slightly different spatial patterns between spring and summer or fall lost the inter-season time stability at scales <72 m mainly at the first half of the transect. The loss of time stability at these scales may be attributed to the change in landform elements and micro-topography within the first half of the transect that altered the hydrological processes from spring to summer or fall. However, the spatial pattern was similar over time in the second half of the transect with fewer variations in landform elements. The spatial pattern created by alternating knolls and depressions or the macro-topography did not change over time and showed strong time stability during any time at the scales > 72 m.

A slight different picture was observed in the time stability of the spatial patterns of soil water storage at the surface soil layer (0 to 20 cm) than that for the whole soil profile. Generally, the surface soil is highly dynamic due to heavy root activity and the plants take up majority of their water need from the top 50% of the root zone. In addition to this, surface layers are very

susceptible to change in any meteorological conditions. The dynamic nature of surface soil yielded less similar spatial patterns at different seasons and makes surface soil loose the inter-season time stability at small and medium scales. However, the time stability at large scales contributed from alternating knolls and depressions was still there with reduced magnitude.

Similarity in the overall spatial pattern as well as at different scales between surface and deep soil layers was examined in this dissertation and the phenomena was termed as depth persistence (Chapter 5). There was strong similarity in the overall spatial patterns of soil water storage between surface and subsurface layers indicating high degree of depth persistence. However, the degree of similarity gradually reduced with the increase in distance between surface and subsurface layers. This is because the impact of soil water processes that control the spatial pattern of soil water storage at the surface layer gradually decreased with the increase in depth and thereby providing a smooth change in the control of soil water dynamics. Similarly, the intensity of the processes operating at the recharge period is also different from the intensity of the processes operating at the discharge period. Therefore, the degree of depth persistence was slightly different from the recharge to discharge period.

The similarity in the spatial patterns of soil water storage was also observed at different scales. The large-scale (> 72 m) spatial patterns were similar between the surface and any sub-surface layers. Strong effect from alternating knolls and depressions or macro-topography yielded very similar large-scale spatial patterns at surface and subsurface layers during the recharge period. Similarity in medium-scale (18 to 72 m) spatial patterns was slightly different from the similarity at large scales. The locations within depressions with more variations in landform elements yielded very similar spatial patterns at medium scales. This means that the hydrological processes that operate at the medium scales are quite similar between the surface and subsurface layers at the locations with more variations in landform elements. However, the small-scale processes are less similar at different depths indicating loss of depth persistence at any locations. While, the surface layer is exposed to the atmospheric forcing and is more dynamic, the subsequent deep layers are less affected by meteorological changes and the hydrological dynamics is more stable.

Though the large-scale spatial patterns were similar between different depths during the discharge period, the degree of similarity was reduced compared to the recharge period. This

indicated the change in the intensity of hydrological processes from the recharge to the discharge period. A careful comparison between the spatial patterns of soil water storage at different depths during the recharge and discharge period indicated the similarity of the hydrological processes over time at a particular depth. While the surface layers showed the least similar spatial patterns between the recharge and the discharge period, the deepest layer showed the strongest similarity in the spatial patters at medium and large scales.

The similarity of the spatial patterns of soil water storage was used to identify benchmark locations that represent the field averaged soil water storage at different depths. For the surface layer (0 to 20 cm), 22nd sample point that was located at a mid-slope position was identified as the benchmark location. Similarly, 61st and 62nd points were identified as the benchmark location for the root zone (0 to 60 cm) and total active soil profile (0 to 120 cm), which were also located at mid-slope positions. The soil water storage at these points was used to predict the average soil water of the field. There were 16, 7, and 8% error, respectively for the surface, root zone, and total active soil profile associated with the average soil water prediction from the benchmark location measurements. Not surprisingly, the dynamic nature of the surface layer increased error in the prediction. However, with depth the stability of the soil water dynamics identified the benchmark location next to each other but different from the surface layer. The benchmark location can greatly improve the sampling efficiency by reducing the number of samples needed to characterize a field.

10.3 Dominant Controls of Soil Water Storage

Soil water storage is not controlled by a single factor but by a complex suite of environmental factors and processes that work independently or in combination to determine the soil water storage in a field. The importance of topography, soil properties, water routing processes, depth to water table, meteorological conditions, geology and vegetation have been studied by various authors in different landscapes. The hummocky landscape of the prairie pothole region of North America is unique because of its topographic settings. The landscape contains millions of wetlands with almost close hydrological basins thus making the hydrology of the area also unique. Chapter 6 provides comprehensive information on the factors that control the distribution of soil water in the landscape and the time evolution of those factors. The spatial

distribution of soil water storage in this type of landscape could not be explained by a single factor; rather the distribution was influenced by multiple factors that exerted an interactive effect. Various soil properties such as texture, BD, OC, depth of C- and A-horizon, depth of $CaCO_3$ as well as terrain indices such as wetness index, slope, aspect, convergence index, and flow connectivity showed strong correlation with soil water storage at any time.

In spite of strong visual similarity, there was almost no correlation between soil water storage and relative elevation. In the study area, knolls or high elevation locations contribute water to the depressions or low elevation locations. Therefore, the origin of the factors and their influence on soil water storage is different, which mean that the scale of influence is different from the scale of measurement. Chapter 7 examines the scale as well as location dependent controlling factors of soil water storage using wavelet coherency. Though, Pearson correlation could not identify any relationship between relative elevation and soil water storage, wavelet coherency identified significant correlation at different scales and locations. While, the large-scale (>70 m) spatial patterns in soil water storage all over the transect may be attributed to alternating knolls and depressions or the macro-topography, the medium scale spatial patterns within depressions may be attributed to the variations in landform elements and micro-topography. Similar to the relative elevation, the organic carbon content was also strongly correlated with soil water storage at medium and large scales. The organic carbon, which reflects the long-term history of soil water storage also strongly correlated with relative elevation. However, sand was only correlated with soil water storage at medium scales during spring and at large scales during summer and fall. In spite of low correlation at the scale of measurement, relative elevation had the largest area of significant coherency over the scales irrespective of seasons. This may be due to the presence of different types of correlation (e.g. positive or negative) at different scales, which neutralize the effect yielding a low overall correlation. The wavelet coherency identified the dominant scales and the types of correlation between soil water storage and relative elevation at different locations.

The strong correlation between the soil water storage and soil properties as well as various terrain indices indicated a combined influence from the controlling factors. Moreover, the relationship between the soil properties and the terrain indices make it difficult to identify the most dominant controlling factor. The principle component analysis was performed to identify

the group of variables that can have major influence on soil water storage by converting a set of correlated variables to a set of values of uncorrelated variables called principle components (PCs). However, low variance contribution of each principle component indicated mutual influences among the group of variables on soil water storage. Among the groups, the PC1 that explained maximum variation (~31%) in soil water storage was correlated with the factors that control soil water storage nonlocally (e.g. terrain indices). Similarly, the PC2 explained the second largest variation (17%) and correlated to the factors that control soil water storage locally (e.g. soil properties).

While, the local factors determine the infiltration and transmission of water in soil mostly as vertical fluxes, the nonlocal factors controls the lateral redistribution of surface and subsurface water in the landscape (Grayson et al., 1997). Therefore, one location in the landscape influences the soil water storage at another location and there is a lag/lead in distance between the origin of the nonlocal controlling factors and its response in soil water storage. The effect of nonlocal factors at different scales was identified by modifying the Pearson correlation coefficients in Chapter 8. The correlation coefficients were calculated by physically shifting the spatial series of soil water storage with respect to that of controlling factors. The shifting distance indicated the difference in the origin of a factor and its response in controlling soil water storage. For example, the correlation between soil water storage and relative elevation was very weak (r^2 = 0.02 to 0.08) at the measurement scale. However, the value of r^2 increased many folds (r^2 = 0.47 to 0.61) after shifting the spatial series of soil water storage by 54 m, which was almost equal the average length of the existing slopes. This indicated the nonlocal effect from the relative elevation. The correlation at the measurement scale is an indicative of local effects. Some local factors were also correlated with soil water storage at scales larger than the scale of measurement. For example, the depth of C and A horizon, $CaCO_3$ layer, organic carbon were correlated with soil water storage at a lag/lead of 54 m. This may be due to the inter-correlation of these factors with relative elevation.

Chapter 9 identified the dominant controls at different scales using HHT. The spatial series of soil water storage was decomposed into 6 different IMFs (IMF 1 through IMF 6) according to the scales of variations present. The lowest scales of variations (e.g. 5 to 10 m) were not correlated to any controlling factors and were attributed to the localized variations in soil

water storage resulting from the random processes in the landscape during the recharge period. The variations at the scales around 30 to 40 m were attributed to the variations in landform elements and micro-topography and separated around 10 percent of total variations during the recharge period. However, the variations at the scales around 80 to 100 m (IMF3) separated the variations (around 41 percent) more than other IMFs combined. The IMF3 was strongly correlated with relative elevation that had alternating knolls and depressions at the scales around 80 to 100 m. At very large scales, the variations were separated as the landscape scale variations and were correlated with almost all factors. However, these scales contributed a small amount of total variations. Sometimes, at a particular scale, different processes can have mutual influences. The mutual influences were identified from the correlation between IMFs and the controlling factors.

Soil water storage was predicted at different scales (or at IMFs) from the regression models. The IMFs contributing maximum variation and the factors that were included in the regression can help to identify the dominant controlling factor of soil water storage. For example, the IMF3 contributed more than 41% of total variation and the relative elevation was the main predictive variable at that scale. In this situation, relative elevation can be identified as the dominant control of soil water storage at the scales of 80 to 100 m. The individual prediction at different scales was added together to compare with the prediction at measurement scale. The overall prediction computed from scale specific predictions provided improvement over the measurement scale predictions.

Though, the trend in the variations in soil water storage and its correlation with different factors at different scales were persistent throughout the measurement period, the magnitude of the variation and the correlation changed over time. This indicated only the change in the degree of control from different factors at different time, but not the switch of controls from one factor to another. This may be because the set of processes dominate in one season may not be at the same intensity at other seasons. It is the intensity of the processes that change over time. For example, the IMF3 was strongly correlated with relative elevation and contributed the highest variation compared to the other IMFs at all measurements. This indicated the strongest control from the relative elevation at the scale of 80 to 100 m irrespective of measurement times or the initial soil water conditions. In the hummocky landscape of the prairie pothole region, water

redistributes along the topography during the recharge period. The depressions accumulate so much water during this time that the effect persisted throughout the discharge period. However, only a small change in the magnitude of correlation was observed over time at different scales.

10.4 Implications and Future Research

The similarity in the spatial pattern of soil water storage provides insight about various important ongoing hydrological and ecological processes in the landscape. The information on the similarity of the spatial pattern can help catchment managers to identify the management units in a more cost effective manner for precision management of crop biomass production and the environment. Similarity in the spatial pattern was used to identify the benchmark locations with field averaged soil water storage, which can greatly improve the sampling efficiency by reducing the number of samples or observations. This provides considerable promise in reducing the cost, time, and labor necessary for field averaged soil water storage monitoring. The benchmark point can be used to calibrate the soil water measurement using satellite images. However, the benchmark point was identified based on four years of soil water measurement. Since the identification procedure requires a large amount of work, the next step for this research is to find the landscape characteristics for the benchmark sites.

The change in the similarity of the spatial patterns of soil water storage over time at different scales is an indicative of the change in the hydrological processes operating at those scales. Therefore, the scales of similarity can be used to identify the change in the sampling domain as controlled by the hydrological processes operating at different scales delivering the maximum information with minimum sampling effort. The information on the scales of similarity in the spatial pattern of soil water storage will guide designing the experiment for any hydrological studies. The similarity of scales can be used for the scale specific prediction of soil water storage. The transformation of information from one scale to another is possible from the information of scales of spatial pattern and its similarity over times and at depths. The field scale measurement can be up scaled to a large area for environmental management. In this study, the spatial scales of hydrological processes were analyzed at discrete point of time. However, to understand the time evolution of various hydrological processes, it is necessary to collect the soil water data continuously. Setting up long term monitoring network would provide comprehensive

information on the exact time evolution of hydrological processes and can be future direction of work. The benchmark location will greatly help to reduce the number of monitoring location.

The similarity in the spatial pattern of soil water storage between the surface and subsurface soil layers help understand the hydrological dynamics of deep soils from the easily measured surface soil water. Measuring soil water over a large area using satellite images is popular among hydrologists. However, it only measures water in the surface layer. The similarity in the overall spatial pattern of soil water storage as well as at different scales between the surface and subsurface soil layers provide a better picture on the soil profile hydrological dynamics. The hydrological dynamics of soil is also controlled by the groundwater. Therefore, the similarity in the spatial patterns of soil water can provide potential inference on ground water dynamics. However, in depth future studies are necessary to understand the interaction between the groundwater and the soil water dynamics.

The similarity in the spatial patterns of soil water storage over time and at different depths is a great source of information for understanding the soil hydrological dynamics. In current research, soil water was measured along a transect and at different depths. Therefore, it was confined to only two spatial dimensions. However, information in three dimensions would provide a complete picture and needs to be understood through future studies. Similarly, current study was conducted in a uniform vegetation type. The presence or absence, type, density also determines the water use. Therefore, future studies are necessary over a large area and multi-land uses to better understand the spatial pattern and its controlling factors at the watershed to the regional scales.

The similarity in the spatial patterns and thus the hydrological process can be a great source of information in understanding various landscape processes. The information can also be incorporated in a large number of surface and subsurface hydrological models and is another scope of future work. The similarity in the spatial patterns of soil water storage can be used as a natural analog for reclamation. The open pit mining provides considerable amount to country's economy, yet the destruction of landscape threaten the environment. The persistence spatial patterns of soil water in the landscape and its scales of variability can be used during the reconstruction of disturbed land landscapes.

11.0 REFERENCES

Abramovich, F., and Y. Benjamini. 1996. Adaptive thresholding of wavelet coefficients. Comput. Stat. Data Anal. 22:351–361.

Acton, D.F., and J.G. Ellis. 1978. The soils of Saskatoon Map area 73B Saskatchewan. Pub. S4. Saskatchewan Inst. Pedology, Univ. of Saskatchewan, Saskatoon, SK.

AES. 1997. Canadian daily climate data for Western Canada. *In* [CD-ROM]. Atmospheric Environment Service, Environment Canada, Downsview, ON.

Albertson, J., and N. Montaldo. 2003. Temporal dynamics of soil moisture variability: 1. Theoretical basis. Water Resour. Res. 39:1274, doi:10.1029/2002WR001616.

Anctil, F., R. Mathieu, L.E. Parent, A.A. Viau, M. Sbih, and M. Hessami. 2002. Geostatistics of near-surface moisture in bare cultivated organic soils. J. Hydrol. 260:30–37.

Anderson, M.G., and P.E. Kneale. 1982. The influence of low-angled topography on hill slope soil-water convergence and stream discharge. J. Hydrol. 57:65–80.

Anderson, M.G., and T.P. Burt. 1978. The role of topography in controlling throughflow generation. Earth Surf. Processes. Landforms 3:331–344.

Bárdossy, A., and W. Lehmann. 1998. Spatial distribution of soil moisture in a small catchment. Part 1: Geostatistical analysis. J. Hydrol. 206:1–15.

Barling, R.D., I.D. Moore, and R.B. Grayson. 1994. A quasi-dynamic wetness index for characterizing the spatial distribution of zones of surface saturation and soil water content. Water Resour. Res. 30:1029–1044.

Bedard-Haughn, A.K., and D.J. Pennock. 2002. Terrain controls on depressional soil distribution in a hummocky morainal landscape. Geoderma 110:169–190.

Bedrosian, E. 1963. A product theorem for Hilbert Transform. Proc. IEEE 51:868–869.

Bell, K.R., B.J. Blanchard, T.J. Schmugge, and M.W. Witczak. 1980. Analysis of surface moisture variations within large-field sites. Water Resour. Res. 16:796–810.

Beven, K. 2001. How far can we go in distributed hydrological modeling? Hydrol. Earth Sys. Sci. 5:1–12.

Beven, K.J., and M.J. Kirkby. 1979. A physically-based, variable contributing area model of basin hydrology. Hydrol. Sci. J. 24:43–69.

Biswas, A., and B.C. Si. 2011a. Season and depth dependent time stability and benchmarking of soil water storage in a hummocky landscape. Soil Sci. Soc. Am. J. (accepted).

Biswas, A., and B.C. Si. 2011b. Identifying scale specific controls of soil water storage in a Hummocky landscape using wavelet coherency. Geoderma (accepted).

Biswas, A., and B.C. Si. 2011c. Application of continuous wavelet transform in examining soil spatial variation: a review. Math. Geosci. 43:379–396.

Biswas, A., and B.C. Si. 2011d. Revealing the controls of soil water storage at different scales in a Hummocky landscape. Soil Sci. Soc. Am. J. (in press).

Biswas, A., B.C. Si, and F.L. Walley. 2008. Spatial relationship between $\delta^{15}N$ and elevation in agricultural landscapes. Nonlinear Proc. Geoph. 15:397–407.

Biswas, A., H.W. Chau, A.K. Bedard-Haughn, and B.C. Si. 2011. Factors controlling soil water storage in the Hummocky landscape of the prairie pothole region of North America. Can. J. Soil Sci. (in review).

Biswas, A., L.K. Tallon, and B.C. Si. 2009. Scale-specific relationships between soil properties: Hilbert-Huang transform. Pedometron 28:17–20.

Blöschl, G. 1999. Scaling issues in snow hydrology. Hydrol. Proc. 13:2149–2175.

Blöschl, G., and M. Sivapalan. 1995. Scale issues in hydrological modeling: a review. Hydrol. Proc. 9:251–290.

Blöschl, G., R. Merz, R.B. Grayson, and A.W. Western. 2001. Looking for scale invariant processes: From point to mesoscale. *In* Abstracts, Chapman Conf. State Art Hillslope Hydrol., AGU, Sun River, OR, 8–12 Oct. 2001.

Bosch, D.D., V. Lakshmi, T.J. Jackson, M. Choi, and J.M. Jacobs. 2006. Large scale measurements of soil moisture for validation of remotely sensed data: Georgia soil moisture experiment of 2003. J. Hydrol. 323:120–137.

Bosch, E.H., M.A. Oliver, and R. Webster. 2004. Wavelets and generalization of variogram. Math. Geol. 36:147–186.

Braud, I., A.C. Dantasantonino, and M. Vauclin. 1995. A stochastic approach to studying the influence of the spatial variability of soil hydraulic-properties on surface fluxes, temperature and humidity. J. Hydrol. 165:283–310.

Brillinger, D.R. 2001. Time series: Data analysis and theory. p. 540. Soc. Ind. Appl. Math. Philadelphia, PA.

Brinson, M.M. 1993. A hydrogeomorphic classification for wetlands. Wetlands Research Program Technical Report WRP-DE-4. p. 103. US Army Corps Eng., Waterways Expt. Stn., Vicksburg, MP.

Brocca, L., F. Melone, and T. Moramarco. 2008. On the estimation of antecedent wetness conditions in rainfall-runoff modeling. Hydrol. Proc. 22:629–642.

Brocca, L., F. Melone, T. Moramarco, and R. Morbidelli. 2009. Soil moisture temporal stability over experimental areas in Central Italy. Geoderma 148:364–374.

Brocca, L., F. Melone, T. Moramarco, and R. Morbidelli. 2010. Spatial-temporal variability of soil moisture and its estimation across scales. Water Resour. Res. 46:W02516, doi:10.1029/2009WR008016.

Brocca, L., R. Morbidelli, F. Melone, and T. Moramarco. 2007. Soil moisture spatial variability in experimental areas of central Italy. J. Hydrol. 333:356–373.

Bromley, J., J. Brouwer, A.P. Barker, S.R. Gaze, and C. Valentin. 1997. The role of surface water redistribution in an area of patterned vegetation in a semi-arid environment, south-west Niger. J. Hydrol. 198:1–29.

Bronstert, A., and A. Bárdossy. 1999. The role of spatial variability of soil moisture for modelling surface runoff generation at the small catchment scale. Hydrol. Earth Sys. Sci. 3:505–516.

Burgess, T.M., and R. Webster. 1980. Optimal interpolation and isarithmic mapping of soil properties. I. The semivariogram and punctual kriging. J. Soil Sci. 31:315–331.

Burrough, P.A. 1983. Multiscale sources of spatial variation in soil. 1. The application of fractal concepts to nested levels of soil variation. J. Soil Sci. 34:577–597.

Burt, T.P., and D.P. Butcher. 1985. Topographic controls of soil moisture distributions. J. Soil Sci. 36:469–486.

Buttafuoco, G., A. Castrignanò, E. Busoni, and A.C. Dimase. 2005. Studying the spatial structure evolution of soil water content using multivariate geostatistics. J. Hydrol. 311:202–218.

Cassel, D.K., O. Wendroth, and D.R. Nielsen. 2000. Assessing spatial variability in an agricultural experiment station field: opportunities arising from spatial dependence.

Agron. J. 92:706–714.

Castrignanò, A., G. Lopez, and M. Stelluti. 1994. Temporal and spatial variability of electrical conductivity, Na content and sodium adsorption ratio of saturation extract measurements. Eur. J. Agron. 3:221–226.

Chang, R.K. 1968. Component potentials and hysteresis in water retention by compacted clay soil aggregates. Soil Sci. 105:172–176.

Charpentier, M.A., and P.M. Groffman. 1992. Soil moisture variability within remote sensing pixels. J. Geophys. Res. 97:18987–18995.

Chen, Y.J. 2006. Letters to the editor on "Rank Stability or Temporal Stability". Soil Sci. Soc. Am. J. 70:306–306.

Choi, M., J.M. Jacobs, and M.H. Cosh. 2007. Scaled spatial variability of soil moisture fields. Geophys. Res. Lett. 34:L01401, doi:10.1029/2006gl028247.

Chui, C.K. 1992. An introduction to wavelets. Academic Press, New York, NY.

Comegna, V., and A. Basile. 1994. Temporal stability of spatial patterns of soil-water storage in a cultivated Vesuvian soil. Geoderma 62:299–310.

Corwin, D.L., J. Hopmans, and G.H. de Rooij. 2006. From field- to landscape-scale vadose zone processes: scale issues, modeling, and monitoring. Vadose Zone J. 5:129–139.

Cosh, M.H., T.J. Jackson, P. Starks, and G. Heathman. 2006. Temporal stability of surface soil moisture in the Little Washita River watershed and its applications in satellite soil moisture product validation. J. Hydrol. 323:168–177.

Cosh, M.H., T.J. Jackson, R. Bindlish, and J.H. Prueger. 2004. Watershed scale temporal and spatial stability of soil moisture and its role in validating satellite estimates. Remote Sens. Environ. 92:427–435.

Cosh, M.H., T.J. Jackson, S. Moran, and R. Bindlish. 2008. Temporal persistence and stability of surface soil moisture in a semi-arid watershed. Remote Sens. Environ. 112:304–313.

Crow, W.T., and E.F. Wood. 2002. The value of coarse-scale soil moisture observations for regional surface energy balance modeling. J. Hydrometeor. 3:467–482.

da Silva, A.P., A. Nadler, and B.D. Kay. 2001. Factors contributing to temporal stability in spatial patterns of water content in the tillage zone. Soil Till. Res. 58:207–218.

Daubechies, I. 1992. Ten lectures on wavelets. *In* Proc. CBMS-NSF Reg. Conf. Series App. Math., Soc. Indust. Appl. Math., Philadelphia, PA.

De Lannoy, G.J.M., P.R. Houser, N.E.C. Verhoest, V.R.N. Pauwels, and T.J. Gish. 2007. Upscaling of point soil moisture measurements to field averages at the OPE3 test site. J. Hydrol. 343:1–11.

Delworth, T., and S. Manabe. 1993. Climate variability and land-surface processes. Adv. Water Resour. 16:3–20.

Douaik, A., M. Van Meirvenne, and T. Toth. 2006. Temporal stability of spatial patterns of soil salinity determined from laboratory and field electrolytic conductivity. Arid Land Res. Manag. 20:1–13.

Douaik, A., M. Van Meirvenne, and T. Toth. 2007 Statistical methods for evaluating soil salinity spatial and temporal variability. Soil Sci. Soc. Am. J. 71:1629–1635.

Ducks Unlimited Canada. 2006. Values and benefits of wetland habitats. Available at http://www.ducks.ca/conserve/wetland_values/ (Verified on 18/04/2011). Ducks Unlimited. Canada, Stonewall, MB.

Dunne, T., and R.D. Black. 1970. Partial area contributions to storm runoff in a small new-England watershed. Water Resour. Res. 6:1296–1311.

Dunne, T., T.R. Moore, and C.H. Taylor. 1975. Recognition and prediction of runoff-producing zones in humid regions. Hydrol. Sci. B. 20:305–327.

Elliott, J.A., and A.A. Efetha. 1999. Influence of tillage and cropping system on soil organic matter, structure and infiltration in a rolling landscape. Can. J. Soil Sci. 79:457–463.

Entin, J.K., A. Robock, K.Y. Vinnikov, S.E. Hollinger, S. Liu, and A. Namkhai. 2000. Temporal and spatial scales of observed soil moisture variations in the extra tropics. J. Geophys. Res. 105:11865–11877.

Environment Canada. 2001. Threats to Sources of Drinking Water and Aquatic Ecosystem Health in Canada. p. 72. *In* NWRI Scientific Assessment Report Series No. 1, National Water Research Institute, Burlington, ON.

Environment Canada. 2004. Threats to water availability in Canada. p. 11. *In* NWRI Scientific Assessment Report Series No. 3, National Water Research Institute, Burlington, ON.

Environment Canada. 2010. National climate data and information archive. Available at www.climate.weatheroffice.gc.ca. (Verified on 18/04/2011). Environ. Can., Fredericton, NB.

Famiglietti, J.S., and E.F. Wood. 1994. Multiscale modeling of spatially variable water and energy-balance processes. Water Resour. Res. 30:3061–3078.

Famiglietti, J.S., and E.F. Wood. 1995. Effects of spatial variability and scale on aerially-averaged evapotranspiration. Water Resour. Res. 31:699–712.

Famiglietti, J.S., J.A. Devereaux, C.A. Laymon, T. Tsegaye, P.R. Houser, T.J. Jackson, S.T. Graham, M. Rodell, and P.J. van Oevelen. 1999. Ground-based investigation of soil moisture variability within remote sensing footprints during the Southern Great Plains 1997 (SGP97) Hydrology Experiment. Water Resour. Res. 35:1839–1851.

Famiglietti, J.S., J.W. Rudnicki, and M. Rodell. 1998. Variability in surface moisture content along a hill slope transect: Rattlesnake Hill, Texas. J. Hydrol. 210:259–281.

Fang, X., and J.W. Pomeroy. 2007. Snowmelt runoff sensitivity analysis to drought on the Canadian prairies. Hydrol. Proc. 21:2594–2609.

Fang, X., and J.W. Pomeroy. 2009. Modeling blowing snow redistribution to prairie wetlands. Hydrol. Proc. 23:2557–2569.

Farahani, H.J., and G.W. Buchleiter. 2004. Temporal stability of soil electrical conductivity in irrigated sandy fields in Colorado. Trans. ASAE 47:79–90.

Farge, M. 1992. Wavelet transform and their applications to turbulence. Annul. Rev. Fluid. Mech. 24:395–457.

Feddes, R.A., P.J. Kowalik, and H. Zaradny. 1978. Simulation of field water use and crop yield. Halsted Press, John Wiley and Sons Inc., New York, NY.

Fernández-Gálvez, J., L.P. Simmonds, and E. Barahona. 2006. Estimating detailed soil water profile records from point measurements. Eur. J. Soil Sci. 57:708–718.

Fitzjohn, C., J.L. Ternan, and A.G. Williams. 1998. Soil moisture variability in a semi-arid gully catchment: implications for runoff and erosion control. Catena 32:55–70.

Flerchinger, G.N., and K.R. Cooley. 2000. A ten-year water balance of a mountainous semi-arid watershed. J. Hydrol. 237:86–99.

Foussereau, X., A.G. Hornsby, and R.B. Brown. 1993. Accounting for variability within map units when linking a pesticide fate model to soil survey. Geoderma 60:257–276.

Francis, C.F., J.B. Thornes, A. Romero Diaz, L. Lopez Bermudez, and G.C. Fisher. 1986. Topographic control of soil moisture, vegetation cover and land degradation in a moisture stressed Mediterranean environment. Catena 13:211–225.

Frantziskonis, G. 2002. Wavelet based analysis of multiscale phenomena: Application of material porosity and identification of dominant scales. Probab. Eng. Mech. 17:349–357.

Fugal, D.L. 2007. Conceptual wavelets in digital signal processing. Available at http://www.conceptualwavelets.com/index.html. (Verified on 18/04/2011), Spring Valley, CA.

Furon, A.C., C. Wagner-Riddle, C.R. Smith, and J.S. Warland. 2008. Wavelet analysis of wintertime and spring thaw CO_2 and N_2O fluxes from agricultural fields. Agric. Forest Meteor. 148:1305–1317.

Gajem, Y.M., A.W. Warrick, and D.E. Myers. 1981. Spatial dependence of physical properties of a Typic Torrifluvent soil. Soil Sci. Soc. Am. J. 45:709–715.

Gautama, T., D.P. Mandic, and M.A. Van Hulle. 2004. The delay vector variance method for detecting determinism and nonlinearity in time series. Physica D. 190:167–176.

Giorgi, F., and R. Avissar. 1997. Representation of heterogeneity effects in earth system modeling: Experience from land surface modeling. Rev. Geoph. 35:413–437.

Gleason, R.A., and B.A. Tangen. 2008. Floodwater storage. *In* R.A. Gleason et al. (ed.) Ecosystem services derived from wetland conservation practices in the United States prairie pothole region with an emphasis on the U.S. Department of Agriculture Conservation Reserve and Wetlands Reserve Programs. Professional Paper 1745. U.S. Geol. Survey, Reston, VA.

Goderya, F.S. 1998. Field scale variations in soil properties for spatially variable control: a review. J. Soil Contam. 7:243–264.

Gómez-Plaza, A., J. Alvarez-Rogel, J. Alabaladejo, and V.M. Castillo. 2000. Spatial patterns and temporal stability of soil moisture a range of scales in a semi-arid environment. Hydrol. Proc. 14:1261–1277.

Gómez-Plaza, A., M. Martínez-Mena, J. Albaladejo, and V.M. Castillo. 2001. Factors regulating

spatial distribution of soil water content in small semi-arid catchments. J. Hydrol. 253:1261–1277.

Goovaerts, P. 1998. Geostatistical tools for characterizing the spatial variability of microbiological and physico-chemical soil properties. Biol. Fertil. Soils 27:315–334.

Goovaerts, P., and C.N. Chiang. 1993. Temporal persistence of spatial patterns for mineralizable nitrogen and selected soil properties. Soil Sci. Soc. Am. J. 57:372–381.

Goovaerts, P., and R. Webster. 1994. Scale-dependent correlation between topsoil copper and cobalt concentrations in Scotland. Eur. J. Soil Sci. 45:79–95.

Grant, L., M. Seyfried, and J. McNamara. 2004. Spatial variation and temporal stability of soil water in a snow-dominated, mountain catchment. Hydrol. Proc. 18:3493–3511.

Graps, A. 1995. An introduction to Wavelets. IEEE Comput. Sci. Eng. 2:1–18.

Gray, D.M., P.G. Landine, and R.J. Granger. 1985. Simulating infiltration into frozen prairie soils in streamflow models. Can. J. Earth Sci. 22:464–472.

Grayson, R.B., A.W. Western, F.H.S. Chiew, and G. Blöschl. 1997. Preferred states in spatial soil moisture patterns: Local and nonlocal controls. Water Resour. Res. 33:2897–2908.

Grayson, R.B., and A.W. Western. 1998. Towards areal estimation of soil water content from point measurements: time and space stability of mean response. J. Hydrol. 207:68–82.

Grayson, R.B., I.D. Moore, and T.A. McMahon. 1992. Physically based hydrologic modeling, II: Is the concept realistic? Water Resour. Res. 28:2659–2666.

Grinsted, A.J., C. Moore, and S. Jevrejeva. 2004. Application of the cross wavelet transform and wavelet coherence to geophysical time series. Nonlinear Proc. Geoph. 11:561–566.

Guber, A.K., T.J. Gish, Y.A. Pachepsky, M.T. van Genuchten, C.S.T. Daughtry, T.J. Nicholson, and R.E. Cady. 2008. Temporal stability of estimated soil water flux patterns across agricultural fields. Int. Agroph. 22:209–214.

Guber, A.K., W.J. Rawls, E.V. Shein, and Y.A. Pachepsky. 2003. Effect of soil aggregate size distribution on water retention. Soil Sci. 168:223–233.

Hawley, M.E., T.J. Jackson, and R.H. McCuen. 1983. Surface soil moisture variation on small agricultural watersheds. J. Hydrol. 62:179–200.

Hayashi, M., G. van der Kamp, and D.L. Rudolph. 1998. Water and solute transfer between a prairie wetland and adjacent uplands, 1. Water balance. J. Hydrol. 207:42–55.

Hayashi, M., G. van der Kamp, and R. Schmidt. 2003. Focused infiltration of snowmelt water in partially frozen soil under small depressions. J. Hydrol. 270:214–229.

He, Y.H., X.L. Guo, and B.C. Si, 2007. Detecting grassland spatial variation by a wavelet approach. Int. J. Remote Sens. 28:1527–1545.

Heathman, G.C., P.J. Starks, L.R. Ahuja, and T.J. Jackson, 2003. Assimilation of surface soil moisture to estimate profile soil water content. J. Hydrol. 279:1–17.

Heuvelink, G.B.M., and E.J. Pebesma.1999. Spatial aggregation and soil process modeling. Geoderma 89:47–65.

Hills, T.C., and S.G. Reynolds. 1969. Illustrations of soil moisture variability in selected areas and plots of different sizes. J. Hydrol. 8:27–47.

Hogan, J.M., and F.M. Conly. 2002. St. Denis national wildlife area land cover classification: 1997. *In* Technical Report Series Number 384. Canadian Wildlife Service, Prairie and Northern Region, Prairie Northern Wildlife Research Centre, Saskatoon, SK.

Horton, R.E. 1933. The role of infiltration in the hydrologic cycle. EOS Am. Geophys. Union Trans. 14:446–460.

Houser, P.R. 2000. Challenges and progress towards multi-scale hydrologic data assimilation. p. 1259-1261 (doi:10.1109/IGARSS.2000.858086). *In* Proc. Geosci. Remote Sens. Symp. 2000, IGARSS 2000, IEEE 2000 Int. Honolulu, HI.

Houser, P.R., W.J. Shuttleworth, J.S. Famiglietti, H.V. Gupta, K.H. Syed, and D.C. Goodrich. 1998. Integration of soil moisture remote sensing and hydrologic modeling using data assimilation. Water Resour. Res. 34:3405–3420.

Hu, S., D.C. Coleman, C.R. Carroll, P.F. Hendrix, and M.H. Beare. 1997. Labile soil carbon pools in subtropical forest and agricultural ecosystems as influenced by management practices and vegetation types. Agri. Ecosyst. Environ. 65:69–78.

Hu, W., M.A. Shao, and K. Reichardt. 2010b. Using a new criterion to identify sites for mean soil water storage evaluation. Soil Sci. Soc. Am. J. 74:762–773.

Hu, W., M.A. Shao, F. Han, K. Reichardt, and J. Tan. 2010a. Watershed scale temporal stability of soil water content. Geoderma doi:10.1016/j.geoderma.2010.04.030.

Hu, W., M.A. Shao, Q.J. Wang, and K. Reichardt. 2008. Soil water content temporal-spatial variability of the surface layer of a Loess Plateau hillside in China. Scientia Agricola

65:277–289.

Hu, W., M.A. Shao, Q.J. Wang, and K. Reichardt. 2009. Time stability of soil water storage measured by neutron probe and the effects of calibration procedures in a small watershed. Catena 79:72–82.

Huang, J.W., and B. Milkereit. 2009. Empirical mode decomposition based instantaneous spectral analysis and its applications to heterogeneous petrophysical model construction. p. 1–6. *In* Proc. Frontiers + Innovations - 2009 CSPG CSEG CWLS Convention, Calgary, AB,

Huang, N.E. 2005. Empirical mode decomposition for analyzing acoustical signals, Patent 6862558, US Patent and Trademark Off. Washington DC. Date issued: 1 March 2005.

Huang, N.E., and S.S.P. Shen. (ed.) 2005. Hilbert-Huang transform and its applications. World Sci., Singapore.

Huang, N.E., and Z. Wu. 2008. A review of Hilbert-Huang transform: method and its applications to geophysical studies. Rev. Geoph. 46:RG2006, doi:10.1029/2007RG000228.

Huang, N.E., Z. Shen, S.R. Long, M.C. Wu, H.H. Shih, Q. Zheng, N.C. Yen, C.C. Tung, and H.H. Liu. 1998. The empirical mode decomposition and the Hilbert spectrum for nonlinear and non-stationary time series analysis. Proc. Math. Phy. Eng. Sci. 454:903–995.

Hubbard, B.B. 1998. The world according to wavelets: The mathematical technique in the making. 2nd ed. AK Press, Natrick, MA.

Hubbard, D., and R.L. Linder. 1986. Spring runoff retention in prairie pothole wetlands. J. Soil Water Conserv. 41:122–125.

Huel, D. 2000. Managing Saskatchewan Wetlands: A landowner's guide. p. 69. Saskatchewan Wetland Conserv. Corp., Regina, SK.

Hupet, F., and A. Vanclooster. 2005. Micro-variability of hydrological processes at the maize row scale: implications for soil water content measurements and evapotranspiration estimates. J. Hydrol. 303:247-270.

Hupet, F., and M. Vanclooster. 2002. Intraseasonal dynamics of soil moisture variability within a small agricultural maize cropped field. J. Hydrol. 261:86–101.

Isaaks, E.H., and R.M. Srivastava. 1989. An introduction to applied geostatistics. Oxford Uni. Press, Toronto, ON.

Jackson, T.J. 1993. Measuring surface soil-moisture using passive microwave remote-sensing. Hydrol. Proc. 7:139–152.

Jacobs, J.M., B.P. Mohanty, E.C. Hsu, and D. Miller. 2004. SMEX02: Field scale variability, time stability and similarity of soil moisture. Remote Sens. Environ. 92:436–446.

Jaynes, D.B., and D.J. Hunsaker. 1989. Spatial and temporal variability of water-content and infiltration on a flood irrigated field. Trans. ASAE 32:1229–1238.

Jenkins, G.M., and D.G. Watts. 1968. Spectral analysis and its application. Holden-Day, San Francisco, CA.

Jenny, H. 1941. Factors of Soil Formation. McGraw-Hill, New York, NY.

Johnson, W.C., B.V. Millett, T. Gilmanov, R.A. Voldseth, G.R. Guntenspergen, and D.E. Naugle. 2005. Vulnerability of northern prairie wetlands to climate change. Biosci. 55:863–872.

Kachanoski, R.G., and E. de Jong. 1988. Scale dependence and the temporal persistence of spatial patterns of soil-water storage. Water Resour. Res. 24:85–91.

Kachanoski, R.G., D.E. Rolston, and E. de Jong. 1985. Spatial and spectral relationships of soil properties and microtopography. 1. Density and thickness of A-horizon. Soil Sci. Soc. Am. J. 49:804–812.

Kamgar, A., J.W. Hopmans, W.W. Wallender, and O. Wendroth. 1993. Plot size and sample number for neutron probe measurements. Soil Sci. 156:213–224.

Keim, R.F., A.E. Skaugset, and M. Weiler. 2005. Temporal persistence of spatial patterns in throughfall. J. Hydrol. 314:263–274.

Keitt, T.H., and J. Fischer. 2006. Detection of scale-specific community dynamics using wavelets. Ecology 87:2895–2904.

Kijewski-Correa, T., and A. Kareem. 2006. Efficacy of Hilbert and wavelet transforms for time-frequency analysis. J. Eng. Mech. 132:1037–1049.

Kim, G., and A.P. Barros. 2002. Space-time characterization of soil moisture from passive microwave remotely sensed imagery and ancillary data. Remote Sens. Environ. 81:393–403.

Koster, R.D., P.A. Dirmeyer, Z. Guo, G. Bonan, E. Chan, P. Cox, C.T. Gordon, S. Kanae, E. Kowalczyk, D. Lawrence, P. Liu, C.H. Lu, S. Malyshev, B. McAvaney, K. Mitchell, D. Mocko, T. Oki, K. Oleson, A. Pitman, Y.C. Sud, C.M. Taylor, D. Verseghy, R. Vasic, Y. Xue, and T. Yamada. 2004. Regions of strong coupling between soil moisture and precipitation. Science 305:1138–1140.

Kumar, P., and E. Foufoula-Georgiou. 1993. A multicomponent decomposition of spatial rainfall fields: 1. Segregation of large- and small-scale features using wavelet transforms. Water Resour. Res. 29:2515–2532.

Kumar, P., and E. Foufoula-Georgiou. 1997. Wavelet analysis of geophysical applications. Rev. Geoph. 35:385–412.

Kydland, F.E., and E.C. Prescott. 1990. Business cycles, real facts and a monetary myth. p. 3–18. *In* Federal Reserve Bank Minneapolis Quarterly Rev. Report Volume-14, Issue-2. Federal Reserve Bank Minneapolis, Minneapolis, MN.

LaBaugh, W.L., T.C. Winter, and D.O. Rosenberry. 1998. Hydrological functions of prairie wetlands. Great Plains Res. 8:17–37.

Lakhankar, T., A.S. Jones, C.L. Combs, M. Sengupta, T.H. Vonder Haar, and R. Khanbilvardi. 2010. Analysis of large-scale spatial variability of soil moisture using Geostatistical method. Sensors 10:913–932.

Lark, R.M. 2006. The representation of complex soil variation on wavelet packet bases. Eur. J. Soil Sci. 57:868–882.

Lark, R.M. 2007. Inference about soil variability from the structure of the best wavelet packet basis. Eur. J. Soil Sci. 58:822–831.

Lark, R.M., A.E. Milne, T.M. Addiscott, K.W.T. Goulding, R. Webster, and S. O'Flaherty. 2004. Scale- and location-dependent correlation of nitrous oxide emissions with soil properties: an analysis using wavelets. Eur. J. Soil Sci. 55:611–627.

Lark, R.M., and R. Webster. 1999. Analysis and elucidation of soil variation using wavelets. Eur. J. Soil Sci. 50:185–206.

Lark, R.M., and R. Webster. 2001. Changes in variance and correlation of soil properties with scale and location: analysis using an adapted maximal overlap discrete wavelet transform. Eur. J. Soil Sci. 52:547–562.

Lark, R.M., and R. Webster. 2004. Analysing soil variation in two dimensions with the discrete wavelet transform. Eur. J. Soil Sci. 55:777–797.

Lark, R.M., S.R. Kaffka, and D.L. Corwin. 2003. Multiresolution analysis of data on electrical conductivity of soil using wavelets. J. Hydrol. 272:276–290.

Lau, K.M., and H. Weng. 1995. Climate signal detection using wavelet transform: How to make a time series sing. Bull. Am. Meteor. Soc. 76:2391–2402.

Li, B.L., and C. Loehle. 1995. Wavelet analysis of multiscale permeabilities in the subsurface. Geophys. Res. Lett. 22:3123–3126.

Lin, H.S., W. Kogelmann, C. Walker, and M.A. Bruns. 2006. Soil moisture patterns in a forested catchment: A hydropedological perspective. Geoderma 131:345–368.

Lindsay, R.W., D.B. Perceval, and D.A. Rothrock. 1996. The discrete wavelet transform and the scale analysis of the surface properties of sea ice. IEEE Trans. Geosci. Remote Sens. 34:771–787.

Litaor, M.I., M. Williams, and T.R. Seastedt. 2008. Topographic controls on snow distribution, soil moisture, and species diversity of herbaceous alpine vegetation, Niwot Ridge, Colorado. J. Geophys. Res. – Biogeosci. 113:G02008, doi:10.1029/2007jg000419.

Liu, Y., X.S. Liang, and R.H. Weisberg. 2007. Rectification of the bias in the wavelet power spectrum. J. Atom. Ocean. Tech. 24:2093–2102.

Loague, K.M., R.E. Green, C.C.K. Liu, and C. Liang. 1989. Simulation of organic chemical movement in Hawaii soils with PRZM: 1. Preliminary results for Ethylene Dibromide. Pacific Sci. 43:67–95.

Lungal, M.A. 2009. Hydrological response to spring snowmelt and extreme rainfall events of different landscape elements within a Prairie wetland basin. Master's Thesis, Univ. of Saskatchewan, Saskatoon, SK, Canada.

Mallat, S. 1999. A wavelet tour of signal processing. Second edition. Academic Press, New York, NY.

Maraun, D., J. Kurth, and M. Holschneider. 2007. Nonstationary Gaussian processes in wavelet domain: Synthesis, estimation, and significance testing. Phys. Rev. E 75:doi:10.1103/PhysRevE.75.016707.

Martínez-Fernández, J., and A. Ceballos. 2003. Temporal stability of soil moisture in a large-

field experiment in Spain. Soil Sci. Soc. Am. J. 67:1647–1656.

Martínez-Fernández, J., and A. Ceballos. 2005. Mean soil moisture estimation using temporal stability analysis. J. Hydrol. 312:28–38.

Matheron, G. 1963. Principles of geostatistics. Econ. Geol. 51:1246–1266.

McBratney, A.B., T.F.A. Bishop, and I.S. Teliatnikov. 2000. Two soil profile reconstruction techniques. Geoderma 97:209–221.

McNamara, J.P., D. Chandler, M. Seyfried, and S. Achet. 2005. Soil moisture states, lateral flow, and streamflow generation in a semi-arid, snowmelt-driven catchment. Hydrol. Proc. 19:4023–4038.

Meyles, E., A. Williams, L. Ternan, and J. Dowd. 2003. Runoff generation in relation to soil moisture patterns in a small Dartmoor catchment, Southwest England. Hydrol. Proc. 17:251–264.

Miller, J.B. 1971. Shoreline-area ratios as a factor in rate of water loss from small sloughs. J. Hydrol. 14:259–284.

Miller, J.J., D.F. Acton, and R.J. St. Arnaud. 1985. The effect of groundwater on soil formation in a morainal landscape in Saskatchewan. Can. J. Soil Sci. 65:293–307.

Milne, A.E., and R.M. Lark. 2009. Wavelet transforms applied to irregularly sampled soil data. Math. Geosci. 41:661–678.

Minke, A.G.N. 2009. Estimating water storage of Prairie pothole wetlands. Master's Thesis, Univ. of Saskatchewan, Saskatoon, SK, Canada.

Mohanty, B.P., and T.H. Skaggs. 2001. Spatio-temporal evolution and time-stable characteristics of soil moisture within remote sensing footprints with varying soil, slope, and vegetation. Adv. Water Resour. 24:1051–1067.

Mohanty, B.P., J.S. Famiglietti, and T.H. Skaggs. 2000. Evolution of soil moisture spatial structure in a mixed vegetation pixel during the Southern Great Plains 1997 (SGP97) hydrology experiment. Water Resour. Res. 36:3675–3686.

Moore, I.D., E.M. Oloughlin, and G.J. Burch. 1988a. A contour based topographic model for hydrological and ecological applications. Earth Surface Proc. Landforms 13:305–320.

Moore, I.D., G.J. Burch, and D.H. MacKenzie. 1988b. Topographic effects on the distribution of surface soil water and the location of ephemeral gullies. Trans. ASAE 31:1098–1107.

Moore, I.D., P.E. Gessler, G.A. Nielsen, and G.A. Peterson. 1993. Soil attribute prediction using terrain analysis. Soil Sci. Soc. Am. J. 57:1548–1548.

Morris, M. 2006. Soil moisture monitoring: low cost tools and methods. Publication number IP277. Available at http://attra.ncat.org/attra-pub/soil_moisture.html. (Verified 18/04/2011), ATTRA- National Sustain. Agri. Inform. Service, Butte, MT.

Munoz-Pardo, J., P. Ruelle, and M. Vauclin. 1990. Spatial variability of an agricultural field-geostatistical analysis of soil texture, soil-moisture and yield components of 2 rain-fed crops. Catena 17:369–381.

Myers, R.H. 1990. Classical and modern regression with applications. Duxbury Press, PWS Publishers, Pacific Groove, CA.

Narayan, U., and V. Lakshmi. 2005. A simple method for spatial disaggregation of radiometer derived soil moisture using higher resolution radar observations. p. 123–127. *In* Proc. Electromagnetics Res. Symp. 2005, Hangzhou, China, August 22–26, 2005.

National Wetlands Working Group. 1997. The Canadian wetland classification system. *In* B.G. Warner and C.D.A. Rubec (ed.) Wetlands Research Centre, 2nd ed., Univ. of Waterloo, ON.

Natural Resources Canada. 2001. Available at http://www.atlas.nrcan.gc.ca. (Verified on 18/04/2011), Ottawa, ON.

Neupauer, R.M., and K.L. Powell. 2005. A fully anisotropic Morlet wavelet to identify dominant orientations in porous medium. Comput. Geosci. 31:465–471.

Neupauer, R.M., K.L. Powell, X. Qi, D.H. Lee, and D.A. Villhauer. 2006. Characterization of permeability anisotropy using wavelet analysis. Water Resour. Res. 42:W07419, doi:10.1029é2005WR004364.

Nielsen, D.R., and O. Wendroth. 2003. Spatial and temporal statistics: sampling field soil and their vegetation. Catena Verlag Pub., Reiskirchen, Germany.

Nielsen, D.R., J.W. Biggar, and K.T. Erh. 1973. Spatial variation of field measured soil water properties. Hilgardia 42:214–259.

Nyberg, L. 1996. Spatial variability of soil water content in a covered catchment at Gårdsjön, Sweden. Hydrol. Proc. 10:89–103.

Ogaard, L.A., J.A. Leitch, D.F. Scott, and W.C. Nelson. 1981. The fauna of the prairie wetlands:

research methods and annotated bibliography. *In* Agricultural Experiment Station Research Report No. 86. North Dakota State Univ., Fargo, ND.

Oladosu, G. 2009. Identifying the oil price-macroeconomy relationship: An empirical mode decomposition analysis of US data. Energy Policy 37:5417–5426.

Oliver, M.A. 1987. Geostatistics and its application to soil science. Soil Use Manag. 3:8–20.

Oliver, M.A., and R. Webster. 1991. How geostatistics can help you. Soil Use Manag. 27:206–217.

Owe, M., E.B. Jones, and T.J. Schmugge. 1982. Soil moisture variation patterns observed in Hand County, South Dakota. Water Resour. Bull. 18:949–954.

Pachepsky, Y.A., A.K. Guber, and D. Jacques. 2005. Temporal persistence in vertical distributions of soil moisture contents. Soil Sci. Soc. Am. J. 69:347–352.

Pai, P.F., and A.N. Palazotto. 2008. Detection and identification of nonlinearities by amplitude and frequency modulation analysis. Mech. Syst. Signal Process. 22:1107–1132.

Pan, F., C.D. Peters-Lidard, and M.J. Sale. 2003. An analytical method for predicting surface soil moisture from rainfall observations. Water Resour. Res. 39:1314, doi:10.1029/2003WR002142.

Pan, Y.X., and X.P. Wang. 2009. Factors controlling the spatial variability of surface soil moisture within revegetated-stabilized desert ecosystems of the Tengger Desert, Northern China. Hydrol. Proc. 23:1591–1601.

Pardo-Iguzquiza, E., and F.J. Rodriguez-Tovar. 2000. The permutation test as a non-parametric method for testing the statistical significance of power spectrum estimation in cyclo-stratigraphic research. Earth Planet. Sci. Lett. 181:175–189.

Parent, A.C., F. Anctil, and L.E. Parent. 2006. Characterization of temporal variability in near surface soil moisture at scales from 1 h to 2 weeks. J. Hydrol. 325:56–66.

Parkhurst, R.S., T.C. Winter, D.O. Rosenberry, and A.M. Sturrock. 1998. Evaporation from a small prairie wetland in the Cottonwood Lake area, North Dakota - An energy-budget study. Wetlands 18:272–287.

Parkin, T.B. 1987. Soil microsites as a source of denitrification variability. Soil Sci. Soc. Am. J. 51:1194–1199.

Parsons, D.F., M. Hayashi, and G. van der Kamp. 2004. Infiltration and solute transport under a

seasonal wetland: bromide tracer experiments in Saskatoon, Canada. Hydrol. Proc. 18:2011–2027.

Penna, D., S. Degli Esposti, P. Boscolo, and M. Borga. 2006. Spatial variability and temporal stability of soil moisture in an alpine catchment. Geophys. Res. Abs. 8:02608

Pennock, D.J. 2005. Field Handbook for Saskatchewan soils. p. 4-5. Dept. of Soil Sci., Univ. of Saskatchewan, SK.

Pennock, D.J., B.J. Zebarth, and E. de Jong. 1987. Landform classification and soil distribution in hummocky terrain, Saskatchewan, Canada. Geoderma 40:297–315.

Percival, D.B., and A.T. Walden. 2000. Wavelet methods for time series analysis. Cambridge University Press, New York, NY.

Perfect, E., and J. Caron, 2002. Spectral analysis of tillage-induced differences in soil spatial variation. Soil Sci. Soc. Am. J. 66:1587–1595.

Petrone, R.M., J.S. Price, S.K. Carey, and J.M. Waddington. 2004. Statistical characterization of the spatial variability of the soil moisture in a cutover peatland. Hydrol. Proc. 18:41–52.

Piñuela, J.A., D. Andian, K.J. McInnes, and A.M. Tarquis. 2007. Wavelet analysis in a structured clay soil using 2D images. Nonlinear Proc. Geoph. 14:425–434.

Pomeroy, J.W., and D.M. Gray. 1995. Snowcover, accumulation, relocation, and management. p. 144. *In* NHRI Science Report No. 7, Environment Canada, Saskatoon, SK.

Pomeroy, J.W., D. de Boer, and L.W. Martz. 2007. Hydrology and water resources. p. 63–80. *In* B. Thraves et al. (ed.) Saskatchewan: Geographic Perspectives. Regina: CRRC.

Porporato, A., E. Daly, and I. Rodriguez-Iturbe. 2004. Soil water balance and ecosystem response to climate change. Am. Natural. 164:625–632.

Price, J.S. 1993. Water level regimes in prairie sloughs. Can. Water Resour. J. 18:95–105.

Qi, X., and R.M. Neupauer. 2008. Wavelet analysis of dominant scales of heterogeneous porous media. Water Resour. Res. 44:W09406, doi:10:1029/2006WR005720.

Qui, Y., B.J. Fu, J. Wang, and L.D. Chen. 2001. Soil moisture variation in relation to topography and land use in a hill slope catchment of the Loess Plateau, China. J. Hydrol. 240:243–263.

Quinn, P. 2004. Scale appropriate modeling: representing cause-and-effect relationships in nitrate pollution at the catchment scale for the purpose of catchment scale planning. J.

Hydrol. 291:197–217.

Raats, P.A.C. 2001. Developments in soil-water physics since the mid-1960s. Geoderma 3-4:355–387.

Renault, P., and P. Stengel. 1994. Modeling oxygen diffusion in aggregated soils: I. anaerobiosis inside the aggregate. Soil Sci. Soc. Am. J. 58:1017–1023.

Reynolds, S.G. 1970. The gravimetric method of soil moisture determination- II: typical required sample sizes and methods of reducing variability. J. Hydrol. 11:274–287.

Reynolds, S.G. 1974. A note on the relationship between size of area and soil moisture variability. J. Hydrol. 22:71–76.

Robinson, M., and T.J. Dean. 1993. Measurement of near surface soil water content using a capacitance probe. Hydrol. Proc. 7:77–86.

Rocha, G.C., P.L. Libardi, L.A. Carvalho, and A.C. Rodríguez Cruz. 2005. Estabilidade temporal da distribuição espacial da armazenagem de água em um solo cultivado com citros. Revista Brasileira de Ciencia do Solo 29:41–50.

Rodríguez-Iturbe, I., and A. Porporato. 2004. Ecohydrology of water-controlled ecosystems: Soil moisture and plant dynamics. Cambridge University Press, Cambridge, UK.

Rodríguez-Iturbe, I., P. D'Odorico, A. Porporato, and L. Ridolfi. 1999. On the spatial and temporal links between vegetation, climate, and soil moisture. Water Resour. Res. 35:3709–3722.

Rodríquez-Iturbe, I., G. Vogel, R. Rigon, D. Entekhabi, F. Castelli, and A. Rinaldo. 1995. On the spatial organization of soil moisture fields. Geophys. Res. Lett. 22:2757– 2760.

Rolston, D.E., J.W. Biggar, and H.I. Nightingale. 1991. Temporal persistence of spatial soil-water patterns under trickle irrigation. Irrig. Sci. 12:181–186.

Rosenberry, D.O., and T.C. Winter. 1997. Dynamics of water-table fluctuations in an upland between two prairie-pothole wetlands in North Dakota. J. Hydrol. 191:266–289.

Saskatchewan Centre for Soil Research. 1989. Rural municipality of Grant, Number 372: Preliminary soil map and report. Publication# SK372. Saskatchewan Centre Soil Res., Univ. of Saskatchewan, Saskatoon, SK.

Schneider, K., J.A. Huisman, L. Breuer, Y. Zhao, and H.G. Frede. 2008. Temporal stability of soil moisture in various semi-arid steppe ecosystems and its application in remote

sensing. J. Hydrol. 359:16–29.

Schume, H., G. Jost, and K. Katzensteiner. 2003. Spatio-temporal analysis of the soil water content in a mixed Norway spruce (*Picea abies* L. -Karst.) - European beech (*Fagus sylvatica* L.) stand. Geoderma 112:273–287.

Seghieri, J., S. Galle, J.L. Rajot, and M. Ehrmann. 1997. Relationships between soil moisture and growth of herbaceous plants in a natural vegetation mosaic in Niger. J. Arid Environ. 36:87–102.

Seyfried, M. 1998. Spatial variability constraints to modeling soil water at different scales. Geoderma 85:231–254.

Shapiro, J.M. 1993. Embedded image coding using zerotrees of wavelet coefficients. IEEE Trans. Signal Process. 41:3445–62.

Sharma, M.L., G.A. Gander, and C.G. Hunt. 1980. Spatial variability of infiltration in a watershed. J. Hydrol. 45:101–122.

Sharon, D. 1980. The distribution of hydrologically effective rainfall incident on sloping ground. J. Hydrol. 46:165–188.

Shen, X., H. Huang, and N. Cressie. 2002. Nonparametric hypothesis testing for a spatial signal. J. Am. Stat. Assoc. 97:1122–1140.

Shiklomanov, I. 1993. World fresh water resources. *In* P.H. Gleick (ed.) Water in Crisis: A Guide to the World's Fresh Water Resources. Oxford University Press, New York, NY.

Shu, Q., Z. Liu, and B.C. Si. 2008. Characterizing scale and location dependent correlation of water retention parameters with soil physical properties using wavelet techniques. J. Environ. Qual. 37:2284–2292.

Shumway, R.H., and D.S. Stoffer. 2000. Time series analysis and its applications. Springer, New York, NY.

Si, B.C. 2003. Spatial and scale dependent soil hydraulic properties: a wavelet approach. p. 163–178. *In* Y. Pachepsky et al. (ed.) Scaling method in soil physics. CRC Press, New York, NY.

Si, B.C. 2008. Spatial scaling analyses of soil physical properties: A review of spectral and wavelet methods. Vadose Zone J. 7:547–562.

Si, B.C., and E. de Jong. 2007. Determining long-term (decadal) deep drainage rate using

multiple tracer. J. Environ. Qual. 36:1686–1694.

Si, B.C., and R.E. Farrell. 2004. Scale dependent relationships between wheat yield and topographic indices: A wavelet approach. Soil Sci. Soc. Am. J. 68:577–588.

Si, B.C., and T.B. Zeleke. 2005. Wavelet coherency analysis to relate saturated hydraulic properties to soil physical properties. Water Resour. Res. 41:W11424, doi:10.1029/2005WR004118.

Si, B.C., R.G. Kachanoski, and R.D. Reynolds. 2007. Analysis of soil variation. p. 1163–1191. *In*: E.G. Gregorich (ed.) Soil sampling and methods of analysis. CRC Press, New York, NY.

Sivapalan, M. 1992. Scaling of hydrologic parameterizations, 1. Simple models for the scaling of hydrologic state variables, examples and a case study. *In* Report DE 614MS. Center Water Res., Univ. of Western Australia, Nedlands, Western Australia.

Smith, R., H.F. Dufresne, and H.A. Hanson. 1964. Northern watersheds and deltas. p. 51–66. *In* J.P. Linduska (ed.) Waterfowl tomorrow. U.S. Fish and Wildlife Service, Washington, D.C.

Soil Classification Working Group. 1998. The Canadian System of Soil Classification. 3rd ed. NRC Research Press.

Starks, P.J., G.C. Heathman, T.J. Jackson, and M.H. Cosh. 2006. Temporal stability of soil moisture profile. J. Hydrol. 324:400–411.

Starr, G.C. 2005. Assessing temporal stability and spatial variability of soil water patterns with implications for precision water management. Agri. Water Manag. 72:223–243.

Sun, M. 1986. Groundwater ills: Many diagnoses, few remedies. Science 232:1490–1493.

Tallon, L.K., and B.C. Si. 2004. Representative soil water benchmarking for environmental monitoring. J. Environ. Inform. 4:31–39.

Tang, C., and T. Piechota. 2009. Spatial and temporal soil moisture and drought variability in the upper Colorado river basin. J. Hydrol. 379:122–135.

Teuling, A.J., R. Uijlenhoet, F. Hupet, E.E. van Loon, and P.A. Troch. 2006. Estimating spatial mean root-zone soil moisture from point-scale observations. Hydrol. Earth Sys. Sci. 10:755–767.

Thierfelder, T.K., R.B. Grayson, D. von Rosen, and A.W. Western. 2003. Inferring the location

of catchment characteristic soil moisture monitoring sites. Covariance structures in the temporal domain. J. Hydrol. 280:13–32.

Tomer, M.D., and J.L. Anderson. 1995. Variation of soil-water storage across a sand plain hill slope. Soil Sci. Soc. Am. J. 59:1091–1100.

Topp, G.C., and W.D. Reynolds. 1998. Time domain reflectometry: a seminal technique for measuring mass and energy in soil. Soil Till. Res. 47:125–132.

Torrence, C., and G.P. Compo. 1998. A practical guide to wavelet analysis. Bull. Am. Meteor. Soc. 79:61–78.

Torrence, C., and P.J. Webster. 1999. Interdecadal changes in the ENSO-monsoon system. J. Clim. 12:2679–2690.

Trangmar, B.B., R.S. Yost, and G. Uehara. 1985. Application of geostatistics to spatial studies of soil properties. Adv. Agro. 38:45–94

Vachaud, G., A.P. Desilans, P. Balabanis, and M. Vauclin. 1985. Temporal stability of spatially measured soil-water probability density-function. Soil Sci. Soc. Am. J. 49:822–828.

van der Kamp, G., and M. Hayashi. 1998. The groundwater recharge function of small wetlands in the semi-arid northern prairies. Great Plains Res. 8:39–56.

van der Kamp, G., M. Hayashi, and D. Gallen. 2003. Comparing the hydrology of grassed and cultivated catchments in the semi-arid Canadian prairies. Hydrol. Proc. 17:559–575.

van der Kamp, G., W.J. Stolte, and R.G. Clark. 1999. Drying out of small prairie wetlands after conversion of their catchments from cultivation to permanent brome grass. Hydrol. Sci. J. 44:387–397.

van der Valk, A.G. (ed.). 1989. Northern Prairie Wetlands. Iowa State University Press, Ames, IA.

van Genuchten, M.T. 1980. A closed-form equation for predicting the hydraulic conductivity of unsaturated soils. Soil Sci. Soc. Am. J. 44:892–898.

Van Pelt, R.S., and P.J. Wierenga. 2001. Temporal stability of spatially measured soil matrix potential probability density function. Soil Sci. Soc. Am. J. 65:668–677.

Van Wambeke, A., and R. Dulal. 1978. Diversity of soils in the Tropics. Am. Soc. Agron. Spec. Publ. 34:13–28.

Van Wesenbeeck, I.J., R.G. Kachanoski, and D.E. Rolston. 1988. Temporal persistence of spatial

patterns of soil-water content in the tilled layer under a corn crop. Soil Sci. Soc. Am. J. 52:934–941.

Vereecken, H., T. Kamai, T. Harter, R. Kasteel, J. Hopmans, and J. Vanderborght. 2007. Explaining soil moisture variability as a function of mean soil moisture: a stochastic unsaturated flow perspective. Geophys. Res. Lett. 34:L22402, doi:10.1029/2007GL031813.

Viera, S.R., J.L. Hatfield, D.R. Nielsen, and J.W. Biggar. 1982. Geostatistical theory and application to variation of some agronomical properties. Hilgardia 51:1–75.

Vivoni, E.R., A.J. Rinehart, L.A. Mendez-Barroso, C.A. Aragon, G. Bisht, M.B. Cardenas, E. Engle, B.A. Forman, M.D. Frisbee, H.A. Gutierrez-Jurado, S.H. Hong, T.H. Mahmood, K. Tai, and R.L. Wyckoff. 2008. Vegetation controls on soil moisture distribution in the Valles Caldera, New Mexico, during the North American monsoon. Ecohydrol. 1:225–238.

Walker, J.P., G.R. Willgoose, and J.D. Kalma. 2001. One-dimensional soil moisture profile retrieval by assimilation of near-surface observations: a comparison of retrieval algorithms. Adv. Water Res. 24:631–650.

Walker, J.S. 1999. A primer on wavelets and their scientific applications. Chapman and Hall, New York, NY.

Wang, J., B.J. Fu, Y. Qui, L.D. Chen, and Z. Wang. 2001. Geostatistical analysis of soil moisture variability on Da Nangou catchment of the loess plateau, China. Environ. Geol. 41:113–120.

Warrick, A.W., R. Zhang, M.M. Moody, and D.E. Myers. 1990. Kriging versus alternative interpolators: errors and sensitivity to model inputs. p. 157–164. *In*: K. Roth et al. (ed.) Field-scale Water and Solute Flux in Soils. Birkhaůser Verlag, Basel.

Watkins, L., R.M. Neupauer, and G.P. Compo. 2009. Wavelet analysis and filtering to identify dominant orientations of permeability anisotropy. Math. Geosci. 41:643–659.

Webster, R. 1977. Spectral analysis of gilgai soil. Aust. J. Soil Res. 15:191–204.

Webster, R., and M.A. Oliver. 2001. Geostatistics for Environmental Scientists. Wiley, Chichester.

Western, A.W., and G. Blöschl. 1999. On the spatial scaling of soil moisture. J. Hydrol.

217:203–224.

Western, A.W., G. Blöschl, and R.B. Grayson. 1998. Geostatistical characterization of soil moisture patterns in the Tarrawarra catchment. J. Hydrol. 205:20–37.

Western, A.W., R.B. Grayson, and G. Blöschl. 2002. Scaling of soil moisture: A hydrologic perspective. Ann. Rev. Earth Planet. Sci. 30:149–180.

Western, A.W., R.B. Grayson, G. Blöschl, and D.J. Wilson. 2003. Spatial variability of soil moisture and its implications for scaling. p. 119– 142. *In* Pachepsky, Y. et al. (ed.) Scaling Methods in Soil Physics. CRC Press, New York, NY.

Western, A.W., R.B. Grayson, G. Blöschl, G.R. Willgoose, and T.A. McMahon. 1999. Observed spatial organization of soil moisture and its relation to terrain indices. Water Resour. Res. 35:797–810.

Western, A.W., S.L. Zhou, R.B. Grayson, T.A. McMahon, G. Blöschl, and D.J. Wilson. 2004. Spatial correlation of soil moisture in small catchments and its relationship to dominant spatial hydrological processes. J. Hydrol. 286:113–134.

Westfall, P.H., and S.S. Young. 1993. Resampling-based multiple testing: Examples and methods for *p*-value adjustment. John Wiley & Sons, New York, NY.

Whigham, D.F., and T.E. Jordan. 2003. Isolated wetlands and water quality. Wetlands 23:541–549.

Wilding, L.P., J. Bouma, and D. Goss. 1994. Impact of spatial variability on modeling. p 61–75. *In* R. Bryant, and R.W. Arnold (ed.) Quantitative modeling of soil forming processes. SSSA Special Publication #39. Soil Sci. Soc. Am. Inc. Madison, WI.

Williams, C.J., J.P. McNamara, and D.G. Chandler. 2008. Controls on the temporal and spatial variability of soil moisture in a mountainous landscape: the signatures of snow and complex terrain. Hydrol. Earth Sys. Sci. Discuss. 5:1927–1966.

Wilson, G.V., S.M. Dabney, K.C. McGregor, and B.D. Barkoll. 2004. Tillage and residue effects on runoff and erosion dynamics. Trans. ASAE 47:119–128.

Winter, T.C., and D.O. Rosenberry. 1995. The interaction of ground water with prairie pothole wetlands in the cottonwood lake area, east-central North Dakota, 1979–1990. Wetlands 15:193–211.

Woo, M.K., and R.D. Rowsell. 1993. Hydrology of a prairie slough. J. Hydrol. 146:175–207.

Wu, W., M.A. Geller, and R.E. Dickinson. 2002. The response of soil moisture to long-term variability of precipitation. J. Hydrometeor. 3:604–613.

Yan, R., and R.X. Gao. 2007. A tour of the Hilbert-Huang transform: An empirical tool for signal analysis. IEEE Instru. Meas. Mag. 1094-6969/07:40–45.

Yates, T.T., B.C. Si, R.E. Farrell, and D.J. Pennock. 2006a.Probability distribution and spatial dependence of nitrous oxide emission: Temporal change in hummocky terrain. Soil Sci. Soc. Am. J. 70:753–762.

Yates, T.T., B.C. Si, R.E. Farrell, and D.J. Pennock. 2006b. Wavelet spectra of nitrous oxide emission from hummocky terrain during spring snowmelt. Soil Sci. Soc. Am. J. 70:1110–1120.

Yates, T.T., B.C. Si, R.E. Farrell, and D.J. Pennock. 2007. Time, location, and scale dependence of soil nitrous oxide emission, water, and temperature using wavelet coherency analysis. J. Geophys. Res. 112:D09104, doi:10.1029/2006JD007662.

Zeleke, T.B., and B.C. Si. 2007. Wavelet based multifractal analysis of field scale variation in soil water retention. Water Resour. Res. 43:W07446, doi:10.1029/2006WR004957.

Zhang, T., and R. Berndtsson. 1988. Temporal patterns and spatial scale of soil water variability in a small humid catchment. J. Hydrol. 104:111–128.

Zhao, Y., S. Peth, X.Y. Wang, H. Lin, and R. Horn. 2010. Controls of surface soil moisture spatial patterns and their temporal stability in a semi-arid steppe. Hydrol. Proc. 24:2507–2519.

Zhou, X., H. Lin, and Q. Zhu. 2007. Temporal stability of soil moisture spatial variability at two scales and its implication for optimal field monitoring. Hydrol. Earth Syst. Sci. Discuss. 4:1185–1214.

APPENDIX A

A.0 SCALE-SPECIFIC SPATIAL VARIABILITY: A COMPARISON OF MULTI-RESOLUTION ANALYSIS AND EMPIRICAL MODE DECOMPOSITION

A.1 Preface

Soil spatial variability is scale dependent. In separating out the scale specific variability, wavelet based multi-resolution analysis is an established method, whereas, empirical mode decomposition has recently introduced in soil science. Therefore, the new method is subjected to comparison with available methods. This chapter compares multi-resolution analysis and empirical mode decomposition in revealing the scale specific variations using artificial spatial series as well as measured soil water data.

A.2 Introduction

Soil varies considerably from location to location (Nielsen et al., 1973). A combination of soil physical, chemical, and biological processes operating at different intensities and at different scales results in a high degree of spatial variability (Goovaerts, 1998). Adequate understanding of soil variability as a function of space and scales is necessary for developing logical, empirical and physical models of soil landscape processes (Burrough, 1983; Foussereau et al., 1993; Wilding et al., 1994; Corwin et al., 2006).

Geostatistical analysis has been used to describe the variability of a soil property (Burgess and Webster, 1980; Webster and Oliver, 2001) or the correlation between two soil properties (Goovaerts and Webster, 1994) as a function of spatial scales. Spectral analysis, which approximates the spatial series by a sum of sine and cosine functions, has been used to quantify variations at different scales. The squared amplitude of the functions at a particular frequency or scale represents the variance contribution of that frequency component towards the total variance in the spatial series (Webster, 1977; Shumway and Stoffer, 2000; Brillinger, 2001). Geostatistics assumes intrinsic stationarity and spectral analysis assumes that the mean and variance of the process are constant (stationarity) in space. However, the existence of the spatial trend creates nonstationarity in the spatial series. Wavelet analysis (Mallat, 1999) of a nonstationary spatial

series produces a set of coefficients, known as wavelet coefficients. Each coefficient is nominally associated with a different scale and location and can be used to view the series information content at various spatial resolutions through multi-resolution analysis (MRA). This generally enables us to visualize structures buried in different spatial scales as one can see the sub-cellular structures of living bodies using a microscope (Hubbard, 1998; Walker, 1999). Wavelet based MRA has been used widely in different fields of science including soil science (Lark and Webster, 1999, 2001; Lark et al., 2003) to separate out the scale specific variations. The main advantage of wavelet analysis is that it does not rely on any stationarity assumption about the data series. However, this analysis assumes the controlling processes of the spatial series are linear (Huang et al., 1998). Similar to this, another MRA based on the wavelet packet analysis has also been used to represent the complex soil variation at different scales (Lark, 2006, 2007). In wavelet packet analysis, the spatial series can also be decomposed to more or less number of spatial scales with more flexibility than discrete wavelet transform (DWT) (Percival and Walden, 2000). However, in this paper we will limit our scope in discussing only the discrete wavelet based MRA.

Another advanced analysis technique, the empirical mode decomposition (EMD), extracts oscillations from the data series into a finite and often small number of mode functions according to the energy associated with different space scales (Huang et al., 1998; Huang and Wu, 2008). These mode functions are known as intrinsic mode functions (IMFs). Unlike spectral and wavelet methods, EMD does not consider any mathematical function in the analysis and works directly in the spatial domain with the basis completely derived from the data. Therefore, it is intuitive, direct, *a posteriori* and adaptive (Huang et al., 1998; Huang and Wu, 2008). The locality and adaptivity of EMD can deal with different types of spatial series including nonstationary and nonlinear (Huang et al., 1998). EMD has been applied to different fields of science and a comprehensive review in geosciences can be found in Huang and Wu (2008). Biswas et al. (2009) used the EMD in soil science to reveal the scale specific controls of soil water storage.

Since the EMD has just been introduced, it is subjected to comparison with available methods. Therefore, the goal of our paper was to compare the well-established wavelet based MRA and EMD in revealing the scale specific variations hidden in a spatial series. To do this,

first we have discussed the basic steps in revealing variations at different scales for both methods. Then we have compared the methods using different type of artificial spatial series composed of pure cosine waves and an example of soil property.

A.3 Theory

A.3.1 Multi-Resolution Analysis (MRA)

In MRA, we back transform the wavelet coefficients of a particular scale to obtain a component of the signal corresponding to that scale. The detail theory of DWT is available elsewhere (Walker, 1999; Percival and Walden, 2000) and is beyond the scope of this paper. Briefly, a spatial series of length n with x regular intervals contains information on the scale range of $2x$ to nx. The DWT partitions this information into non-overlapping intervals that double in size with scale (although there is some leakage), i.e. $2x – 4x$, $4x – 8x$, $8x – 16x$, … The wavelet transform is invertible, i.e. if we back transform the wavelet coefficients; we obtain the original series (Daubechies, 1992). However, if we set all of the wavelet coefficients to zero except those associated with a certain scale interval and back transform, we obtain a component of the series associated with that given scale interval. For example, the number of coefficients of scale ranges $2x – 4x$ and $4x – 8x$ for a data series of 1024 are 512 and 256, respectively. As the scale range doubles, the number of coefficients decreases by half of the number of the previous scale range coefficients. Therefore, for the scale range of $2x – 4x$, keep the 512 coefficients and set rest 512 points as zero and for the scale range of $4x – 8x$, keep 256 coefficients and set rest 768 points to zero. A similar procedure is followed for each scale range and back transformed the coefficients with zeros. The back transformed new series will only contain the pattern of the specific scale range at which the coefficients were retained. The spatial pattern at different scales can be represented separately and the original series can be obtained by adding the resulting patterns together due to the additive nature of MRA.

A.3.2 Empirical Mode Decomposition (EMD)

The EMD is based on a simple assumption that at a given space, there might be different simple oscillatory modes of significantly different frequencies or scales superimposing one another (Huang et al., 1998; Huang and Wu, 2008). EMD extracts the intrinsic oscillations of the

signal through their characteristic space scale (i.e., local properties of the signal itself). Each component is defined as an Intrinsic Mode Function (IMF) and satisfies the following conditions: 1) the mode may or may not be linear and the number of extrema and zero crossings must either equal or differ at most by one. Zero crossing is a point where the sign of function changes. 2) The oscillation will be symmetric with respect to the local mean. Thus at any data point the average value of the envelopes defined by local maxima and local minima is zero. The IMFs of a spatial series $Y(x)$ can be obtained in the following steps:

1. Find the local maxima and local minima of the spatial series.
2. Create the upper envelope (UE) by joining the maxima and the lower envelope (LE) by joining the minima using a cubic spline line. The envelopes will include all the data points.
3. Calculate the mean of the envelope at each location [$m_1 = (UE + LE)/2$].
4. Subtract the mean m_1 from the data $Y(x)$ to get the first prototype (h_1); $h_1(x) = Y(x) - m_1(x)$ which is a function of space. By construction, the prototype will be an IMF provided h_1 satisfies the definition of an IMF. However, changing a local zero from a rectangular to curvilinear coordinate system may introduce new extrema and needs sifting processes (Huang and Wu, 2008).
5. Take h_1 as the data and repeat the steps from 1 to 4. This will produce the next prototype $h_{11}(x)$; $h_{11}(x) = h_1(x) - m_{11}(x)$.
6. Repeat the steps until the prototype satisfies the definition of an IMF. For example, after k times of iteration, the prototype $h_{1k}(x)$, $h_{1k}(x) = h_{1(k-1)}(x) - m_{1k}(x)$ will be produced. If the prototype meets the local envelope symmetry condition, the $h_{1k}(x)$ will be defined as first IMF, C_1 as a function of space, i.e., $C_1(x) = h_{1k}(x)$. The approximate symmetry of local envelopes in the sifting process or in the iteration is called stoppage criteria for the EMD. Huang et al. (1998) defined this stoppage criterion based on a Cauchy type of convergence test, which is the normalized squared difference between two successive sifting operations and is given as

$$SD_k = \frac{\sum_{x=0}^{X} |h_{k-1}(x) - h_k(x)|^2}{\sum_{x=0}^{X} h_{k-1}^2(x)} \quad [A.1]$$

The SD value determines the time to stop the iteration so that the IMF components retain enough physical sense of both amplitude and frequency modulations. Usually, a threshold value for SD is set between 0.2 and 0.3 (Huang et al., 1998) and the sifting process needs to stop below this value.

7. Extract the rest of the oscillations of the signal or the residuals $r_1(x)$, after subtracting the first IMF that contained the finest scale or the shortest period oscillations;

$$Y(x) - C_1(x) = r_1(x) \quad [A.2]$$

8. Treat the residue as the new data series to separate low frequency variations by the sifting or iteration procedure as described in steps 1 thorough 6. If the sifting is carried out for subsequent $r_j(x)$'s, the result can be written as

$$r_1(x) - C_2(x) = r_2(x), \cdots, r_{n-1}(x) - C_n(x) = r_n(x) \quad [A.3]$$

where, $C_n(x)$ are the empirical modes and $r_n(x)$ are the residues.

9. Carry out the decomposition process until the residue $r_n(x)$ is left with only one extremum or the residue becomes a monotonic function. The final residue represents the underlying trend in the data (Huang et al., 1998). The original signal can be reconstructed after adding all IMFs and the final residue and is written as

$$Y(x) = \sum_{j=1}^{n} C_j(x) + r_n(x) \quad [A.4]$$

A.4 Comparison of MRA and EMD using artificial signals

Elevation, soil properties, and total biomass have been shown to be quasi-cyclic in rolling and undulating landscapes (Si and Farrell, 2004). Very often, the spatial series are characterized by nonstationary and/or nonlinear in nature. To illustrate MRA and EMD in separating the scale specific variations, four artificial signals of different types: stationary-linear, stationary-nonlinear, nonstationary-linear, and nonstationary-nonlinear, composed of three cosine waves with different frequencies were used as a surrogate spatial series for measurements taken along a

rolling and undulating landscape. The artificial signals are created following Yan & Gao (2007), who used similar signals with only one frequency. To represent the stationary-linear series, an artificial spatial series sampled at regular intervals (1 m) was generated by combining three cosine waves; $Y^{[1]}(x) = \cos(2\times\pi\times100\times x) + \cos(2\times\pi\times25\times x) + \cos(2\times\pi\times10\times x)$, where x = 0, 1, 2, ..., 1023. The frequencies for three cosine waves were 100, 25 and 10 Hz, respectively, which can also be converted to the cycles per meter (cpm). There were 100 cycles per 1000 m, 25 cycles per 1000 m and 10 cycles per 1000 m, respectively for the frequency of 100, 25 and 10 Hz. Therefore, three cosine waves have frequencies of 0.1 cpm, 0.025 cpm, and 0.01cpm, respectively. The spatial frequencies were converted to spatial scales (= 1/frequency) and they were 10, 40 and 100 m, respectively.

The artificial stationary-nonlinear, nonstationary-linear and nonstationary-nonlinear spatial series we considered are defined as
$Y^{[2]}(x) = \cos(2\times\pi\times100\times x + 0.3\times\sin(2\times\pi\times200\times x)) + \cos(2\times\pi\times25\times x + 0.3\times\sin(2\times\pi\times50\times x)) + \cos(2\times\pi\times10\times x + 0.3\times\sin(2\times\pi\times20\times x))$, $Y^{[3]}(x) = \cos(2\times\pi\times100\times x^{0.5}) + \cos(2\times\pi\times25\times x^{0.5}) + \cos(2\times\pi\times10\times x^{0.5})$, and $Y^{[4]}(x) = \cos(2\times\pi\times100\times x^{0.5} + 0.3\times\sin(2\times\pi\times200\times x^{0.5})) + \cos(2\times\pi\times25\times x^{0.5} + 0.3\times\sin(2\times\pi\times50\times x^{0.5})) + \cos(2\times\pi\times10\times x^{0.5} + 0.3\times\sin(2\times\pi\times20\times x^{0.5}))$, respectively. The nonlinear series was generated following the mathematical model

$$Y(x) = \cos(\omega x + \varepsilon \sin 2\omega x) \qquad [A.5]$$

where ω is the frequency in Hz, x is the sampling point, and ε is the amplitude for the sine function. The model is derived numerically from the Duffing equation, which is a classic form of simplest nonlinear equation. In the nonlinear series, a sine wave within a cosine wave created subcyclic or intra-wave frequencies thus making the series nonlinear. However, the equation with square root of the location created the gradual change in frequency, which is known as inter-wave or supercyclic frequency modulation thus making the series nonstationary. The nonstationary-nonlinear series contains both intra-wave and inter-wave frequency modulation. Figure A.1 shows four different spatial series. The stationary-linear signal was identified the by a constant function of frequency and the stationary-nonlinear signal by a steady oscillation along the spatial axis. The nonstationary-linear was identified by smoothly decreasing amplitude with time and the nonstationary-nonlinear series by time varying oscillation with decaying envelope of the amplitude (Yan and Gao, 2007).

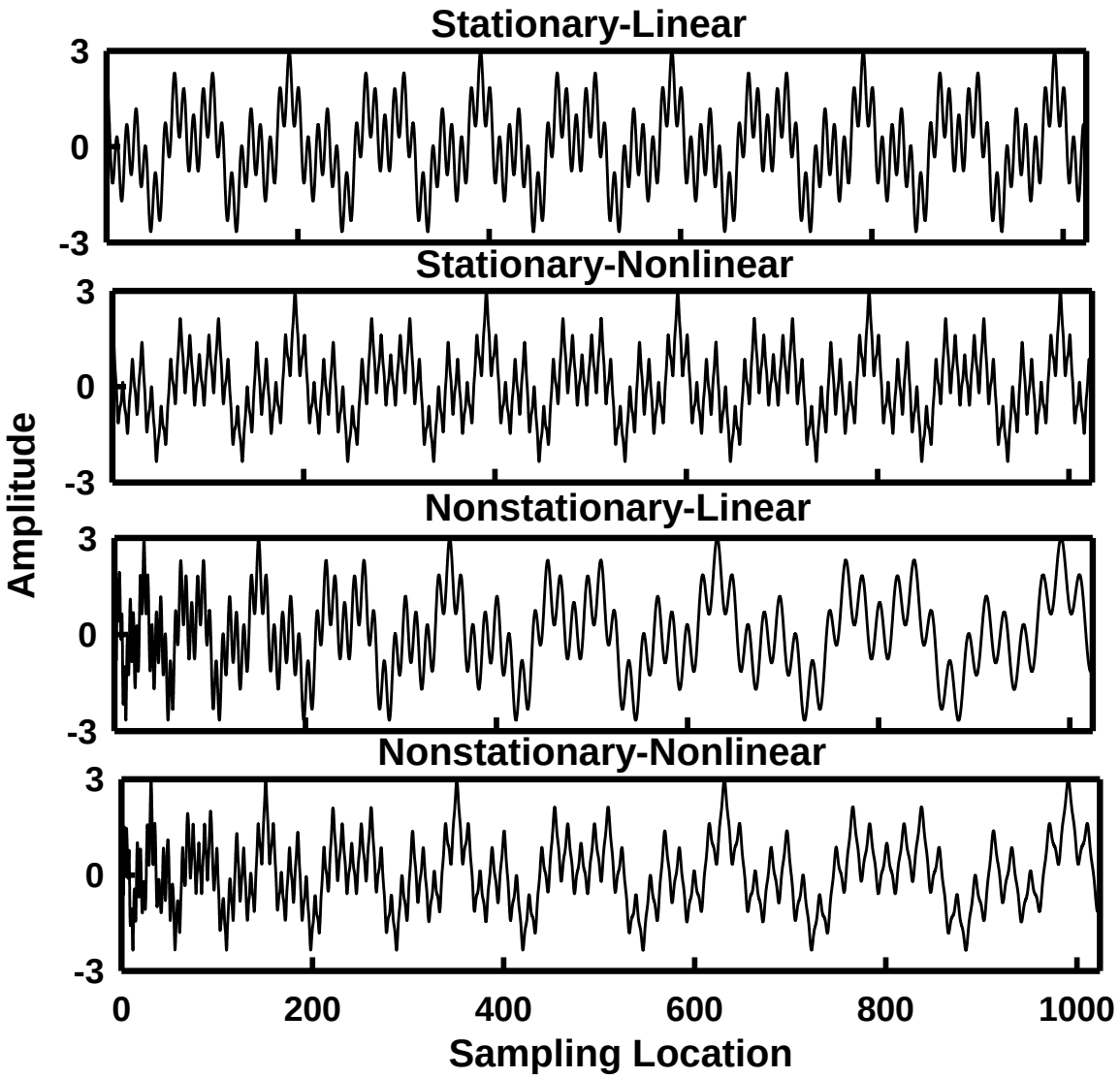

Figure A.1. Four types of synthetic signals; a) stationary-linear, b) stationary-nonlinear, c) nonstationary-liner and d) nonstationary nonlinear with three cosine waves of frequencies 10 Hz, 25 Hz and 100 Hz. Total numbers of samples are 1024. X-axis indicates the distance along the sampling locations (m) and Y-axis indicates the amplitude of the signal (m).

The MRA of the artificial signal was completed using the wavelet toolbox in MATLAB (MathSoft Inc.) software. Daubechies 4 wavelet was used in the manuscript for illustrating the MRA. All four types of signals were decomposed into predefined scale intervals using MRA. The EMD of the artificial signal was completed using a MATLAB (MathSoft Inc.) program written by Dr. Wu. (available at http://rcada.ncu.edu.tw/research1_clip_program.htm). All four types of signals were decomposed into IMFs using the EMD.

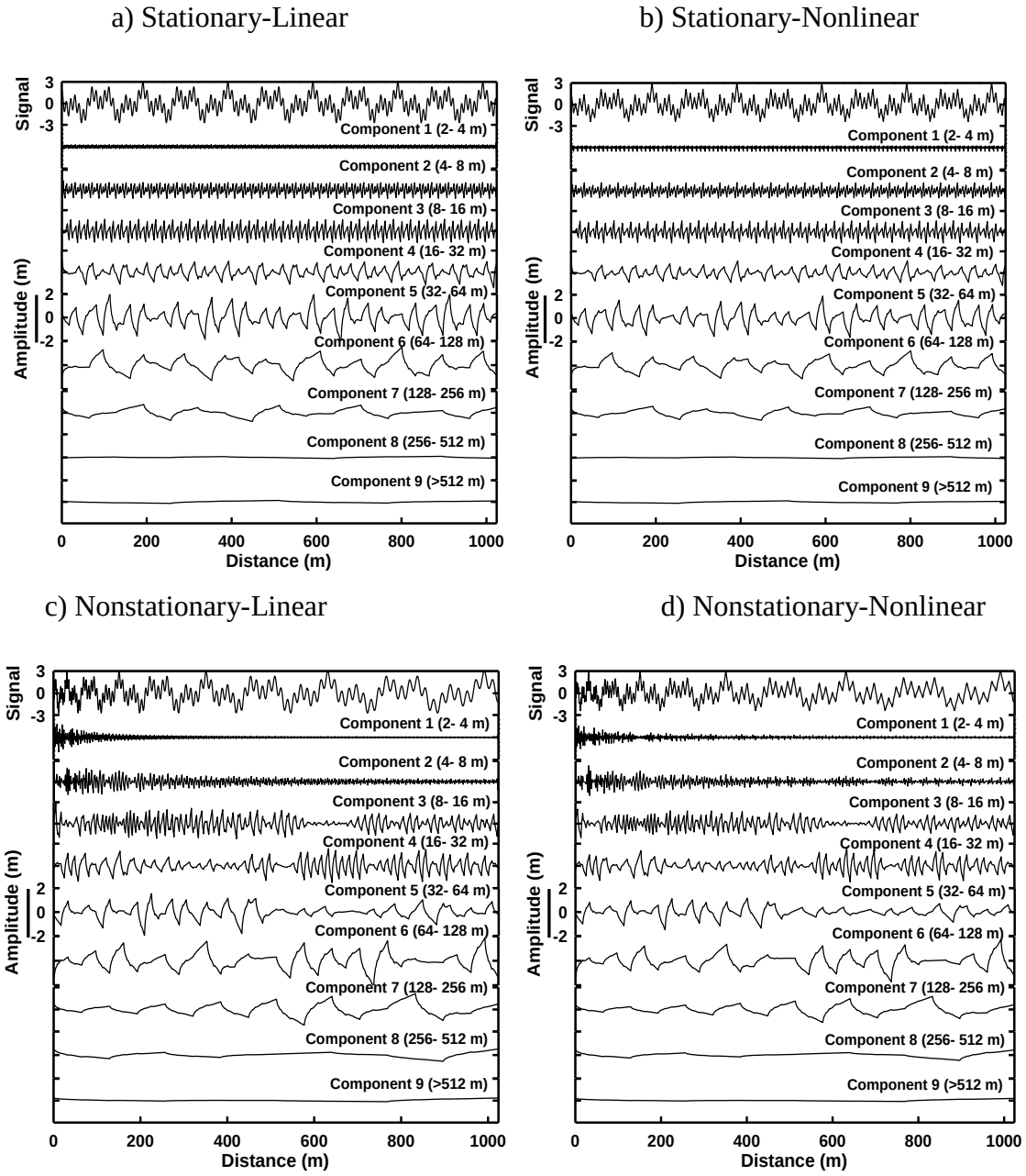

Figure A.2. The scale components of the MRA of synthetic a) stationary-linear, b) stationary-nonlinear, c) nonstationary-linear, and d) nonstationary-nonlinear signal with the original signal at top. X-axis indicates the distance along the sampling locations (m) and Y-axis indicates the amplitude (m). The vertical solid bar in Y-axis shows the scale of the amplitude of the components and is equivalent to 4 m.

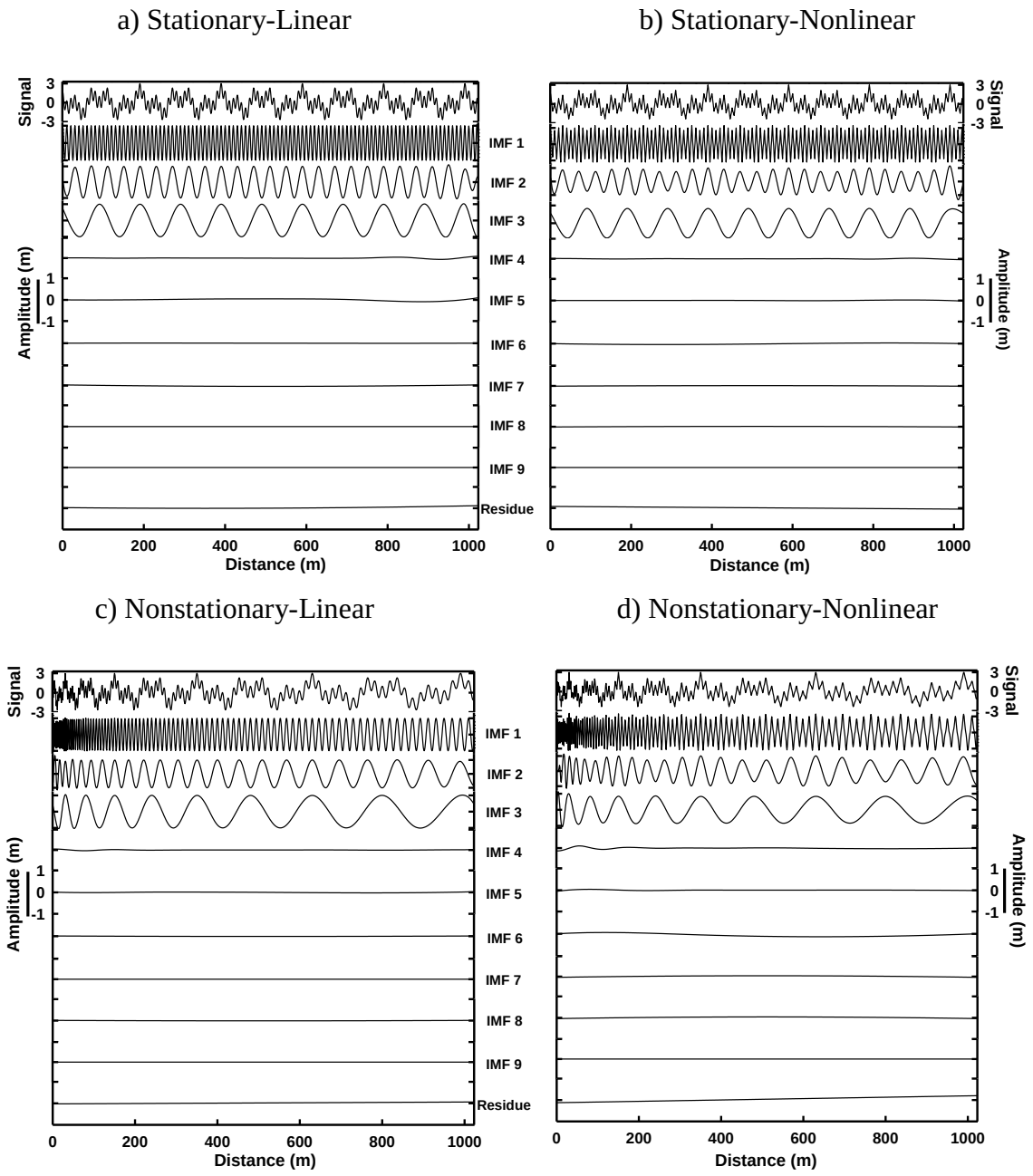

Figure A.3. The IMFs (IMF 1 through IMF 9) of synthetic a) stationary-linear, b) stationary-nonlinear, c) nonstationary-linear, and d) nonstationary-nonlinear signal of three cosine waves with the original signal at top. The residue is shown at the bottom. X-axis indicates the distance along the sampling locations (m) and Y-axis indicates the amplitude (m). The vertical solid bar in Y-axis shows the scale of the amplitude of IMFs and is equivalent to 2 m.

All four types of series were decomposed into 9 different scale components using MRA, which separates the variations at different scale intervals. Figures A.2a, A.2b, A.2c, and A.2d showed the scale components of stationary-linear, stationary-nonlinear, nonstationary-linear and nonstationary-nonlinear series, respectively. The component 1, which separates the variations at 2 to 4 m scale interval, contained rapidly changing variations. The component 2 separated the variations at the scale of 4 to 8 m and component 3 separated the variations at the scale of 8 to 16 m (Figure A.2a). The scales separated by subsequent components increased gradually to the scale interval of > 512 m for component 9, which was almost a flat line indicating that there were almost no variations at the scale > 512 m.

In case of stationary-nonlinear series, a similar decomposition was obtained from MRA (Figure A.2b). For both stationary series, the variations separated as fluctuations were similar and repetitive over the space. However, in the component 1 of nonstationary-linear series, there were more fluctuations separated at the beginning of the sampling period and gradually decreased at the later part (Figure A.2c).The frequency modulation over the space resulted variations in the fluctuations. Similar fluctuations were also separated in component 2 and component 3. However, the fluctuations at the later part of component 4 were stronger than fluctuations at the beginning. A similar type of decomposition was obtained from nonstationary-nonlinear series (Figure A.2d). Therefore, the pattern was similar for two stationary series and for two nonstationary series. However, MRA could not identify the variations due to linear/nonlinear series.

EMD separated the artificial series into 9 IMFs (IMF 1 through IMF 9) and the final residue (R). IMF1 of the stationary-linear series separated the smallest scale representing rapidly changing variation in the original signal (Figure A.3a). The average scale of each IMF can be determined by counting the number of oscillations over the entire length of sampling. In average, there were 10 oscillations per 100 m distance indicating the scale of 10 m. However, more accurate scale information can be obtained by decomposing the IMFs using Hilbert transform. The Hilbert-transform can calculate physically meaningful instantaneous frequency from the IMFs. The instantaneous frequency is the local frequency, which identifies both intra-wave, inter-wave frequencies in any signal, and thus deals with the nonstationarity and nonlinearity together. The instantaneous frequencies can be converted to the scales (=1/frequency) (Huang et

al., 1998). The Hilbert transform of IMF 1 of the stationary-linear series identified the frequency of exactly 0.1 cpm or the scale of 10 m. The scale of first cosine wave was also 10 m. While, the IMF 2 separated the oscillations with a scale of 40 m, IMF 3 separated the oscillations with a scale of 100 m (Figure A.3a). The scales of other IMFs were extremely large as the IMFs were represented by almost a straight line. The residual trend in the dataset was also zero (Figure A.3a).

Similar decomposition of the stationary-nonlinear signal with three important IMFs was presented in Figure A.3b. It also separated a constant frequency oscillation along the sampling space. There is a change in the magnitude of the oscillations representing the nonlinear effect, which MRA was not able to detect. Figure A.3c presented the IMFs of the nonstationary-linear series. The gradual change in the frequency with space or the frequency modulation was clear in all three important IMFs. The change in the frequency within an IMF represented a range of scales for each IMF. The changing frequency and the amplitude of the nonstationary-nonlinear signal were identified in all three important IMFs presented in Figure A.3d. Therefore, MRA only deals with nonstationarity but EMD deals with both nonstationarity and nonlinearity together (Huang et al., 1998; Huang and Wu, 2008).

The MRA decomposed the series into some pre-defined scale intervals that double in size with scales (Fugal, 2007), and only separates the variations corresponding to those scale intervals. For example, MRA decomposed the signal into nine different scale components with the scale interval of 2 to 4, 4 to 8, 8 to 16, 16 to 32, 32 to 64, 64 to 128, 128 to 256, 256 to 512, and > 512 m. However, though the EMD decomposed the original signal into 9 different IMFs and the final residue, the scales were not defined in advance of decomposition. Rather, EMD decomposed the data according to the variations present in the signal. The EMD is adaptive and explain the hidden physical mechanism directly from the data (Huang et al., 1998; Huang and Wu, 2008). It did not consider any mathematical function in the decomposition such as mother wavelet in wavelet transform or sine and cosine function in Fourier transform (Huang et al., 1998). The EMD adapts to the localized changes as it present in the data and separate the variations into different scales. Though EMD produced nine IMFs, only the first three IMFs of each series represented the dominant three frequencies present in the signal separately. The variations of different frequencies were separated accurately according to the scales. However, in

identifying the accurate scales, EMD is not self-sufficient; as it requires Hilbert transform to get the actual scale information, while MRA directly separated the variations at accurate scale intervals. Therefore, in correlating different data series, MRA is a direct method, while EMD needs to be combined with other method.

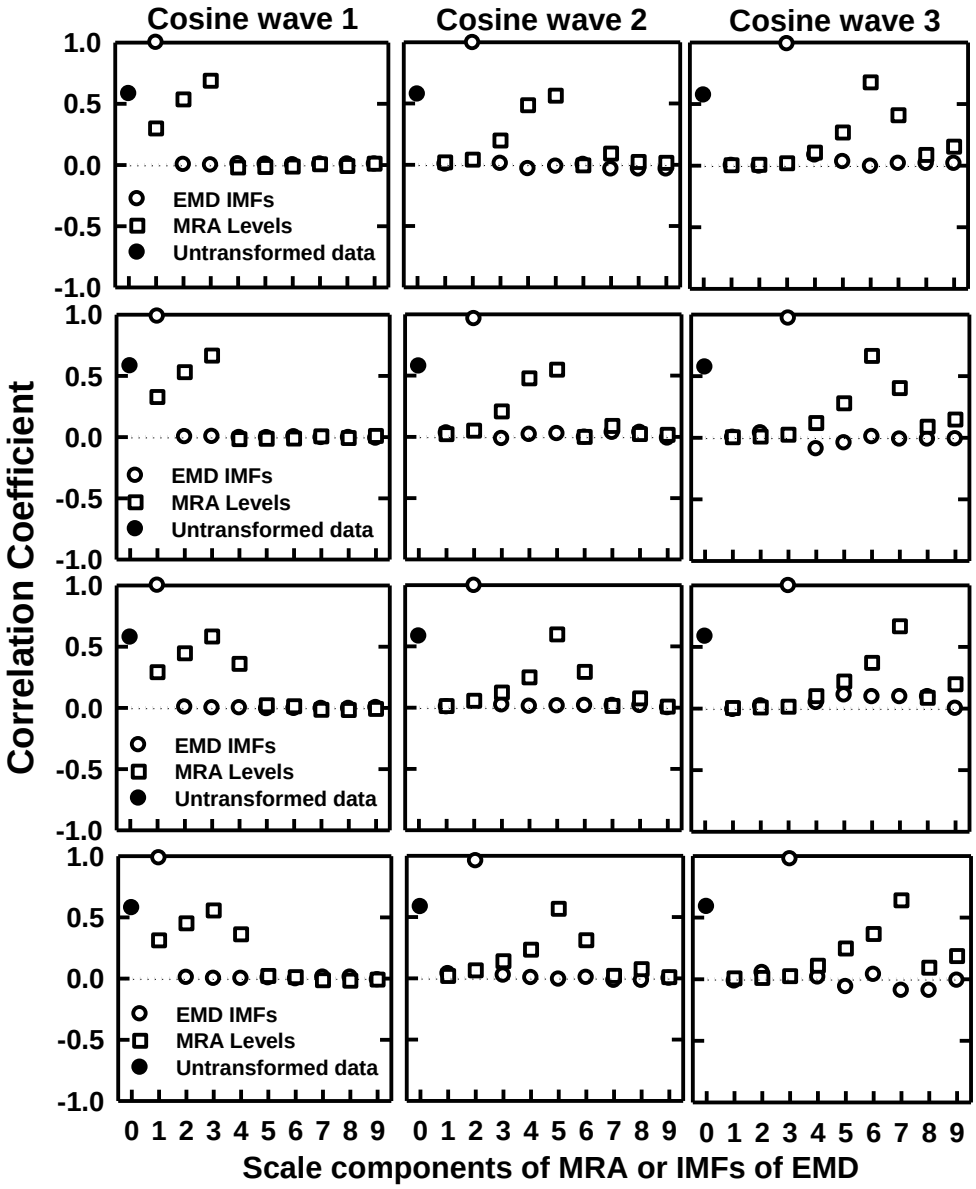

Figure A.4. Correlation coefficients between the cosine waves of four synthetic signals (stationary-linear, stationary-nonlinear, nonstationary-linear, and nonstationary-nonlinear) and the EMD decomposed IMFs (open circle legend) and MRA decomposed scale components (open square legend). X-axis indicates the scale components of MRA and IMFs of EMD. Y-axis indicates the magnitude of correlations. The correlation between untransformed data and the cosine waves at 0 value on X-axis (solid circle legend).

Table A.1. Percent variance contribution of each scale component of MRA and IMFs of EMD of stationary-linear, stationary-nonlinear, nonstationary-linear, and nonstationary-nonlinear series with three different frequencies.

Component	MRA				Component	EMD			
	Stationary-Linear	Stationary-Nonlinear	Nonstationary-Linear	Nonstationary-Nonlinear		Stationary-Linear	Stationary-Nonlinear	Nonstationary-Linear	Nonstationary-Nonlinear
	Percent variation					Percent variation			
1 (2-4 m)	1.0	1.8	1.8	2.1	IMF 1	33.6	33.8	33.4	33.5
2 (4-8 m)	9.2	9.3	5.7	6.4	IMF 2	32.8	34.1	32.8	32.2
3 (8-16 m)	16.5	16.6	15.7	15.1	IMF 3	33.3	31.9	33.7	32.9
4 (16-32 m)	11.9	11.9	16.3	17.6	IMF 4	0.0	0.0	0.0	0.1
5 (32-64 m)	33.6	33.4	15.2	14.0	IMF 5	0.1	0.0	0.0	0.0
6 (64-128 m)	20.7	20.1	26.2	26.6	IMF 6	0.0	0.1	0.0	0.4
7 (128-256 m)	6.7	6.5	16.1	15.3	IMF 7	0.0	0.0	0.0	0.0
8 (256-512 m)	0.1	0.1	2.5	2.5	IMF 8	0.0	0.0	0.0	0.0
9 (> 512 m)	0.3	0.3	0.4	0.4	IMF 9	0.0	0.0	0.0	0.0
					Residue	0.1	0.1	0.0	0.8

The correlation coefficients between the signal components (cosine waves) and the scale components (scale intervals for MRA and IMFs for EMD) of four series were presented in Figure A.4. The correlation coefficient (r) between the first cosine wave and IMF 1 of stationary-linear series was 1.00 (Figure A.4). IMF 2 to IMF 9 was not correlated with first cosine wave. Similarly the second cosine wave was strongly correlated (r = 1.00) to only IMF 2 and third cosine wave was strongly correlated (r = 1.00) to only IMF 3 of stationary-linear series (Figure A.4). There were three cosine waves present in the signal and they were strongly correlated with only three IMFs. If each cosine wave represents an ongoing process and the reciprocal of frequency of the cosine wave represented the scale of the processes, the IMFs separated the scale of the processes accurately without dividing the effects into different IMFs. Similar scale of processes was represented by only one IMF. Identical strong correlation was observed between the cosine waves and the stationary-nonlinear, nonstationary-linear and nonstationary-nonlinear series (Figure A.4). However, this was not the case for MRA decomposition. In case of stationary-linear signal, the first cosine wave was correlated with scale component 1 (r = 0.27) and 2 (r = 0.55) and 3 (r = 0.69; Figure A.4). The first cosine wave had a scale of 10 m and should have been correlated only with scale component 3 as it separated the variations of the scale interval of 8 - 16 m. However, first cosine wave was correlated with three different scale intervals. There were moderate correlations between second cosine wave and the scale component 4 (r = 0.49) and 5 (r = 0.56) and weak correlation between second cosine wave and the scale component 3 (r = 0.20; Figure A.4).

The period of second cosine wave was 40 m and should have been correlated only with component 5 representing the scale interval of 32 – 64 m. Similarly, the cosine wave 3 was also weak to moderately correlated with the scale components 5 (r = 0.27) and 7 (r = 0.41; Figure A.4) and moderately with the scale component 6 (r = 0.68). As the third cosine wave had a scale of 100 m, it should have been correlated with only scale component 6. Though each cosine wave represented only one scale process, MRA separated the process into more than one scale intervals. Similar correlation was also observed between the cosine waves and different scale components of stationary-nonlinear, nonstationary-linear, and nonstationary-nonlinear series. The overall correlation between three cosine waves and the untransformed data was separated into three IMFs by EMD, while MRA separated into seven different scale components or into

seven different scale intervals. This may be due to the leakage in the MRA, which smooth the variation along the scale. Therefore, in these examples, the EMD is more parsimonious in representing the signal content than MRA, which lost the parsimony during decomposition. Representation of the cosine waves through IMFs was more physically meaningful than the different scale components of MRA. In this situation, EMD is a better choice in revealing the accurate scale of the processes.

Both MRA and EMD partitioned the overall variation present in the data into a number of components. These components were additive and we can obtain the original signal by adding them up (Huang et al., 1998; Walker, 1999; Fugal, 2007). Therefore, the addition of variations separated by components will be equal to the total variation in the data (Shapiro, 1993). The variance of each component of all four types of series was calculated and presented in Table A.1 as the percent contribution of each component towards the total variation. In the MRA, the component 1 to component 7 of stationary-linear series had varying contribution towards the total variations with the maximum in component 5 (33.6 %). The artificial series comprised of three scale processes; 10 m, 40 m and 100 m. The variations at these scales should have been separated only in three scale intervals as presented by component 3, 5, and 6, respectively for 10, 40 and 100 m processes. Though the variance contribution of these scale components was higher among the components, the combined contribution was only 70 percent. Rest 30 percent of the variations was smoothed out to other scale components; in spite of the absence of those scale processes. Similar contribution from the three scale components (component 3, 4 and 6) was observed for stationary-nonlinear series. However, for nonstationary-linear and nonstationary-nonlinear series, combined variance contribution from those three scale components was only 48 percent and 45 percent, respectively. This may be due to the gradual change in the scales, which was identified by MRA as the different scale interval discretely. Therefore, the variations were spread over other scales.

The EMD separated the variations into very first three IMFs (Table A.1). Three IMFs combined explained 99.8, 99.8, 100, and 98.7 percent of the data variations respectively present in stationary-linear, stationary-nonlinear, nonstationary-linear, and nonstationary-nonlinear series. This indicated almost perfect separation of the variation of a spatial series into its component scale processes. As the signal was composed of equal magnitude cosine waves, the

percent contribution of each frequency component was equal as represented by the contribution of the different IMFs (Table A.1). Each IMF contributed almost one third of the total variation in the data. This suggested that the EMD not only separated the scale specific processes accurately, but also the magnitude or the contribution of variation towards the total variation.

A.5 Comparison of MRA and EMD using a Soil Variable

Soil water storage measured along a transect of 128 points (4.5 m regular interval) at St. Denis National Wildlife Area (SDNWA), Saskatchewan, Canada was used to compare MRA and EMD. A detailed description of the study site can be found in Biswas and Si (2011b). Briefly, a transect of 576 m was established over several rounded knolls and depressions representing different landform cycles. The dominant landscape of the study area is hummocky with slopes varying from 10 to 15%. The relative elevation along the transect is presented in Figure A.5 at the top. The soil of this area is Dark Brown Chernozem, which is developed from glacio-lacustrine deposits and modified glacial till (Acton and Ellis, 1978). The climate of the study area is semi-arid in nature with the average annual air temperature of 2^{o}C. The 90-year average precipitation of the area is 360 mm (AES, 1997).

The soil water was measured from 0.2 m to 1.4 m depth at an interval of 0.2 m using a neutron probe (CPN 501 DR Depthprobe, CPN International Inc.) in field. Surface soil water (0 - 0.2 m) was measured using time domain reflectometry probe and a metallic cable tester (Model 1502B Tektronix, Beaverton, OR). The soil water measurements were taken over a four year (2007-2010) period at different times. For this study, we only considered one measurement series completed on 12 October 2007 to compare two methods. The spatial distribution of measured soil water storage along the transect was presented in Figure A.5. The statistical distribution of soil water storage was approximately normal, with average soil water storage of 37.37 cm and standard deviation of 6.18 cm. The soil water storage series was decomposed using MRA and EMD following the procedure described earlier.

Relative elevation along the transect was measured using Trimble Pro XRS Global Positioning System (Trimble Navigation, Sunnyvale, CA, USA). The particle size distribution of surface soil samples was characterized using HORIBA LA-950 Laser diffraction particle-size

analyzer (HORIBA Scientific Inc., Edison, NJ, USA). The organic carbon (OC) of surface soil was determined using LECO-C6235 carbon determinator (LECO Corp., St. Joseph, MI, USA).

Figure A.5 showed six different scale components obtained from MRA along with the spatial distribution of soil water storage and the relative elevation. The scale components separated the scale intervals of 9 to 18, 18 to 36, 36 to 72, 72 to 144, 144 to 288, and > 288 m, respectively. The component 1 represented very small-scale (9 to 18 m) processes operating frequently in space along the transect (Figure A.5), and may be contributed from measurement errors, or the localized variations in soil water storage. However, the variance contribution of the scale component 1 towards the total variation was very low (3.83 %; Table A.2).

Table A.2. The percent variance contribution of each scale component of MRA and IMFs of EMD of the soil water storage.

MRA		EMD	
Component	Percent variation	Component	Percent variation
1 (9 – 18 m)	3.83	IMF 1	5.52
2 (18 – 36 m)	6.92	IMF 2	9.08
3 (36 – 72 m)	8.13	IMF 3	43.84
4 (72 – 144 m)	21.06	IMF 4	10.45
5 (144 – 288 m)	25.55	IMF 5	2.70
6 (> 288 m)	34.52	IMF 6	2.36
		Residual	26.05

The variance contribution of the scale component 2 was also small (6.92 %) compared to the total variations in the soil water storage. This indicated that the processes operating at these scales did not have a strong influence on soil water storage. The variance contribution towards the total variation was increased with the increase in scales (Table A.2). The component 6 had the highest variance contribution (34.52 %) and separated the variations > 288 m scale representing the overall landscape variations or the overall trend in the data. The scale component 5 had the second highest variance contribution (25.55 %) towards the total variation, which represented the large-scale processes (144 to 288 m). The component 4 contributed about 21 percent of the total variations present in the data (Table A.2). There were repetitive variations in the topography around the scale of 90 to 100 m (Figure A.5). The component 4 might explain the controls from these topographic variations in the landscape. The component 3 separated the

variations at the scale of 36 to 72 m and contributed a small amount of variations (8.13 %), which might explain the variations from micro-topography and the landform elements (Figure A.5) within the landscape.

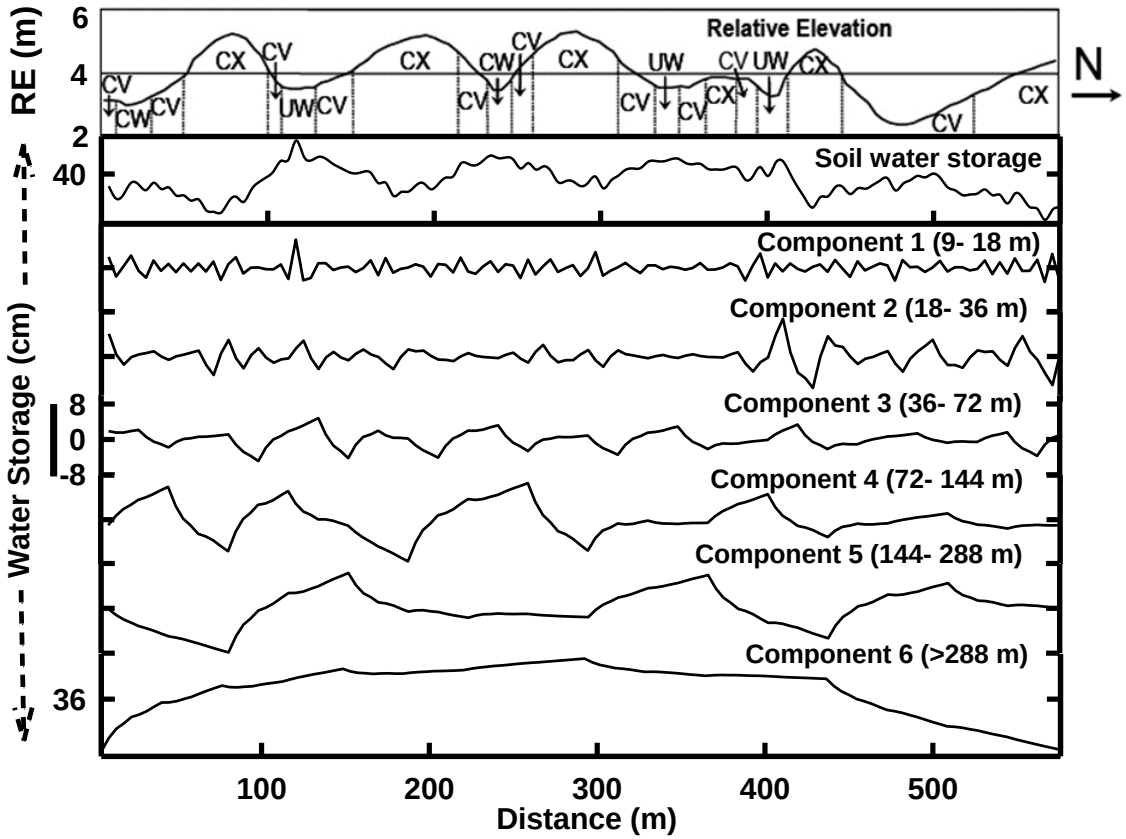

Figure A.5. Scale components presenting different scale intervals of soil water storage using MRA. The relative elevation is at the top; the soil water storage series is at second top; the final residue is at the bottom. CX in the elevation graph indicates convex, CV indicates concave, CW indicates cultivated wetland and UW indicates uncultivated wetlands, which are different landform units along the transect. The vertical solid bar in Y-axis shows the scale of soil water storage and is equivalent to 16 cm. X-axis indicates the distance along the transect (m).

In the MRA, all the variations with in the scale interval were combined together. Whereas, the EMD separated the variations present in the soil water storage into 6 different IMFs (Figure A.6) as they were present at different scales. The overall trend in the data was separated as the residue. The decomposition was completely based on the oscillations or variations present in the data. The oscillations of similar scales were separated in one IMF. The IMF 1 (Figure A.6)

separated very small scale variations present in the soil water storage representing the small scale processes, and the contribution of variation towards the total variation at this scale was small (5.52%). The IMF 2 represented the variations at the medium scales of 30 to 40 m (Figure A.6) that contributed towards the variations in soil water storage. The variations due to landform elements (such as convex and concave) or the micro-topographical variations (Figure A.6) might have controlled the soil water storage at the scales of 30 to 40 m. However, the contribution of variation towards the total variations was moderate at these scales (Table A.2). The contribution was the highest from IMF 3 (43.84%), which was more than the sum of contributions from all other IMFs combined (Table A.2). The IMF 3 represented the scales of around 90 to 100 m, which indicated the variations due to the topography (Figure A.6). There were similarities between IMF 3 and elevation (Figure A.6). The IMF 4 represented the variations at large scales (almost > 200 m). The contribution of variations towards the total variation at this scale was little higher than the variations at small scales (Table A.2). The residue had moderate contribution towards the overall variation (Figure A.6). This variation may be a result of the movement of ground water towards the both ends as the large ponds were located not very far from the end of the transect.

To understand the physical mechanisms explained by IMFs and the different level coefficients, a scale specific correlation analysis was carried out. Correlation coefficients (r) between the scale components and IMFs of soil water storage decomposed through MRA and EMD, respectively and the measured controlling factors were calculated and presented in Figure A.7. It was assumed that the controlling factors had its dominant scale of control. The control from these factors was represented at particular spatial scale in soil water storage series. Therefore, only the soil water storage series was decomposed by EMD or MRA and compared with the measured controlling factors. At the measurement scale (or before decomposition by EMD or MRA), soil water storage was strongly correlated to sand (r = -0.64) and OC (r = 0.66). Elevation showed a weak correlation (r = -0.21) with soil water storage at measurement scale (Figure A.7). However, elevation was strongly correlated with IMF 3 (r = -0.61) and contributed the highest towards overall variation (Table A.2). IMF 3 was also correlated with OC (r = 0.60).

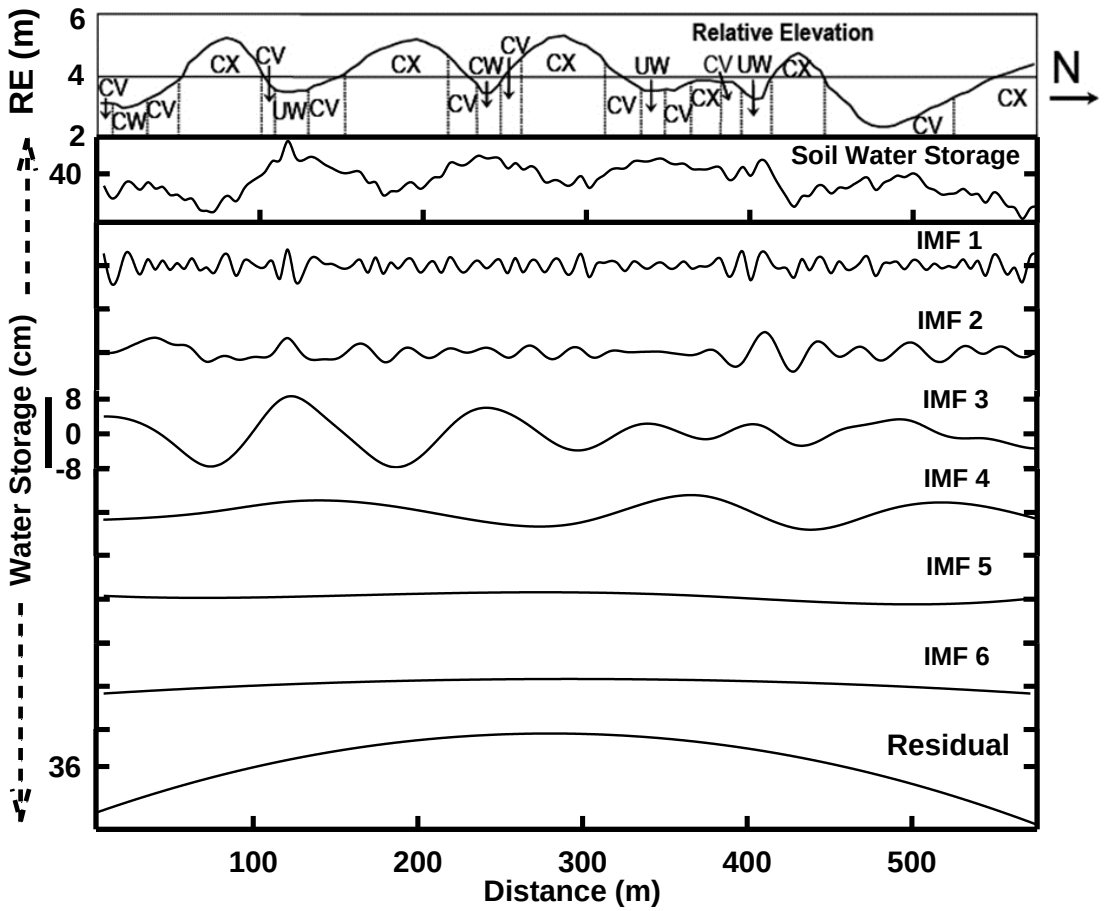

Figure A.6. IMFs of soil water storage using EMD are shown. The relative elevation is at the top; the soil water storage series is at second top; the final residue is at the bottom. CX in the elevation graph indicates convex, CV indicates concave, CW indicates cultivated wetland and UW indicates uncultivated wetlands, which are different landform units along the transect. The vertical solid bar in Y-axis shows the scale of soil water storage and is equivalent to 16 cm. X-axis indicates the distance along the transect (m).

Generally, the variation in OC in a field reflects the long-term history of water storage, which might be the reflection of historical topography, micro-topography or landform elements in that field (Gómez-Plaza et al., 2001). Therefore, the elevation was considered as the major control of soil water storage. Sand (r = 0.71) and elevation (r = 0.60) had also strong correlation with IMF 5 (Figure A.7) showing the large-scale association between soil water storage and sand and elevation. Therefore, the scale specific correlation with controlling factors explained the physical meaning of the IMFs. MRA decomposed the soil water storage into six different components or scale intervals. Component 3 (r = -0.34), 4 (r = -0.55), and 6 (r = 0.48) showed moderate to

strong correlation with elevation (Figure A.7). The variations due to elevation at the scale of 90-100 m were separated in the component 4 or at the scale interval of 72 to 144 m. OC also had a strong correlation with the component 4 (r = 0.53). Sand had a strong correlation with the component 6 (r = -0.56) representing the large-scale controls (Figure A.7). However, the variance contributions from different components were different (Table A.2). This indicated that the different factors control soil water storage at a range of scales with no dominating control at a specific scale.

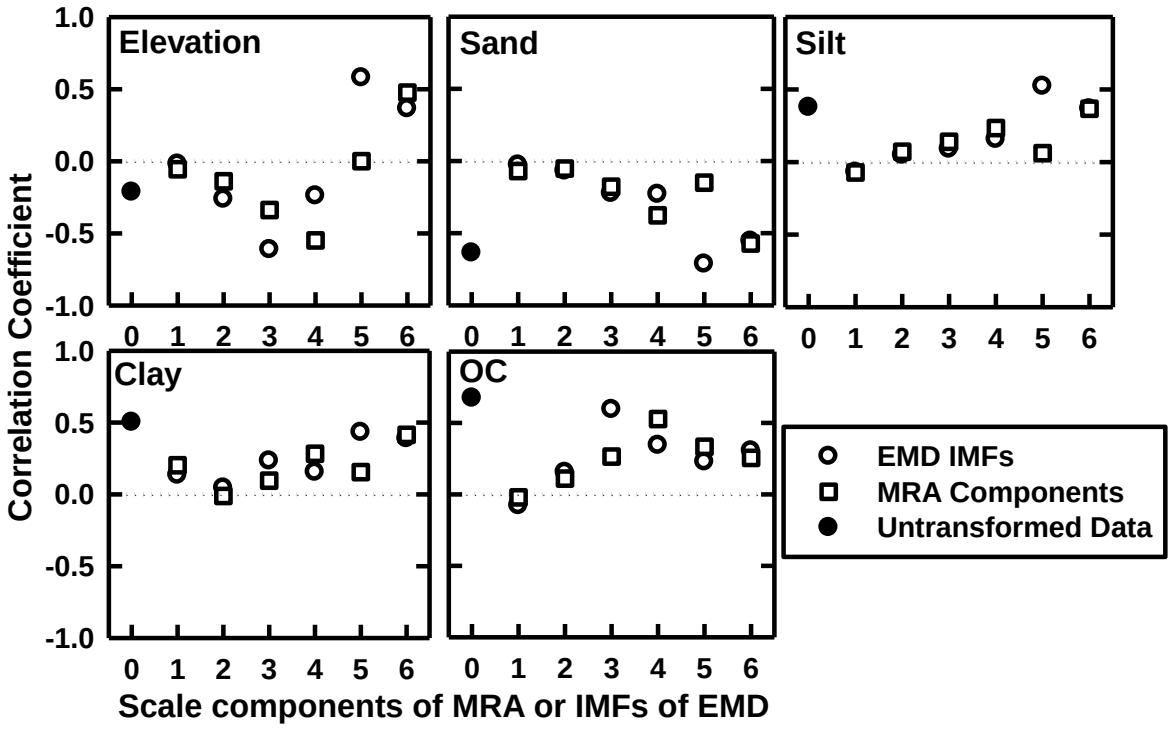

Figure A.7. Correlation coefficients between the controlling factors of soil water storage and the EMD decomposed IMFs (open circle legend) and MRA decomposed levels (open square legend). X-axis indicates the scale components of MRA and IMFs of EMD. Y-axis indicates the magnitude of correlations. The correlation between untransformed data and the cosine waves at 0 value on X-axis (solid circle legend).

Both MRA and EMD decomposed the variations in soil water storage into different scales. The MRA partitioned the variation at some fixed and predefined scales, whereas EMD was adaptive and data driven. In nature, soil processes and their controls do not vary regularly; rather they can occur at any scales. Identification of variations at a particular scale provides

better understanding of the spatial variability of soil properties and can be helpful in finding the scale-specific controls of the variability. The EMD produced better result in isolation of scale-specific spatial variability than MRA.

Comparison of MRA and EMD conducted in this study was based on cyclic and quasi-cyclic spatial series. Therefore, we selected four cyclic surrogate spatial series with different characteristics and a realistic spatial series from a rolling landscape for the purpose. However, our conclusion may also be valid for soil properties collected along a transect in other forms of landscapes. A comprehensive comparison of the two methods for different case scenarios is needed and is subjected to future research.

A.6 Conclusions

In this study, a comparison was made between wavelet based MRA and newly introduced EMD in the isolation of scale specific variability of soil properties. The Daubechies 4 wavelet function was used to separate the variations in the data series into different scale components using MRA.

Four artificial signals composed of three cosine waves with equal amplitudes but different frequencies were decomposed using MRA and EMD. The MRA decomposed variations into different scale components with predefined scale intervals and each scale contributed differently towards the overall variation. Whereas, EMD separated the three frequencies present in the artificial signal accurately in the first three IMFs each of that contributed one third of the total variation. Therefore, EMD can accurately identify the scales of variations along with the exact contribution of variance from each scale, which makes the scale specific decomposition physically meaningful. Similarly, on decomposition of a soil water storage series, MRA separated the overall variation into 6 different predefined scale intervals contributing differently towards the total variations. The EMD also decomposed the soil water storage series into 6 IMFs and the residue, among which, IMF 3 separated oscillations of around 90 to 100 m scale and represented the variations due to alternative knolls and depressions along the transect. IMF 3 had the highest contribution to the total variation and was strongly correlated with elevation indicating the elevation to be a major control of soil water storage at that scale. The IMFs from EMD explained the scale-specific data variations with better physical meaning than MRA.

However, the choice of these tools for identifying scale specific variation will depend on the information to be needed. For example, while EMD can be used to identify the scales, as they are present in the data, MRA may be a better choice in some applications such as correlating soil water content at one scale to satellite radar images with a fixed pixel size.

APPENDIX B

B.0 SCALE–LOCATION SPECIFIC SOIL SPATIAL VARIABILITY: A COMPARISON OF CONTINUOUS WAVELET TRANSFORM AND HILBERT–HUANG TRANSFORM

B.1 Preface

Soil spatial variability is the rule and not the exception, which is complicated by issues of spatial dependence, periodicity, nonstationarity, and nonlinearity. Geostatistics and spectral analysis deal with spatial dependence and periodicity, respectively. Development of continuous wavelet transform (CWT) has been crucial in dealing with nonstationary soil spatial series. Although CWT reveals scale and location specific information of nonstationary soil properties, it is a linear analysis, thus limiting its scope of analysis. Recently, Hilbert–Huang transform (HHT) has been introduced in soil science to reveal scale and location specific information of both nonstationary and nonlinear soil properties concurrently. This chapter compares CWT and HHT in revealing the scale and locations of variations using artificial spatial series as well as measured soil water series.

B.2 Introduction

Soil spatial variability is the rule, not the exception, and is generally a product of the combined effect of soil physical, chemical, and biological processes that operate in different intensities and at different scales (Goovaerts, 1998). Therefore, adequate understanding of variability as a function of space and scale is necessary for environmental prediction (Trangmar et al., 1985), precision agriculture (Goderya, 1998), soil quality assessment (Heuvelink and Pebesma, 1999; McBratney et al., 2000), and natural resource management. A detailed description of soil spatial variability also provides critical information for the development of various logical, empirical, and physical models of soil landscape processes (Burrough, 1983; Foussereau et al., 1993; Wilding et al., 1994; Corwin et al., 2006).

Since the classic study of Nielsen et al. (1973), systematic study of soil spatial variability has identified various complicating issues such as spatial dependence, periodicity, nonstationarity, and nonlinearity. Geostatistical analysis (Trangmar et al., 1985) and spectral

analysis (Webster, 1977; Shumway & Stoffer, 2000; Brillinger, 2001) can explain the spatial dependence and the periodicity, respectively. However, more often than not, soil spatial variations are nonstationary and soil processes at differing scales may be localized in space relative to the entire spatial domain (Si, 2003). Therefore, the assumption of stationarity and the loss of spatial information (Oliver and Webster, 1991; Goderya, 1998) restricted the use of geostatistics and spectral analysis in analyzing nonstationary soil spatial variation. Wavelet analysis can be used to examine the variability of a nonstationary spatial series by partitioning the sample variation into positions (or locations) and frequencies (or scales) (Si, 2003; Lark et al., 2004; Si and Farrell, 2004).

Wavelet analysis has been used for over a decade to study multi–scale (Bosch et al., 2004) stationary/nonstationary soil processes (Lark and Webster, 1999; Lark et al., 2004; Si and Farrell, 2004; Neupauer and Powell, 2005; Biswas et al., 2008; Watkins et al., 2009). There are different types of wavelet analyses such as continuous wavelet transform (CWT), discrete wavelet transform (DWT), maximum overlap discrete wavelet transform (MODWT) and wavelet packet transform (WPT). These are a suite of tools used for different purposes, each with inherent advantages and disadvantages. CWT is particularly suited for scale analysis as it partitions the overall variations in a spatial series into continuous scales and locations (Lau and Weng, 1995; Si and Zeleke, 2005). It has previously been used to examine the scale–location specific variability of various soil properties. A comprehensive review on the applications of CWT in soil science can be found in Biswas and Si (2011c).

While CWT has proven to be extremely useful in revealing the underlying variability of any soil properties, it typically suffers from a deficiency; that is, the analysis assumes the spatial series to be linear (Huang et al., 1998). In complex natural systems, however, the total effect from multiple processes is non–additive. Therefore, the principle of superposition does not apply to the overall system, thus indicating a nonlinear system (Yan and Gao, 2007). Alternatively, in a nonlinear system, the target or dependent variable cannot be written as a linear sum of its independent components (Pai and Palazotto, 2008). In discussing a nonlinear system, the concept of subcyclic and supercyclic oscillations is introduced (Huang et al., 1998; Kijewski-Correa and Kareem, 2006). Subcyclic oscillations denote the changes in frequency that occur within a single cycle of oscillations, supercyclic oscillations denote changes in frequency that occur over the

course of one or more cycles. As a result, in nonlinear systems the frequency or scales of a spatial series will be locally unpredictable (Gautama et al., 2004). Although wavelet analysis is capable of capturing supercyclic variations, the subtle variations of subcyclic frequency are not elucidated by this technique. In CWT, the mother wavelet (e.g., Morlet wavelet) is essentially used to identify the frequency of a best–fit sinusoid to the data over a short span of time/space. However, if the signal deviates from the sinusoid form as is often the case with subcyclic frequency modulations, the deviations must be examined locally (Huang et al., 1998; Kijewski-Correa and Kareem, 2006). Hilbert-Huang transform (HHT) can capture both super and subcyclic oscillations simultaneously through the calculation of instantaneous frequency, a local frequency (Huang et al., 1998; Kijewski-Correa and Kareem, 2006).

HHT can simultaneously deal with both nonlinear and nonstationary spatial series (Huang et al., 1998) and has been recently extended to explore the scale–location specific information of a spatial series in soil science (Biswas et al., 2009; Biswas and Si, 2011d). The main advantage of HHT is that it identifies the hidden physical trends directly from data without imposing any mathematical rule in the analysis. Unlike other data analysis methods, HHT does not have any *a priori* basis; rather it is intuitive, direct, adaptive and completely data driven (Huang et al., 1998). In the two–step process, HHT separates the dominant scales of variations and calculates the instantaneous frequency or scales (= sampling interval / frequency) in a spatial series. The separation of scales can deal with trends in nonstationary series and the instantaneous frequency or the localized frequency in a spatial domain can deal with nonlinearity (Huang et al., 1998). Recently, CWT has also been modified to calculate the instantaneous frequency (Kijewski-Correa and Kareem, 2006) using a modified Morlet wavelet. However, CWT using the regular Morlet wavelet is still the widely used method for identifying scale and location specific variations in soil science and will be the subject of investigation for this manuscript.

While CWT is a well–established spatial analysis method that deals with nonstationarity, HHT is a new method to deal with both nonstationarity and nonlinearity. Before HHT is to be used as a research tool a careful comparison to existing standard methods is needed. In this study, we have compared the relative merits of CWT and HHT in revealing the scale–location specific variations that are hidden in a spatial series. To do this, we have divided the manuscript into three parts. In part one we have discussed the theory in brief. In part two we have used

different types of artificial signals composed of pure cosine waves to compare the CWT and HHT. Finally, we have used two examples of soil properties to compare the methods in identifying scale–location specific variations.

B.3 Theory

B.3.1 Continuous Wavelet Transform (CWT)

The CWT decomposes the overall variations in a spatial series into different locations (sample positions) as a function of continuous scales (frequencies). Different wavelet functions such as Haar, Maxican Hat, and Morlet can be used to calculate the wavelet coefficients. These functions are called the mother wavelet function that can be stretched or contracted in space (x) and at different scales (s). The detailed theoretical description of the CWT is well established in the literature and is beyond the scope of this paper. For reader's interest, full descriptions can be found in Farge (1992), and Kumar and Foufoula–Georgiou (1993, 1997) among many others. Briefly, CWT can be defined as the convolution of a spatial series Y_i of length N ($i = 1, 2, \cdots, N$) along a transect with equal increments of distance δx (Torrence and Compo, 1998),

$$W_i^Y(s) = \sqrt{\frac{\delta x}{s}} \sum_{j=1}^{N} Y_j \psi\left[(j-i)\frac{\delta x}{s} \right] \qquad \text{[B.1]}$$

which can be implemented through a series of Fast Fourier Transform (FFT). The function $\psi[\ ]$ is called wavelet function or 'basic wavelet'. The parameter s is the dilation–contraction factor (Kumar and Foufoula–Georgiou, 1997). Wavelet coefficients, $W_i^Y(s)$ are expressed as $a + ib$, where a and b are the real and imaginary components of $W_i^Y(s)$, respectively. The energy associated with each scale and location can be calculated from the magnitude of wavelet coefficients (Qi and Neupauer, 2008). Similar to the Fourier power spectrum, the wavelet power spectrum can be calculated as $\left|W_i^Y(s)\right|^2$. These wavelet power spectra are a function of scales and locations. Therefore, a better visualization of power spectra can be given by contour plot with locations on the horizontal axis and scales on the vertical axis. The wavelet spectrum at a location and scale represents the local variance, and the sum of all local spectra is equal to the total variance. Therefore, it can used to examine the scale–location specific variations in soil properties.

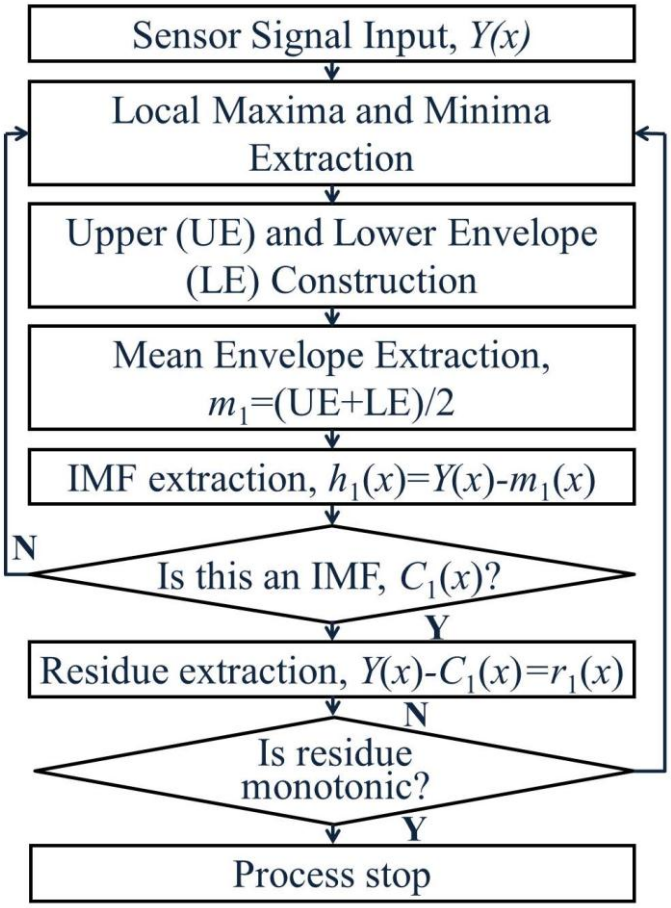

Figure B.1. Shifting steps for extracting intrinsic mode functions (IMFs) through empirical mode decomposition (EMD).

B.3.2 Hilbert–Huang Transform (HHT)

The HHT is a two–step method. The first step, empirical mode decomposition (EMD), separates the oscillations present in a spatial series according to their characteristic space scales. It decomposes the overall spatial pattern into a finite and often small number of intrinsic modes that are known as intrinsic mode functions (IMFs). Each IMF represents the characteristics scales of variability. In the second step, Hilbert–spectral analysis (HSA), the instantaneous frequencies are calculated after applying the Hilbert transform to each IMF. The energy is calculated from the instantaneous amplitude, a product of Hilbert transform, which is a function of frequency or scale and space or location. Detailed theory on HHT can be found in Huang et al. (1998) and Huang and Wu (2008).

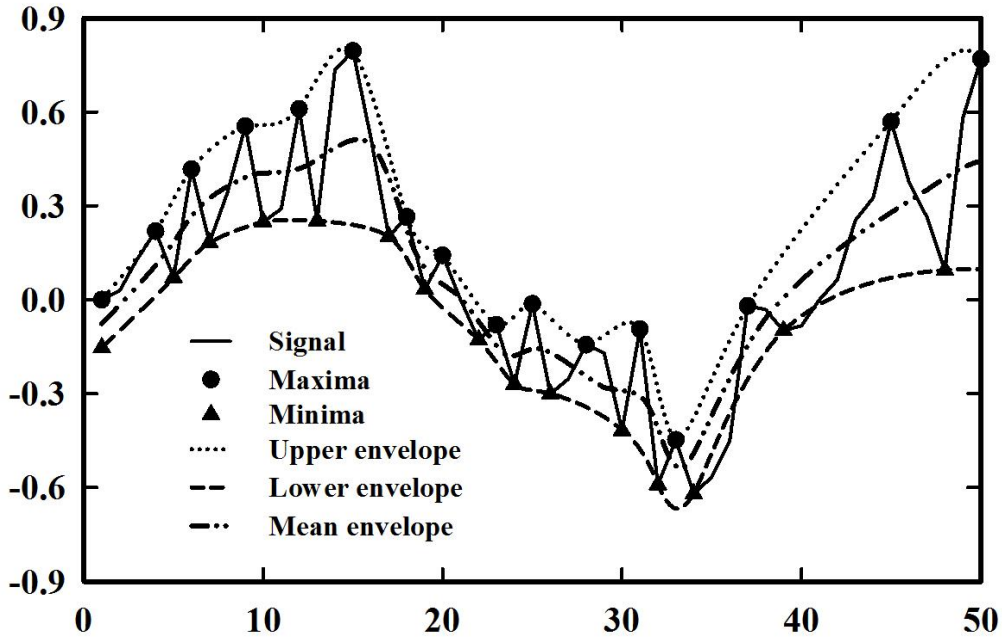

Figure B.2. Different parts of a signal including maxima and minima. Maxima's are joined by spline interpolation to create upper envelope, and minima's are joined by spline interpolation to create lower envelope. Mean envelope is the local mean of upper and lower envelope.

Briefly, IMFs are extracted through a sifting process (Figure B.1). For a spatial signal $Y(x)$, we can identify the local maxima and local minima (Figure B.2). The maxima and minima are then joined by a cubic spline line to create the upper (UE) and lower (LE) envelope (Figure B.2). The mean value of the envelopes $m_1 = (UE + LE)/2$ can be calculated locally and subtracted from the original spatial series to get the first prototype $h_1(x) = Y(x) - m_1(x)$, which is a function of space. This prototype will be an IMF provided it has satisfied the following conditions: 1) the mode may or may not be linear and the number of extrema and zero crossings must either equal or differ at most by one, and 2) the oscillation will be symmetric with respect to the local mean; which says that at any data point the mean value of the envelopes defined by local maxima and local minima is zero (Huang et al., 1998). If the prototype does not satisfy the conditions, the procedure needs to be repeated and the prototype will be considered as the new data. After k times of iterations $h_{1(k-1)}(x) - m_{1k}(x) = h_{1k}(x)$, when the conditions are satisfied, $h_{1k}(x)$ is defined as the first IMF (C_1) as a function of space, $C_1(x) = h_{1k}(x)$. However, the number of iterations needs

to be finite and will be stopped at approximate symmetry of local envelopes. This is known as stoppage criteria, which ensures that the IMF components retain enough physical sense of both amplitude and frequency modulations. The stoppage criterion was defined based on a Cauchy type of convergence test, which is the normalized squared difference between two successive sifting operations and is given as (Huang et al., 1998)

$$SD_k = \frac{\sum_{x=0}^{X} \left| h_{k-1}(x) - h_k(x) \right|^2}{\sum_{x=0}^{X} h_{k-1}^2(x)} \qquad \text{[B.2]}$$

where, X represents maximum of x. When the SD value is smaller than a predetermined value (usually set between 0.2 and 0.3), the iteration has to stop.

The first IMF separates the highest frequency oscillations or finest scale of variations in the spatial series and can be extracted from the data as $Y(x) - C_1(x) = r_1(x)$. Thereafter the residue is treated as the new data and the sifting procedure is carried out to separate subsequently larger scales of variations until the final residue is left with only one extremum, or becomes a monotonic function. If the sifting is carried out for subsequent $r_j(x)'s$, where j = 1, 2, 3, …, n and the final residue can be written as $r_1(x) - C_2(x) = r_2(x), \ldots, r_{n-1}(x) - C_n(x) = r_n(x)$ where, $C_n(x)$ are the IMFs. Therefore, the spatial series will be the sum of all empirical modes and final residue and can be written as

$$Y(x) = \sum_{j=1}^{n} C_j(x) + r_n(x) \qquad \text{[B.3]}$$

Once the IMFs are extracted, Hilbert transform can be carried out for each IMF. For the first IMF $C_1(x)$, the Hilbert transform is given as

$$D_1(x) = \frac{1}{\pi} P \int_{-\infty}^{\infty} \frac{C_1(\tau)}{x - \tau} d\tau \qquad \text{[B.4]}$$

where P is the Cauchy principle value and τ is the sample location. This produces an analytical function $Z_1(x) = C_1(x) + iD_1(x) = a(x)e^{i\theta(x)}$, where $i = \sqrt{-1}$, a is the instantaneous amplitude, $a(x) = \sqrt{\left(C_1^{\,2} + D_1^{\,2}\right)}$, and θ is the instantaneous phase function, $\theta(x) = \tan^{-1}\left(\frac{D_1}{C_1}\right)$. Thereafter,

the instantaneous frequency is calculated as $\omega(x) = \frac{d\theta(x)}{dx}$. The final form of data can be written as

$$Y(x) = \sum_{j=1}^{n} a_j(x) e^{i\int_{\tau=0}^{x} \omega_j(\tau) d\tau} \quad [B.5]$$

However, one limitation of Hilbert transform is that it cannot satisfy the Bedrosian theorem, which states that the Hilbert transform of the product of a low-pass and a high-pass signal with non-overlapping spectra is given by the product of the low-pass signal and the Hilbert transform of the high-pass signal (Bedrosian, 1963). According to the theorem, H [$e(x)$ $C(x)$] = $e(x)$ H [$C(x)$], only if the Fourier spectra for envelope function $e(x)$, and IMF function , $C(x)$ are totally disjointed in frequency space when the amplitude of the transform varies slowly. However, this condition is seldom satisfied in nature. Therefore, normalization, as given by the iterative process can overcome this problem (Huang, 2005). In doing so, the envelopes, $e_i(x)$ are defined by the extrema points of the IMFs, $C_j(x)$ and the normalization is given by the iterative process

$$f_1(x) = C_j(x)/e_1(x),\ f_2(x) = f_1(x)/e_2(x), \quad \text{till } f_n(x) = f_{n-1}(x)/e_n(x) \quad [B.6]$$

when $e_n(x)$ is unity and $e_i(x)$ is obtained from $f_{i-1}(x)$ by interpolation process (Huang and Milkereit, 2009). Therefore, the IMFs can be expressed as

$$C_j(x) = a_j(x)\cos\left(\int_{\tau=0}^{x} \omega_j(\tau) d\tau\right) \quad [B.7]$$

and the original spatial series can be expressed as

$$Y(x) = \sum_{i=1}^{n} a_j(x)\cos\left(\int_{\tau=0}^{x} \omega_j(\tau) d\tau\right) + r_n(x) \quad [B.8]$$

which is an instantaneous amplitude and instantaneous frequency modulated signal. The amplitude and the frequency both are function of time. Therefore, the energy (squared amplitude) can be expressed as a joint function of space and frequency $H(\omega, x)$. The frequency is converted to the scale (= sampling interval / frequency). The graphical representation of space–frequency–energy [x, $\omega(x)$, $a(x)$] (known as Hilbert spectra) through contour plot can provide a better visualization of scale–location specific soil spatial variability.

B.4 Comparison of CWT and HHT Using Artificial Signals

A spatial series of various soil and landscape properties can often be characterized as being nonstationary and nonlinear. At the same time, these properties may show a quasi–cyclic behavior in rolling and undulating landscapes (Si and Farrell, 2004). Therefore, to compare CWT and HHT, four artificial series; stationary–linear, stationary–nonlinear, nonstationary–linear, and nonstationary–nonlinear, composed of three cosine waves with different frequencies (80, 25 and 10 Hz) were used as a surrogate spatial series for measurements taken along a rolling and undulating landscape. The artificial series were generated with 1024 points regular interval in space and were similar to the form of series used by Yan and Gao (2007). The stationary–linear series can be identified as a constant function of frequency and is written as $Y^{[1]}(t)$ = $\cos(2\times\pi\times80\times x) + \cos(2\times\pi\times25\times x) + \cos(2\times\pi\times10\times x)$, where x = 0, 1, 2, ..., 1023 (Figure B.3A). Therefore, the frequencies of the spatial series were 80, 25, and 10 Hz. The spatial frequency can be converted to spatial scale.

To generate a nonlinear series, we have used the mathematical model $Y(x) = \cos(\omega x + \varepsilon \sin 2\omega x)$, which is derived numerically from the Duffing equation, a classic form of the simplest nonlinear equation. Hence, the stationary–nonlinear series can be written as $Y^{[2]}(x) = \cos(2\times\pi\times80\times x + 0.3\times\sin(2\times\pi\times160\times x)) + \cos(2\times\pi\times25\times x + 0.3\times\sin(2\times\pi\times50\times x)) + \cos(2\times\pi\times10\times x + 0.3\times\sin(2\times\pi\times20\times x))$ (Figure B.3B). The sine function within the cosine function creates intra-wave or subcyclic oscillations, which can be identified by the steady oscillations along the space axis. Therefore, the nonlinearity is identified from the changing period of the oscillations thus making the scale locally unpredictable (Gautama et al., 2004).

The nonstationary–linear series was generated by using the square root of time, which creates gradual changes in frequency or inter-wave (supercyclic) frequency modulation over space. The series can be written as $Y^{[3]}(x) = \cos(2\times\pi\times80\times x^{0.5}) + \cos(2\times\pi\times25\times x^{0.5}) + \cos(2\times\pi\times10\times x^{0.5})$, which has a smoothly decreasing amplitude with space (Figure B.4A). The nonstationary–nonlinear series can be written as $Y^{[4]}(x) = \cos(2\times\pi\times80\times x^{0.5} + 0.3\times\sin(2\times\pi\times160\times x^{0.5})) + \cos(2\times\pi\times25\times x^{0.5} + 0.3\times\sin(2\times\pi\times50\times x^{0.5})) + \cos(2\times\pi\times10\times x^{0.5} + 0.3\times\sin(2\times\pi\times20\times x^{0.5}))$. The series is in a form of the numerically derived Duffing equation with frequency modulation over space (Figure B.4B). Therefore, the series contains both intra-wave

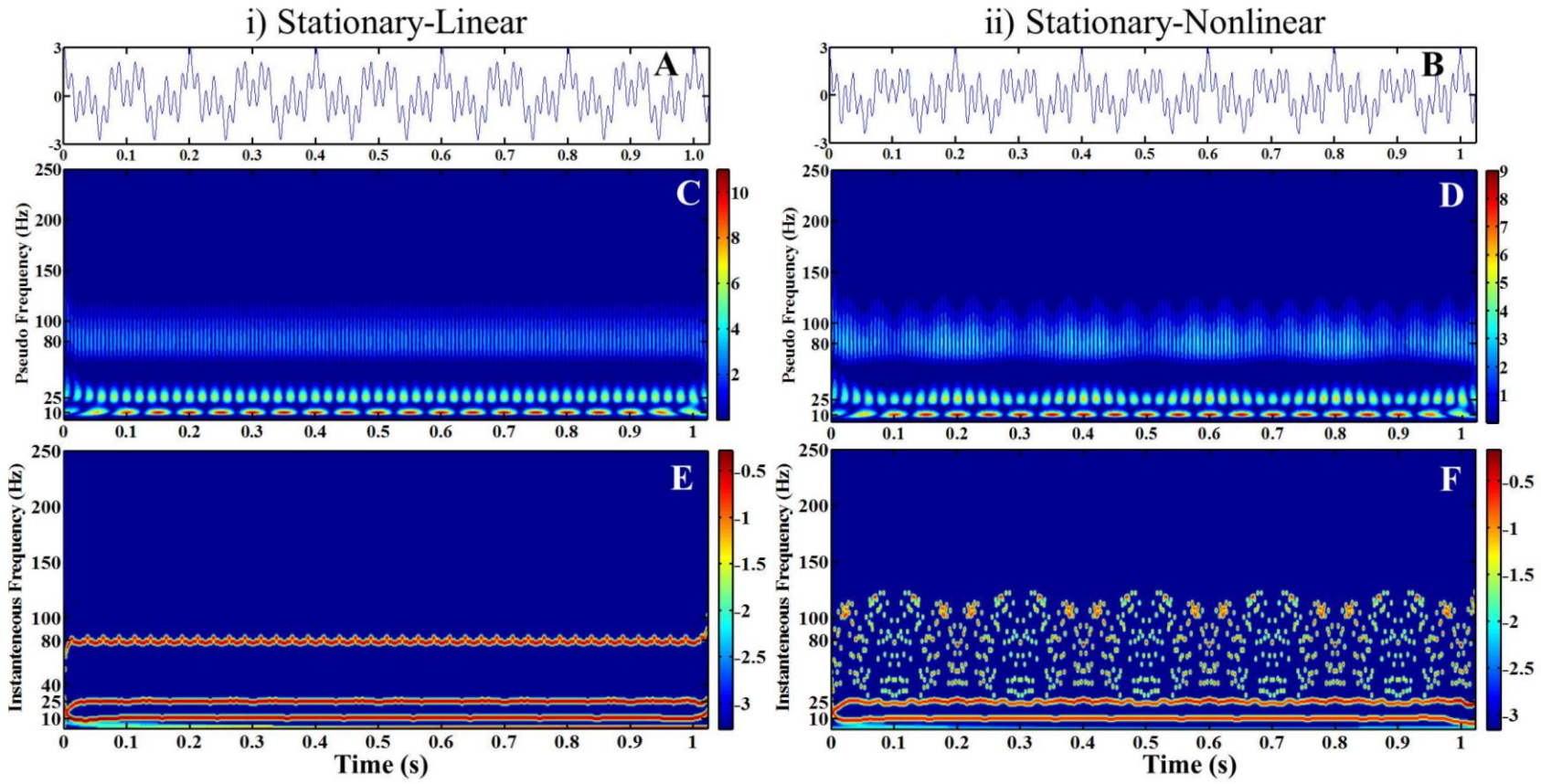

Figure B.3. A) Stationary-linear signal and its C) wavelet spectra, E) Hilbert spectra are shown. B) Stationary-nonlinear signal and its D) wavelet spectra and F) Hilbert spectra.

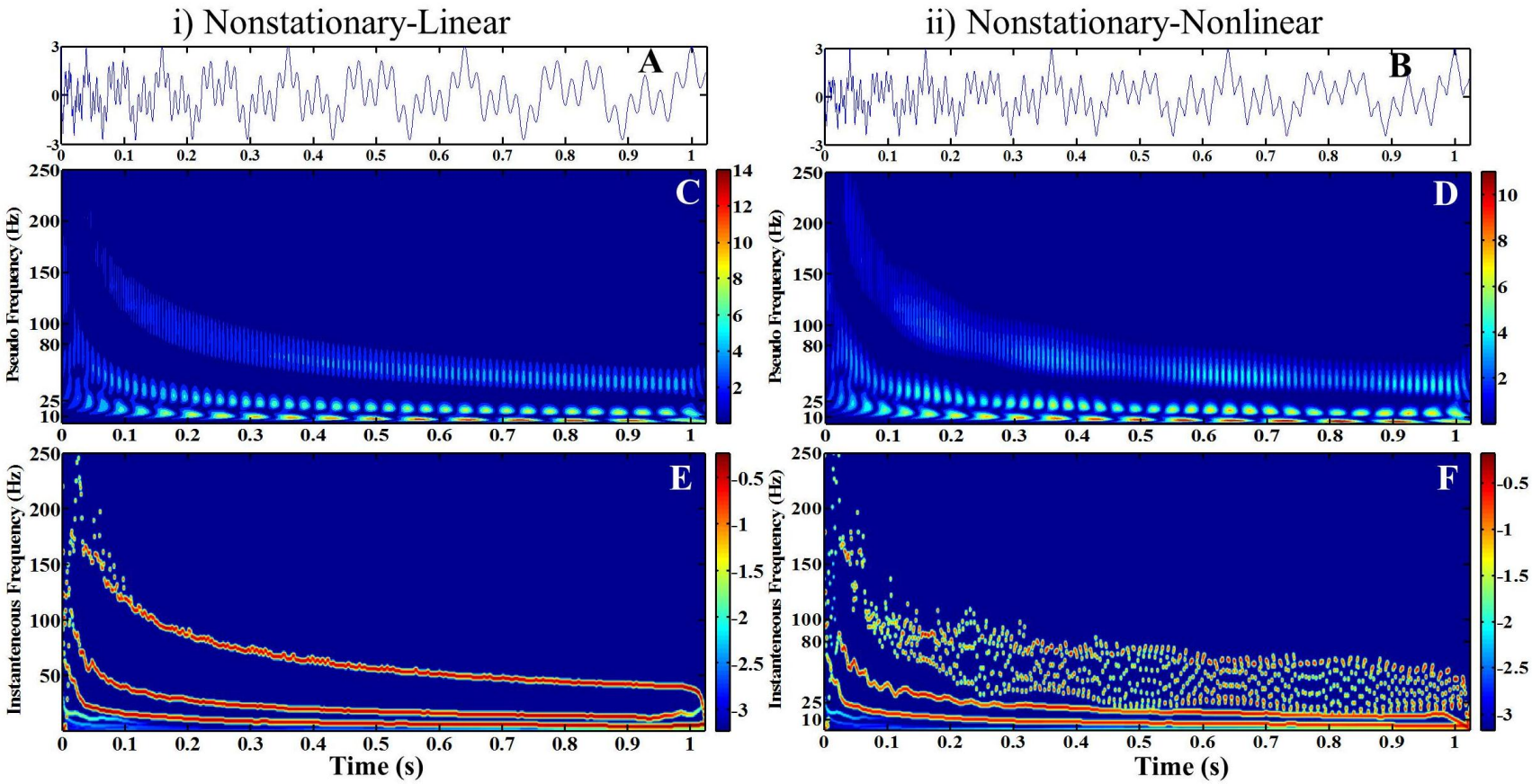

Figure B.4. A) Nonstationary-linear signal and its C) wavelet spectra, E) Hilbert spectra are shown. B) Nonstationary-nonlinear signal and its D) wavelet spectra and F) Hilbert spectra.

and inter-wave frequency modulation and can be identified by the time varying oscillations with decaying envelope of the amplitude (Yan and Gao, 2007).

The CWT was performed in MATLAB (MathSoft Inc.) using the built-in wavelet toolbox. In the transform, the scale is converted to pseudo–frequency by a MATLAB internal function 'scal2frq' based on $F_a = F_c / (a \cdot \Delta)$, where a is a scale, Δ is the sampling period, F_c is the center frequency in Hz and F_a is the pseudo–frequency corresponding to the scale a, in Hz. The wavelet power spectrum was plotted as a function of space and frequency. The HHT was also performed in MATLAB (MathSoft Inc.) using the code written by Dr. Wu (available at http://rcada.ncu.edu.tw/research1_clip_program.htm). For display purposes, a Gaussian weighted filter was applied to the spectrum skeleton obtained directly from HHT, which showed the energy as a function of space and frequency.

CWT identified the variations in the stationary–linear series into three components ranging over a diffuse band of frequencies with varying color (Figure B.3C). Although there was only one frequency component of 80 Hz, the CWT identified the frequency over the range of 60 to 120 Hz. Similarly, a range of frequencies was identified for 25 and 10 Hz frequency components (Figure B.3B). However, HHT identified the frequency components of the signal exactly at those particular frequencies and not over a range of frequencies (Figure B.3E). Similarly, for the stationary–nonlinear series, CWT produced similar spectra identifying three bands of frequency components (Figure B.3D). Wavelet analysis assumes the series is linear, and therefore, is not able to identify the localized changes in the frequency caused by subcyclic oscillations. Each frequency component was identified as a diffuse frequency band. However, HHT was able to identify the small changes in the frequency created by nonlinearity (Figure B.3F) as it considers both sub and supercyclic frequencies (Huang et al., 1998; Kijewski-Correa and Kareem, 2006). The changes in the frequency was identified as discrete points with varying color intensities over a range of frequencies as opposed to distinct bands, thus providing a clearer indication that nonlinearity exists. The discrete points for the other two frequencies were not show up in the figure due to the linear representation of frequency scales.

For the nonstationary–linear series, CWT identified the gradual change in frequencies over time as expected (Figure B.4C). However, a range of frequencies was observed for each particular frequency component. A gradual change in color intensity was also observed within a

particular frequency band indicating a change in energy content of that frequency component over time (Figure B.4C). Conversely, HHT was able to identify different frequency components as it varied over scape with similar energy representation (Figure B.4E). In addition, variations at 200 Hz were identified in HHT (Figure B.4E), while the CWT spectra were not able to discern any kind of variations at that particular frequency (Figure B.4C). The CWT spectra of nonstationary–nonlinear series identified three gradually changing frequency bands with differing color intensities for three frequency components (Figure B.4D). Increasing color intensity was also observed within the band of frequencies. However, the changes in the frequency due to nonlinearity were not identified from CWT spectra. The gradual change of frequency (inter-wave) due to nonstationarity and the localized changes (intra-wave) in the frequency due to nonlinearity were clearly identified in HHT (Figure B.4F).

In CWT, continuous comparison of the sinusoid mother wavelet within the signal produces redundant information of the signal content. Therefore, the variation due to a particular frequency is spread over a diffuse band of frequencies (Lau and Weng, 1995; Percival and Walden, 2000). However, the spread of the frequency band can be modified to certain extent by altering the center frequency of the mother wavelet (Kijewski-Correa and Kareem, 2006). Given the aforementioned qualities of HHT (no *a* priori basis, empirical, data driven), the technique was much better suited in resolving variations at each individual frequency. Spreading the frequency information content over a range of frequencies in CWT can lead to erroneous conclusions. In addition, the CWT could not identify the subcyclic frequency changes due to nonlinearity and produced similar spectra for linear and nonlinear series. Conversely, the calculation of instantaneous amplitude and frequency allowed HHT to identify the variations in a nonlinear series due to sub and supercyclic frequencies more accurately (Huang et al., 1998; Kijewski-Correa and Kareem, 2006). The instantaneous frequency can also be calculated by modifying the mother wavelet (Kijewski-Correa and Kareem, 2006). However, this is not the commonly used technique.

In spite of equal amplitude, CWT identified different frequency components with varying color intensities, indicating unequal energy levels associated with those frequency components. For example, CWT identified the small frequency component with high energy (red color) and high frequency component with low energy (light blue color). Distortion of wavelet power

spectra in favor of large scales, or low frequencies, has been previously identified in the literature, and has been termed as spectral 'bias' (Torrence and Compo, 1998; Liu et al., 2007). The discrimination in identifying the energy may mislead the researcher when explaining scale–location specific variability. However, HHT did not show any such bias and equally identified the variations associated with each frequency component.

B.5 Comparison of CWT and HHT Using Spatial Series of Soil Properties

Two examples of soil properties, organic carbon (OC in %) and soil water storage (SWS in cm) were considered to compare CWT and HHT. Organic carbon (0 to 20 cm) and SWS (0 to 140 cm) was measured along a transect of 128 points (576 m long) from St. Denis National Wildlife Area, Saskatchewan, Canada. The landscape of the study site is dominantly hummocky with a complex sequence of slopes of 10 to 15 % extending from rounded depressions to complex knolls and knobs. The soil of this area is classified as a Dark Brown Chernozem (following the Canadian System of Soil Classification), which is developed from a moderately fine to fine textured, moderately calcareous, clayey glacio–lacustrine deposit and modified glacial till (Acton and Ellis, 1978). The climate of this area is dry semi–arid with the mean annual air temperature of 2°C with the monthly mean of −19°C in January and 18°C in July. The 90-year average precipitation is 360 mm, 84 mm of which occurs as snow (AES, 1997). The vegetation of the study site is grass.

Organic carbon in the collected soil samples was analyzed using LECO–C6235 carbon determinator (LECO Corp., St. Joseph, MI, USA) (Figure B.5A). Soil water was measured up to 140 cm with 20 cm vertical depth intervals using a neutron probe (model– CPN 501 DR Depthprobe, CPN International Inc., Martinez, CA). Surface (up to 20 cm) soil water was measured using time domain reflectometry (TDR) probe and a metallic cable tester (Model 1502B Tektronix, Beaverton, OR). Soil water (Figure B.5E) was calculated from the site-specific calibration equation for neutron probe and the standard calibration equation for TDR (Topp and Reynolds, 1998). The SWS was measured on several occasions over a four–year period (2007 to 2010). The current case study will use one measurement collected on 6 April 2010 as an example to compare the methods. A topographic survey of the site was completed by Light Detection and Ranging (LiDAR) and a Trimble Pro XRS Global Positioning System (Trimble Navigation,

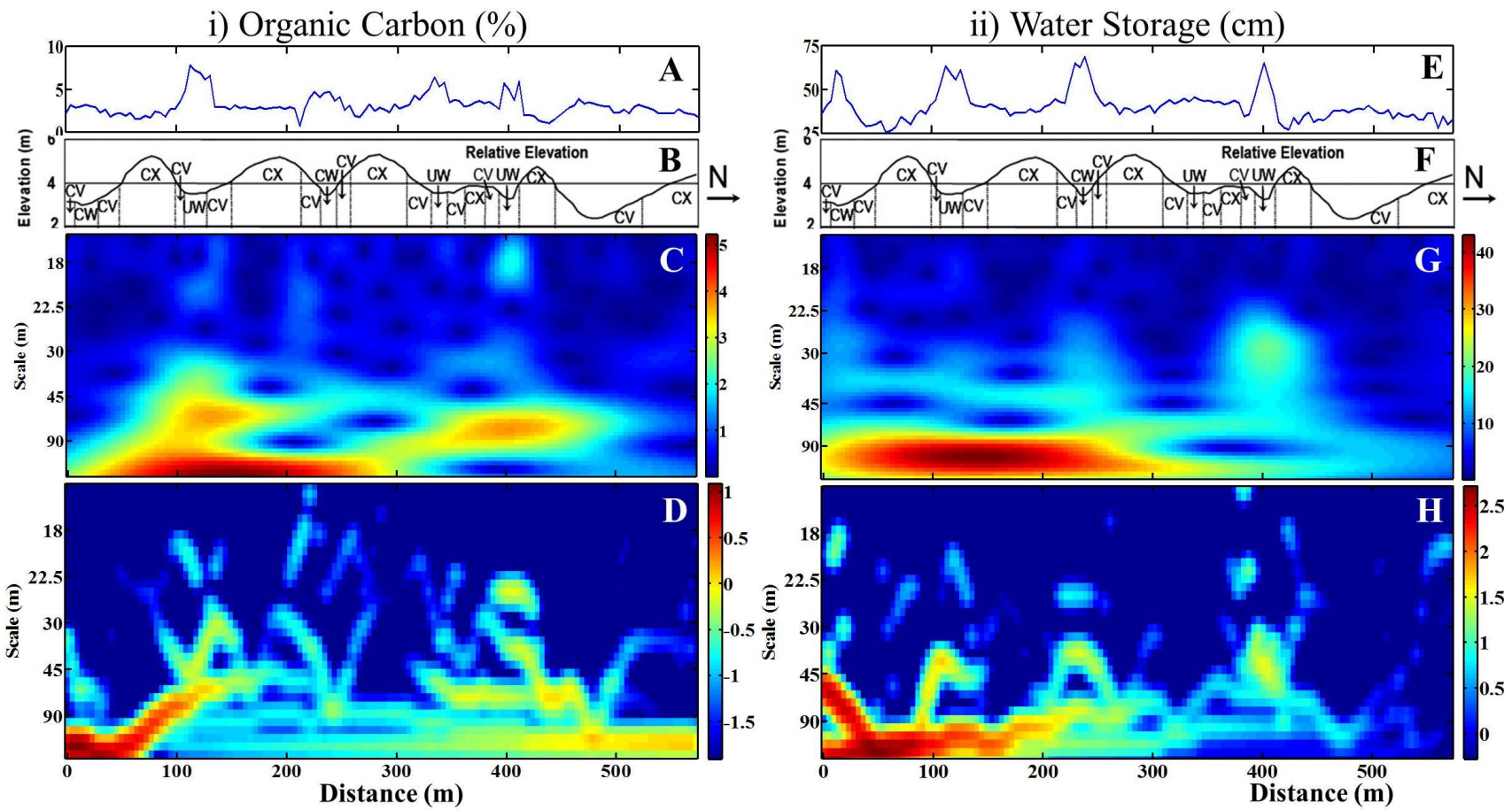

Figure B.5. A) Spatial distribution of organic carbon (%) along B) the transect with different landform elements are shown. C) The Wavelet spectra and D) Hilbert spectra of organic carbon. E) Spatial distribution of soil water storage (cm) along F) the transect with different landform elements. G) Wavelet spectra and H) Hilbert spectra of soil water storage.

Sunnyvale, CA). Different landform elements along the transect were also identified as concave (CV), convex (CX), cultivated wetlands (CW) and uncultivated wetlands (UW) (Figures B.5B, B.5F). The CWT and HHT were performed following the same methods described earlier.

Wavelet spectra showed strong variations (denoted in red) in the spatial distribution of OC within the scale range of 45 to 90 m at the locations of 100 to 180 and 350 to 460 m along the transect (Figure B.5C). In addition, strong variation at scales > 90 m were evident over most of the first half of the transect. Moderate variations (light blue) were also observed at small scales (< 30 m) at almost all locations (Figure B.5C). In contrast, the Hilbert spectra identified the variations with much better resolution with respect to both scale and location (Figure B.5D). For example, HHT demonstrated that the variations at 350 to 460 m were actually a moderate to strong variation at the scale of 50 to 70 m concentrated at the locations of 350 to 400 and 420 to 460 m (Figure B.5D). The wide band of variation from 100 to 180 m as shown by CWT was further resolved by HHT as being concentrated from 0 to 125 m.

The redundancy and smoothing over multiple scales and space of CWT identified a wider range of variability than what exists. In contrast, HHT more precisely identified the variations associated with very specific locations. For example, the variations at the scales of 30 to 45 m concentrating at the locations of 100 to 140 and 390 to 420 m (Figure B.5D) were attributed to the variations due to landform elements present within those two depressions (Figure B.5B). Similarly, the variations at the scales > 90 m can be attributed to the variations due to alternating knolls and depressions, or the topographical variations. The topographical variations in the dataset occur over a few tens of meters. The precision of HHT allows for a more exact interpretation of landscape / OC interactions, whereas the smoothing of CWT precludes any exact interpretation.

The strongest variations identified by CWT (dark red) in the spatial distribution of SWS were at scales > 90 m, and were concentrated in the first half of the transect (Figure B.5G). However, HHT further resolved these variations to very specific scales and locations (Figure B.5H). Similarly, while CWT identified a moderate variation (light blue color) at the 20 to 80 m scale at the locations of 375 to 450 m (Figure B.5H), HHT was able to localize the variation more precisely to occur at the 30 to 60 m scale from 390 to 420 m (Figure B.5H). The artificial diffusion of scale and location as given by CWT may provide misleading results when

identifying the scale and location specific soil spatial variation. There were many random variations at small and medium scales, which may be indicative of any possible existence of intra-wave frequencies resulting from nonlinearity. However, a more rigorous testing of nonlinearity in the spatial series is necessary and requires future work.

The lack of precision in scale at large scales from CWT can be a problem in applications. For example, if one is interested in selecting appropriate satellite image resolution based on the dominant scales of variation identified from CWT, one could miss the dominant scale of variations completely due to the imprecise scale information of CWT. In that case, HHT would be more desirable. Another advantage of HHT lies in its ability to differentiate nonstationarity and nonlinearity. However, a more extensive research is necessary with different types of possible spatial series. Though, we have only considered four artificial series and two realistic example of soil properties showing the cyclic and quasi-cyclic variations along a transect or in one dimension of space, it can be valid for other type of spatial series. However, a more extensive comparison is still necessary considering different other case scenarios.

B.6 Conclusions

In this study, a comparison was made between the well–established CWT and newly introduced HHT in the isolation of scale–location specific variability of soil properties. Four artificial signals (stationary–linear, stationary–nonlinear, nonstationary–linear, and nonstationary–nonlinear) composed of three cosine waves with equal amplitude but different frequencies were analyzed using CWT and HHT. While CWT identified a range of frequency bands for a particular frequency present in the signal, HHT identified the frequency exactly. The redundancy in CWT analysis and the smoothing of the wavelet function identified a frequency band, rather than correctly identifying the exact frequency. In addition, in spite of equal amplitude, CWT placed a greater emphasis on larger scales than on smaller scales. In CWT, a gradual change in the energy representation was also observed within a frequency component. The deficiencies of CWT were clearly contrasted with the superiority of HHT for analyses of this type. The adaptive basis of HHT did not consider any mathematical function to extract the variations and worked directly with the data, thus allowing frequencies to be represented equally at all locations. Though CWT separated the nonstationary variations, it could not identify the

nonlinear variations in the data, which were present as subcyclic variations in frequency. Alternatively, HHT identified the change in frequencies locally (subcyclic variations in frequency) and was therefore able to address nonlinearity in the analysis. Using HHT, the scale–location specific variations were better resolved, while nonstationary and nonlinear soil spatial variations were analyzed concurrently. Similarly, in comparing these methods using soil properties as a case study, HHT identified the variations in OC and SWS with much better resolution in terms of both scale and location. The variations separated through HHT more easily lent themselves to physical interpretation than those from CWT.

APPENDIX C

C.0 APPLICATION OF CONTINUOUS WAVELET TRANSFORM IN EXAMINING SOIL SPATIAL VARIATION: A REVIEW

C.1 Preface

Soil spatial variation can be partitioned into frequencies (scale) and positions (location) by the wavelet transform. This review focuses mainly on different applications of the continuous wavelet transform in identifying the scale and location dependence of soil attributes. The main discussion focussed on the application of i) wavelet spectra in analysing soil spatial variation and ii) wavelet coherence in examining scale and location-specific relationship between two variables.

C.2 Introduction

Soil varies considerably from location to location (Nielsen et al., 1973). Information about soil spatial variation is necessary for environmental prediction (Trangmar et al., 1985), soil-landscape process modelling (Burrough, 1983; Corwin et al., 2006), precision agriculture (Goderya, 1998), soil quality assessment (Heuvelink and Pebesma, 1999; McBratney et al., 2000) and natural resources management. Over the last thirty years, much effort has been made to quantify soil spatial variation. Soil is a function of environmental factors such as parent material, climate, living organisms, relief and time (Jenny, 1941). These factors work independently or in combination at a range of spatial scales to produce different types of soil. Each soil type occupies an area rather than a point, therefore, soil properties measured at places close together are more likely to be similar than those at places further apart (Gajem et al., 1981; Viera et al., 1982; Oliver, 1987). This is known as spatial autocorrelation or spatial dependence.

Sometimes features of the soil repeats at a certain distance beyond its spatial dependence. Repetition or quasi-cyclic behaviour of soil can arise from features in the topography (Kachanoski et al., 1985), geology or parent material, tillage operations (Perfect and Caron, 2002), and cultivation practices (van Wesenbeeck et al., 1988). The cyclic behaviour of soil properties is known as periodicity.

The change in soil properties can be also smooth and predictable over space resulting in linear or nonlinear spatial trends, which are referred to as non-stationary. Non-stationarity can arise from the effects of topography, lithology, parent material, climate and vegetation (Van Wambeke and Dulal, 1978), resulting in distinct strata, such as different types of soil. The mean and/or variance of the soil properties in one stratum may differ from that of another.

Table C.1. Some basic information on geostatistics, spectral analysis and wavelet transform.

	Geostatistics	Spectral analysis	Wavelet transform
Measurement basis	Semivariance (autocorrelation)	Sine and cosine functions (Fourier transform)	Mother wavelet (Fast Fourier transform)
Presentation	Semivariogram	Spectral plot	Wavelet spectra
Measurement result	Spatial dependence	Periodicity	Scales and locations
Type of information	Global	Global	Local
Stationarity assumptions	Yes (Intrinsic)	Yes (Second order)	No

Stationary or nonstationary soil spatial variation can be represented by a number of cyclic Fourier series with different periods. Each series with a characteristic frequency and period can represent an underlying process creating the variability (Si, 2003). When one or a few processes contribute the most to the total variance, we want to know their periods or scales to aid sampling and management, and to gain insight into soil behaviour. Some processes may be dominant at one scale, others at another scale, making the overall variation scale dependent. Processes operate at a range of spatial scales that are superimposed on one another, which sometimes result in nested variation.

Soil spatial variation has long been recognized. Earlier efforts to characterize the spatial variation mainly focused on spatial similarity in properties over a given area and did not quantify the variation of soil properties with respect to their spatial arrangement, spatial dependence or periodicity (Goderya, 1998). Spatial dependence can be quantified by the variogram (Matheron, 1963) from the autocorrelation of a variable. A variogram helps in revealing patterns in data

series and identifying the scale of major ongoing processes (Si et al., 2007). However, a necessary assumption in calculating a meaningful variogram is that the variable is spatially stationary and the sum of squared differences depends only on the separation of measurements, not on their absolute locations (Table C.1; Oliver and Webster, 1991; Goderya, 1998). The periodicity in the spatial variation can be quantified from the spectral analysis, which approximates a spatial data series by a sum of sine and cosine functions. Each of the functions has an amplitude and a frequency or period. The squared amplitude at a given frequency is equal to the variance contribution of the frequency component to the total variance in the spatial series (Webster, 1977; Shumway and Stoffer, 2000; Brillinger, 2001). The spikes and peaks in the frequency domain signify the cycle or repetition in the variation, whereas equal variances across all scales or frequencies indicate a random spatial distribution of the variables.

Frequency domain analysis or spectral analysis assumes that a spatial series is second-order stationary (i.e. the mean and variance of the series are finite and constant; Table C.1). This assumption is generally stricter than the intrinsic stationarity assumptions of geostatistics. Both geostatistical and spectral analyses mainly deal with global information or the mean states (Si, 2008; Table C.1). However, soil spatial variations are sometimes non-stationary and different frequency regimes representing different processes will be localized in space relative to the entire spatial/time domain (Si, 2003). Non-stationarity excludes direct application of geostatistics and spectral analysis. Although there are methods to remove trends, such as removing fitted polynomials from the data, selection of the functional form of the trends (such as the order of polynomials) is quite arbitrary. Furthermore, the physical meaning of the detrended data can be difficult to interpret. Furthermore, these natural trends, localized features or transient features are an integral part of the nature of soil and need to be analysed to understand soil-related landscape processes. Therefore, a method is required that can accommodate trends in data. Wavelet analysis (Mallat, 1999), an advanced mathematical method, can be used to examine both trends and localized features of soil processes by partitioning the sample variation into positions (or locations) and frequencies (or scales) (Si, 2003; Lark et al., 2004; Si and Farrell, 2004). The objective of this review is to demonstrate what wavelet analysis can do in examining the scale and location dependent soil spatial variation. To do this, a selection of spatial data series was taken from literature published in the soil science community.

C.3 Wavelet and Wavelet Transform

A wavelet is a mathematical function that can be used to study multi-scale (Bosch et al., 2004), stationary/nonstationary processes occurring over finite spatial and temporal domains (Lau and Weng, 1995; Graps, 1995). The mathematical function represents a finite small waveform, unlike the Fourier series that stretches infinitely (Graps, 1995). Wavelet analysis has been applied widely in diverse fields of science, such as seismic signal detection, atmospheric turbulence, image processing, optics, data compression, simulation, quantum mechanics, chaos, fractal and medical research and more. Wavelets have also been used in the analysis of one dimensional spatial data series (Lark and Webster, 1999; Bosch et al., 2004; Lark et al., 2004; Si and Farrell, 2004; Parent et al., 2006; Biswas et al., 2008; Furon et al., 2008) or two dimensional spatial field (Neupauer and Powell, 2005; Neupauer et al., 2006, Watkins et al., 2009) in soil science.

Basic tools in wavelet analysis are the integral wavelet transform and wavelet series. The integral wavelet transform is the convolution with respect to the dilation of some functions and known as the 'basic wavelet', whereas the wavelet series is expressed in terms of a single function by means of two simple operations: binary dilations and integral transformations (Chui, 1992). For example, if we measure a spatial series y_i at location x_i (i = 1, 2, ... , m) along a transect, the integral wavelet transform is defined as:

$$W(s,\tau) = \int_{-\infty}^{\infty} y(x)\overline{\psi}_{s,\tau}(x)\mathrm{d}x, \qquad [C.1]$$

where $\psi_{s,\tau}(x) = \frac{1}{\sqrt{s}}\psi_{s,\tau}\left(\frac{x-\tau}{s}\right)$. [C.2]

The function $\psi(x)$ is called as a wavelet function or 'basic wavelet' and $\overline{\psi}_{s,\tau}$ is the complex conjugate. The parameter s is the dilation-contraction factor and τ is the temporal or spatial translation of the wavelet function (Kumar and Foufoula-Georgiou, 1997; Si, 2008). There are many basic functions with different shapes and characteristics that can be used in the wavelet transform, whereas Fourier transform uses just the sine and cosine functions (Graps, 1995).

Table C.2: Characteristics of CWT, DWT, and MODWT

	CWT	DWT	MODWT
Scale	Continuous	Dyadic	Dyadic
Redundancy in information	Yes	No	Yes
Orthogonality	No	Yes	No
Global wavelet covariance (frequency domain)	No	Yes	Yes
Global wavelet correlation (frequency domain)	No	Yes	Yes
Cross wavelet spectra (frequency and spatial domain)	Yes	No	No
Wavelet coherency (frequency and spatial domain)	Yes	No	No
Significance testing	Comparatively difficult (requires advanced computational power)	Easy	Easy
Usefulness	Scale analysis, signal or noise extraction	Decomposition and reconstruction of signal, signal compression, noise reduction	Scale analysis, noise extraction
Restriction	Continuous scales, large number of coefficients, require advanced computational power	Coefficients represent range of scales, predefined scales	Coefficients overlap at end, requires large number of data, predefined scales

In the analysis, wavelet coefficients are calculated at each possible scale and location. Therefore, the wavelet transform turns a one-dimensional data series into a two-dimensional matrix. The continuous wavelet transform (CWT) partitions the spatial series into continuous scales and locations by interpolating between them. At the same time, it preserves all the information in the original data series giving us the possibility of gaining insight into the original data (Shu et al., 2008). The wavelet coefficients at consecutive scales and locations carry common information and provide a redundant representation of a signal (Table C.2). This redundancy or overlapping of the information can produce enhanced information of scale localization, which means that the different scale processes can be represented simultaneously.

On the other hand, the discrete wavelet transform (DWT) is a judicious sub-sampling from the CWT with dyadic scales or the scales with two fold increments (Percival and Walden, 2000; Table C.2). The wavelet coefficients at different scales and locations are orthogonal to each other and contain no redundant information. Thus, a spatial series can be represented by a minimum number of wavelet coefficients at fixed scales or the scales with only two fold increments, not continuously. The independence of wavelet coefficients of the DWT at different scales enables us to compare the coefficients by an analysis of variance, whereas the dependence among the wavelet coefficients of the CWT makes it less straightforward to test the statistical significance between wavelet coefficients (Si and Zeleke, 2005; Table C.2). However, with the advancement of computational power, various methods have been developed to test the statistical significance of continuous wavelet spectra, which is discussed in brief at the later part of this review. The orthogonal or discrete coefficients in the DWT help in the decomposition and reconstruction of a time series with minimal bases, synthesis and compression of signals and reduction of noise (Lau and Weng, 1995). However, in DWT, the scales are analyzed only at octaves (integer powers of 2) and not at the voices (fractional powers of 2) that may not always yield most physically meaningful scale analysis (Lau and Weng, 1995). On the contrary, the continuity of coefficients over scales in the CWT yields enhanced information on timescale localization providing a better scaling analysis and the extraction of signal or noise (Lau and Weng, 1995; Si 2003; Grinsted et al., 2004). Some scale and location information can also be extracted discretely from the DWT, but redundancy in the CWT allows better representation of the signal's information content (Farge, 1992; Lau and Weng, 1995; Keitt and Fischer, 2006; Furon et al., 2008; Table E.2). A comparison of DWT and CWT with examples is given by Shu et al. (2008). In addition, the DWT and the maximal overlap discrete wavelet transform (MODWT) can calculate global wavelet covariance and global wavelet correlation coefficients to describe linear relationships between two data series in the frequency domain (Percival and Walden, 2000). However, the scale and location specific cross spectra and wavelet coherency in both frequency and spatial domains are readily available using CWT, but not DWT or MODWT. CWT, DWT, and MODWT are a suite of tools for different purposes. Each has its advantage and disadvantage. It is our opinion that CWT is particularly suited for scale analysis, particularly for elucidating scale- and location- dependent relationships between two variables. Therefore, in the following,

we limit the scope of our discussion to the application of the CWT in elucidating soil spatial variation. The details of the methodology or theory of the CWT is readily available in literature and beyond the scope of our discussion. A detailed description of wavelet analysis can be found in Farge (1992), Kumar and Foufoula-Georgiou (1993, 1997) and many more. For readers' interest, detailed information on the DWT can be found in Lindsay et al. (1996), Lark and Webster (1999, 2004), and on wavelet packet analysis in Lark (2006, 2007) which is beyond this review.

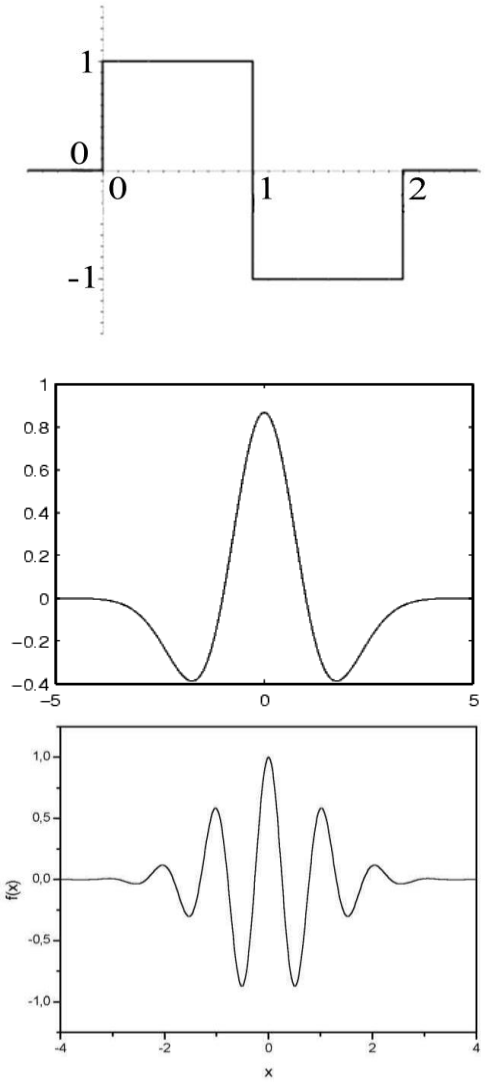

Figure C.1. A typical example of a) Haar wavelet, b) Mexican Hat wavelet and c) Morlet wavelet (real part).

C.4 Methodology

Commonly used wavelet functions, also known as mother wavelets, for the CWT include the Haar, Mexican hat and Morlet wavelets (Figure C.1) (Torrence and Compo, 1998). The Haar wavelet is simple, asymmetric and detects sharp changes in the data series, whereas the Mexican hat wavelet is a real symmetric function that detects peaks and valleys. A Morlet wavelet is a complex symmetric function that can also detect peaks and valleys. The wavelet transform using a Morlet wavelet results in complex wavelet coefficients, while the same transform using a Mexican hat wavelet produces real wavelet coefficients. A complex wavelet coefficient is in the form of $a + ib$, where a is the real and b is the imaginary component of the coefficient and $i = \sqrt{-1}$. Generally, a complex number extends the idea of one dimensional line to two-dimensional complex plane using the one dimension line for the real part and a vertical axis to the plot for the imaginary part. Therefore, the phase information that can be extracted from the imaginary part of the wavelet coefficients is conserved in the wavelet transform with a Morlet wavelet, but not with a Mexican hat. The real and imaginary part of the Morlet wavelet is directionally dependent and can be used to identify the dominant orientations in a random field. It can also identify the anisotropy in two-dimensional fields. The details of the anisotropic Morlet wavelet can be found in Neupauer and Powell (2005) and Neupauer et al. (2006). In general, the directional Morlet wavelet can be represented as (Torrence and Compo, 1998):

$$\psi(\eta) = \pi^{-1/4} e^{i\varpi\eta - 0.5\eta^2} \qquad [C.3]$$

where ω is the dimensionless frequency and η is the dimensionless space. This mother wavelet function can be stretched in space (x) at different scales (s). The CWT can be defined as the convolution of a spatial series Y_i of length N ($i = 1, 2, \cdots, N$) along a transect with equal increments of distance δx (Torrence and Compo, 1998).

$$W_i^Y(s) = \sqrt{\frac{\delta x}{s}} \sum_{j=1}^{N} Y_j \psi\left[(j-i)\frac{\delta x}{s}\right] \qquad [C.4]$$

which can be implemented through a series of Fast Fourier Transform (FFT). Wavelet coefficients, $W_i^Y(s)$, are expressed as $a + ib$, where a and b are the real and imaginary components of $W_i^Y(s)$, respectively. The magnitude of the wavelet coefficients for a given scale and location is a measure of the energy at that scale and location (Qi and Neupauer, 2008). As

for the Fourier power spectrum, the wavelet power spectrum is defined as $\left|W_i^Y(s)\right|^2$. As wavelet coefficients are a function of the location and width (or scale), a better visualization of wavelet coefficients (or power spectra) can be given by a contour plot with location on the horizontal axis and scale on the vertical axis. The wavelet spectrum at a location and scale represents the local variance, and the sum of all local spectra is equal to the total variance. Therefore, the wavelet power spectrum can be used to examine the spatial variation of soil properties at different scales and at different locations.

If wavelet spectra in the space-scale domain are like variances in the spatial domain, cross wavelet spectra in the space-scale domain are equivalent to the covariance in the spatial domain. Wavelet cross spectra are the product of the spectra of two variables at a given scale and location (Si and Zeleke, 2005). If we have the wavelet coefficients, W_i^X and W_i^Y for two spatial series, *X* and *Y*, respectively, the cross wavelet power spectrum can be calculated from Equation C.5.

$$\left|W_i^{XY}(s)\right| = \left|W_i^Y(s)\overline{W_i^X(s)}\right|, \qquad [C.5]$$

where $\overline{W_i^X}$ is the complex conjugate of W_i^X and the complex argument of W_i^{XY} can be interpreted as the local relative phase between X_i and Y_i in the spatial frequency domain (Si and Zeleke, 2005).

While, wavelet cross spectra are similar to the covariances in the spatial domain, the wavelet coherence spectra are similar to the coefficients of determination in the space-scale domain for two variables. The wavelet coherency explains the correlation between two variables at each scale and location. The squared wavelet coherence is defined as (Torrence and Webster, 1999):

$$R_i^2(s) = \frac{\left|S\left(s^{-1}W_i^{XY}(s)\right)\right|^2}{S\left(s^{-1}\left|W_i^X(s)\right|^2\right)S\left(s^{-1}\left|W_i^Y(s)\right|^2\right)}, \qquad [C.6]$$

where *S* is defined as a smoothing operator and can be written as

$$S(W) = S_{\text{scale}}\left(S_{\text{space}}\left(W(s,\tau)\right)\right) \qquad [C.7]$$

where τ denotes the location and S_{scale} and S_{space} denote the smoothing along the wavelet scale axis and the spatial domain, respectively (Si and Zeleke, 2005). Now if we have the smoothing

function $\frac{1}{s\sqrt{2\pi}}\exp\left(-\frac{\tau^2}{2s^2}\right)$, the smoothing along the locations can be written as (Torrence and Webster, 1999):

$$S_{\text{space}}\left(W(s,\tau)\right)=\sum_{k=1}^{N}\left(W(s,\tau)\frac{1}{s\sqrt{2\pi}}\exp\left(-\frac{(\tau-x_k)^2}{2s^2}\right)\right)\Bigg|_s \qquad \text{[C.8]}$$

and the smoothing along scales can be written as (Torrence and Webster, 1999):

$$S_{\text{scale}}\left(W(s_k,x)\right)=\frac{1}{2m+1}\sum_{j=k-m}^{k+m}\left(S_{scale}\left(W(s_j,x)\right)\Pi\left(0.6s_j\right)\right)\Big|_x \qquad \text{[C.9]}$$

where Π is the rectangle function, $\big|_x$ means at a fixed x value and j is the index for the scales.

C.5 Application of Continuous Wavelet Transform

The wavelet power spectrum can be used to identify the dominant scale and location of variation of soil properties, and the cross wavelet spectrum and wavelet coherence can be used to identify the scale- and location-dependent correlation between two variables.

C.5.1 Identification of Dominant Scale and Location of Variation of Soil Properties

Study of scale-dependent spatial variation of soil properties is important because the scale at which the soil has been sampled may be different from the scale at which the information about soil properties will be applied. There is a need for data sampled at one scale or location, for example, to be extended or generalized to other scales or locations. However, conversion of the information from one scale to another or the data re-scaling and data integration are relatively difficult for scale-dependent spatial variation. In addition, it is often desirable to focus on a particular (dominant) spatial scale that results from a specific process (such as denitrification and nitrification). A priori information on the approximate scales of variation is also required for designing an efficient sampling scheme because the scale of spatial variation varies with the support (area of measurement averages), resolution (sample spacing) and extent (total area covered) of measurement (Western et al., 2002).

The global wavelet spectra (GWS), σ^2_W, can be obtained by integrating the local wavelet spectra across the transect (Si and Farrell, 2004); it is given by (Li and Loehle, 1995),

$$\sigma_W^2(s) = \frac{1}{A}\int_\tau \left|W_i^Y(s,\tau)\right|^2 \mathrm{d}\tau, \qquad [C.10]$$

where A is the size of the spatial domain. The global wavelet energy spectra (GWES), $E(s)$ can be calculated from GWS to identify the dominant scale and is defined as

$$E(s) = \frac{\sigma_W^2(s)}{s}. \qquad [C.11]$$

Another concept, the energy of the wavelet transform (EWT), $E_W(s)$, has been used by Frantziskonis (2002) to identify the dominant scale in a one-dimensional field; it is defined by

$$E_W(s) = \frac{\sigma_W^2(s)}{s^2}. \qquad [C.12]$$

Qi and Neupauer (2008) explained the superiority of GWES in identifying the characteristic scale of a spatial series. While GWES identifies the dominant scale, GWS explains the contribution of a scale towards the total variation.

Patterns can be repeated along a transect (a global event) or restricted to only one or a few small regions along the transect (localized events). The global and localized features jointly provide a complete picture of scale-location information of different processes in the field. Guidance in designing efficient management practices such as soil management of the field (based on global features) and site-specific soil management (based on localized features) can be obtained by differentiating between localized and global features (Si and Farrell, 2004).

In field situations the presence of global and localized features are common. Si and Farrell (2004) examined crop yield in an undulating landscape. Wheat yields were recorded at 103 sites along a transect with a sampling interval of 6 m. The transect traversed several cycles of knolls and depressions. The characteristics of the cycles changed over distance indicating an acyclic pattern. The wheat yield and other topographic indices of the area showed strong non-stationarity that restricted the use of geostatistical and spectral analyses. Si and Farrell (2004) found considerable variation in wheat yield at scales of 60 to 180 m along the transect at spatial locations 30, 90, 160, 200, 260, 300, 380, 430, and 520 m as identified from the wavelet spectra (Figure C.2, Original Figure 3 in Si and Farrell, 2004). This variation was explained as a global feature because these positions correspond to locations of knolls and depressions along the transect. There were relatively small and uniform variances at scales of 0 to 60 m. At the large scales (> 180 m), marked variation in wheat yield was centered at only a few locations, such as

90, 240, 430 and 570 m along the transect (Figure C.2), which corresponded to the locations of large depressions and knolls only. This variation was considered as localized features.

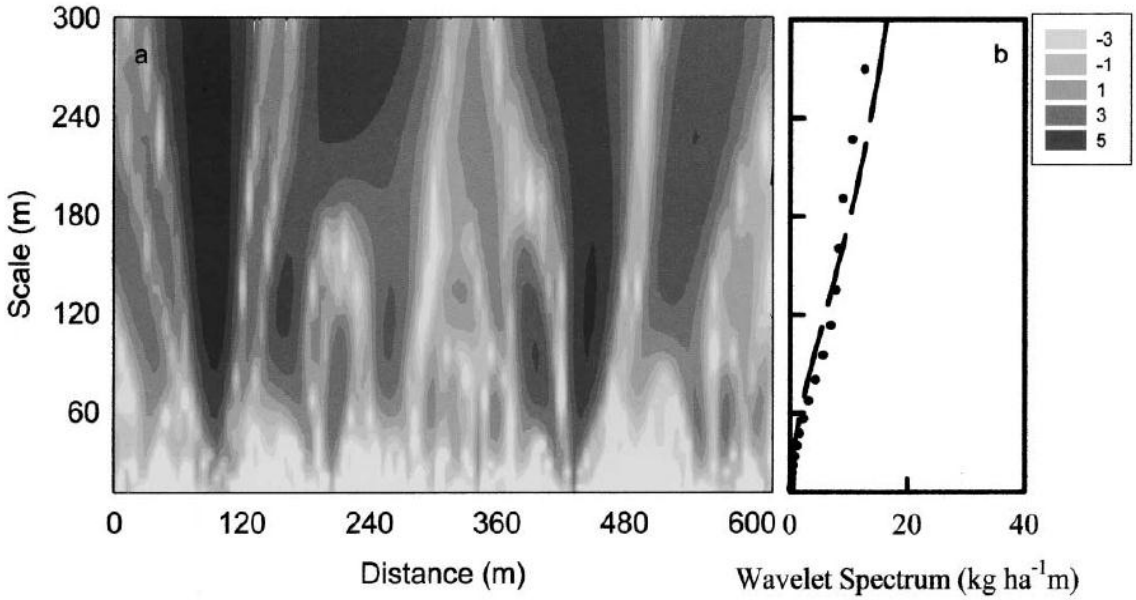

Figure C.2. Local (a) wavelet spectrum and (b) global wavelet spectrum of grain yield. Gray scale is expressed as the natural logarithm of local wavelet spectrum. The dashed line in (b) is the power spectra of red noise at a confidence level of 99% (Reproduced from Si and Farrell, 2004)

Biswas et al. (2008) examined the spatial variation of soil $\delta^{15}N$ from two different soil zones of Saskatchewan, Canada. One hundred twenty eight samples were taken along each transect at 3 m sampling intervals. Large variations in $\delta^{15}N$ concentrated at the beginning and the end of the transect in Davidson field at small scales. These localized variations correspond mainly to relatively high elevations. The wavelet spectrum of soil $\delta^{15}N$ had a few significant small-scale variations across the transect indicating the localized features of spatial variation. The location- and scale-dependent spatial variation of $\delta^{15}N$ acts as an indicator of varying soil N cycling processes.

Yates et al. (2007) investigated the spatial variation of N_2O emission from a grassland. One hundred and twenty eight monitoring locations with 4.5 m sampling intervals were established in a hummocky landscape. The N_2O emission rates were measured at each location using a chamber method during a two-year period. Generally the denitrification rate, the

important process controlling N_2O emission, varied intermittently across the landscape as the process can only occur at microsites, where the soil conditions are anaerobic and the supply of substrate to denitrifying bacteria is not limiting (Parkin, 1987). The large values of N_2O emission made the data very localized and resulted in a very skewed, 'J' shaped, lognormal or non-normal distribution of N_2O emission (Yates et al., 2006a). The spatial trend in mean and variance of nitrous oxide emission made the spatial series strongly nonstationary.

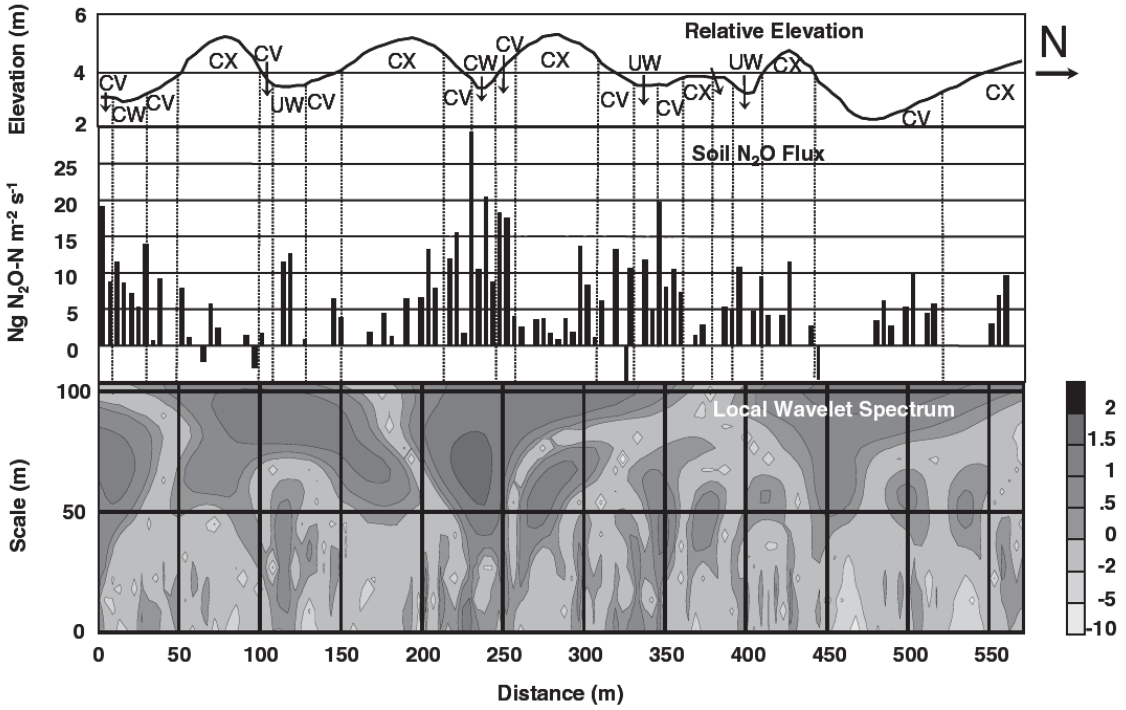

Figure C.3. Relative elevation, soil N_2O flux, and local wavelet spectrum for seeded grass transect, 3 June, 2004. Convex (CX), concave (CV), cultivated wetland (CW), and uncultivated wetland (UW) landscape elements are indicated. Color bar is log of wavelet variance. Scales <65 m are not significant according to a permutation test (p<0.05). (Reproduced from Yates et al., 2006b)

The continuous wavelet transform was used by Yates et al. (2006b, 2007) to analyze the spatial variation and scale dependency of gas emission in the agricultural field. The large variance features in the wavelet spectra at the early period of snowmelt were associated mainly with peak N_2O fluxes at the convex elements of landscape (Yates et al., 2006b), resulting in a cyclical pattern in the variance (Figure C.3; Original Figure 4 in Yates et al., 2006b). When snowmelt water had concentrated in cultivated and uncultivated wetlands, the position of the large fluxes

shifted from convex to concave elements of the landscape. The distribution of variance (form wavelet spectra) showed periodicity at scales of 30 to 50 m, which was associated with both large fluxes from the concave elements and small fluxes from flooded cultivated and uncultivated wetlands. In a snow-free field, the mean N_2O flux increased by an order of magnitude. The extreme value occurred at the location that was 320 m from the beginning of the transect, which appeared as a non-repetitive variance anomaly (i.e., localized feature). This location-specific N_2O emission was not prominent in the later part of the season when the snowmelt water was more widespread over the landscape. At the end of March and beginning of June N_2O measurements did not show any strong localized features, but they did show evolving scales of spatial variation. The small-scale variation (measurement errors) of gas fluxes was not significant, whereas the large-scale variation was significant. The local wavelet spectra showed that landscape position was an important control on the spatial variation of soil N_2O emissions, because the periodicity in the flux distribution was mainly controlled by landform elements. Beside the physical controlling factors, different environmental events also controlled the N_2O emission from agricultural soils (Furon et al., 2008). During the spring thaw events, N_2O emissions from agricultural soils were highly temporally variable with a time scale of 10 days. The thaw events control the water content in field thus modifying the N_2O emission from soils. Similarly the other environmental events like rainfall also control the temporal variability of surface soil moisture (Parent et al., 2006) than at deeper depths at a temporal scale of 1 to 48 h. Parent et al. (2006) depicted a close relationship between surface soil moisture and the precipitation from the similarity of the wavelet spectrum.

The spatial variation of two water retention model parameters (α and n in the van Genuchten (1980) water retention function) was studied by Shu et al. (2008) together with soil properties such as bulk density, sand and organic carbon contents. Similar to Si and Zeleke (2005), spatial variation of sand and organic carbon content showed three different scales of variation. These location- and scale-specific spatial variations can be explained easily with wavelet spectra.

The spatial variation in the two dimensional spatial field can be explained from the wavelet spectra calculated using a modified anisotropic Morlet wavelet. To understand the variability in two-dimensional fields, the directionality of the variation is calculated at a series of

possible scales. The dominant scales and the orientations of the spatial variations can be identified from three global measures (Neupauer and Powell, 2005; Neupauer et al., 2006).

C.5.2 Identification of Dominant Scale and Location Dependent Correlation Between two Soil Properties

Two questions are frequently asked: 1) is the relationship between two variables scale-dependent and 2) what is the dominant scale of correlation? Pearson correlation coefficient is a common measure of linear correlation between two variables strictly at the measurement scale. However, the behaviour of the variables may not be the same at all locations and scales. One variable can be positively correlated to another at some places within the measurement area, whereas at other places the two variables may be negatively correlated. Similarly, the relationships can also vary with scale. The opposite correlations may neutralize each other over the entire measurement area and scales. It is not possible to separate out the relationship at scales and locations using traditional statistics, therefore, the overall relationship can be misleading sometimes.

The cross wavelet spectrum can be used to study the correlation between two variables, but is not sufficient on its own (Si and Zeleke, 2005). A relationship between two variables can be examined by combining wavelet spectrum and coherence analyses. In addition, the phase spectrum can be used to determine if the wavelet coherence is in phase (positive correlation), out of phase (negative correlation) or random (no correlation) between two variables.

Though the Pearson correlation showed a very low coefficient value, Si and Zeleke (2005) found a significant correlation between saturated hydraulic conductivity (K_s) and sand content using the wavelet coherence and phase spectrum. There were stronger coherent relationships between them at the scales of 30 to 60 m than at the scales of 6 to 18 m. The sand and K_s were positively correlated as identified from the phase spectrum (Figure C.4; Original Figure 4 in Si and Zeleke, 2005). The K_s was strongly negatively correlated to organic carbon at scales of 30 to 90 m. In addition to these strong correlations, some weak correlations at other scales and locations were variable in nature (sometimes negative, sometimes positive or random).

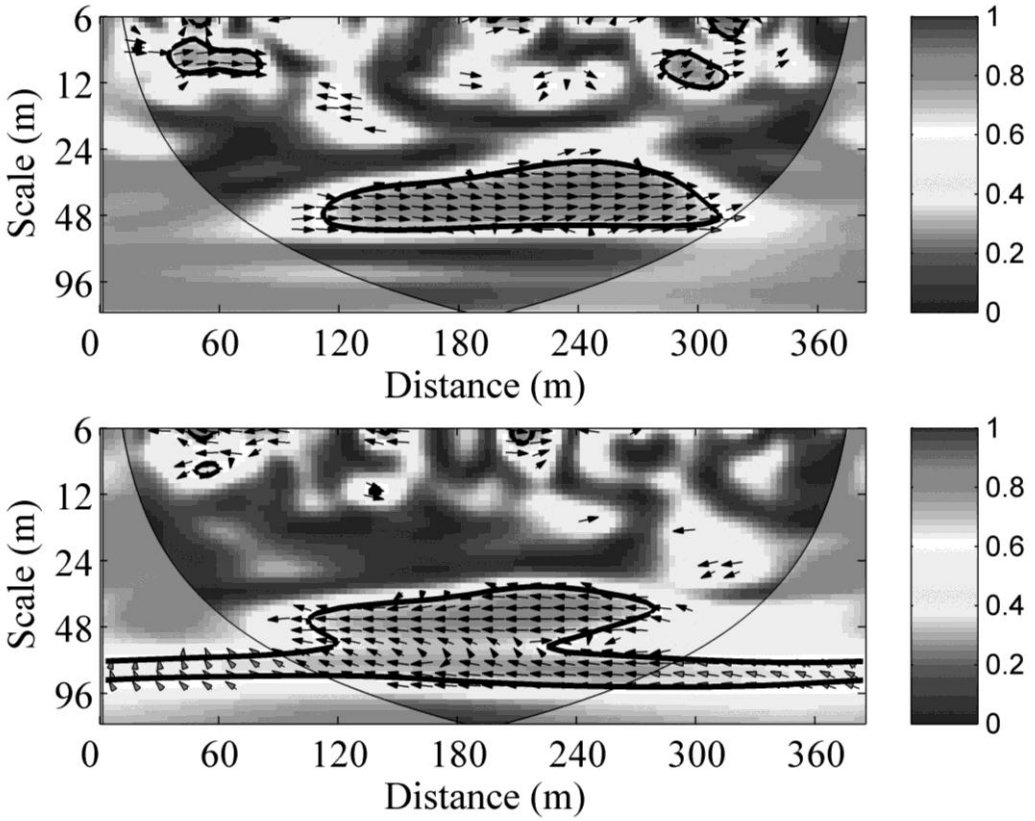

Figure C.4. Local wavelet coherency between saturated hydraulic conductivity and sand content (upper panel) and between saturated hydraulic conductivity and OC (lower panel). Horizontal axis is the distance between a sampling location and the origin of the transect. Arrows indicated the phase angles of wavelet spectra. Thin solid lines indicate the cone of influence and thick solid lines indicate the 90% confidence level. (Reproduced from Si and Zeleke, 2005)

The positive correlations might have been neutralized by negative correlations or vice versa, thus resulting in a weak linear overall correlation between K_s and sand. Shu et al. (2008) found a scale- and location-dependent relationship between the water retention parameter (α) and soil physical properties. Strong coherence between the water retention parameter, *n* and organic carbon content was also reported at the scales of 8 to 20 m and 160 to 240 m, but because of their inconsistent phase spectra, the overall correlations between them were weak for almost all scales. As the relationships between soil physical and hydraulic properties change with scale and location, these scale and location dependent relationships should be used in developing any pedotransfer functions for predicting one variable from others (Si and Zeleke, 2005; Shu et al., 2008).

A similar advantage of wavelet coherence over the traditional Pearson correlation was also reported by Biswas et al. (2008). The Pearson correlation coefficient between soil $\delta^{15}N$ and elevation was close to zero. However, at some locations and scales there were strong coherence spectra. Further, the phase spectra indicated that some of these coherence spectra were out of phase (negative) and some were in phase (positive). The in-phase and out-of-phase coherence spectra neutralized each other, resulting in weak overall correlations between the two variables. These different levels of coherence at different scales and locations also reflected varying controls of landscape position on the biological activity in soil. The strong coherence spectra indicated a linear predictive relationship at the scales and locations of its occurrence. A similar predictive relationship between water content and gas flux was indicated by Yates et al. (2007). Their study suggested that the landscape was the major controlling factor on the spatial distribution of soil temperature and water, which modified the processes responsible for nitrous oxide gas emission. Furon et al. (2008) took the advantage of wavelet coherency analysis to understand the effect of agricultural management practices on the temporal trend of N_2O emission. The thaw event was found to be the most important environmental events controlling the N_2O and CO_2 emission from soils. Beside these events, the gas emission had a coherent relationship with surface (air) temperature (Furon et al., 2008).

Wavelet coherence analysis is a powerful tool for identifying correlation between two variables over a range of scales and locations. Strong coherence between two variables at a few scales does not necessarily mean better prediction of one variable from another. The large coherence values can result from different scenarios including: i) low power spectra for both variables and low cross spectra and ii) high power spectra for both variables and high cross spectra. For scenario i), large coherence is meaningless because the contribution of variance from the scale and location to the total variance is negligible. Therefore, for locations and scales with larger coherencies, we must also refer to the power spectra to determine if the location and scales also have large variances for each of the variables and large covariances between the two variables to guarantee that the strong coherence is physically meaningful (Si and Zeleke, 2005).

C.6 Test of Statistical Significance

The test of statistical significance can be done in different ways and was reviewed by Si (2008). A common way of testing the significance of wavelet coherence is the Monte Carlo method that generates a large ensemble of surrogate data series pairs (such as K_s series and sand content series) with the same lag-1 autoregressive coefficients as the original data (Grinsted et al., 2004). To be statistically valid, at least 1000 surrogate data series pairs are required and the wavelet coherence is calculated for each of them. The 1000 wavelet coherence coefficients at a specific scale and location are then sorted in ascending order. The 95 % confidence level is the 950^{th} wavelet coherence coefficient. For a given scale and location, if the wavelet coherence coefficient calculated from the measured data (such as K_s and sand content) is larger than the 950^{th} of the 1000 wavelet coherence coefficients, the coherence is significantly different from the background red noise. As the soil properties are generally auto-correlated (Isaaks and Srivastava, 1989), the statistical significance test is performed against a red noise; a red noise is a data series that is autocorrelated in short lag distance; a typical red noise is a univariate lag-1 autoregressive process (Torrence and Compo, 1998; Si and Farrell, 2004). If the calculated wavelet coherence for the measured data is smaller than 950^{th} of the 1000 wavelet coherence coefficients, the coherence is not significantly different from red noise at the 95% confidence level.

For normally distributed data, Monte Carlo simulation is very effective (Grinsted et al., 2004; Si and Zeleke, 2005; Biswas et al., 2008). However, it is not applicable to non-normally distributed data because a theoretical probability distribution cannot be formulated for sampling. To avoid the problem, Yates et al. (2006a, 2007) used the permutation method: The data series pairs (i.e. K_s and sand series) are re-sampled without replacement for exactly N times (N is the number of data points in the series). Similar to Monte Carlo simulation, this is repeated a large number of times. In this way, each realization has an identical statistical distribution with the original data because a permutation is exactly the measured data series with a different order. However, the re-sampling completely destroys spatial dependence in the data, whereas Monte Carlo simulation can assume any type of autocorrelation such as one-step autocorrelation.

The above-mentioned Monte Carlo simulation and permutation methods test a single hypothesis at a time: whether one wavelet transform statistic (spectra or coherence) at a location and scale is different from that of background noise or not. However, there are many wavelet

coefficients, and the null hypothesis for this situation is that none of the wavelet transform statistics is different from that of the background noise. That is equivalent to testing if all the wavelet coefficients are simultaneously different from that of background noise. This is a multiple testing problem and needs a different approach to avoid inflated type I errors (Si, 2008). Maraun et al. (2007) developed an area-wise significance test for continuous wavelet spectra to overcome the difficulties of multiple testing. More research is needed to establish standard testing methods for wavelet analysis.

C.7 Conclusions and Future Research

In this paper, we have reviewed the application of the CWT to spatial studies in soil science. Spatial variation of soil has spatial dependence, periodicity, non-stationarity and many other characteristics. Geostatistics quantifies spatial dependence and spectral analysis can analyse the scale information, but loses spatial information. Wavelet analysis is an advanced mathematical technique that can provide the scale and location information of spatial variation. The CWT is superior in analysing the scale information compared with DWT. Wavelet spectra from CWT can be used to identify the dominant scales and locations of the variation. The global wavelet spectra can identify the dominant scales of variation and the local wavelet spectra can identify the localized features. Some variations at a particular scale persist over all locations, indicating a global feature. The combined information on localized and global features yields a complete picture of scale-location information of different processes in field and may provide guidance in designing efficient management practices. While wavelet spectra explain the spatial variation of a variable, wavelet coherency provides information on correlation between two variables at a scale and location. The phase spectrum, a wavelet transform product, provides information on the sign of their correlations. In combination with the phase spectrum, the wavelet coherency can explain the type and magnitude of the correlation. The positive correlation at some scales and negative correlation at other scales can neutralize each other resulting in a non-significant measurement-scale correlation between the two. Traditional statistics can measure the linear correlation only at the measurement scale and sometimes fail to identify existing correlation between the variables. Wavelet coherency partitions the overall

correlation to different scales and locations and reveals the scale and location-specific correlation between variables.

The advantage of CWT in analyzing spatial variation of nonstationary soil properties is the versatility in dealing with natural phenomenon. Wavelet cross spectra and wavelet coherence can identify only the dominant scale and location dependent correlation between two variables. Many soil processes are controlled by not only one or two variables, but rather by multiple variables. Wavelet coherence needs to be extended to analyse scale- and location-dependent correlation among multiple variables.

Understanding soil processes requires intensive sampling of soil, but soil scientists are always restricted by the number of sampling points. The present wavelet analysis deals mainly with regularly spaced samples. It is not always possible to obtain soil samples at regular intervals. Wavelet analysis needs to be extended for dealing with irregularly spaced samples and there is one instance to use discrete wavelet analysis for irregularly sampled data (Milne and Lark, 2009). Only the second moments of wavelet coefficients can explain the spatial series completely by wavelet spectra and coherence analysis, provided the data series is normally distributed. However, for other distributions, higher order moments are needed, which may provide more complete description of nonlinear spatial variation. The combination of wavelet and multifractal analysis through the wavelet transform modulus maxima (WTMM) effectively alleviate the weakness of standard multifractal analysis (cannot deal with non-positive data and non-stationary data series) (Piňuela et al., 2007; Zeleke and Si, 2007). More innovative use of the wavelet transform would provide new insights that cannot otherwise be obtained from the original data. Regression based on wavelet coefficients may provide better predictions such as linear and nonlinear regression and neural network modeling.

APPENDIX D

Permission to publish and republish different sections and chapters of this dissertation was given to the following journals.

Chapter 3: Season and depth dependent time stability and benchmarking of soil water storage in a hummocky landscape – Soil Science Society of America Journal (Accepted with minor revision) (Authors: Asim Biswas and Bing C. Si)

Chapter 4: Scales and locations of the time stability of soil water storage in a hummocky landscape – Journal of Hydrology (Accepted with minor revision) (Authors: Asim Biswas and Bing C. Si)

Chapter 5: Depth persistence of the spatial pattern of soil water storage in a hummocky landscape – Soil Science Society of America Journal 75, doi:10.2136/sssaj2010.0399 (Authors: Asim Biswas and Bing C. Si)

Chapter 7: Identifying scale specific controls of soil water storage in a hummocky landscape using wavelet coherency – Geoderma (Accepted with minor revision) (Authors: Asim Biswas and Bing C. Si)

Chapter 9: Revealing the controls of soil water storage at different scales in a hummocky landscape – Soil Science Society of America Journal (In press) (Authors: Asim Biswas and Bing C. Si)

Appendix E: Application of Continuous Wavelet Transform in Examining Soil Spatial Variation: A Review – Mathematical Geosciences 43:379-396. (Authors: Asim Biswas and Bing C. Si)

APPENDIX E

Up to date publications related to the Ph.D. work.

PUBLISHED

1. **Biswas, A.,** and B.C. Si. 2011. Revealing the controls of soil water storage at different scales in a hummocky landscape. Soil Sci. Soc. Am. J. (in press)
2. **Biswas, A.,** and B.C. Si. 2011. Depth persistence of the spatial pattern of soil water storage in a hummocky landscape. Soil Sci. Soc. Am. J. 75, doi:10.2136/sssaj2010.0399
3. **Biswas, A.,** and B.C. Si. 2011. Application of Continuous wavelet transform in examining soil spatial variation: A review. Math. Geosci. 43:379-396.
4. **Biswas, A.,** and B.C. Si. 2010. Scaling soil physical properties. *In* J. Gliński et al. (ed.) Encyclo. Agrophy. doi:10.1007/978-90-481-1.
5. **Biswas, A.,** L.K. Tallon, and B.C. Si. 2009. Scale Specific relationships between soil properties: Hilbert-Huang transform. Pedometron 28: 17-20.
6. **Biswas, A.,** and B.C. Si. 2009. Spatial relationship between soil physical and hydraulic properties along a transect. Can. J. Soil Sci. 89:473-488.
7. **Biswas**, **A**., B.C. Si, and F.L. Walley. 2008. Spatial relationship between $\delta^{15}N$ and elevation in agricultural landscapes. Nonlinear Proc. Geophy. 15:397-407.

ACCEPTED WITH MINOR REVISION

1. **Biswas, A.,** and B.C. Si. 2011. Identifying scale specific controls of soil water storage in a hummocky landscape using wavelet coherency analysis. **Geoderma.**
2. **Biswas, A.,** and B.C. Si. 2011 Scale and location specific time stability of soil water storage in a hummocky landscape. **J. Hydrol.**
3. **Biswas, A.,** and B.C. Si. 2010. Season and depth dependent time stability and benchmarking of soil water storage in a hummocky landscape. **Soil Sci. Soc. Am. J.**
4. Zou, W., A. **Biswas,** B.C. Si, and X. Han. 2011. Extracting soil water storage pattern using self-organizing map. **Geoderma.**

CONFERENCE PUBLICATIONS

1. **Biswas, A.**, and B.C. Si. 2011. Depth persistence of the spatial pattern of soil water storage in a hummocky landscape. *In* Abstracts, Annu. Meet., Can. Geophy. Union, Banff, AB. 15 May – 18 May 2011.
2. **Biswas, A.,** and B.C. Si. 2010. Hilbert-Huang transform: A new approach of analyzing non-stationary and nonlinear soil spatial variation. *In* Abstracts, Int. Annu. Meet., Am. Soc. Agro. - Crop Sci. Soc. Am. - Soil Sci. Soc. Am., Long Beach, CA. 31 Oct. – 4 Nov. 2010.
3. **Biswas, A.,** E. Lamb, and B.C. Si. 2010. Direct and indirect control of soil water storage in a hummocky landscape. *In* Abstracts, Int. Annu. Meet., Am. Soc. Agro. - Crop Sci. Soc. Am. - Soil Sci. Soc. Am., Long Beach, CA. 31 Oct. – 4 Nov. 2010.
4. Tallon, L., and **A. Biswas.** 2010. Time scales of variability in unsaturated soil cover system water content and temperature. *In* Abstracts, Int. Annu. Meet., Am. Soc. Agro. - Crop Sci. Soc. Am. - Soil Sci. Soc. Am., Long Beach, CA. 31 Oct. – 4 Nov. 2010.
5. **Biswas, A.,** and B.C. Si. 2010. Scale dependent spatial variability of soil properties in the high Arctic. *In* Abstracts, Joint Annu. Conf., Can. Soc. Soil Sci. – Can. Soc. Agro., Saskatoon, SK. 20 – 24 June, 2010.
6. **Biswas, A.,** and B.C. Si. 2010. Scale specific spatial pattern of soil water storage and its relation to topographic indices. *In* Abstracts, Joint Annu. Conf., Can. Soc. Soil Sci. – Can. Soc. Agro., Saskatoon, SK. 20 – 24 June, 2010.
7. Zou, W., A. **Biswas,** B.C. Si, and X. Han, X. 2010. Nonlinearity detection in the spatial variation of nitrous oxide emission by delay vector variance. . *In* Abstracts, Joint Annu. Conf., Can. Soc. Soil Sci. – Can. Soc. Agro., Saskatoon, SK. 20 – 24 June, 2010.
8. **Biswas, A.,** and B.C. Si. 2010. Soil water storage patterns in Chernozemic soil of hummocky landscapes. *In* Abstracts, Int. Work. Manag. Black Soil., Harbin, China.
9. **Biswas, A.,** and B.C. Si. 2009. Scaling analysis of irregularly sampled soil properties using second generation wavelet. *In* Abstracts, Int. Annu. Meet., Am. Soc. Agro. - Crop Sci. Soc. Am. - Soil Sci. Soc. Am., Pittsburgh, PA. 1 – 5 Nov. 2009.
10. **Biswas, A.,** and B.C. Si. 2009. Elucidation of controls of soil water storage in the landscape using Hilbert-Huang Transform. *In* Abstracts, Int. Annu. Meet., Am. Soc. Agro. - Crop Sci. Soc. Am. - Soil Sci. Soc. Am., Pittsburgh, PA. 1 – 5 Nov. 2009.

11. **Biswas, A.,** and B.C. Si. 2009. Analyzing landscape variability in soil water storage using Hilbert-Huang transform. *In* Abstracts, Bi-annu. Meet. Comm. 1.5 Pedometrics Div. 1 Int. Union Soil Sci., Beijing, China.
12. **Biswas, A.,** and B.C. Si. 2009. Examining temporal stability of soil water storage using wavelet coherency analysis. *In* Abstracts, Joint Annu. Conf., Can. Soc. Soil Sci. – Can. Soc. Agro. – Can. Soc. Agric. Forest Meteor., Guelph, ON. 5 – 7 Aug. 2009.
13. **Biswas, A.,** and B.C. Si. 2009. Revealing the controls of nonstationary and nonlinear soil water storage in the landscape. *In* Abstracts, Joint Annu. Conf., Can. Soc. Soil Sci. – Can. Soc. Agro. – Can. Soc. Agric. Forest Meteor., Guelph, ON. 5 – 7 Aug. 2009.
14. **Biswas, A.,** and B.C. Si. 2009. Is the soil water storage pattern stable over time? *In* Abstracts, Prairie Reg. Student Conf., Can. Water Resour. Asso., Saskatoon, SK. 25 – 26 Feb. 2009.
15. **Biswas, A.,** and B.C. Si. 2009. Soil water benchmarking for environmental monitoring. *In* Abstracts, Soils Crops, Saskatoon, SK. 25 – 26 Feb. 2009.
16. **Biswas, A.,** and B.C. Si. 2008. Scaling properties of depth controlled spatial pattern of soil water storage. *In* Abstracts, Annu. Meet., Can. Soc. Soil Sci., Prince George, BC. 6 – 10 July 2008.
17. **Biswas, A.,** and B.C. Si. 2008. Model averaging for Water Retention Curve. *In* Abstracts, Annu. Meet., Can. Soc. Soil Sci., Prince George, BC. 6 – 10 July 2008.
18. **Biswas, A.,** and B.C. Si. 2008. Spatial relationship between soil hydraulic and soil physical properties along a transect. *In* Abstracts, Can. Geophy. Union – Hydrol. Sec. Prairie Student Conf., Saskatoon, SK. 26 Jan. 2008.

PROCEEDING PUBLICATION

1. **Biswas, A.,** and B.C. Si. 2009. Soil water benchmarking for environmental monitoring. *In* Soils Crops Proc. [CD ROM], Univ. of Saskatchewan, Saskatoon, SK. 25 – 26 Feb. 2009.